PETROGENESIS OF THE MCGERRIGLE PLUTONIC COMPLEX, GASPE, QUEBEC

by
Graeme M. B. Wallace
Department of Geological Sciences
McGill University, Montreal
January, 1988

A thesis submitted to the Faculty of Graduate Studies and Research in partial fulfillment of the requirements for the degree of Master of Science.

PETROGENESIS OF THE MCGERRIGLE PLUTONIC COMPLEX, GASPE, QUEBEC

This thesis is dedicated to my father

ABSTRACT

The Devonian McGerrigle Complex is a shallow pluton dominated by granite, with lesser volumes of quartz monzonite, syenite, gabbro, monzodiorite, and nepheline syenite. The gabbro crystallized at low to moderate $f(O_2)$ conditions (below the Ni-NiO buffer); titansalite and labradorite are the only liquidus phases. The syenites are genetically distinct from most granites. In these felsic rock types the $f(O_2)$ was internally buffered at relatively high values (near the Ni-NiO buffer); evidence for magmatic oxidation is restricted to the more evolved samples. The nepheline syenites crystallized under a wide range of magmatic conditions; their observed mineralogy depends principally on the agpaitic index and $f(O_2)$ of the magma.

Xenocrysts, typically derived from more primitive material, are observed in all rock types. Contamination of the felsic rocks is interpreted to have occurred predominantly through hybridization, rather than magma mixing.

The observed range in $\delta^{18}O$(whole-rock) is 5.6 to 9.3°/oo with all rock types typically exhibiting low values (6.0-7.0°/oo). Quartz (6.4-8.1°/oo) and feldspar (5.9-7.4°/oo) typically achieved approximate subsolidus isotopic equilibrium. The predominantly low $\delta^{18}O$ values exhibited by the felsic rocks and their transitional A- to I-type character are consistent with an origin in the lower crust from isotopically primitive material. The higher $\delta^{18}O$ values probably reflect interaction with upper crustal materials at a late (subsolidus?) stage.

RESUME

Le complexe de McGerrigle, un pluton polyphasé d'âge dévonien, mis en place à faible profondeur, est constitué principalement de granite et de quantités moins importantes de monzonite quartzique, syénite, gabbro, monzodiorite et syénite à néphéline.

Le gabbro a cristallisé à des fugacités d'oxygène faibles à modérées (en-dessous du tampon Ni-NiO); les seuls minéraux présents sur le liquidus sont la titansalite et la labradorite.

Les syénites sont génétiquement distinctes de la plupart des granites. Durant la cristallisation des roches felsiques, la fugacité d'oxygène a été maintenue à un niveau relativement élevé (près du tampon Ni-NiO); les signes d'oxydation magmatique sont limités aux échantillons les plus évolués.

Les syénites néphéliniques ont cristallisé sous des conditions variables; leur minéralogie reflète principalement leur index agpaïtique et la fugacité d'oxygène du magma pendant la cristallisation.

Tous les types de roches contiennent des xénocristaux, typiquement dérivés de source(s) plus primitive(s). La contamination des roches felsiques semble avoir pris place principalement par hybridation plutôt que par brassage et mélange de magmas.

Les valeurs de $\delta^{18}O$ des roches totales s'échelonnent de 5.6 à 9.3°/oo. Dans l'ensemble, tous les faciès montrent des valeurs plutôt basses (6.0-7.0°/oo). La composition isotopique du quartz (6.4-8.1°/oo) et des feldspaths (5.9-7.4°/oo) reflète leur réequilibration subsolidus. Les valeurs de $\delta^{18}O$

généralement basses des roches felsiques et leur caractère transitionnel (type A à I) s'accordent avec une source isotopiquement primitive dans la partie inférieure de la croûte. Les valeurs les plus élevées de $\delta^{18}O$ reflètent probablement l'interaction tardive (sous le solidus?) du pluton avec la partie supérieure de la croûte.

Acknowledgements

To me this thesis always represented more than a degree, it was the chance to do a piece of work that was original, stimulating and provided a large dose of self-satisfaction. However, its completion was only possible through the support and patience of many people to whom I will always be grateful.

I am especially thankful to the Geological Survey of Canada which supplied the funds for most of the analyses presented and supported the author in the field during the summer of 1984. Dr. J. B. Whalen of the Survey collected most of the samples studied here and showed the author exactly how the field study of an igneous pluton should be carried out.

I wish to thank my thesis advisor, Bob Martin, who patiently read several drafts of this thesis, and was always available to answer questions. Furthermore, Dr. Martin collected all the X-Ray data for the feldspars.

Dr. C. Gariépy of the Université du Québec provided much needed advice and technical assistance, that considerably facilitated the arduous task of obtaining mineral separates.

I would never have started work on the McGerrigle Plutonic Complex without the support and encouragement of R. Wares and J. Van Bosse. Luciano Venditteli and Scott Green provided invaluable assistance and much needed company in the field. I would like to thank all the graduate students who discussed with me different aspects of this thesis, particularly Serge Nadeau, Tom Skulski, Christine Payette and Abdel Rahman.

I am grateful to Dr. M. Mackinnon for introducing me to the electron microprobe and especially for making herself available

for after work inquiries. Richard Yates carried out some of the photographic work and gave much needed advice on drafting. The technical assistance of Dr. K. Muehlenbachs, Mr. T. Ahmedali, Mr. T. Shahzada and Dr. G. Pouliot at various stages of this thesis is also appreciated.

I would like to acknowledge the financial support that I received from the Reinhardt Fund of the Department of Geological Sciences of McGill University, the McGill Summer Award and the Fonds FCAR.

There are many people who helped me keep going during the rough times and made the time spent much more enriching than it otherwise would have been. I am especially thankful to Heidi, Carissa, Sally and Brent. Finally, it is to Jeanne Paquette that I owe my greatest debt, particularly for her huge contribution to the shaping of this thesis.

TABLE OF CONTENTS

LIST OF FIGURES

LIST OF TABLES

CHAPTER 1. INTRODUCTION

OBJECTIVES

This thesis presents data on the field relations, petrography and mineralogy, as well as a preliminary study of the oxygen isotope geochemistry, of the McGerrigle Plutonic Complex, a polyphase intrusive body located in the north-central zone of the Gaspé Peninsula, Québec. This work was carried out as part of a broader project undertaken by the Geological Survey of Canada on the petrogenesis of the major granites in Gaspé. Related studies of the whole-rock major- and trace-element geochemistry, lead isotope geochemistry and geochronology (K-Ar dating of biotite and amphibole separates, U-Pb dating of accessory minerals) are still in progress at the time of writing (cf. Whalen and Garièpy 1986, Whalen and Roddick 1987).

Field, petrographic and mineralogical data (Chapters 2-5) are presented in order to: 1) describe the principal rock types of the intrusion and their relationships, 2) document the compositional, textural and, in some cases, structural variations of the major rock-forming minerals (mafic minerals and feldspar), 3) identify the accessory minerals, especially in the nepheline syenites, and 4) integrate the available data to gain insight into the petrogenetic processes that have contributed to the origin and evolution of each rock type. Oxygen isotope data (Chapter 6) were obtained for representative samples (including several quartz and feldspar pairs) to further constrain the magmatic and subsolidus histories of the principal rock types.

LOCATION AND ACCESS

The pluton occupies a region of Gaspé known as the monts McGerrigle, which includes mont Jacques-Cartier (1248 m), the highest peak of the Canadian Appalachians. It is located in the north-central part of the Gaspé Peninsula, approximately 40 km ESE of Sainte-Anne-des-Monts (Fig. 1.1). Except for its northeasternmost portion, the pluton lies entirely within Gaspé Provincial Park. It is nearly completely encircled by La Rue de Ceinture, which cross-cuts the pluton at its NE corner. Access onto the plateau on which the bulk of the pluton outcrops is largely restricted to the northern half of the pluton and, even there, is difficult by car. The main access routes are: 1) the trail that climbs up mont Jacques-Cartier on the west side, 2) a dirt road that starts from the Madeleine mine on the east side, 3) an old prospector's road that climbs toward mont Auclair on the north side, and 4) old prospector's roads that lead toward the top of mont Richardson near lac aux Américains (cf. de Romer 1977).

DATA BASE

The pluton was mapped during the summer of 1984 by the author and Dr. J. B. Whalen of the Geological Survey of Canada. The results of this project are published as a 1:25 000 map (Whalen 1986). Within the pluton, the proportion of outcrop is variable, being high in some areas (e.g., north of mont Richardson and along the trail up mont Jacques-Cartier) but generally is poor to moderate. Mountain tops are typically bare of trees and are commonly covered by large fields of blocks (felsenmeer) rather than solid outcrop. These blocks

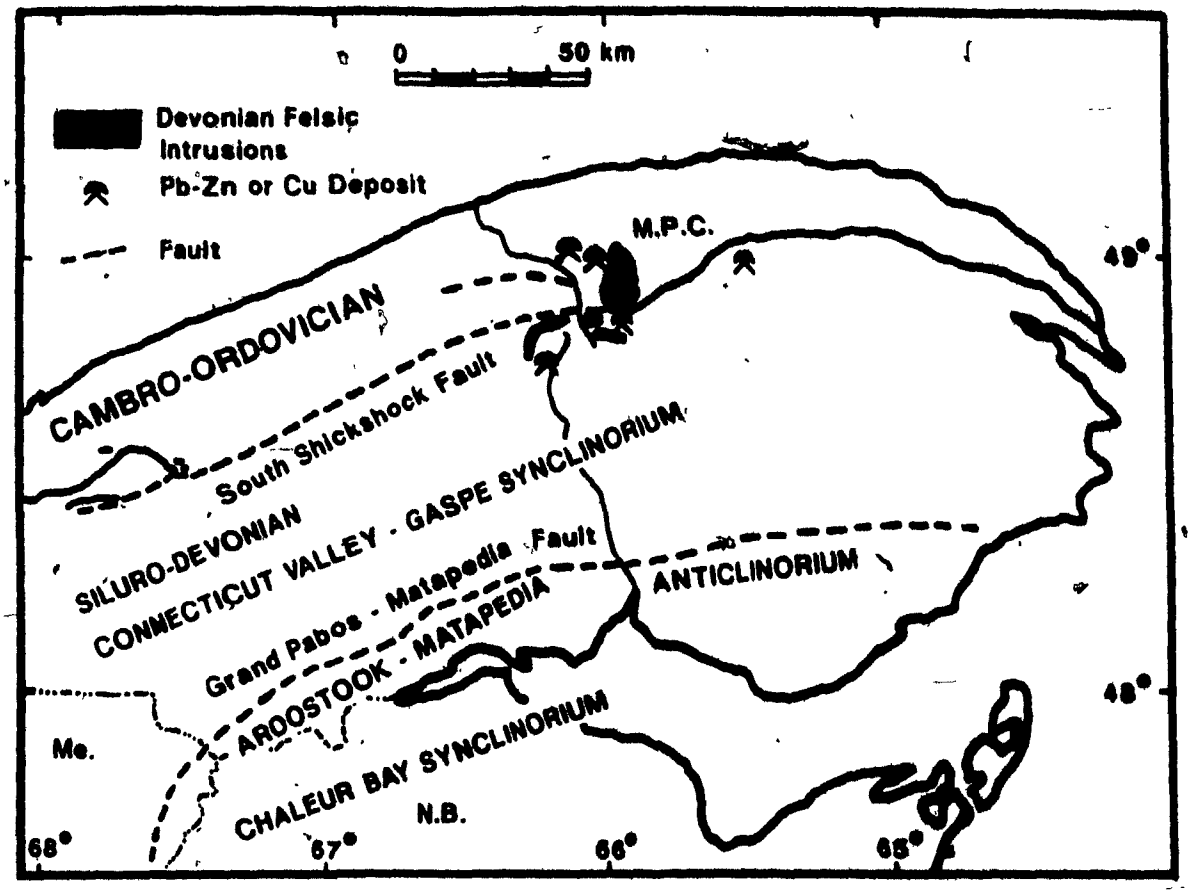

Figure 1.1. Setting of the McGerrigle Plutonic Complex in the Gaspe Peninsula. M.P.C.: McGerrigle Plutonic Complex. Modified from Van Bosse (1985).

commonly form stripes (on slopes) or polygonal patterns and are assumed to be approximately *in situ* (*cf.* Payette and Boudreau 1984). Some areas, such as around mont Auclair in the northern part of the pluton, are notable for their general lack of outcrop. The uneven quality of exposure and the complex relationships between many rock types complicates the separation of different units. Therefore, for the purpose of this study, the pluton has been roughly divided into two suites (Fig. 1.2, see below).

Over 300 hand specimens were collected, from which more than 200 thin sections were studied. 83 "chemical samples", each several kilograms in weight, were collected from the freshest material available to document the compositional variability of the pluton. Polished thin sections were made of nearly every sample (80), and modal analyses were carried out on 39 samples (J. Whalen, pers. comm. 1985). Major- and trace-element analyses were carried out by C. Gariépy on all the chemical samples. A subset of approximately 40 chemical samples were selected for more detailed study, including lead-isotope, rare-earth and oxygen-isotope geochemistry. This thesis presents mineral chemistry data for 35 of these samples. Oxygen-isotope data were obtained for 18 whole-rock (plus four replicate) samples and four pairs of quartz and feldspar mineral separates.

PREVIOUS WORK

The first surveys of the monts McGerrigle region to describe briefly the igneous rocks present were carried out by Richardson (1859) and Low (1885). Systematic mapping of the

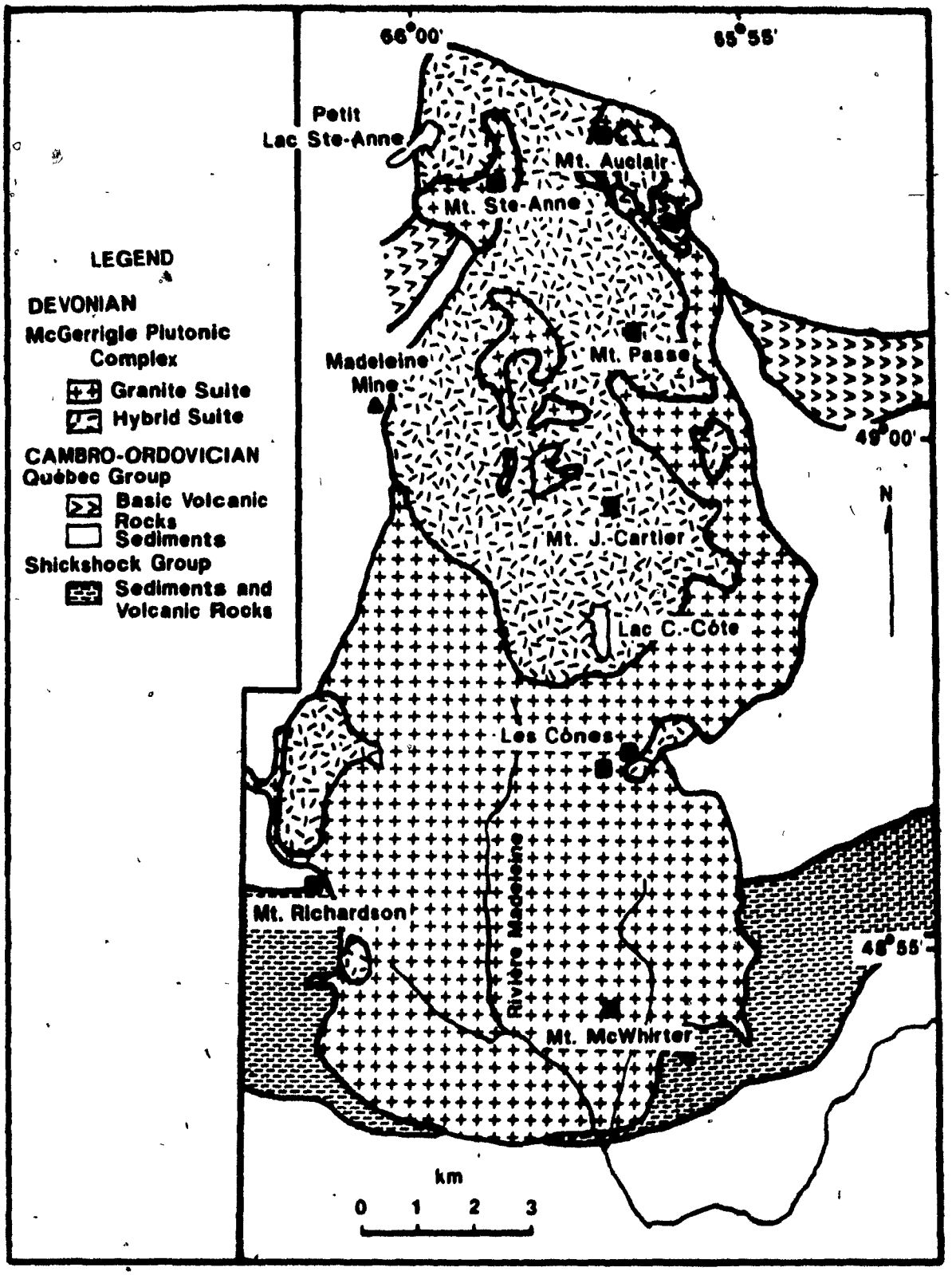

Figure 1.2. General geological map of the McGerrigle Plutonic Complex. Modified from Whelan (1985a).

region, however, did not take place until the 1920s and 1930s (e.g., Jones 1933) when regional mapping at a scale of 1:63 360 was carried out. Even though several different rock types (granite, granodiorite, syenite, diorite, felsite and pegmatite) were recognized, their distribution was not shown on the map.

During the sixties and early seventies, a detailed (1:12,000) mapping program of the area was carried out by the Québec Department of Natural Resources (Robert 1966, 1967, Girard 1967, Lachance and Duquette 1977, de Römer 1977), inspired in part by the discovery of the Madeleine Mines copper deposit in 1964, after the park had been opened to prospecting in the fall of 1963.

Of these studies, de Römer's (1974, 1977) provided the most complete description of the pluton and its metamorphic aureole. De Römer concluded that the pluton represents a polyphase intrusive complex that could be subdivided into an early hybrid suite consisting of xenoliths of gabbro, nepheline syenite, hornfels and metavolcanics within quartz-poor felsic rocks (syenite, granodiorite and monzonite) and a later granite suite. He interpreted the quartz-poor felsic rocks of the hybrid suite to result from the large-scale incorporation and assimilation of xenoliths. De Römer deduced that the pluton was forcibly intruded at a depth corresponding to 2 kbar and that the presently exposed surface is the roof portion.

Wanless et al. (1973) obtained a 358±16 Ma date for a biotite concentrate from a granite as well as a date of 342±14 Ma from a hornblende separate from quartz diorite. De Römer (1974,

1977) obtained three whole-rock K-Ar dates for the pluton; two were interpreted to represent a minimum age of crystallization (356±4 Ma for a porphyritic granite and 346±7 Ma for a biotite granodiorite).

La Rocque (1986) carried out a combined Rb-Sr and geochemical study of the Gaspé granites, including the McGerrigle Plutonic Complex. She dated the hybrid suite of de Romer (1974, 1977) at a Middle Devonian age of 380±5 Ma, and the granite suite at a Late Devonian to early Carboniferous age, ranging from 362±5 Ma to 356±8 Ma. She also concluded that the granites display a transitional A- to I- type character and that they were either derived by partial melting of different crustal sources or had been contaminated by a fluid rich in radiogenic strontium. The quartz-bearing rocks of the hybrid suite are attributed to heterogeneous crustal contamination of a mantle-derived magma; however, this primary magma does not correspond to the gabbro observed in the intrusive complex.

Other studies of interest include a detailed study of the metamorphic aureole of the pluton by Van Bosse (1985), who inferred that the aureole equilibrated at a maximum temperature of approximately 610°C and a lithostatic pressure of 2 kbar. Conductive heat transfer was deduced to have predominated east of the pluton, whereas in the western and southern portions of the aureole, heat is interpreted to have been partly transferred by infiltrating fluids. Van Bosse also documented the occurrence of a second phase of prograde metamorphism in the pelitic hornfels in the southern half of the pluton, consistent with the hypothesized younger intrusive phase of La

Rocque (1986). P. Girard (1969, 1971) studied the Madeleine copper deposit, work which is being continued today by A. E. Williams-Jones and co-workers (1986).

REGIONAL GEOLOGY

The McGerrigle Plutonic Complex intrudes an ENE-trending belt of sedimentary and volcanic rocks (Fig. 1.1, 1.2) from the Cambro-Ordovician Shickshock Group, and the Middle Ordovician Deslandes and Lower Ordovician (and older) Cap-des-Rosiers formations of the Québec Group (de Romer 1977, Lachance and Duquette 1977, Islam et al. 1982). St.-Julien and Hubert (1975) subdivided the Cambro-Ordovician rocks of the Québec Appalachians into three major tectonic domains; the Shickshock Group was included in the internal domain, whereas the Deslandes and Cap-des-Rosiers formations form part of the allochthonous nappes of the external domain. In their maps of the tectonic lithofacies for the Appalachian Orogen, Williams (1979) and Williams and Hatcher (1983) included these units within the St. Lawrence Terrane that makes up part of the Humber zone.

The Shickshock Group represents sedimentary, volcanic and rare plutonic rocks formed at a continental slope and rise (Gagnon and Jamieson 1985). Several ultramafic bodies including the mont Albert peridotite, a layered harzburgite, are observed in the Shickshock Group and are interpreted to represent transported alpine peridotite (Beaudin 1980, Gagnon and Jamieson 1985). In the McGerrigle area the Shickshock Group forms an E- to ENE trending, 2.5 to 4 km wide belt that is

cross-cut by the southern half of the pluton and is bounded by rocks of the Québec Group both to the north and south (Fig. 1.2; de Römer 1977). In this area the belt consists of sandstone, shale, slate, limestone and basalt as well as their contact-metamorphosed equivalents (de Römer 1977). The nature of the contact between the Shickshock Group and the Québec Group is unclear; de Römer (1977) reported examples of both faulted and conformable contacts in the McGerrigle region.

The Deslandes and Cap-des-Rosiers formations represent allochthonous deep-water sediments that were deposited on the continental slope and rise (R. Hesse, pers. comm. 1987). Flysch sequences dominate both formations, with shales, siltstones, slates, phyllites, sandstone, conglomerate and limestone being present in the McGerrigle area (de Römer 1977, Lachance and Duquette 1977). Within the Cap-des-Rosiers Formation, a band (1.5 to 3 km wide and 25 km long) of massive or amydaloidal basalt and associated tuff (Fig. 2.1; de Römer 1977, Lachance and Duquette 1977) is cross-cut by the northern half of the pluton.

Geophysical data have been interpreted to indicate the presence of Precambrian (Grenville?) basement underlying the Québec and Shickshock groups (Seguin 1982).

Immediately to the south of the pluton, Siluro-Devonian sequences unconformably overlie the Cambro-Ordovician rocks (Duquette et al. 1984) within the Connecticut-Gaspé Synclinorium (Fig. 1.1). The Siluro-Devonian sequences consist of a wide range of predominantly sedimentary rock types, including sandstone, reef-bearing limestone, calcareous

siltstone and conglomerates (de Römer 1977, Duquette et al. 1984). During the Lower Devonian a transition from a shallow marine (Lower and Upper Gaspé Limestone groups) to a non-marine environment (Gaspé Sandstone Group) occurred (de Römer 1977, Rust 1981). The York River Formation of the Gaspé Sandstone Group contains a bimodal volcanic sequence of silica-undersaturated alkali basalt and oversaturated rhyolite tuffs with alkaline tendencies, dated at 380±3 Ma (La Rocque and Doig 1984, La Rocque 1986).

The McGerrigle Plutonic Complex is one of several major intrusive bodies located within the north-central zone of the Gaspé Peninsula (Fig. 1.1, McGerrigle and Skidmore 1967, de Römer 1974, La Rocque 1986). Several plutons (e.g., mont Hogsback, mont Vallières-de-Saint-Réal) cut the Siluro-Devonian sediments south of the McGerrigle Plutonic Complex and consist of various types of felsic porphyry (Duquette et al. 1984, La Rocque 1986). A small inclusion of medium-grained gabbro occurs within the quartz monzonite at mont Vallières-de-Saint-Réal (Duquette et al. 1984). Numerous felsic and mafic dykes and sills are also observed cross-cutting the Siluro-Devonian rocks (Wares 1983, Duquette et al. 1984, Girard, unpubl. manuscript). Both Duquette et al. (1984) and de Römer (1973, 1977) concluded that the southern plutons intruding the Siluro-Devonian rocks and the McGerrigle Plutonic Complex are probably contemporaneous and that at least in some cases the plutons may belong to the same igneous mass at depth. However, data obtained by La Rocque (1986) indicate a range of ages from 381±4 to 338±6 Ma for the southern plutons.

One of the principal structures of the Gaspé Peninsula, the South Shickshock fault (Fig. 1.1) is located within two kilometres of the southern contact of the pluton. This fault can be followed from Matapedia Lake to just east of the McGerrigle Plutonic Complex. Some authors (e.g., Lachance and Duquette 1977) have speculated that the fault may extend as far as the eastern end of the Gaspé Peninsula. To the west of the pluton the fault defines the boundary between the Siluro-Devonian and Cambro-Ordovician sediments; however, to the east the fault apparently continues within the Québec Group (de Römer 1977, Wares 1983). A long history of fault movement which may have spanned most of the Paleozoic, has been inferred by many authors (e.g., Beaudin 1980, Duquette et al. 1984) but the exact amount of displacement is unknown. Recent studies (e.g., Lebel and Hubert 1986, Berger and Hubert, unpubl. manuscript) suggest that it may represent a major, dextral wrench fault.

TECTONIC HISTORY OF THE GASPE PENINSULA

The northern Appalachians have been affected by several orogenies (e.g., Avalonian, Taconian, Acadian and Alleghanian; St.-Julien and Béland 1982); in the Gaspé area, however, widespread evidence has only been reported for the Taconic and Acadian Orogenies.

The Ordovician Taconic Orogeny affected the rocks of the Québec and Shickshock groups, resulting in polyphase deformation, development of northwesterly-vergent nappes and thrust faults, emplacement of ophiolites and regional metamorphism (Béland 1969, 1974, St.-Julien and Hubert 1975, Gagnon and Jamieson 1985). The most commonly suggested model

for the Taconic Orogeny involves a collision between North America and either an island arc or a microcontinent (e.g., Bird and Dewey 1970, Osberg 1978, Williams and Hatcher 1983).

The Lower to Middle Devonian (Keppie et al. 1983) Acadian Orogeny resulted in mild to moderate deformation in the Gaspé area (Béland 1969, 1982). Acadian deformation of the Siluro-Devonian rocks of Gaspé resulted in tight to broad, upright, generally northeasterly-trending folds (Béland 1969, 1982, de Römer 1977, Duquette et al. 1984). In the Quebec Appalachians, the Acadian deformation did not involve transport of nappes and imbrication of slices as was the case for the Taconian episode (Béland 1982). Recent studies (e.g., Bourque et al. 1985, Lebel and Hubert 1986) indicate that wrench tectonics involving major displacements along strike-slip faults (e.g., South Shickshock Fault) occurred during the Acadian Orogeny. Major Acadian flat thrusting has also been inferred from seismic profiles near Anticosti Island, located to the north-east of the Gaspé Peninsula (Roksandic and Granger 1981, Béland 1982).

Whereas most authors relate the Acadian Orogeny to closure of an oceanic basin culminating in a continent-continent collision (e.g., Bird and Dewey 1970, Bradley 1983, Williams and Hatcher 1983), any such collision must have occurred far to the south of the study area (e.g., Williams 1979). Futhermore, a recent study (Bédard 1986) of the Siluro-Devonian volcanic and intrusive rocks in the southern half of the Gaspé indicates that they are not directly associated with subduction. His preferred model for the generation of these magmas calls for local tensional environments in an orogenic foreland or a wide

intracontinental shear. Therefore, there appears to be little basis for the existence of a subduction zone dipping beneath the Gaspé during the Siluro-Devonian (cf. Bradley 1983).

MCGERRIGLE PLUTONIC COMPLEX

The McGerrigle Plutonic Complex forms an elongate body whose axis trends approximately north-south (perpendicular to the regional structural grain) and is exposed over an area of approximately 130 km^2 (Figs. 1.1, 1.2). The pluton is surrounded by a prominent 1.5- to 3-km wide aureole of hornfels and skarn (de Römer 1977, Van Bosse 1985). A much broader epimetamorphic halo was identified by Islam et al. (1982) using illite crystallinity and asphaltic pyrobitumen. This was interpreted to indicate that the intrusion extends over a much larger area at relatively shallow depths than is exposed at the surface. The isotropic fabric and lack of deformational structures within the pluton indicate that the pluton postdated the Acadian Orogeny.

The pluton can be roughly subdivided into two suites; the granite suite is concentrated in the southern half of the pluton, whereas the hybrid suite dominates the northern half (Fig. 1.2, de Römer 1977, Whalen 1986). Small areas of rocks mapped as part of the hybrid suite occur in the southern half of the pluton, specifically to the north and southeast of mont Richardson and to the east of Les Cônes. Areas of granite mapped as part of the granite suite are also present within the northern half of the pluton; they occur both marginal to and within the hybrid suite. Granite containing a large amount of mafic or intermediate inclusions was mapped as part of the

hybrid suite. The granites in the hybrid and granite suites are lithologically similar except for the presence or absence of inclusions. The contact relationships between the two types are generally ambiguous and probably in part gradational.

The dominant characteristic of the hybrid suite is its heterogeneous appearance on both the outcrop and regional scales. This results from the presence of inclusions of intermediate to mafic composition (only very rare felsic inclusions were observed). Relative to the granite suite, the evolved rock types in the hybrid suite are commonly quartz-poor (<10%), though many exceptions exist. A wide variety of rock types are observed in the hybrid suite, including monzonite (quartz), syenite (quartz), alkali-feldspar syenite, monzodiorite (quartz), granite, granodiorite, diorite, and gabbro (Whalen and Gariepy 1986). Xenoliths of Quebec Group metasedimentary (principally hornfels) and metavolcanic rock types derived from the country rock (de Römer 1977) are occasionally observed in the hybrid rocks. These xenoliths vary in size from several square metres to large patches up to 600 metres in length and 300 metres in width, interpreted to represent roof pendants (e.g., S and SE of mont Auclair). The presence of these country-rock xenoliths and the distribution and typically fine-grained nature of the hybrid rocks suggest that the hybrid rocks represent the roof facies of the intrusive complex (de Römer 1977).

The granite suite is relatively homogeneous relative to the hybrid suite. Its rocks make up approximately 75% of the total outcrop area of the pluton. Typically, the granites are medium-

to coarse-grained, equigranular to porphyritic and plot in the granite field of the IUGS classification scheme for plutonic rocks (Streckeisen 1976). Mafic inclusions are typically uncommon, rarely exceeding 2 cm in size.

The pluton is also crosscut by several generations of mafic and felsic dykes; these generally trend in a northwesterly direction within the pluton, following the prevalent system of joints in the area (de Römer 1977). The mafic dykes (up to 4 m wide) are typically alkaline and, following Irvine and Baragar (1971), they are classified as alkali basaltic or hawaiitic (C. Gariépy, pers. comm. 1985). The latter type seems more abundant, especially in the southern half of the pluton (e.g., south of Les Cônes). Aplite dykes, rhyolite porphyry dykes (commonly exhibiting a micrographic texture) and rare pegmatite dykes are the felsic varieties observed. Field evidence indicates that the emplacement of the hawaiitic dykes postdated at least in part that of the rhyolite porphyry dykes. Tinguaite dykes and sills (Sørensen 1974a, b) as well as rare pods(?) of miaskitic nepheline syenite are observed in the northern half of the pluton (cf. Whalen 1986). Quartz veins, commonly with a metasomatized (bleached) halo, are predominantly found in the southern half of the pluton (cf. de Römer 1977).

ECONOMIC GEOLOGY

There are three mineral deposits located within the immediate vicinity of the McGerrigle Plutonic Complex. The Candego mine, located approximately 6 km northwest of the pluton, is a lead-zinc-silver deposit (62 000 tonnes mined between 1948 and 1954). Mineralization occurs in quartz-carbonate veins along or

near a schistose zone (the Candego Fault; Lachance and Duquette 1977). In the northwestern part of the aureole, the Madeleine mine contained approximately 8.7×10^6 tonnes of ore grading 1.15% Cu and 7 g/t Ag and was mined from 1969 until 1982. The ore occurs in an en échelon array of five steeply plunging, chimney-shaped, zoned bodies (bornite core, chalcopyrite and pyrrhotite toward the rim) consisting of closely spaced sulfide and quartz-sulfide veins and stringers located within pelitic hornfels (Williams-Jones et al. 1986). Mineralization in the Candego and Madeleine deposits has been related to fluids derived from the McGerrigle Plutonic Complex (Lachance and Duquette 1977, Williams-Jones et al. 1986). However, the detailed mechanism and source of the sulfur and metals are still poorly understood. The third deposit, Sullipek, is located 2.5 km south of the southern limit of the pluton, within the Siluro-Devonian rocks of the Saint-Léon Formation. It contains approximately 509 000 tonnes of ore grading 1.35% Cu (Duquette et al. 1984). The deposit is formed in skarn, which appears to be associated with dacite porphyry dykes that may or may not be related to the McGerrigle Plutonic Complex (Wares 1983). Many other occurrences of mineralization have been reported, the principal ones being described by de Römer (1977) and Lachance and Duquette (1977). Apart from rare molybdenite flakes, mineralization was not observed in the pluton itself.

CHAPTER 2. FIELD RELATIONSHIPS, PETROGRAPHY AND MINERALOGY OF THE MESOCRATIC INTERMEDIATE TO MAFIC ROCK TYPES

INTRODUCTION

A wide range of mafic to mesocratic intermediate rock types (characterized by SiO_2 contents of 45 to 60 wt. % and color indices greater than 30) are observed within the McGerrigle Plutonic Complex. They make up less than 5 % of the exposure of the plutonic complex (cf. Whalen 1986). The samples studied (Fig. 2.1) are subdivided into four groups on the basis of compositional and textural characteristics: 1) gabbro, 2) fine-grained mafic inclusions, 3) mesocratic intermediate rock types, and 4) endoskarn.

FIELD RELATIONSHIPS AND PETROGRAPHY

Gabbro

Gabbro forms small scattered bodies up to 1500 m in length in the northern half of the pluton (Whalen 1986). It is typically black, equigranular and massive (rare porphyritic varieties were also sampled). Grain size varies from fine to coarse. Fine-grained mafic (likely cognate) inclusions and rare miarólitic cavities were observed.

Mineralogical, textural and field evidence indicates that emplacement of most, if not all, gabbro predated that of the surrounding more evolved host lithologies (e.g., syenite, granite, etc.). However, the presence of fine-grained inclusions of alkali basalt that exhibit textural evidence of coexistence as a liquid with the host melt (Whalen 1985a; see below) as well as the cross-cutting of typical felsic rocks from the hybrid suite (e.g., quartz monzonite and white

Figure 2.1. Sample location map showing the distribution of samples for which electron microprobe data were obtained. Open circles: mafic and mesocratic intermediate rock types, filled circles: compound samples of granite and fine-grained mafic inclusions, open triangles: quartz monzonite, closed triangles: syenites, squares: granites, hexagons: nepheline syenites. Refer to Figure 1.2 for definition of the map units.

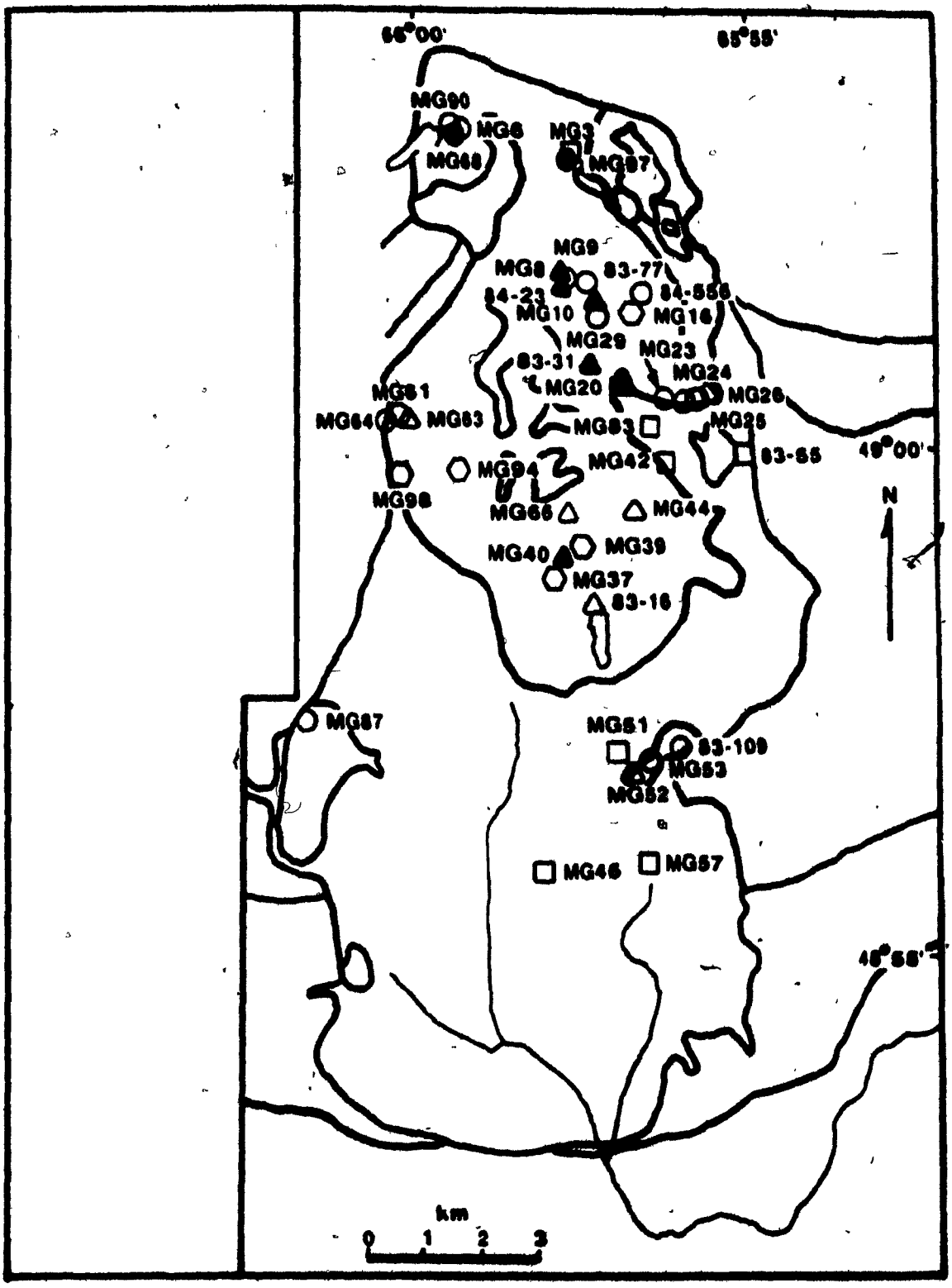
66°00'
65°55'
MG90
MG6
MG3
MG68
MG67
MG9
MG8
83-77
84-23
84-556
MG10
MG16
MG29
MG23
83-31
MG24
MG20
MG26
MG61
MG64
MG63
MG83
MG25
83-55
49°00'
MG94
MG42
MG98
MG66
MG44
MG40
MG39
MG37
83-16
N
MG87
MG51
83-109
MG53
MG52
MG46
MG57
49°55'
km
0 1 2 3

granodiorite east of the Madeleine mine) by alkali basaltic dykes (up to 1 m across) also indicate that the basaltic magmatism was in part contemporaneous with, and may even have outlasted, felsic magmatism. Some outcrops of medium-grained gabbro show apparent chilled margins near felsic veins, indicating that the gabbro must have been at least partly liquid at the time it came in contact with the felsic magma.

Plagioclase forms anhedral to euhedral, unzoned to weakly zoned (normal, rare oscillatory) laths or phenocrysts up to 1.2 cm. K-feldspar is rare, occurring as weakly perthitic, interstitial grains or lining fractures.

Amphibole is the dominant mafic mineral in all samples studied, with subordinate amounts of biotite and clinopyroxene also present. The alkali basaltic dyke (MG61) contains mafic pseudomorphs, possibly after olivine phenocrysts; if olivine was present this is the only sample in which it was tentatively identified. Primary accessory minerals are magnetite, ilmenite, pyrite, chalcopyrite, pyrrhotite, apatite and zircon. The alkali basaltic dyke is also exceptional in that sulfides (dominantly pyrite) are the only opaque phases present.

Fine-grained Mafic Inclusions

Fine-grained mafic inclusions are relatively common in a wide range of rock types at scattered localities, principally in the northern half of the complex (e.g., trail up mont Jacques Cartier, mont Ste-Anne). They are typically black, porphyritic and amygdaloidal, range from less than one centimetre to several metres in size, and exhibit a wide range of shapes,

including pillows (Figs. 2.2.1, 2.2.2) and irregular "blebby" inclusions (Fig. 2.3.1). The fine-grained inclusions commonly occur in swarms; elongate inclusions may exhibit a preferred orientation. Linear arrays of inclusions could represent disrupted dykes (cf. Whalen 1985a).

Many inclusions exhibit textural evidence of coexistence as a mafic liquid with an at least partly liquid host (Whalen 1985a). This evidence includes the presence of chilled margins (Fig. 2.3.2), crenulated irregular contacts (Figs. 2.3.1, 2.4.8), breadcrust structures (round inclusion with contraction cracks visible in the chilled margin; cf. Whalen 1985a), net-vein textures (irregular mafic blebs separated by thin felsic veinlets or veins), and pillow shapes. Similar textures have been described by numerous authors (e.g., Walker and Skelhorn 1966, Reid et al. 1983, Brown and Becker 1986).

Contacts between the fine-grained mafic inclusions and their hosts are typically sharp. Contaminated facies between the host and inclusion (Chapters 3, 4) are typically restricted to a hand specimen or outcrop scale.

Plagioclase forms anhedral to euhedral, typically unzoned to weakly zoned (normal, oscillatory) laths or phenocrysts up to 8 mm. Perthitic K-feldspar is observed in the more felsic inclusions, occurring as interstitial grains, partial rims on plagioclase laths or partly infilling amygdules.

Amphibole and biotite, the dominant mafic minerals, are commonly heterogeneously distributed even on a thin-section scale. Phenocrysts or xenocrysts (see below) of clinopyroxene are common in some samples. Observed primary accessory minerals

Figure 2.2.1. Fine-grained mafic pillows in white granodiorite, Mont Ste-Anne.

Figure 2.2.2. Fine-grained mafic pillows in K-feldspar-dominant granite. Northeast of Les Cônes.

Figure 2.3.1. Irregularly-shaped fine-grained mafic inclusions exhibiting crenulated and chilled margins in white granodiorite. Mont Auclair.

Figure 2.3.2. Fine-grained mafic inclusion exhibiting a well-developed chilled margin, cross-cut by a felsic vein. Mont Passe.

FIGURE 2.4. FINE-GRAINED MAFIC INCLUSIONS

1. Train of apatite grains cross-cutting both plagioclase laths and titanite (T). Apatite apparently crystallized along late-stage microfractures. Scale bar = 0.15 mm. Fine- to medium-grained mafic inclusion (MG24); part of chilled pillow in granite.

2. Garnet(?) (v) and fibrous, pale brown to blue-green pleochroic pumpellyite(?) (p) along cleavages in biotite (B) with titanite (T) and chlorite (c; after biotite) also present. Scale bar = 0.15 mm. Same sample as Fig. 2.4.1 (MG24).

3. Resorbed oscillatory zoned grain of plagioclase (c) that varies in composition from andesine (An_{33}) near the core to calcic oligoclase (An_{23}) at the rim, with an optically discontinuous rim (R) of oligoclase (An_{20}). Crossed polars. Scale bar = 0.15 mm. Porphyritic fine-grained mafic inclusion (MG6).

4. A compound xenocryst of titansalite (P) and labradorite (L; An_{56-57}). The titansalite exhibits alteration to amphibole and minor biotite, mostly along its margin. Under crossed polars the titansalite exhibits patchy cross-hatched polysynthetic twinning. In the upper left-hand part of the grain a slightly deeper-colored zone is visible along an irregular curved contact. Scale bar = 3 mm. Same sample as Fig. 2.4.3 (MG6).

5. Corona texture. A core of pale yellow-green to blue-green pleochroic silicic amphibole (A) plus minor amounts of Fe-Ti oxides and titanite rimmed by biotite (b) plus minor amounts of amphibole. Possible pseudomorph after pyroxene. A similar texture is observed in the white granodiorite host. Crossed polars. Scale bar = 1 mm. Porphyritic fine-grained mafic inclusion (MG68).

6. Infilled amygdule containing concentrically zoned radiating fibrous aggregates of chlorite (c), amphibole (A), titanite (T), pyrite (p), zoned epidote (e), plagioclase (P) as well as calcite. Crossed polars. Scale bar = 1 mm. Fine- to medium-grained mafic inclusion (MG26).

7. Chilled contact between a porphyritic fine-grained mafic inclusion (MG97) and white granodiorite (G). The chilled margin is characterized by the presence of prismatic grains of salite (P) and platy iron oxides (dominantly ilmenite). Biotite (b) is the dominant mafic mineral on the inclusion side of the contact. Scale bar = 0.15 mm.

8. Chilled, cuspate contact between a porphyritic fine-grained mafic inclusion and white granodiorite. Hand specimen obtained from the same locality as MG97.

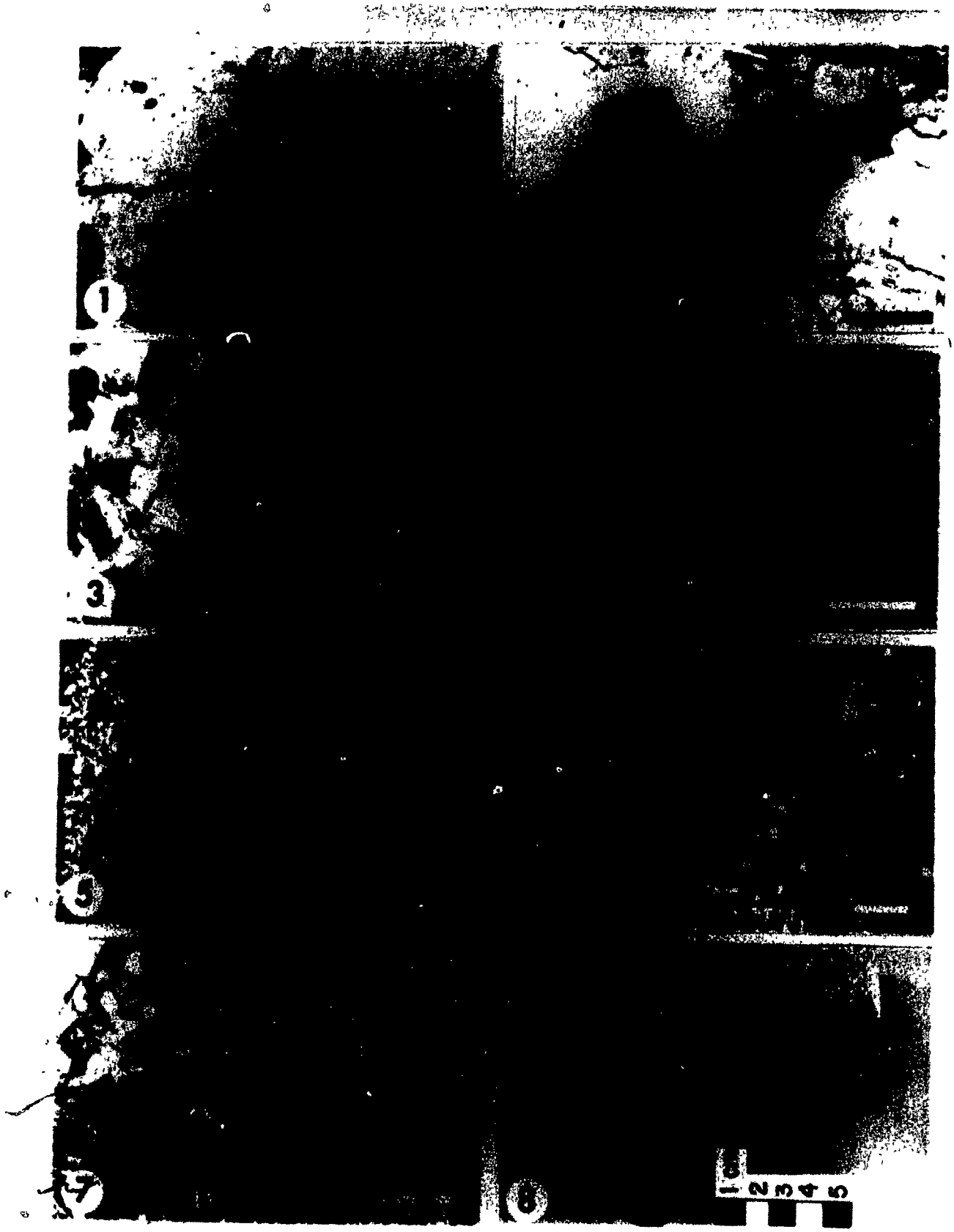

are magnetite, ilmenite, pyrite, chalcopyrite, pyrrhotite, apatite, zircon and allanite(?).

The oval to round or elongate amygdules (Fig. 2.4.6) contain coarser-grained minerals than the surrounding groundmass including K-feldspar, titanite, calcite, epidote, chlorite, apatite, allanite, oxides, pyrite, quartz, plagioclase, zircon, amphibole and biotite. The amygdules may be surrounded by an alteration halo in which the plagioclase is highly altered relative to grains farther from the amygdule.

Chilled margins are characterized by a well-defined decrease in grain size (from fine- to medium-grained interiors to fine- to very fine-grained margins), an abundance of platy oxides and acicular apatite, an increase of biotite relative to amphibole, and a zone of prismatic clinopyroxene crystals at the host-inclusion contact (Fig. 2.4.7).

The Mesocratic Intermediate Rock types

The mesocratic intermediate rock types predominantly consist of monzodiorite, though diorite and quartz monzodiorite are also observed. Field relationships and petrography suggest that they represent inclusions, varying from less than one metre to several tens of metres in size, within a more evolved host. A wide range of textural and compositional variations may occur over short distances. The inclusions range from fine- to coarse-grained, equigranular to porphyritic or even pegmatitic, and are typically grey in color. Some samples contain amygdules and miarolitic cavities.

Fine-grained rounded mafic inclusions or "ghosts" of

inclusions are observed in some samples (e.g., Fig. 2.5.8). These samples are typically fine- to medium-grained and exhibit a heterogeneous color index. Contacts between the mesocratic intermediate rock types and their felsic hosts are typically sharp, but gradational contacts may occur.

Plagioclase typically occurs as anhedral to subhedral, unzoned to weakly zoned (normal) laths or phenocrysts. In the more felsic samples (monzodiorites, etc.), K-feldspar typically forms weakly perthitic, dominantly anhedral grains; it is commonly interstitial to plagioclase and, in some samples, mantles the plagioclase laths. Interlocking contacts between the mantling K-feldspar and plagioclase are only rarely observed (e.g., Fig. 2.5.4). Quartz is present in most samples, typically as interstitial grains. Minor amounts of interstitial nepheline are observed in a sample of diorite (MG9).

The samples studied can be roughly divided into two groups according to their mafic mineralogy: 1) diorite to monzodiorite dominated by biotite, with subordinate amounts of clinopyroxene and typically minor amounts of amphibole (e.g., MG9, 90, 29), and 2) monzodiorite to quartz monzodiorite or monzonite in which amphibole is typically the dominant mafic mineral, with subordinate amounts of biotite and clinopyroxene (e.g., MG23, 53, 84-556). Identified primary accessory minerals include magnetite, ilmenite, pyrite, pyrrhotite, chalcopyrite, apatite, zircon and allanite(?).

Endoskarn

The hybrid zones in the southern half of the pluton (e.g.,

FIGURE 2.5. MESOCRATIC INTERMEDIATE ROCK TYPES

1. Secondary colorless pyroxene (c; white) and chlorite, intergrown and in optical continuity with pink-brown primary pyroxene (r; black). Primary pyroxene is rimmed by amphibole (A) which is locally intergrown with biotite and contains anhedral grains of colorless pyroxene. Crossed polars. Scale bar = 0.5 mm. Medium- to coarse-grained monzodiorite (MG23).

2. Skeletal ilmenite. Scale bar = 0.5 mm. Same sample as Fig. 2.5.1 (MG23).

3. Sector-zoned clinopyroxene (P). Crossed polars. Scale bar = 0.1 mm. Fine- to medium-grained biotite-pyroxene monzodiorite (MG29).

4. Plagioclase phenocryst exhibiting evidence of recrystallization (predominantly along its margin; fading of twin lamellae, development of patchy extinction), and mantled by perthitic K-feldspar (k), along a locally interlocking contact (e.g., below k). Secondary silicic amphibole (A) with minor amounts of biotite infill fractures in the phenocryst. Some of the amphibole may have formed after primary pyroxene. Crossed polars. Scale bar = 1.0 mm. Medium- to coarse-grained (slightly porphyritic) quartz monzodiorite (84-567).

5. Example of coexisting grains of both brownish primary (p) and pale green secondary (S) clinopyroxene. Primary pyroxene is rimmed and partly replaced by amphibole (a) as well as subordinate amounts of biotite (minor amounts of secondary pale green pyroxene are visible at the margin of the primary pyroxene). The secondary pyroxene partially encloses a euhedral lath of biotite (b) with no visible evidence of interaction between the two minerals. Scale bar = 0.5 mm. Fine- to medium-grained porphyritic monzodiorite (84-556).

6. Platy oxides (dark grey or black) as well as acicular apatite (barely visible) in nonturbid, untwinned secondary plagioclase (R; white) surrounding remnants of the primary plagioclase (P; dark grey). The primary plagioclase is alterated to saussurite(?) along fractures. Crossed polars. Scale bar = 0.15 mm. Fine-grained monzodiorite (84-541).

7. Abundant acicular apatite needles concentrated in a nonturbid rim of secondary plagioclase (S; light grey) surrounding unzoned, weakly turbid primary plagioclase (p; black). Some sericitization of the primary plagioclase is visible predominantly along fractures. Crossed polars. Scale bar = 0.15 mm. Same sample as Fig. 2.5.5 (84-556).

8. Rounded, fine-grained biotite-amphibole-pyroxene, highly recrystallized mafic inclusion (I) in fine- to medium-grained amphibole (only rare biotite or pyroxene) monzodiorite (G) (84-424). Scale bar = 0.5 cm.


G

north of mont Richardson, east of Les Cônes; Fig. 1.2), located close to the contact with the country rock, contain mafic and mesocratic intermediate inclusions (Fig. 2.6.1) that exhibit evidence of metasomatism by a fluid that was not in equilibrium with the host granite (see below). These inclusions are therefore classified as endoskarn (Einaudi and Burt 1982).

The inclusions vary from green to brown and from fine- to coarse-grained. At some outcrops, lenses of relatively pristine rock are still preserved within the endoskarn (Fig. 2.6.2). Some highly metasomatized inclusions are cross-cut by veins of pink or white albite(?) (plus quartz), clinopyroxene (±feldspar), and of granite. However, the metasomatism does not appear to be directly related to the granite veins.

Plagioclase is the dominant rock-forming mineral; it occurs as anhedral, rarely subhedral, typically unzoned grains. None of the samples studied show K-feldspar or quartz, though both minerals are relatively common in the unmetasomatized inclusions located in the same area. Clinopyroxene is the only mafic mineral observed in most of the samples studied. Identified accessory minerals are titanite, apatite, rutile, zircon and, exceptionally, oxide phases.

MAJOR-ELEMENT GEOCHEMISTRY

Representative modes, whole-rock compositions and norms are given in Tables A3.1 and A4.1. The interpretation of the whole-rock chemistry is complicated, as many samples exhibit textural and mineralogical evidence of variable degrees of metasomatism and recrystallization (see below). Another potential complication is the possible presence of a cumulate component,

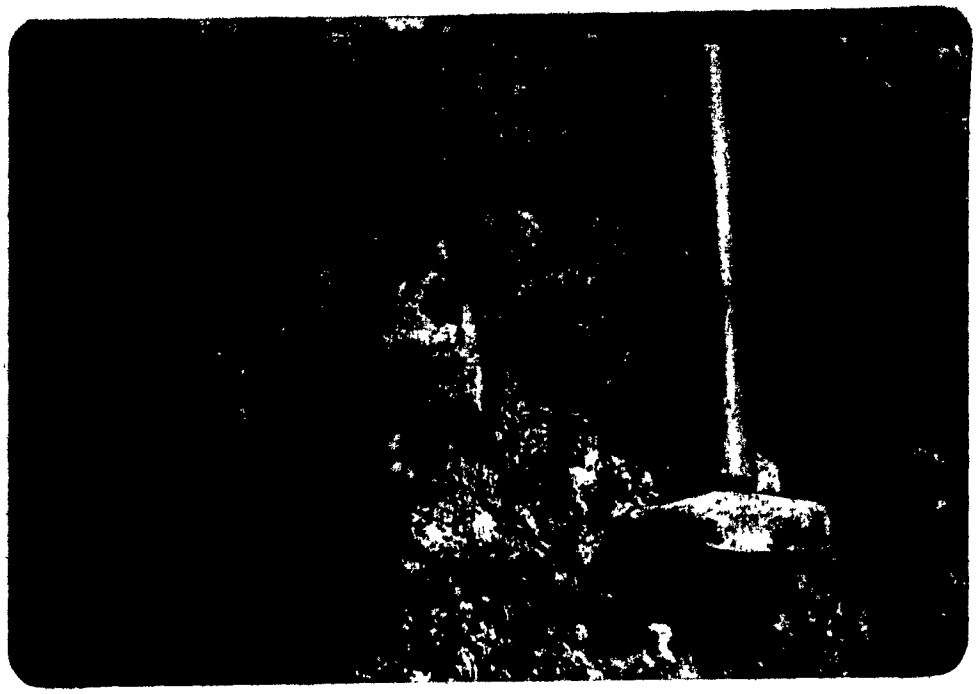

Figure 2.6.1. Inclusions of endoskarn in K-feldspar-dominant granite. East of Les Cônes.

Figure 2.6.2. Monzodiorite inclusion that has undergone metasomatism to form endoskarn. North of mont Richardson.

especially in the coarser-grained rocks (e.g., MG64). Most samples are therefore unlikely to have preserved their primary composition, though some samples of the mafic rocks, particularly the dykes, probably come close. Any detailed geochemical study will have to sort the effect of these processes on different elements in order to determine those most likely to reflect original magmatic abundances.

With the exception of the endoskarn (e.g., MG88), which falls in the subalkaline field, and quartz monzodiorite (e.g., MG87), which plots right on the boundary, the samples studied plot in the alkaline field on a plot of Na_2O+K_2O versus SiO_2 (Whelan and Gariépy 1986).

Most mafic samples are SiO_2-undersaturated, with up to 6 wt. % normative nepheline. Some of the fine-grained mafic inclusions (e.g., MG6) contain a small amount of normative hypersthene, indicating silica saturation. However, these samples show evidence of metasomatism and oxidation.

The biotite-pyroxene diorites and monzodiorites (e.g., MG29, 90) are all SiO_2-undersaturated, whereas the amphibole-dominant monzodiorites (MG23, 84-556) are all oversaturated and contain minor amounts of quartz. Relative to the mafic samples, both types are characterized by lower Fe, Mg and Ca and higher alkali contents (Table A4.1). Ti and P abundances of the more primitive amphibole-dominant monzodiorites are initially as high or higher than those in the mafic samples but decrease in the more evolved samples (e.g., MG87).

The endoskarn (e.g., MG88) is characterized by higher Ca, and lower K, Fe^{3+} and Fe^{2+} (C. Gariépy, pers. comm. 1985) than

unmetasomatized inclusions in the same area (e.g., MG87; Table A4.1). However, in the absence of systematic analyses of samples exhibiting differing degrees of metasomatism, the actual extent of the chemical changes is poorly constrained.

FELSIC MINERALOGY

Plagioclase

Plagioclase ranges from white to grey to dark brown and almost invariably exhibits evidence of recrystallization, principally along grain margins and fractures. Recrystallization results in fading and, ultimately, disappearance of both twinning and primary zoning, development of an anhedral shape, appearance of inclusions of K-feldspar, mafic and accessory minerals, formation of myrmekite and replacement by untwinned, more sodic plagioclase. Extensive recrystallization of the plagioclase within the biotite-pyroxene diorites (e.g., MG90) and the endoskarn (e.g., 83-109) has resulted in nearly complete destruction of the primary igneous textures (i.e., zoning, subhedral shape).

The degree of alteration is variable, with sericitization most commonly observed. The recrystallized areas of the plagioclase grains typically exhibit little or no alteration.

Labradorite (An_{61-67}; Table A5.1) is the primary feldspar in the gabbro studied (MG64). The recrystallized rim exhibits a sodic andesine composition (An_{32-33}). A mineral separate of the lowest-density feldspar fraction of the rock has a composition, estimated from its cell parameters, of sodic oligoclase (An_{17}; Table A6.2).

In the fine-grained mafic inclusion studied (MG6), an unzoned

phenocryst of labradorite (An_{56-57}) forms a compound grain with titansalite (Fig. 2.4.4). Other phenocrysts contain a resorbed, oscillatory-zoned core (Fig. 2.4.3) that varies from calcic andesine in its center to sodic oligoclase (An_{23-45}) outward. The cores are compositionally and petrographically similar to the zoned grains in the white granodiorite that is host to the mafic inclusion. Such resorbed cores may therefore represent xenocrysts derived from the granodiorite (e.g., Didier 1987). The discontinuous rim surrounding the resorbed core exhibits a sodic oligoclase (An_{19}) composition similar to that of the groundmass plagioclase (An_{21}).

In the mesocratic intermediate inclusions, core compositions are typically more An-rich in the amphibole-dominated monzodiorites (e.g., MG23, 53, 84-556), ranging up to An_{53} (labradorite), than in the biotite-pyroxene diorites or monzodiorites (e.g., MG90, 83-77), which are invariably below An_{30} (calcic oligoclase). This may reflect the more highly recrystallized character of the biotite-pyroxene samples, though more sodic primary core compositions may have been typical of some of the biotite-pyroxene monzodiorites. A rounded, resorbed core was only observed in plagioclase from one sample of this rock group (MG87); the core is commonly unzoned and more highly altered than the rim.

In all mesocratic intermediate inclusions the plagioclase rim invariably shows evidence of extensive recrystallization. It is characterized by a more restricted range of compositions than the core, from albite to sodic oligoclase (An_{5-20}). Acicular apatite or even skeletal oxide phases (Figs. 2.5.6, 2.5.7) are

observed in the recrystallized margin of some grains, implying that dissolution of the primary plagioclase preceded precipitation of the secondary feldspar, as it is unlikely that such rapid-growth textures could develop in a solid medium (Vernon 1983; see below).

K-Feldspar

K-feldspar is typically pinkish or brownish, weakly to moderately turbid and microperthitic. In thin section the K-feldspar commonly exhibits textural characteristics similar to those described in Chapter 3. In some samples (e.g., MG90), the K-feldspar is commonly intergrown with and replaces plagioclase and may be partly or completely secondary.

Grid twinning is rare and its occurrence is similar to that observed in more felsic rocks (Chapter 3). Its scarcity is consistent with the X-ray data (Table A6.3); the K-feldspar of all the analyzed samples is monoclinic (orthoclase) to X rays. The samples exhibit a restricted range of Al-Si ordering ($2t_1$ between 0.79 and 0.82; Table A6.1, Fig. 2.7) and Or-content (Or_{90-98}) that overlap that of most of the more evolved samples studied and therefore can be interpreted in a similar way (Chapter 3). The composition of the albite component of the K-feldspar separate (estimated from its cell parameters) varies from An_3 to An_{14} (Table A6.2) and probably reflects the presence of a plagioclase contaminant in the separate analyzed.

MAFIC MINERALOGY

Pyroxene

Two texturally and compositionally distinct varieties of

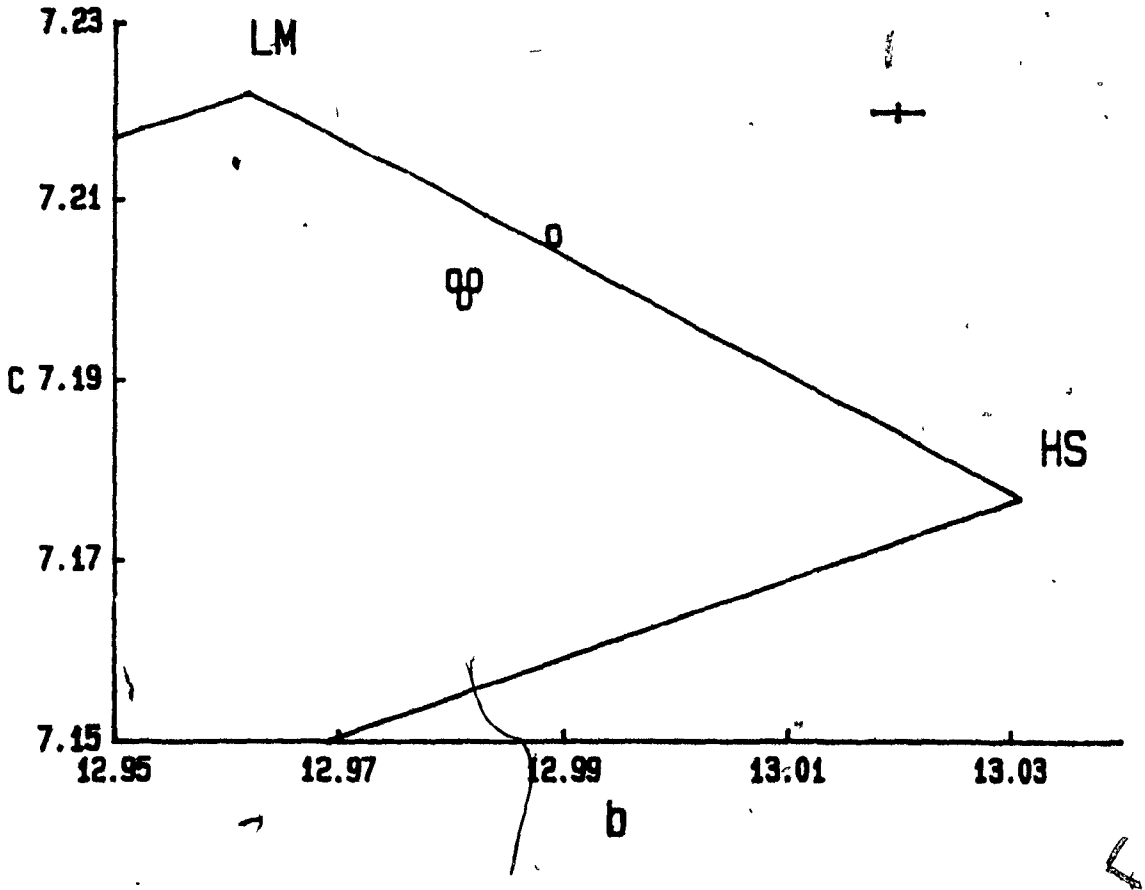

Figure 2.7. Plot of b versus c unit-cell dimensions for K-feldspar from the monzodiorites. LM: low microcline, HS: high sanidine. Units: Å. Error bar is the average for the samples plotted.

clinopyroxene are recognized. One is brownish in color, commonly rimmed and often partly (or completely) replaced by amphibole or biotite; it is considered to represent the primary magmatic pyroxene. The second variety, typically greenish, commonly appears more pristine than its brownish counterpart and is interpreted to be secondary.

Primary Clinopyroxene

The primary clinopyroxene typically exhibits a pale brown to pink-brown pleochroism whose intensity increases with Ti content. The pyroxene exhibits a subophitic texture in the coarser-grained samples (e.g., MG23, MG64); it also occurs as phenocrysts (xenocrysts) in the fine-grained mafic inclusions or as rare grains mantled by kaersutite in the groundmass of an alkali basaltic dyke (MG61). In some samples (e.g., MG25, 84-556), only remnants of the primary clinopyroxene are preserved.

The grains can be subdivided into two groups; those that appear to preserve a primary magmatic composition and those that appear to have been modified through subsolidus recrystallization. Recrystallization is suggested by the wide range of Ti contents within or between grains in the same sample. The distribution of values does not appear to correspond to any primary zonation. Ti is assumed to be a good indicator of the degree of recrystallization, as the solubility of Ti in clinopyroxene increases with increasing temperature (Verhoogen 1962, Akella and Boyd 1973, Otten 1985). In MG23, Ti contents vary from 0.7 to 2.2 wt. % TiO_2. Al (predominantly ^{iv}Al) tends to increase with Ti content, whereas Si and, in

some samples, Mg decrease. The compositional trends resemble those in unrecrystallized clinopyroxene, suggesting that the same schemes of substitution apply to both cases (see below). Na, total Fe and Mn appear to remain constant, whereas the behavior of Ca is irregular. Bleaching of the pyroxene is observed with increasing degree of recrystallization. These changes are similar to those observed by Smith (1970) in recrystallized augite from an olivine diabase sill. In samples (e.g., MG23, 87 and 84-556) in which it was impossible to separate recrystallized from unrecrystallized grains using textural characteristics (e.g., homogeneous extinction, absence of secondary alteration, etc.), compositions that exhibit the highest Ti and Al contents were interpreted to most likely approximate the primary composition.

In the pyroxene quadrilateral (Ca-Mg-FeTotal+Mn), the "magmatic" compositions dominantly fall within the salite and augite fields (Fig. 2.8.1) and would be classified either as titansalite (augite) or titaniferous salite (augite). In general they (Table A7.1) are characterized by high Al, Ti, Na and inferred Fe^{3+}, implying the presence of a large percentage (up to 35.6 %) of nonquadrilateral components (Cameron and Papike 1981). Cr contents are typically less than 0.05 wt. % Cr_2O_3. These characteristics are typical of clinopyroxene that has crystallized from alkaline mafic magmas (e.g., Wilkinson 1956, Kushiro 1960, Fodor et al. 1975, Schweitzer et al. 1979).

Sector (hourglass) zoning was observed in one sample of gabbro (MG64, Fig. 2.9.1). In the two grains analysed the deeper-colored sectors are characterized by higher Al (both

Figure 2.8. Pyroxene compositions plotted in terms of cationic Ca-Mg-(Fe+Mn) in the "pyroxene quadrilateral". Nomenclature is that proposed by Poldervaart & Hess (1951): a: diopside, b: salite, c: ferrosalite, d: hedenbergite, e: endiopside, f: augite, g: ferroaugite, h: ferrohedenbergite. 2.8.1. Selected average compositions of "primary" clinopyroxene. Star: gabbro and fine-grained mafic inclusions, open circle: monzodiorite. 2.8.2. Selected average compositions of secondary clinopyroxene. Filled circle: mafic and mesocratic intermediate rock types (with the exception of the endoskarn), triangle: endoskarn. Lines join irregulary zoned grains.

1.

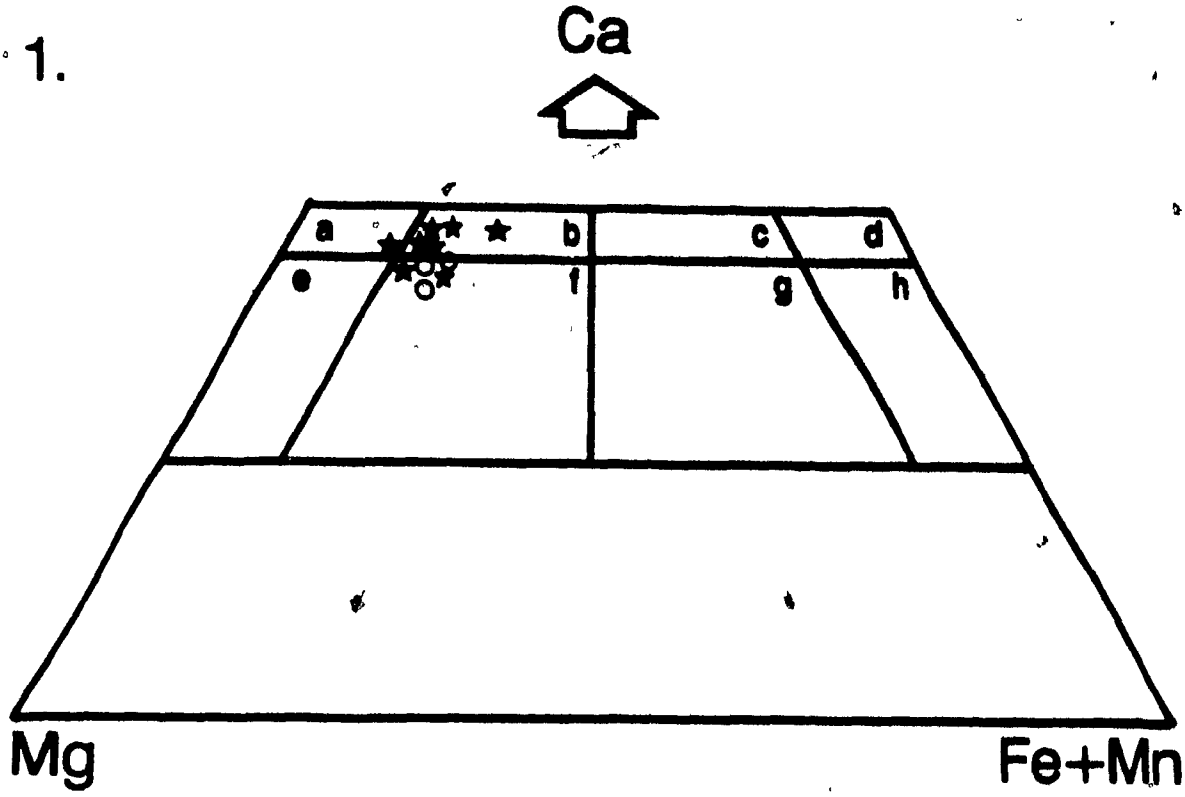

2.

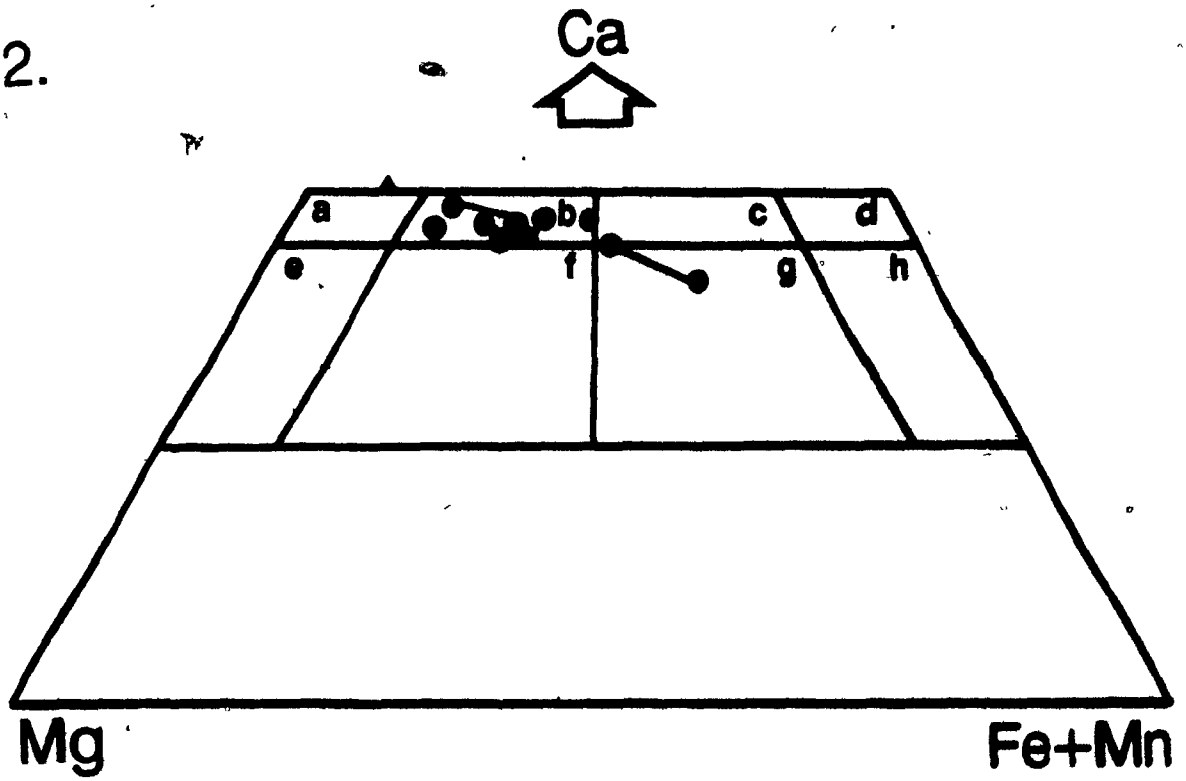

FIGURE 2.9. GABBRO AND ENDOSKARN

1. Hourglass zoning in titansalite. Recrystallization to colorless pyroxene (R) intergrown with kaersutite is visible on the right-hand of the grain. The titansalite also contains several laths of plagioclase (e.g., P). Crossed polars. Scale bar = 0.5 mm. Medium-grained gabbro (MG64).

2. Overgrowth of kaersutite (K) on titansalite (P). The titansalite appears to have been partially recrystallized to form salite (sp; No. 6, Table A7.2). Secondary salite is intergrown with kaersutite. Scale bar = 0.5 mm. Same sample as Fig. 2.9.1 (MG64).

3. Irregular pale green intergrowths of sodian salite (light grey; No. 3, Table A7.2) in a grain of colorless salite (P; No. 4, Table A7.2). Crossed polars. Scale bar = 0.1 mm. Medium- to coarse-grained gabbro (MG25).

4. Iron oxide (black) interstitial to plagioclase laths that has undergone replacement by chlorite (c), epidote (E) and titanite (T). Apparent collapse of one oxide fragment (f) to the bottom of the cavity formed during its partial replacement (the flat face of the oxide apparently was originally in contact with the plagioclase laths). This implies the presence of a time gap between dissolution of the oxide and deposition of the epidote. Scale bar = 0.5 mm. Medium-grained gabbro (84-37).

5. Patchy replacement of amphibole (A) by pyroxene (p) along cleavages and fractures. Scale bar = 0.15 mm. Partly metasomatized fine- to medium-grained mafic inclusion (84-571).

6. Veinlet of diopside (P). Crossed polars. Scale bar = 1 mm. Medium-grained endoskarn (83-110).

7. Radial aggregate of diopside (P). Scale bar = 0.5 mm. Medium-grained endoskarn (84-564).

8. Radial intergrowth of diopside (p; light grey) and plagioclase (f; black). Crossed polars. Scale bar = 1.5 mm. Medium- to coarse-grained endoskarn (83-150).

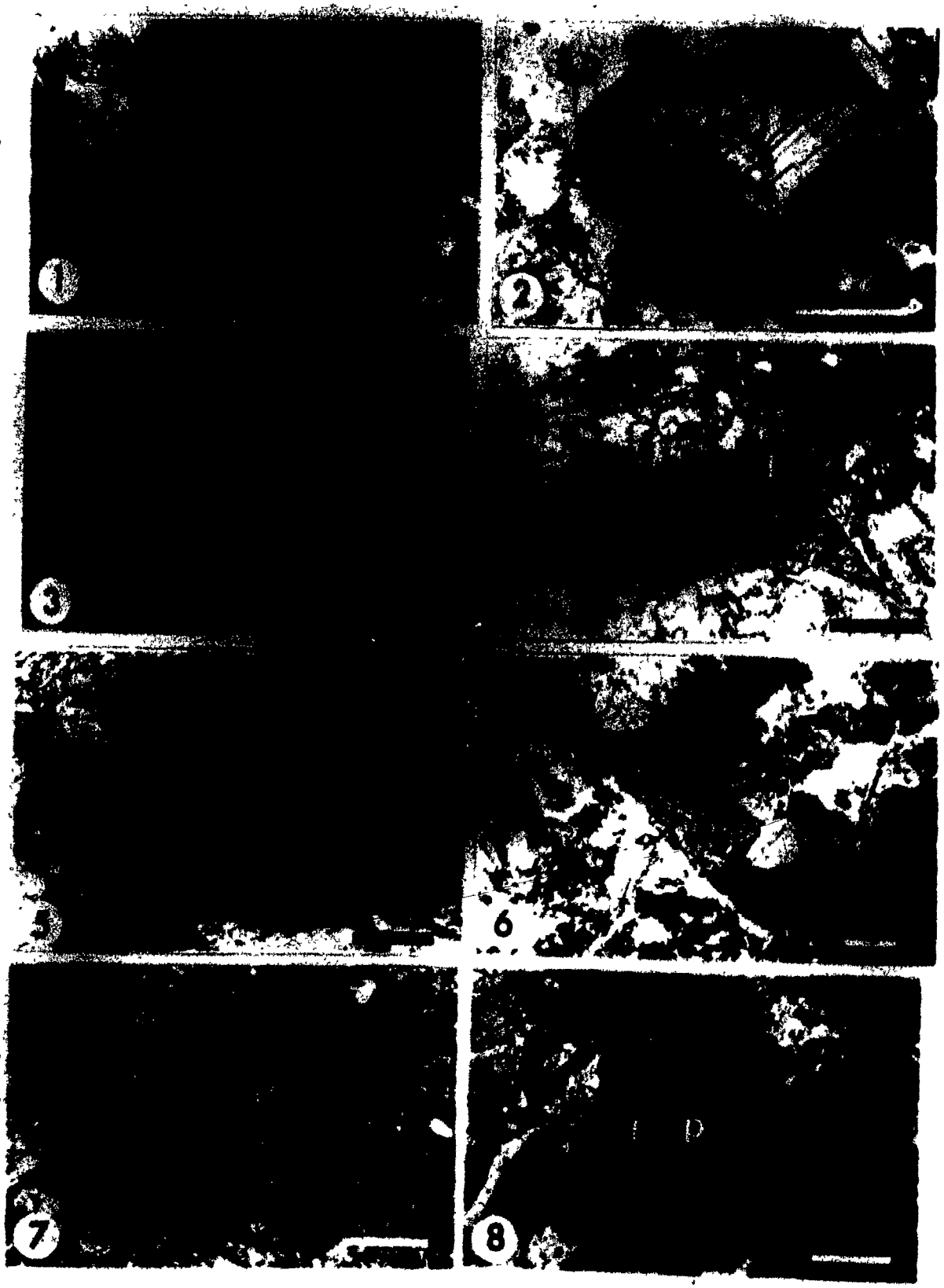
1
2
3
5
6
7
8

tetrahedrally and octahedrally coordinated), Ti and Fe, while the lighter-colored sectors have higher Si and Mg (Nos. 8, 9; Table A7.1). These variations are similar to those reported by others (e.g., Hollister and Gancarz 1971, Downes 1974, Leung 1974). Sector zoning is interpreted to result from metastable (nonequilibrium) growth that is favored by rapid crystallization (e.g., Hollister and Gancarz 1971, Wass 1973, Dowty 1976). No evidence of primary concentric zoning was observed in any of the samples studied.

The alkali basaltic dyke studied contains by far the most Ti-enriched titansalite. The titansalite is also the most Al-rich and Si-poor pyroxene analyzed. The most likely explanation for the enrichment in Ti is the lack of Ti-rich oxides within the dyke. Other contributing factors could be the low a_{SiO2} of the magma (Kushiro 1960, Le Bas 1962, Gupta et al. 1973) indicated by the relatively large amount of normative nepheline (6.03 wt %; Table A4.1), high temperature (Verhoogen 1962) or high $f(H_2O)$ of the magma (Dolfi and Trigila 1983), or rapid crystallization (Dowty 1976, Coish and Taylor 1979).

The Al-rich clinopyroxene of the alkali basaltic dyke contains the highest amount of tetrahedrally co-ordinated aluminum (0.356), but a normal amount of octahedrally co-ordinated aluminum (0.036). However, the average ^{vi}Al-content of the pyroxene phenocrysts in the fine-grained mafic inclusions is high (0.054-0.121). Many investigators (e.g., Le Bas 1962, Kushiro 1969, Thompson 1974, Wass 1979) have shown that for similar magma compositions the amount of ^{vi}Al increases with pressure. The relatively high average Cr content

(0.28 to 0.32 wt. % Cr_2O_3) of many of these phenocrysts is consistent with early crystallization from a relatively primitive magma, as Cr is highly compatible and commonly becomes depleted at a very early stage of magma evolution (e.g., Gibb 1973, Campbell and Borley 1974).

The wide range of temporal relationships observed with the felsic rocks (see above) as well as the dichotomy between SiO_2-undersaturated mafic samples and SiO_2-oversaturated mesocratic intermediate rocks, make it unlikely that these rock types represent different fractions of the same fractionating magma (see below). Therefore, correlations among clinopyroxene compositions of different rocks are more likely the consequence of the limited number of possible chemical substitutions.

This is well illustrated by a plot of Ti versus ^{iv}Al (Fig. 2.10.1). A general trend of increasing ^{iv}Al with increasing Ti is compatible with the occurrence of a coupled substitution involving exchange of $TiAl_2$ for $(Mg,Fe^{2+})Si_2$ (e.g., Tracy and Robinson 1977, Schweitzer et al. 1979). However, the lack of a single trend reflects the variable importance of other schemes involving ^{iv}Al. The average $Ti/^{iv}Al$ ratio varies from 1/2.4 (MG61) to 1/6.9 (MG6), reflecting $CaAl_2SiO_6$ (Ca-Tschermak) and $CaFe^{3+}AlSiO_6$ (Fe^{3+}-Al Tschermak) substitutions (Akasaka and Onuma 1980), particularily in phenocrysts from the fine-grained mafic inclusions (see above). In general, as Ti increases Mg decreases (Fig. 2.10.2). The variation in total Fe is complicated by its occurrence in two valence states whose proportions have only been estimated. A trend of increasing total Fe with increasing Ti, however, is observed (Fig.

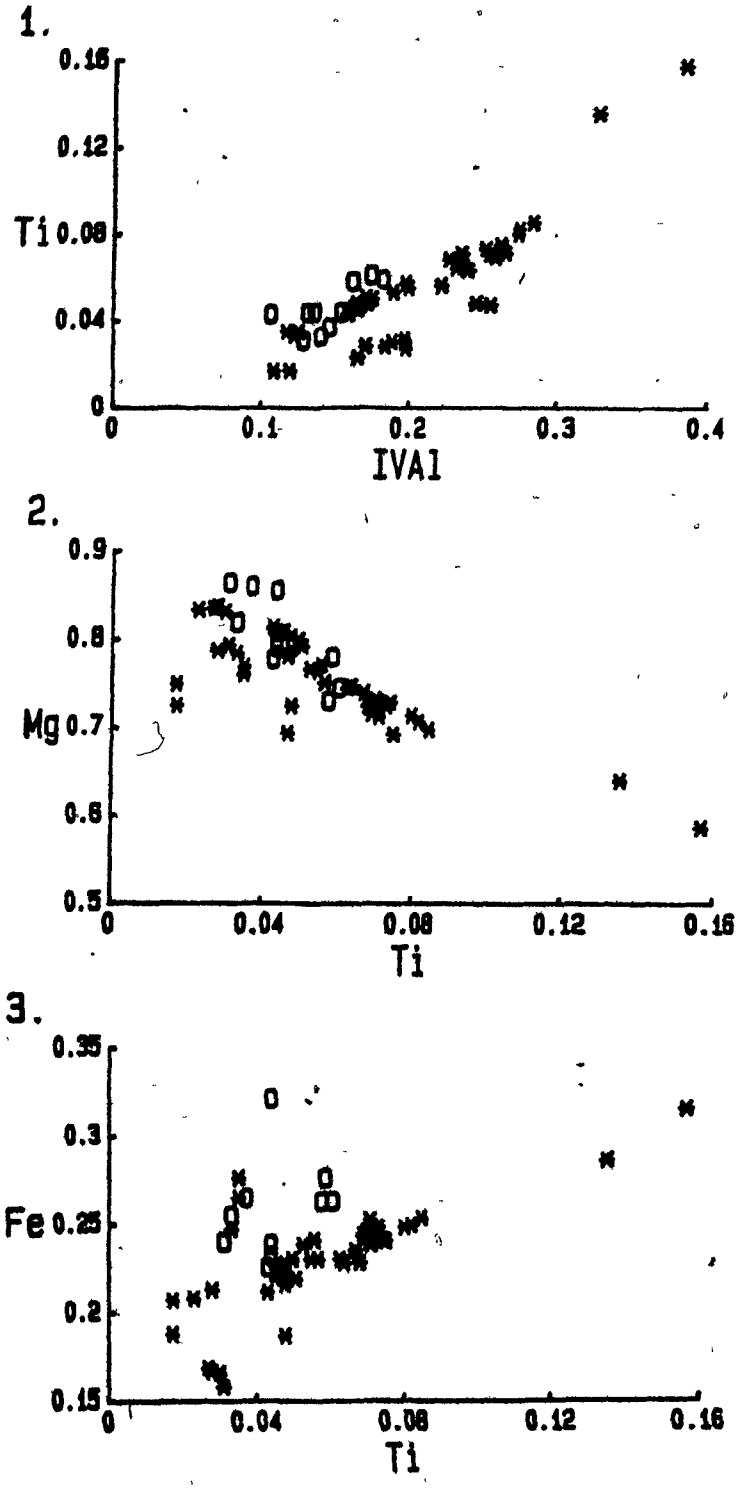

Figure 2.10. Relations between various cations and Ti in "primary" clinopyroxene, based on a stoichiometric formula of four cations and six oxygen atoms. Star: gabbro and fine-grained mafic inclusions, open circle: monzodiorites. 2.10.1. Ti versus tetrahedral Al, 2.10.2. Mg versus Ti, 2.10.3 Total Fe versus Ti.

2.10.3). Clinopyroxene from oversaturated rocks tends to be richer in Fe for a given ^{iv}Al or Ti content, likely reflecting the lower X_{Mg} of the magmas from which it crystallized. These results, consistent with the coupling of Fe^{2+} for Mg and $TiAl_2$ for $MgSi_2$ substitutions, reflect the increased stabilization of Ti in the clinopyroxene by Fe^{2+}-Ti^{4+} intervalence charge-transfer interactions (Sack and Carmichael 1984). Na remains approximately constant, indicating that the $NaTiAlSiO_6$ component is not important here.

Secondary Clinopyroxene

The secondary clinopyroxene typically occurs as pale green (rarely weakly pleochroic), anhedral, commonly interstitial grains that often are intergrown with other mafic minerals. In some samples where both the brownish and pale green clinopyroxenes coexist (e.g., MG23, 64), the pale green clinopyroxene forms intergrowths or a rim in optical continuity with the primary clinopyroxene (Fig. 2.5.1) and anhedral granules in amphibole that incipiently replace the brownish clinopyroxene along its margin. In other samples (e.g., 84-556) the green clinopyroxene predominantly forms discrete grains that show no obvious relationship to brownish clinopyroxene (Fig. 2.5.5). In 84-556, the grains of pale green clinopyroxene commonly contain acicular needles of apatite, which are absent in the brownish clinopyroxene but are commonly observed in secondary plagioclase that replaces the primary plagioclase (Fig. 2.5.7), indicating that both probably formed simultaneously.

The secondary clinopyroxene compositions plot almost entirely within the salite field of the pyroxene quadrilateral (Fig. 2.8.2). The exceptions, from a sample of monzodiorite (83-77), are grains of pale green sodian ferroaugite that commonly have irregular patches of yellow-green to bright green pleochroic Na-rich sodian ferroaugite.

In samples where both the brownish and pale green clinopyroxenes were analyzed (e.g., MG64, 84-556), the latter contains more Si, Fe, Mn and Ca, and less Al, Ti, calculated Fe^{3+}, Mg and nonquadrilateral components (Tables A7.1, A7.2). The green clinopyroxene also commonly shows high average Na contents (up to 2.0 wt. % Na_2O), which likely reflect the alkali-rich environment in which it formed. These results are consistent with those reported from other localities where two clinopyroxenes coexist (Smith 1970, Walker et al. 1973, Girardeau and Mevel 1982, Manning and Bird 1986).

The pale green clinopyroxene grains are commonly irregularly zoned (in rare cases sector-zoned; Fig. 2.5.3) or occur as an intergrowth of two compositionally distinct phases (Fig. 2.9.3). Typically, the colorless to pale green zones are enriched in Si, Mg and Ca and depleted in Al, Fe^{3+}, Ti, Fe and Na (compare Nos. 3 and 4, 7 and 8, 9 and 10, 13 and 14; Table A7.2) relative to the deeper green zones. This zonation is attributed to progressive recrystallization of the clinopyroxene.

Pale green slightly pleochroic salite is observed along the chilled margin of a fine-grained mafic inclusion (Fig. 2.4.7) in a white granodiorite (MG97). The presence of similar grains

of salite in the granodiorite indicates that the clinopyroxene probably formed in equilibrium with the granodiorite. It has a similar chemical composition to the secondary salite in the inclusions (high Si, moderately high Ca and low Ti and Al contents; Table A7.2).

The above textural and compositional data are consistent with a subsolidus origin for the pale green clinopyroxene, due to high-temperature recrystallization and metasomatism of the inclusion by the host magma or fluids at equilibrium with the same. Similar conclusions have been reached where clinopyroxenes coexist at other localities (e.g., Smith 1970, Walker et al. 1973, Manning and Bird 1986). However, in consideration of the field evidence that the biotite-pyroxene monzodiorites (e.g., 83-77, MG29) are hybrid rocks, the possibility that the Na-rich sodian ferroaugite represents variably recrystallized xenocrysts (derived from the felsic end member involved in magma mixing?) cannot be ruled out.

The inclusions of endoskarn in the southern half of the pluton contain a texturally and compositionally distinct variety of clinopyroxene, which is the only stable mafic mineral present. The clinopyroxene is colorless or, rarely, pale green, and its calcium-rich composition plots within or slightly above the diopside field in the pyroxene quadrilateral (Fig. 2.8.2). Similar clinopyroxene is also observed in a bleached halo around quartz veins that cross-cut granite in the southern half of the pluton, in altered dykes and in some samples of plagioclase-dominant granite (Chapter 4); it is almost invariably the only mafic mineral present. Where the

original mineralogy of the inclusion is still partly preserved (Fig. 2.6.2), the clinopyroxene occurs as irregular blebs within amphibole (Fig. 2.9.5), giving the mistaken impression that the pyroxene rather than the amphibole is undergoing replacement. In samples where it is the only mafic mineral, the secondary clinopyroxene typically forms anhedral, commonly interstitial or ragged, grains. Distinctive textures include monomineralic veinlets or veins (Fig. 2.9.6), radial aggregates (Fig. 2.9.7), or intergrowths with plagioclase (Fig. 2.9.8). The two first textures are characteristic of a hydrothermal origin (e.g., Bird et al. 1984). The intergrowths of plagioclase and clinopyroxene are morphologically similar to other examples interpreted to be primary (e.g., MacKenzie et al. 1984); here, however, the texture appears to develop progressively during recrystallization and replacement of the primary plagioclase.

The secondary clinopyroxene from the endoskarn generally contains higher amounts of Si, Mg and Ca, and lower Al, Ti, Fe, Mn and Na (Table A7.2) than those from the mafic and mesocratic intermediate inclusions. It is compositionally similar to the clinopyroxene from the highest-temperature zones of active geothermal systems (e.g., Cavarretta et al. 1982) or from other endoskarns (e.g., Harris and Einaudi 1982). Textural, field and compositional data are therefore consistent with precipitation of the clinopyroxene from a hydrothermal fluid that infiltrated the inclusions at moderately high temperatures (likely above 300^{o}C: Bird et al. 1984).

Amphibole

Pale yellow-brown to red-brown pleochroic kaersutite (Fig. 2.11.1, Table A8.1) is commonly observed in the gabbro as anhedral, principally interstitial grains that rim and replace titansalite (Fig. 2.9.2). Kaersutite also occurs in a compound xenocryst in a plagioclase-phyric syenite (Chapter 3). In all cases, kaersutite has undergone some recrystallization to green calcic amphibole.

The interpretation of the compositional variations of the kaersutite is hampered by the small number of analyses obtained (Table A8.1), the diverse parageneses of the samples and the possiblity of partial recrystallization. The highest Ti and Al, and lowest Si and K contents are observed in the kaersutite from the alkali basaltic dyke (MG61), in agreement with the clinopyroxene (see above). The composition of a kaersutite xenocryst observed in a plagioclase-phyric syenite (MG10) falls in the range of those from the mafic samples and therefore could have been derived from a mafic source.

Pale yellow-brown to brownish green pleochroic magnesio- to actinolitic hornblende (Fig. 2.11.2, Table A8.2) is the main type of amphibole observed in the fine-grained mafic and mesocratic intermediate inclusions, where it forms anhedral to subhedral, commonly interstitial, grains. In one fine-grained mafic inclusion (MG97), compositions also range from magnesian hastingsite to edenitic hornblende (Fig. 2.11.3). Subhedral to euhedral and commonly oscillatory-zoned grains of magnesio- to actinolitic hornblende partly infill amygdules in some fine-grained mafic inclusions.

Figure 2.11. Selected average amphibole compositions from the mafic and mesocratic intermediate rock types plotted in the classification diagrams showing XMg ($Mg/(Mg+Fe^{2+})$) versus Si (in atoms per 23 oxygen atoms) from Leake (1978). Star: gabbro and fine-grained mafic inclusions, open circle: mesocratic intermediate rock types, X: syenite. 2.11.1. Calcic amphiboles in which: 1) $(Ca+Na)_{M4} \geq 1.34$, 2) $Na_{M4} < 0.67$ and 3) $Ti \geq 0.5$. a.f.u. a: kaersutite, b: ferro-kaersutite. 2.11.2. Calcic amphiboles in which: 1) $(Ca+Na)_{M4} \geq 1.34$, 2) $Na_{M4} < 0.67$, 3) $(Na+K)_A < 0.5$, and 4) $Ti < 0.5$ a.f.u. Line delimits the range of average compositions of hornblende from felsic rock types (Chapters 3, 4). Straight lines join extreme compositions in oscillatory zoned grains. a: tremolite, b: tremolitic hornblende, c: actinolite, d: actinolitic hornblende, e: magnesio-hornblende, f: tschermakitic hornblende, g: tschermakite, h: ferro-actinolite, i: ferro-actinolitic hornblende, j: ferro-hornblende, k: ferro-tschermakitic hornblende, l: ferro-tschermakite. 2.11.3. Calcic amphiboles in which: 1) $(Ca+Na)_{M4} > 1.34$, 2) $Na_{M4} < 0.67$, 3) $(Na+K)_A \geq 0.5$, 4) $Ti < 0.5$ a.f.u., and 5) $Fe^{3+} > {}^{VI}Al$. a: silicic edenite, b: edenite, c: edenitic hornblende, d: magnesio-hastingsitic hornblende, e: magnesio-hastingsite, f: silicic ferro-edenite, g: ferro-edenite, h: ferro-edenitic hornblende, i: magnesian hastingsitic hornblende, j: magnesian hastingsite, k: hastingsitic hornblende, l: hastingsite.

1.

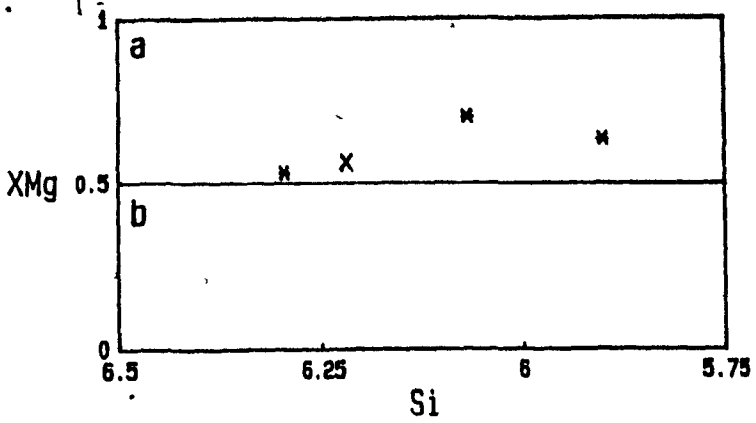
a
b
XMg
0.5
0
6.5
6.25
6
5.75
Si

2.

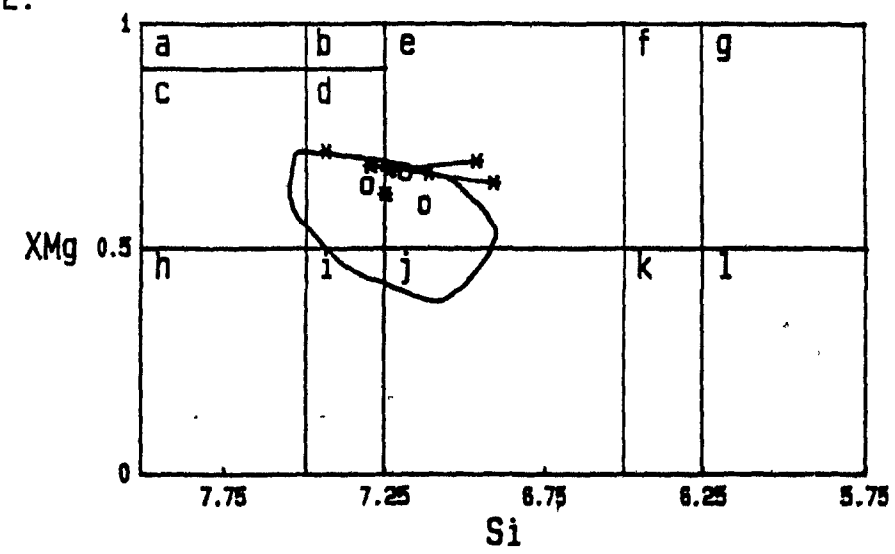
1
a
b
e
f
g
c
d
XMg
0.5
h
i
j
k
l
0
7.75
7.25
6.75
6.25
5.75
Si

3.

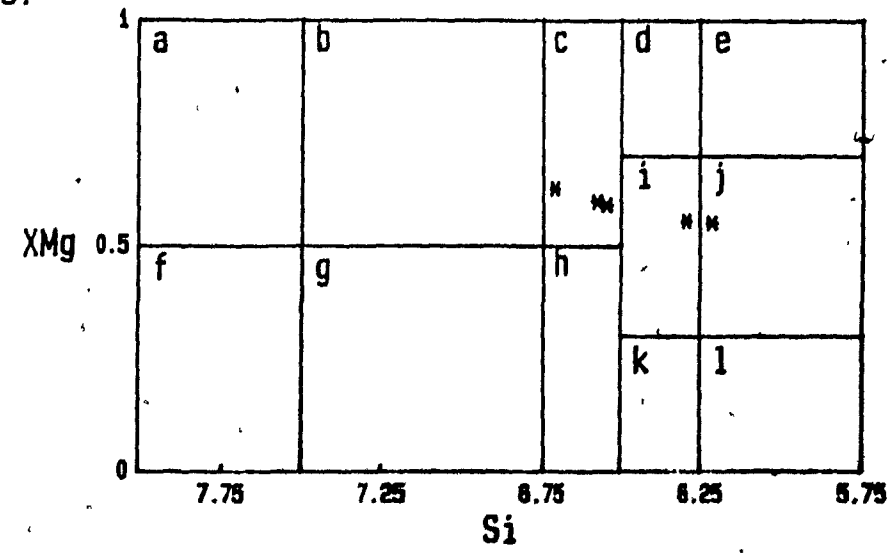
1
a
b
c
d
e
i
j
XMg
0.5
f
g
h
k
l
0
7.75
7.25
6.75
6.25
5.75
Si

The compositional range of the green amphibole in the inclusions is very similar to that in the more felsic rocks (Fig. 2.11.2; 0.3-2.2 versus 0.6-2.1 wt. % TiO2, 0.34-0.51 versus 0.35-0.66 X_{Fe}). The X_{Fe}^{3+} ($Fe^{3+}/(Fe^{3+}+Fe^{2+})$) of magnesio-hornblende from a sample of monzodiorite (MG53) is between 0.19 and 0.22 (Table 2.1), in the range exhibited by the felsic rocks. Trends of decreasing Ti, Al (predominantly in terms of ^{iv}Al), Fe, K, A-site occupancy and Na, and increasing Mg with increasing Si are observed (Fig. 2.12). Other elements do not show obvious trends, except in amphiboles from MG97, where there are slight increases in Ca and Mn with increasing Si (Figs. 2.12.5, 2.12.6). These trends are probably related to the progressive recrystallization of the amphibole to compositions in equilibrium with its more voluminous felsic host, under subsolidus conditions of decreasing temperature and increasing $f(O_2)$ (Helz 1973, Spear 1981).

The oscillatory-zoned amphiboles within the amygdules of the fine-grained mafic inclusions exhibit the same general trends as the groundmass amphiboles. The oscillatory zoning is probably related to small changes in the conditions of crystallization [e.g., T, $f(O_2)$, $f(H_2O)$] in the subsolidus environment and indicates a more complex subsolidus history than would be inferred from the groundmass amphibole alone.

F and Cl contents of the kaersutite are low, with less than 0.1 wt. % F and 0.05 wt. % Cl, respectively. The green amphiboles exhibit slightly higher halogen contents, especially Cl (averages vary from 0.06 to 0.24 wt. % Cl; Table A8.2).

The interpretation of the substitutions in complex phases

Sample	Rock Type	Mineral	FeOM1	FeOM2	Fe2O3M1	Fe2O3M2	FeOT1	FeOT2	FeOTAvg	FeOProbe	XFe3+1	XFe3+2	XFe3+*
M68	SYEN	Amph	15.2	15.3	4.2	4.1	19.0	18.9	19.0	18.4	0.199	0.194	0.196
M616	MIAS	Bio	16.3	16.2	6.0	6.4	22.4	22.8	22.2	22.3	0.273	0.262	0.267
M623	MZDI	Bio	18.9	19.0	2.0	3.3	21.4	22.1	21.7	20.5	0.118	0.135	0.128
M640	PSYN	Amph	20.2	20.1	4.4	4.4	24.1	24.1	24.1	24.2	0.164	0.165	0.164
M640	PSYN	Bio	22.7	-	3.3	-	25.6	-	25.6	27.0	0.116	-	0.113
M644	QTMZ	Amph	19.0	21.4	1.0	2.2	20.7	23.4	22.1	21.8	0.079	0.085	0.083
M646	PDGR	Amph	14.2	14.2	4.1	4.5	17.9	18.3	18.1	17.9	0.286	0.222	0.216
M646	PDGR	Bio	18.0	17.3	4.2	5.1	21.0	21.9	21.0	22.3	0.174	0.210	0.174
M651	GP	Amph	15.6	15.7	4.6	5.9	19.7	21.1	20.4	19.0	0.210	0.253	0.209
M651	GP	Bio	18.4	18.6	4.1	4.4	22.1	22.5	22.3	22.7	0.167	0.176	0.170
M653	MZDI	Amph	14.5	14.2	4.6	3.0	18.7	17.6	18.2	17.9	0.222	0.194	0.212
M653	MZDI	Bio	19.1	18.7	3.3	3.3	22.1	21.6	21.9	21.1	0.135	0.137	0.137
M653	QTMZ	Amph	12.7	12.3	3.9	4.0	16.2	15.0	16.0	15.2	0.217	0.226	0.219
M654	GABB	Bio	14.0	14.3	2.4	2.6	17.0	16.7	16.0	16.0	0.127	0.140	0.135
M666	QTMZ	Amph	16.0	15.0	4.7	4.0	20.3	20.2	20.2	18.7	0.209	0.215	0.215
M666	QTMZ	Bio	15.0	18.6	7.3	4.6	22.4	22.0	22.6	23.1	0.294	0.182	0.183
M683	KFPG	Amph	17.0	16.9	5.0	5.6	21.5	22.0	21.2	21.0	0.209	0.230	0.219
M683	KFPG	Bio	19.5	18.3	5.3	7.4	24.3	24.9	24.6	24.3	0.197	0.267	0.196
M690	DIOR	Bio	19.2	19.4	3.9	3.5	22.7	22.5	22.6	22.4	0.155	0.140	0.145
M694	ITIN	Bio	21.1	-	5.9	-	26.5*	-	26.5	30.4	0.201	-	0.204

Table 2.1. Ferrous-ferric values determined by wet chemistry for biotite and amphibole. FeOM1, FeOM2: FeO determined by wet chemistry. FeOT1, FeOT2: Total Fe expressed as FeO. Fe_2O_3M1, Fe_2O_3M2: Fe_2O_3 determined by the difference between FeOT and FeOM. FeOTAvg: average of FeOT1 and FeOT2. FeOProbe: average total iron determined by electron microprobe analyses expressed as FeO. XFe3+1, XFe3+2: molar fraction of Fe^{3+} ($Fe^{3+}/(Fe^{3+}+Fe^{2+})$). XFe3+*: X_{Fe}^{3+} used to recalculate the electron microprobe analyses. SYEN: syenite, MIAS: miaskitic nepheline syenite, MZDI: monzodiorite, PSYN: plagioclase-phyric syenite, QTMZ: quartz monzonite, PDGR: plagioclase-dominant granite, GP: granite porphyry, GABB: gabbro, KFPG: K-feldspar porphyritic granite, DIOR: diorite, ITIN: intermediate tinguaite. *: the large difference observed between the FeOT and FeOProbe probably reflects the prescence of felsic inclusions in the biotite separate; however, their presence should not affect the X_{Fe}^{3+}.

Figure 2.12. Compositional variations of green calcic amphiboles with Si content (in atoms per 23 oxygen atoms). Cross: fine-grained mafic inclusion (MG97), star: oscillatory-zoned amphiboles present in amygdules of fine-grained mafic inclusions (MG6, 68), hyphen: other green amphiboles from mafic and mesocratic intermediate rock types. 2.12.1. Total Al versus Si. 2.12.2. Ti versus Si. 2.12.3. Mg versus Si. 2.12.4. Total Fe versus Si. 2.12.5. Mn versus Si. 2.12.6. Ca versus Si. 2.12.7. Na versus Si. 2.12.8. K versus Si. 2.12.9. A-site occupancy versus Si.

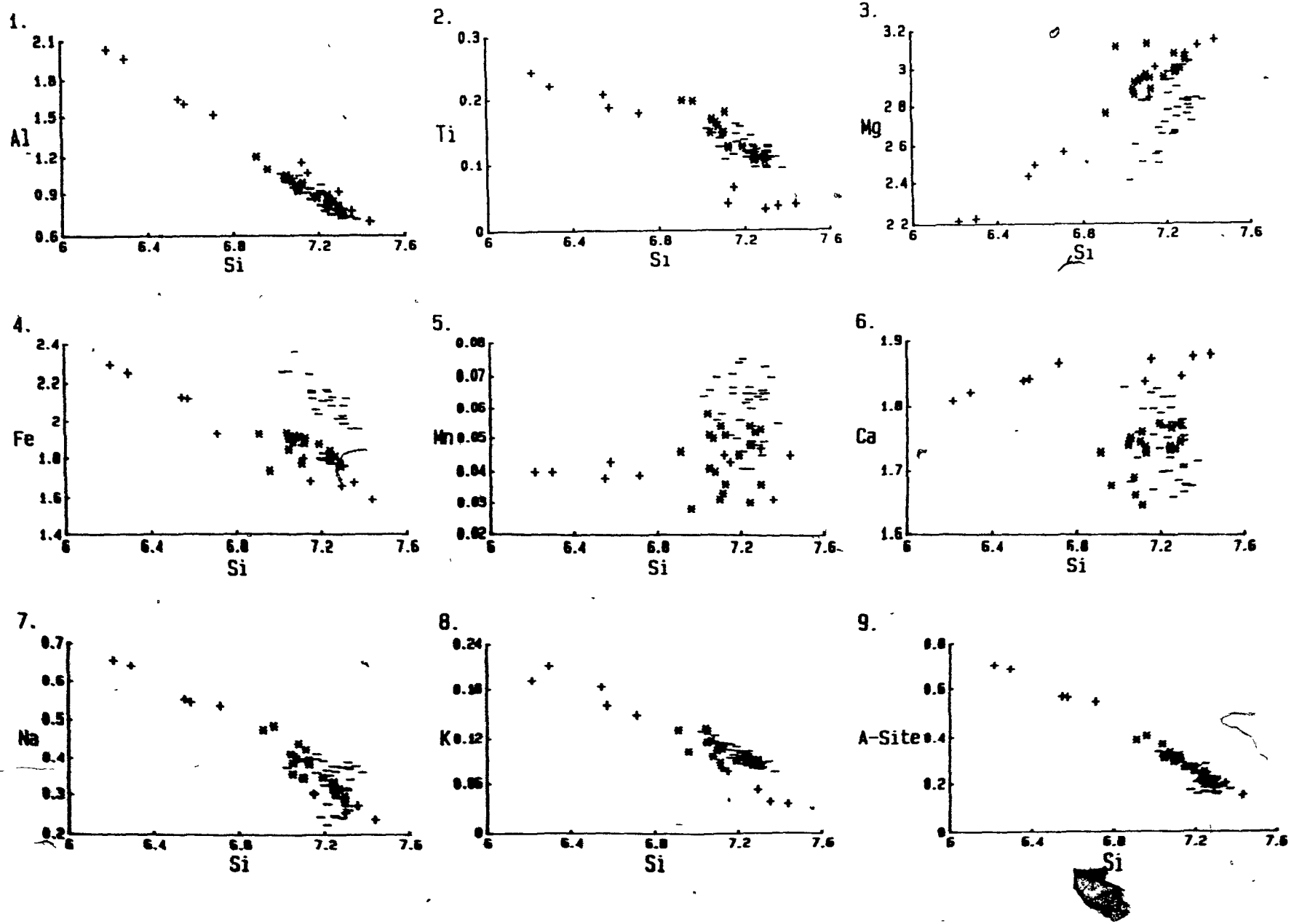
1.
Al
Si
2.
Ti
Si
3.
Mg
Si
4.
Fe
Si
5.
Mn
Si
6.
Ca
Si
7.
Na
Si
8.
K
Si
9.
A-Site
Si

such as amphibole and biotite, for which only partial analyses are generally available, is difficult and commonly ambiguous (Hewitt and Abrecht 1986). A list of some of the coupled substitutions believed to occur in amphiboles is given in Table 2.2. The kaersutite data are scattered and too few, but good correlations between several elements are observed in the green amphibole. Both A-site minus NaM4 (to remove the effects of any richterite substitution; Czamanske and Wones 1973) and Ti (Figs. 2.13.1, 2.13.2) are well correlated with ^{iv}Al, indicating that the edenite and Ti-tschermakite coupled substitutions probably are important. No other significant correlation is observed; however, compositional variations imply that other substitutions such as tschermakite, ferritschermakite and those involving Na in the M4 site (e.g., glaucophane or riebeckite) must occur (Chapter 3, Spear 1981).

Biotite

Light tan to dark brown or red-brown pleochroic titaniferous biotite or titanbiotite forms anhedral, commonly interstitial, to subhedral grains in both the mafic and mesocratic intermediate rock types. Biotite in many samples is at least in part secondary (e.g., Fig. 2.4.5). Grains are relatively free of inclusions, but apatite, oxide phases and, in some samples, zircon are observed. Alteration to chlorite, titanite, epidote and, in rare cases, green biotite occurs to varying degrees.

The biotite compositions (Table A9.1) are generally similar to those obtained from the more felsic rock types; they plot close to the phlogopite-annite join (Fig. 2.14) and exhibit a

TABLE 2.2. SUGGESTED SCHEMES OF COUPLED SUBSTITUTION IN AMPHIBOLE AND THEIR SOURCES

1. $^{A}(Na,K) + {}^{iv}Al$ for $^{A}( ) + {}^{iv}Si$ (edenite) Czamanske & Wones 1973

2a. $^{M1-M3}Al + {}^{iv}Al$ for $^{M1-M3}Mg + {}^{iv}Si$ (Tschermakite) Ibid.

2b. $^{M1-M3}Fe^{3+} + {}^{iv}Al$ for $^{M1-M3}Mg + {}^{iv}Si$ (Ferritschermakite) Ibid.

3a. $^{M4}Na + {}^{M1-M3}Al$ for $^{M4}Ca + {}^{M1-M3}Mg$ (Glaucophane) Ibid.

3b. $^{M4}Na + {}^{M1-M3}Fe^{3+}$ for $^{M4}Ca + {}^{M1-M3}Mg$ (Riebeckite) Ibid.

4. $^{A}Na + {}^{M4}Na$ for $^{A}( ) + {}^{M4}Ca$ (Richterite) Ibid.

5. $^{M1-M3}Ti + 2\,{}^{iv}Al$ for $^{M1-M3}Mg + 2\,{}^{iv}Si$ (Ti-tschermakite) Ibid.

6a. $2\,{}^{M4}Na + {}^{M1-M3}Ti$ for $2\,{}^{M4}Ca + {}^{M1-M3}Mg$ Ibid.

6b. $^{M4}Na + {}^{M1-M3}Ti$ for $^{M4}Ca + {}^{M1-M3}Al$ Ibid.

7. $^{A}( ) + {}^{M1-M3}Mg + 2\,{}^{iv}Si$ for $^{A}(Na,K) + {}^{vi}Al + 2\,{}^{iv}Al$ (Pargasite) Spear 1981

8. $2\,{}^{A}Na + {}^{M1-M3}Ti + 4\,{}^{iv}Al$ for $2\,{}^{A}( ) + {}^{M1-M3}Mg + 4\,{}^{iv}Si$ Fabries et al. 1984

9. $^{M4}Na + {}^{iv}Si$ for $^{M4}Ca + {}^{iv}Al$ Giret et al. 1980

10. $^{A}Na + {}^{M1-M3}Fe^{2+}$ for $^{A}( ) + {}^{M1-M3}Fe^{3+}$ Ibid.

11. $^{M1-M3}Ti + O$ for $^{M1-M3}Fe^{3+} + OH^{-}$ Ibid.

12. $^{A}( ) + {}^{M1-M3}Ti$ for $^{A}Na + {}^{M1-M3}Al$ Ibid.

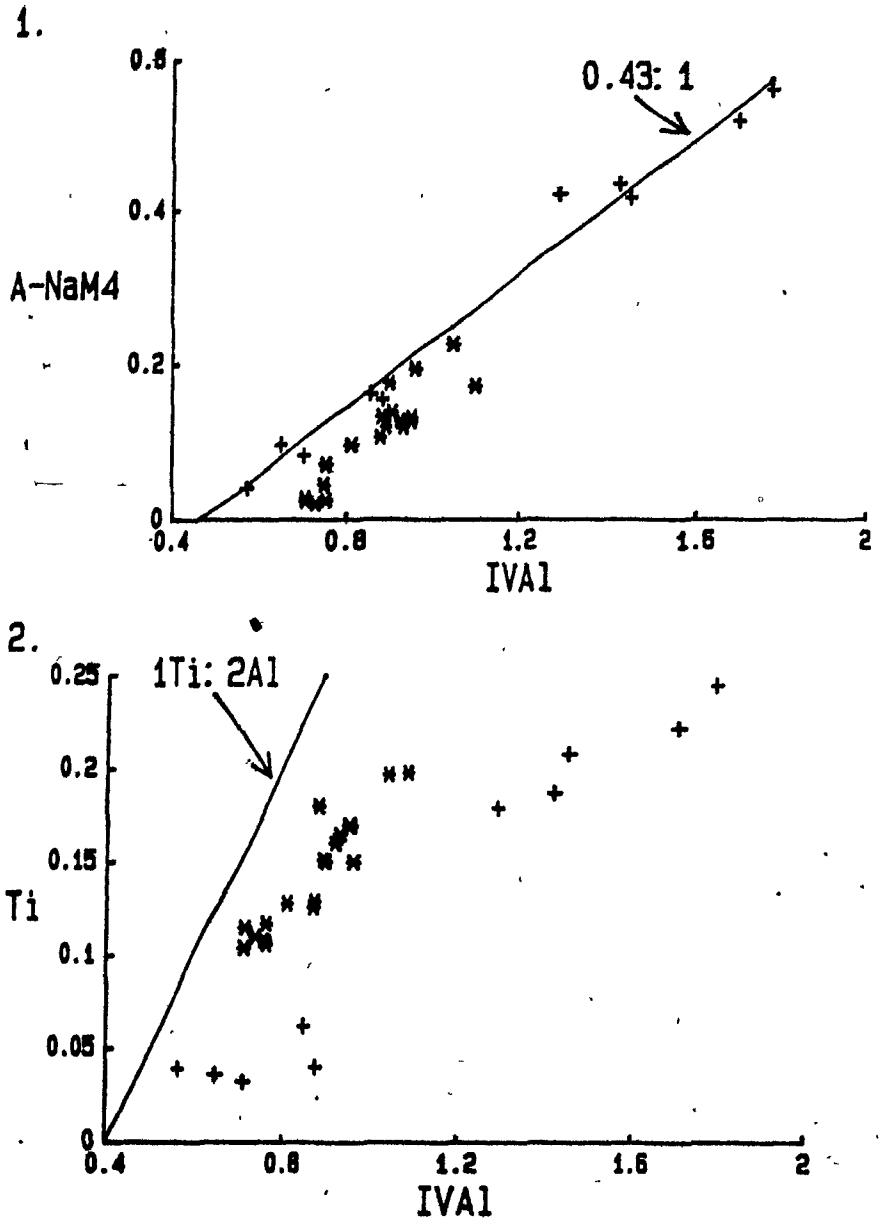

Figure 2.13. Compositional relations indicative of possible coupled substitutions in the green amphiboles of the fine-grained mafic inclusions. Cross: fine-grained mafic inclusion (MG97), star: oscillatory-zoned amphiboles present in the amygdules of the fine-grained mafic inclusions (MG6, 68). 2.13.1 Total A-site cations less Na in the M4 site versus tetrahedral Al. Line represents a least-squares regression of the data represented by the crosses, and has a slope of 0.43. 2.13.2. Ti versus tetrahedral Al.

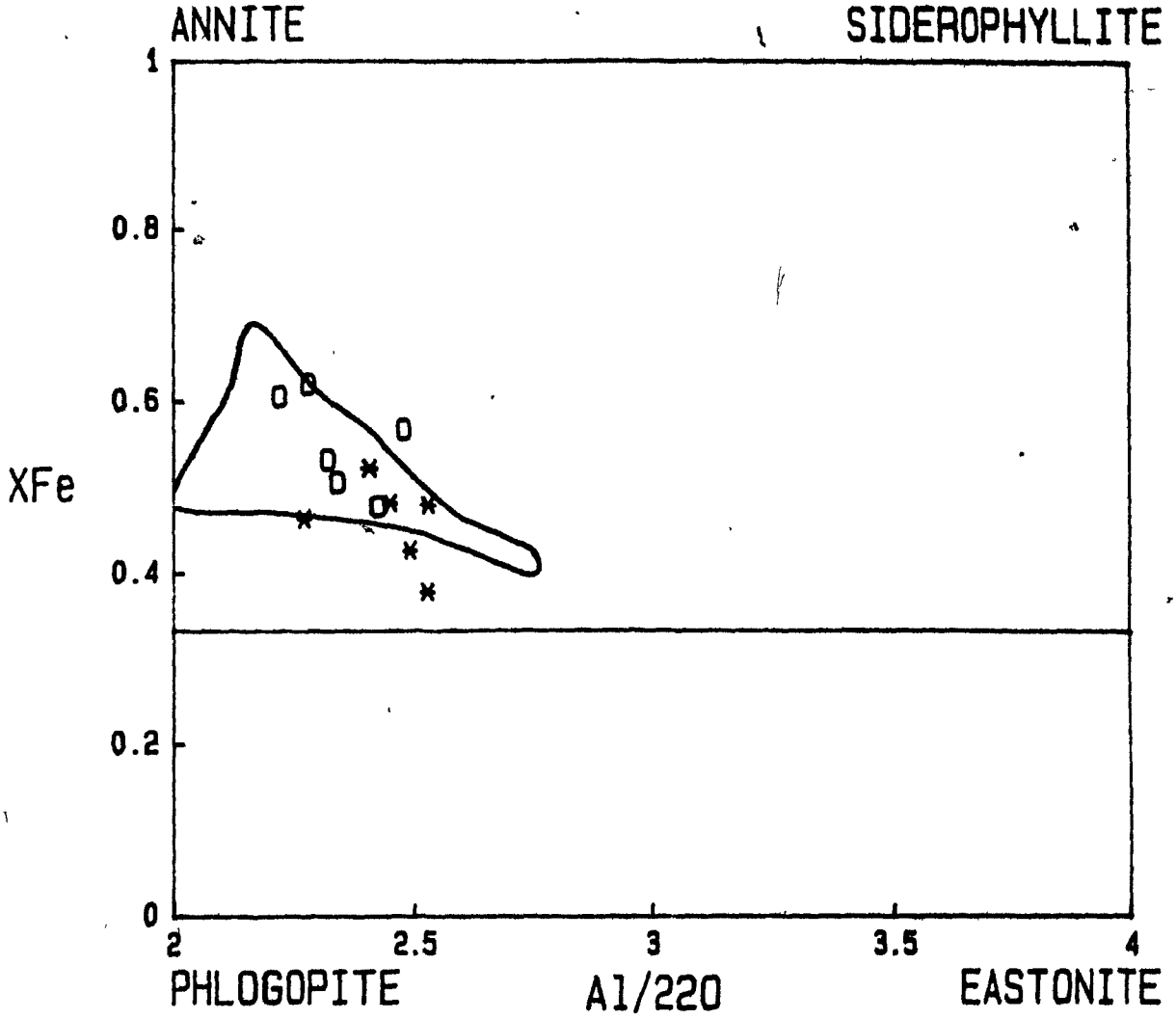

Figure 2.14. Average biotite compositions from the mafic and mesocratic intermediate rock types projected into the phlogopite-annite-eastonite-siderophyllite compositional field. X_{Fe}: Fe/(Fe+Mg). Top subdivision: biotite, bottom subdivision: phlogopite; the division between the two is arbitrarily chosen at Mg:Fe = 2:1 (Deer et al. 1975). Symbols are the same as in Figure 2.10. Line delimits the range of the average biotite compositions from the felsic rock types (Chapters 3, 4)

similar range in X_{Fe} (0.42-0.63 versus 0.44-0.69). The similarity is especially evident if biotite compositions from the mafic inclusion are compared with those from the adjacent white granodiorite host (cf. No. 8, Table A9.1 with No. 8, Table A9.3). These data suggest that in most instances biotite has re-equilibrated with the felsic host.

One possible exception is the biotite from a gabbro (MG64) that exhibits a lower X_{Fe} (0.37-0.38), K (8.14-8.79 wt. % K_2O) and higher Na (0.65-0.96 wt. % Na_2O) than that of the other samples. Of all the mafic samples studied, this one exhibits the least textural evidence of having undergone recrystallization.

X_{Fe}^{3+} in biotite (including duplicates) varies from 0.12 to 0.16 (Table 2.1). $f(O_2)$ can be qualitatively estimated by plotting the average biotite compositions in a Fe^{3+}-Fe^{2+}-Mg diagram (Wones and Eugster 1965, Speer 1984). All the data plot slightly above and parallel to the Ni-NiO buffer (Fig. 2.15) indicating a moderately high $f(O_2)$.

The biotite generally contains less than 0.4 wt. % F and 0.4 wt. % Cl, with the lowest abundances observed in biotite from the gabbro and the inclusions in the white granodiorite. F contents are lower than those from the more felsic rocks (with the exception of the white granodiorite), whereas Cl contents (apart from the gabbro) are similar (Table A9.1-3).

Interrelations of the Mafic Silicates

The distribution coefficients (K_Ds) among clinopyroxene, amphibole and biotite have been calculated for Fe-Mg, Mn and Ti

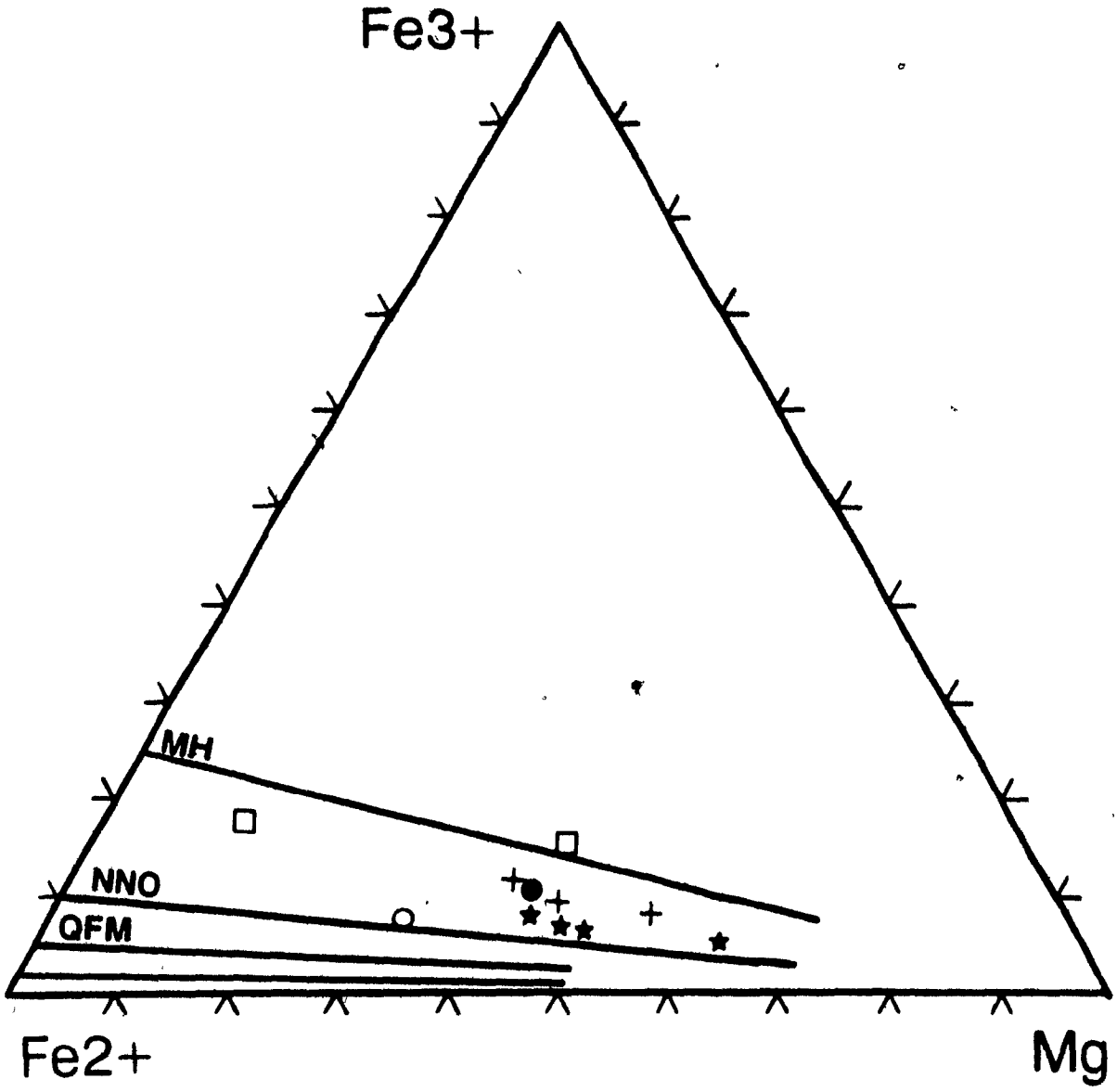

Figure 2.15. The composition of biotite in terms of Fe^{3+}-Fe^{2+}-Mg. Oxygen fugacity curves are from Wones and Eugster (1965). MH: magnetite-hematite, NNO: nickel-nickel oxide, QFM: quartz-fayalite-magnetite. Star: mafic and mesocratic intermediate rock types, open circle: syenite, filled circle: quartz monzonite, cross: granite, open box: nepheline syenite.

(Table 2.3). The values are commonly used to identify whether the minerals present are in equilibrium or not (e.g., Czamanske et al. 1977, Anderson 1980). Interpretation is complicated by many factors, including the presence of Fe^{3+}, the control exerted by the bulk composition of the mineral(s), and the exact scale over which equilibrium can be expected (e.g., Kretz 1960, Helz 1973, Anderson 1980).

The distribution of Fe, Mg and the other elements has been shown to be principally controlled by the composition of the amphibole (Kretz 1960, Gorbatschev 1977, Stephenson 1977). The fact that, in gabbro (MG64), the K_DFe-Mg between kaersutite and biotite (0.71) falls within the range of K_Ds between biotite and the compositionally distinct green amphiboles (0.63-0.75) seems fortuitous. Significantly, if X_{Fe} biotite is plotted versus that of amphibole (Fig. 2.16.1), the green amphibole compositions plot on the extension of a trend formed by the compositionally similar amphiboles from the felsic rocks, whereas MG64 plots well away from this trend. Furthermore, the distribution of Ti (see below) suggests that the kaersutite and biotite in the gabbro are probably not in equilibrium.

On the basis of their crystal structures, Czamanske and Wones (1973) concluded that Ti should increase from clinopyroxene to amphibole to biotite where those phases are in equilibrium. The Ti content, lower for biotite than for amphibole in the gabbro (K_DTiamph/bio=1.6) suggests disequilibrium, consistent with the textural evidence that the biotite may have formed later than the amphibole. In other mafic samples containing green amphibole the order is as predicted; the distribution

			KDFe-Mg		Mn1/Mn2			Ti1/Ti2				
Sample	Unit	Amphibole	Cpx/Amph	Amph/Bio	Amph/Cpx	Bio/Cpx	Amph/Bio	Amph/Cpx	Bio/Cpx	Amph/Bio	FAmph/FBio	ClAmph/ClBio
MB6	MAFI	Mag.-hbl.	-	0.63	-	-	2.33	-	-	0.25	0.92	0.36
MB23	MZDI	Act. hbl.	-	0.69	-	-	2.21	-	-	0.25	0.49	0.49
MB24	MAFI	-	-	-	-	0.33	-	-	63.2	-	-	-
MB26	MAFI	Act. hbl.	-	0.71	-	-	3.64	-	-	0.33	0.39	0.48
MB63	MZDI	Mag.-hbl.	-	0.75	-	-	2.41	-	-	0.30	0.57	0.50
MB61	MDYK	Kaer.	1.25	-	1.0	-	-	1.32	-	-	-	-
MB64	GNBB	Kaer.	1.37	0.71	1.42	0.92	1.55	2.22	1.78	1.31	3.20	0.24
MB68	MAFI	Act. hbl.	-	0.64	-	-	2.91	-	-	0.31	1.72	0.32
83-77a	MZDI	-	-	-	-	0.33	-	-	18.79	-	-	-
83-77b	MZDI	-	-	-	-	0.34	-	-	18.79	-	-	-
MB90a	DIOR	-	-	-	-	0.66	-	-	11.59	-	-	-
MB90b	DIOR	-	-	-	-	0.67	-	-	51.00	-	-	-
MB97	MAFI	Act. hbl.	0.91	0.75	0.53	0.24	2.25	2.30	18.90	0.12	0.13	0.35
84-556a	MZDI	Mag. hbl.	1.12	0.68	0.71	0.39	1.84	2.91	11.18	0.26	0.71	0.39
84-556b	MZDI	Mag. hbl.	0.81	-	0.61	0.33	-	18.67	41.00	-	-	-

Table 2.3. Distribution coefficients (K_D) representing the co-distribution of Fe-Mg, Mn, Ti, F and Cl between the mafic minerals of the mafic and mesocratic intermediate rock types. Fe-Mg distribution coefficient calculated using the formula:

$$K_D Fe\text{-}Mg = \left\{\frac{Fe/(Fe+Mg)}{Mg/(Fe+Mg)}\right\}_1 \times \left\{\frac{Mg/(Fe+Mg)}{Fe/(Fe+Mg)}\right\}_2$$

Other distribution coefficients are simply the ratio of the particular element between the two phases in question. MAFI: fine-grained mafic inclusions, MDYK: alkali basaltic dyke. Other rock types as in Table 2.1. Clinopyroxene compositions used in the calculations are as follows; MG24: salite, MG61: titansalite, MG64: titansalite (average of both high- and low-Ti sectors), 83-77a: sodian ferroaugite (bright green zones), 83-77b: sodian ferroaugite (pale green zones), MG90a: sodian salite (pale green zone), MG90b: salite (colorless zone), MG97: sodian salite, 84-556a: salite (colorless zone), 84-556b: sodian salite (pale green zone).

1.

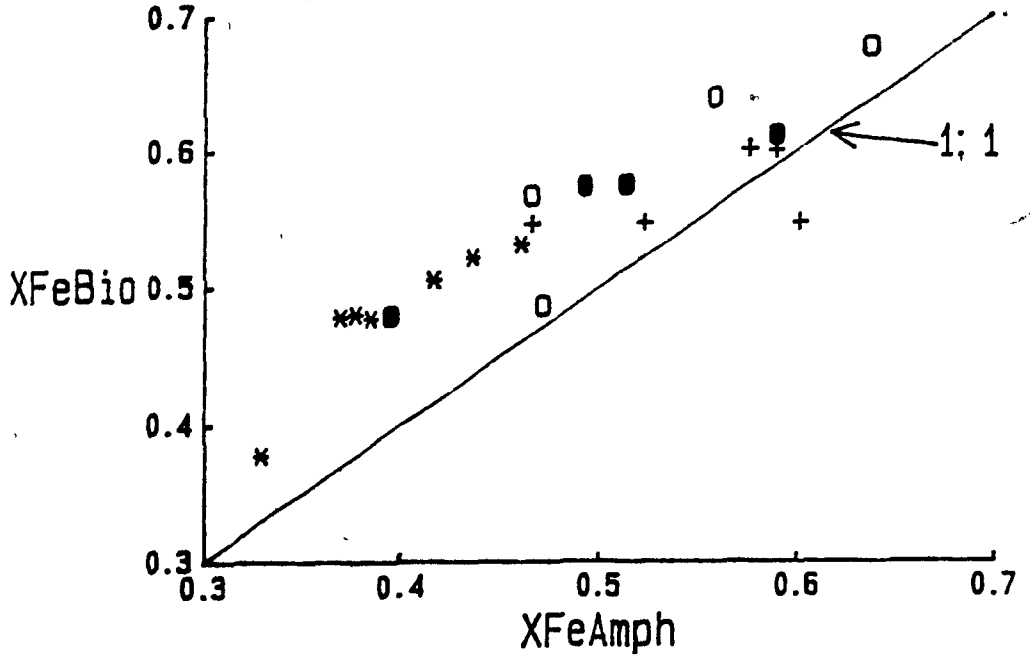

2.

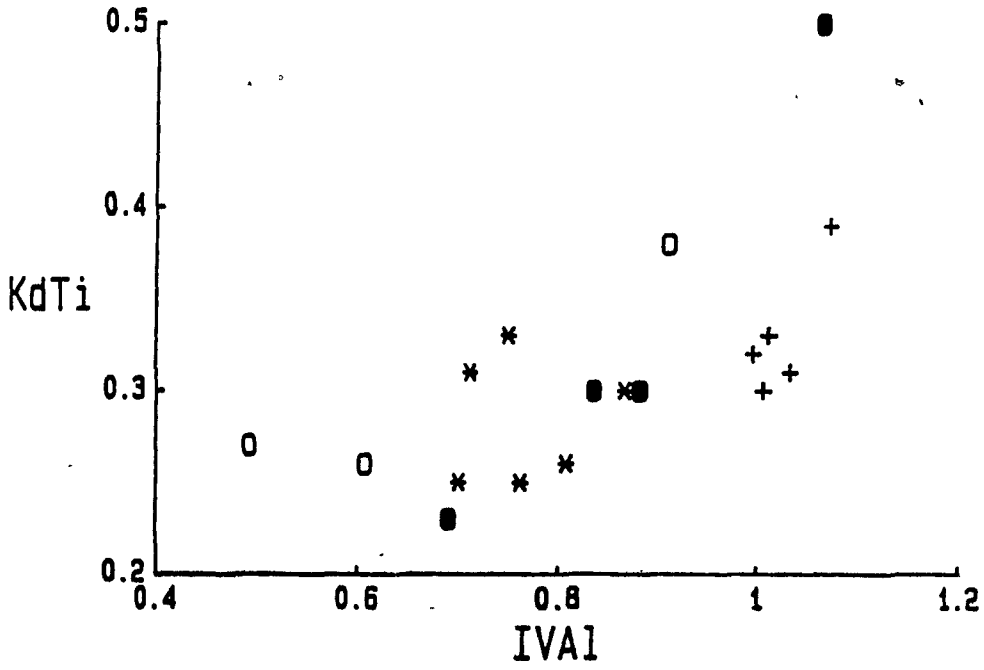

Figure 2.16. Relationships between amphibole and biotite. Symbols are the same as in Figure 2.15. 2.16.1. X_{Fe} (Fe/(Fe+Mg)) of biotite versus X_{Fe} of amphibole. Line has a slope of 1:1. 2.16.2 $K_D Ti$ ($Ti^{amphibole}/Ti^{biotite}$) versus the content of tetrahedral Al in amphibole.

coefficients exhibit a limited range of low values (K_DTiamph/bio= 0.12-0.31) that overlaps the range observed in the felsic samples (Chapters 3, 4). The rough correlation between the K_DTi and the amount of tetrahedral aluminum in the green amphiboles of the pluton (Fig. 2.16.2) suggests that the partitioning of Ti between biotite and amphibole seems to be influenced by the coupled substitutions involving Ti. Furthermore, the charge and size of Ti do not allow it to substitute as readily for Fe as Mn (Czamanske et al. 1981).

The order of increasing Mn should be the reverse of that shown by Ti (Czamanske and Wones 1973). The distribution of Mn between titansalite and kaersutite (K_DTiamph/cpx of 1.0 or 1.42) implies that these two minerals may not be at equilibrium. This inference is consistent with the low Fe-Mg (amph/cpx) distribution coefficients (1.25 or 1.37, cf. Helz 1973) and the occurrence of kaersutite as a rim or replacing titansalite. The distribution of Mn between amphibole and biotite has been related to temperature, Mn-content of the minerals and the degree of subsolidus re-equilibration (Greenland et al. 1968, Stephenson 1977). Distribution coefficients from green amphibole-biotite pairs in mafic rocks span a relatively wide range (K_DMnamph/bio 1.84-3.64) similar to that from the felsic rocks (Chapters 3, 4), whereas the kaersutite-biotite pair in the gabbro exhibits a lower value of 1.55.

ACCESSORY MINERALOGY

Oxide Minerals

Magnetite typically forms anhedral to subhedral, partly

interstitial, or skeletal grains. In the fine-grained mafic inclusions, magnetite may occur as anhedral to subhedral, in some cases possibly resorbed, phenocrysts. Ilmenite is commonly associated with magnetite in sandwich intergrowths, or internal or external granules (terminology of Buddington and Lindsley 1964). Ilmenite also forms discrete, anhedral to euhedral, partly interstitial, or skeletal grains (e.g., Fig. 2.5.2). Both primary magnetite and ilmenite generally appear to have crystallized near the solidus.

The degree of alteration of the oxide minerals is variable. Alteration of ilmenite to titanite is most common, but alteration of magnetite to hematite or titanite also occurs. Only remnants of the original ilmenite are preserved in some samples (e.g., MG90). In the endoskarn, the oxides have typically been completely replaced by titanite (in some cases with rutile).

The presence of granular "exsolved" ilmenite and the low Ti (0.0-1.1 wt. % TiO_2) and Mn contents (0.0-0.13 wt. % MnO) of the magnetite (Table A10.1) indicate that the original titaniferous magnetite underwent extensive subsolidus oxidation and diffusion (Buddington and Lindsley 1964), a common observation in plutonic bodies (e.g., Himmelberg and Ford 1977). Magnetite, therefore, cannot be used for geothermometry (oxybarometry). A high initial ulvospinel (Fe_2TiO_4) content can be inferred, however, from the high proportion of ilmenite relative to magnetite in composite grains (up to about 50 % or more). In contrast to the ilmenite from the more felsic rock types (Chapter 3), there are no distinctive chemical

differences (Table A10.1) between the ilmenite intergrown with magnetite and that occurring as discrete grains.

Other Accessory Minerals

Abundant apatite occurs as prismatic or acicular grains up to 4 mm long in all mafic and mesocratic intermediate samples. The presence of abundant acicular grains, commonly skeletal, partly hollow or containing elongate fluid and mineral inclusions implies rapid growth of the apatite (Wyllie et al. 1962). This is consistent with its late-stage crystallization, reflecting the high solubility of phosphorus in high-temperature, SiO_2-poor magmas (Watson 1979a).

In a fine-grained mafic inclusion (MG24), apatite also forms linear trains of grains (Fig. 2.4.1) or parallel sheaves of acicular crystals that may exhibit a herring-bone texture; these textures result from crystallization of apatite along microfractures. As noted above, abundant acicular apatite occurs within secondary plagioclase and pyroxene in several samples of monzodiorite (e.g., 84-556, Fig. 2.5.7). These textures imply that apatite crystallized in part under subsolidus conditions from deuteric fluids.

Zircon (No. 2, Table A11.1), rare or absent in the gabbro, is common in the more intermediate rock types (e.g., MG23, 53). It forms interstitial to euhedral, in some cases skeletal, grains that may be zoned. In some samples (e.g., MG6, 24, 53) allanite, a late-stage (secondary?) mineral, occurs as rare brownish, commonly hydrated grains either interstitially, along microfractures, or in amygdules.

.Other accessory minerals are secondary: titanite, epidote and chlorite (e.g., No. 3, Table A11.1) result from the breakdown of ferromagnesian and oxide minerals (Fig. 2.9.4). Titanite is especially abundant in samples of biotite-pyroxene diorite and endoskarn (e.g., MG88, 90; Table A3.1) that exhibit evidence of the most intense metasomatism and recrystallization.

In many samples, biotite contains pods or lenses of secondary minerals along its cleavage (Fig. 2.4.2). One secondary mineral is generally colorless to pale brown and fibrous with a low birefringence. Analyses (No. 1, Table A11.1) from this mineral are similar to those from analogous bodies in biotite from granites (Tulloch 1979). Tulloch identified the mineral as a grossular-andradite garnet (grandite). The McGerrigle material is characterized by high Ti (3.76-4.13 wt. % TiO_2) and, surprisingly, contains between 0.88 to 1.31 wt. % F. An alternative possibility is that such lenses consist of vesuvianite $Ca_{19}(Al,Fe)_{10}(Mg,Fe)_3[Si_2O_7]_4[SiO_4]_{10}(O,OH,F)_{10}$. No definitive identification can be made on the basis of the available data.

The occurrence of secondary Ca-Al silicates is relatively common along biotite cleavages (e.g., Phillips and Rickwood 1975, Tulloch 1979). These minerals are generally interpreted to represent a sink for elements derived through the hydrothermal alteration of primary minerals (e.g., Ca-rich to Ca-poor plagioclase, biotite to chlorite, etc.).

DISCUSSION

The presence of alkali basaltic dykes demonstrates conclusively the existence of an alkali basaltic magma. It is

therefore unlikely that the mineralogically similar gabbro represents simple cumulates derived from more evolved rock types (cf. Bonin and Giret 1984, Bédard et al. 1987). According to most investigators, alkali basalts are formed at high pressures, deeper in the upper mantle and by a smaller degree of partial melting than the melts that crystallize as tholeiitic rocks (Sørensen 1986).

The presence of amygdules within the fine-grained mafic inclusions indicates vesiculation of the mafic magma as it crystallized, probably as it chilled against a larger volume of cooler silicic magma (Eichelberger 1980, Huppert et al. 1982, Reid et al. 1983). Mafic magmas are commonly denser than felsic ones (e.g., McBirney et al. 1985). However, vesiculation lowers the bulk density of the mafic liquid (Eichelberger 1980, Huppert et al. 1982) and may thereby facilitate its rise through much more felsic liquids to the roof zone of the pluton (cf. Campbell and Turner 1986).

Petrographic data indicate that plagioclase and clinopyroxene were the liquidus or near-liquidus phases in the alkali basaltic magma. However, the presence of possible pseudomorphs of olivine phenocrysts in the alkali basaltic dyke (MG61), the most primitive sample studied, indicates that the possibility that olivine may have been a liquidus phase in some of the mafic magmas cannot be ruled out. Fractionation of labradorite would drive the mafic compositions to more silica-undersaturated compositions, whereas fractionation of the clinopyroxene could result in silica over- or undersaturated residua depending on its Al content. There is no petrographic

evidence that kaersutite was ever a liquidus phase, and therefore there is no direct evidence that the fractionation of calcic amphibole from the mafic magmas could have resulted in the formation of the oversaturated felsic rock types (e.g., Cawthorn 1976, Bonin and Giret 1984). However, this does not rule out the possibility that all these minerals were fractionated at much deeper levels in the crust.

The origin of the ^{vi}Al-rich clinopyroxene phenocrysts in the fine-grained mafic inclusions is unclear. The presence of a composite labrodorite-clinopyroxene grain (Fig. 2.3.4) in MG6 suggests that they are probably in part xenocrysts that crystallized at higher pressures from a magma of similar but generally more primitive composition (see above). Contamination presumably occurred when the liquid that formed the fine-grained inclusions rose through and was contaminated by a pre-existing gabbroic body (cumulates).

The presence of primary kaersutite in the mafic rocks implies that they crystallized from magmas with a relatively high water content (Otten 1984), at temperatures greater than 950°C and under moderate to low $f(O_2)$ conditions (probably below the Ni-NiO buffer; Helz 1973, Otten 1984, Neumann et al. 1985). This $f(O_2)$ is lower than that inferred from the Fe^{3+} content of the biotite (above the Ni-NiO buffer), indicating either that biotite crystallized at a late stage under a higher $f(O_2)$ than kaersutite (see above) or that the estimate obtained from the biotite is too high. The absence of oxides in the alkali basaltic dyke (MG61) reflects its crystallization at a lower $f(O_2)$, probably below the QFM buffer, and the low a_{SiO2} of the

magma (Carmichael et al. 1974). The lower calculated $X_{Fe}3+$ of titansalite in the alkali basaltic dyke (0.26-0.29) relative to the gabbro (0.34-0.57) is also consistent with lower $f(O_2)$ conditions (e.g., Neumann et al. 1985).

All mafic and mesocratic intermediate samples studied have undergone varying degrees of recrystallization and metasomatism. These changes are reflected in the re-equilibration of biotite and amphibole, replacement of Ca-rich by Na-rich plagioclase, development of secondary clinopyroxene, replacement of oxide phases by titanite, and the precipitation of secondary apatite along microfractures and in secondary minerals. These mineralogical changes resulted in a redistribution of elements both within and between inclusions and the enclosing rocks. For example, the occurrence of biotite-rich zones toward the margin of fine-grained mafic inclusions implies K migration from the felsic host into the mafic inclusion. Though no detailed attempt was made to quantify the extent of metasomatism, the mineralogical changes suggest an increase in Si and alkalis and a decrease in Ca in the inclusion. The presence of secondary accessory minerals such as apatite, titanite, epidote and allanite(?), which commonly contain a large proportion of the whole-rock incompatible trace elements, indicates that trace elements may also have been remobilized (e.g., Exley 1980).

The chemical and mineralogical changes observed in the endoskarn are distinct from those observed in the other inclusions. Some samples of granite show mineralogical changes similar to those in the endoskarn; this implies that the

metasomatizing fluids were not in equilibrium with the granite either. Ca appears to be the principal element enriched in the endoskarn during metasomatism, dominantly through the formation of titanite and diopside. An obvious Ca source would be the calc-silicate rocks located within the aureole of the intrusion (de Römer 1977). Van Bosse (1985), in her study of the aureole, identified metasomatic diopside-anorthite±garnet±titanite skarns in the highest-grade calcareous rocks. She inferred that these rocks formed at minimum temperatures between 500 and 550°C and that metasomatism by infiltrating fluids involved an increase in Ca and a decrease in Na and K; similar to the chemical changes observed in the endoskarn. The high initial $^{87}Sr/^{86}Sr$ values (0.7068-0.7093 depending on the model age used; La Rocque 1986) of the endoskarn are consistent with interaction with fluids that partly originated in the aureole.

The determination of the origin of the mesocratic intermediate rock types is complicated by the variable degrees of recrystallization and metasomatism of the samples studied.

The biotite-pyroxene monzodiorites and diorites appear to be more highly recrystallized than their amphibole-dominated counterparts. The presence of a biotite-pyroxene assemblage probably reflects recrystallization under drier conditions than those samples that also contain abundant amphibole (Naney 1983). The samples of biotite-pyroxene diorite (e.g., MG90) appear to represent recrystallized equivalents of the gabbro, though none of the primary mineralogy is preserved, except perhaps for the accessory phases.

The oversaturated amphibole-dominated monzodiorites are by

far the most abundant mesocratic intermediate rock type sampled. Geochemical data do not support a cogenetic relationship with the gabbros using a simple fractional crystallization model (La Rocque 1986). However, the intimate field association (including apparent gradational contacts) does indicate a close relationship. The presence of primary Ti-rich clinopyroxene in both types also confirms their shared alkaline character. A major problem with a simple model of fractional crystallization is the existence of a low-pressure thermal barrier between undersaturated and oversaturated melts (Yoder and Tilley 1962). Possible mechanisms by which this thermal barrier could be crossed include: 1) fractionation at high pressure or high $f(H_2O)$ of phases such as aluminous clinopyroxene or amphibole (Cawthorn 1976, Presnall et al. 1978, Bonin and Giret 1984), 2) contamination by crustal rocks (e.g., Barker et al. 1975, Bédard et al. 1987) and 3) magma mixing (e.g., Brown and Becker 1986).

Clear evidence of a hybrid origin through magma mixing (i.e., textural heterogeneity, variable color index, etc.) is well developed only in a few monzodiorite samples (e.g., MG29). Therefore, any mixing must have occurred at an early stage, when both magmas were dominantly or completely liquid. One problem with a mixing model is the similar Ti and P contents of the gabbro and more primitive monzodiorites (e.g., MG23; cf. Vogel 1982, Marshall and Sparks 1984). If the monzodiorites cannot be derived through simple fractionation of an alkali basaltic magma, a model of combined assimilation - fractional crystallization (e.g., Taylor 1980) may be more appropriate.

CHAPTER 3. FIELD RELATIONSHIPS, PETROGRAPHY AND MINERALOGY OF THE QUARTZ-POOR FELSIC ROCK TYPES OF THE HYBRID SUITE

INTRODUCTION

The quartz-poor felsic rock types (SiO_2 typically between 60 and 68 wt. %) make up a large part of the hybrid suite (cf. Whalen 1986). Included in this category are alkali syenite, alkali-feldspar syenite, syenite, quartz syenite, monzonite and quartz monzonite. Like the granitic rock types associated with the hybrid suite, they commonly contain inclusions.

For the purpose of this thesis, the quartz-poor felsic rocks of the hybrid suite are subdivided into two groups. The first consists of predominantly syenitic rocks characterized by less than 5 % quartz; the second consists dominantly of quartz monzonites, i.e., with higher amounts of quartz (5-15 %).

FIELD RELATIONSHIPS AND PETROGRAPHY

Syenites

The syenitic rocks seem restricted to the northern half of the pluton. They are concentrated north and west of mont Jacques-Cartier; the most alkaline samples are found northwest of mont Passe (e.g., 84-23, MG8; Fig. 2.1). They are typically reddish or brownish and fine- to medium-grained, and vary from equigranular to porphyritic. The color index is variable, highest (up to 11.4) in the plagioclase-phyric syenites and lowest in the alkali-feldspar syenites. The fine-grained nature of many of the samples limited the collection of representative modal data; however, combined visual and modal data indicate a range of composition from monzonite and syenite to alkali-feldspar syenite. Several samples contain a Na-rich

mafic mineral and therefore are classified as alkali syenites (Streckeisen 1976). In one case (84-23), the alkali syenite is a texturally heterogeneous, fine- to medium-grained, greenish grey and relatively mafic "hybrid"-looking rock.

The contacts between the syenitic rock types and other evolved members of the hybrid suite are generally ambiguous. In some cases the alkali-feldspar syenite appears to grade into alkali-feldspar granite (Chapter 4). The petrographic similarities and field association suggest gradational contacts between plagioclase-phyric and equigranular syenites. Sharp intrusive(?) contacts between syenite and granite, and syenite and other quartz-poor felsic rocks are also observed.

Inclusions are locally prominent and range from less than one centimetre to several tens of metres across. Rock types found as inclusions include fine- to medium-grained syenite or monzonite (possibly cognate), monzodiorite, diorite and gabbro. Fine-grained mafic inclusions may exhibit textural evidence that they coexisted as a liquid with the syenitic melt (Chapter 2). Limited contamination by mafic inclusions is observed in some samples (Fig. 3.1.4); however, inclusion-host contacts are typically sharp.

In the alkali-feldspar and alkali syenites, K-feldspar forms predominantly equigranular anhedral to subhedral grains or tabular laths (up to 8 mm), and typically exhibits a mesoperthitic texture. In the plagioclase-phyric syenites and monzonites, K-feldspar typically occurs as anhedral to subhedral, weakly to strongly perthitic grains in an allotriomorphic-granular groundmass.

FIGURE 3.1. SYENITE

1. Unzoned plagioclase phenocryst (P) mantled by perthitic K-feldspar (k). K-feldspar is intergrown with plagioclase in places along the phenocryst margin. Crossed polars. Scale bar = 0.5 mm. Plagioclase-phyric syenite (MG14).

2. Zoned clinopyroxene consisting of an augite core (white) and an aegirine-augite rim (dark grey). Replacement of the augite along fractures by aegirine-augite is visible. Crossed polars. Scale bar = 0.1 mm. Alkali syenite (84-23).

3. Oscillatory-zoned clinopyroxene grain (P; Nos. 3-7, Table A7.3), rimmed and partly replaced by amphibole (A). Crossed polars. Scale bar = 0.1 mm. Plagioclase-phyric syenite (MG10).

4. Fine- to medium-grained syenite (83-98) of heterogeneous color index is undergoing contamination by finer-grained mafic inclusions. Mafic inclusions (dark areas) are surrounded by a halo with a composition and grain size intermediate between the syenite and the mafic inclusions.

5. Clot of medium- to coarse-grained plagioclase laths (P), kaersutite (a; No. 1, Table A8.1), pyroxene remnants (p) and magnetite (m) in a fine-grained groundmass (G). Clot is mantled by perthitic K-feldspar (k). Plagioclase laths exhibit oscillatory zoning and have undergone partial recrystallization. (lighter zones in the laths). The magnetite is partly rimmed by biotite. Crossed polars. Scale bar = 1 mm. Same sample as Fig. 3.1.3 (MG10).

6. A mafic clot consisting of biotite (predominant), amphibole, apatite and iron oxides. The clot is attached to a mantled, weakly zoned, fractured plagioclase phenocryst (P) and occurs in a fine-grained groundmass (G). Bleached zones in amphibole (a) indicate that it probably formed after pyroxene. Probable pseudomorph after clinopyroxene. Scale bar = 0.5 mm. Plagioclase-phyric syenite (MG40).

7. Mantled plagioclase phenocryst (P) apparently recrystallized, resulting in the formation of K-feldspar (k, dark grey) - plagioclase intergrowths. Inclusions in plagioclase include clinopyroxene (p), biotite, iron oxides and apatite. Crossed polars. Scale bar = 1 mm. Plagioclase-phyric syenite (MG38).

8. Recrystallized margin of a mantled plagioclase phenocryst (P) resulting in the formation of perthitic K-feldspar (k; dark grey) - sodic plagioclase (white) intergrowths. Phenocryst is present within a fine-grained groundmass (G). Scale bar = 0.5 mm. Plagioclase-phyric monzonite (84-40).

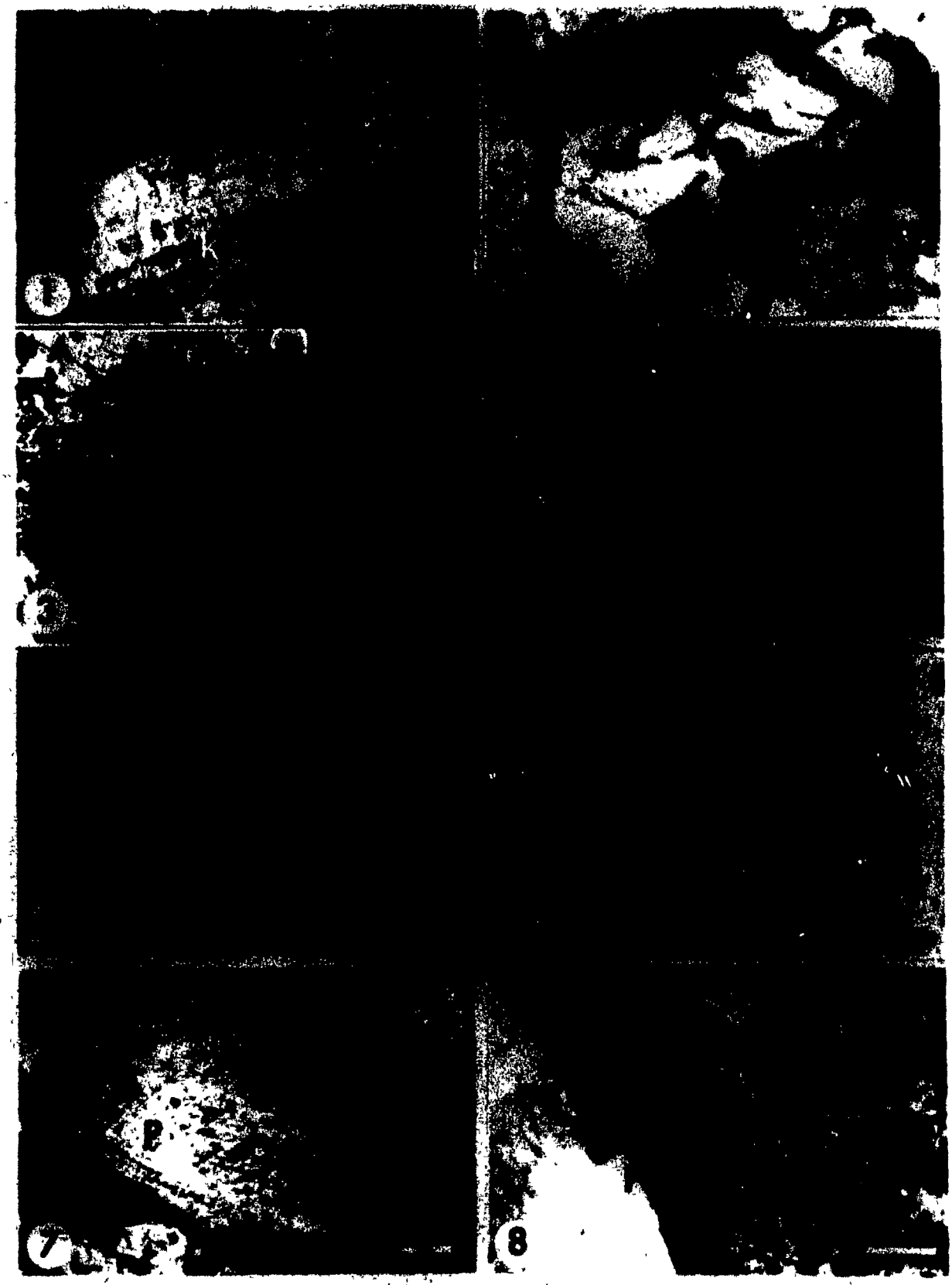

Plagioclase either forms twinned, weakly zoned to unzoned, anhedral to subhedral grains concentrated in the groundmass of plagioclase-phyric samples, or anhedral to subhedral, unzoned to strongly zoned (normal, oscillatory) phenocrysts (up to 1 cm) that are commonly mantled by K-feldspar (Fig. 3.1.1). In one sample of monzonite, a preferred orientation of the plagioclase laths is evident. Quartz typically forms anhedral and interstitial grains.

Clinopyroxene is the dominant mafic mineral observed in the alkali syenite (84-23), with subordinate amounts of amphibole and biotite. In most samples, however, amphibole predominates over biotite and clinopyroxene. Observed primary accessory minerals include magnetite, ilmenite, pyrite, pyrrhotite, apatite, zircon, titanite, allanite and chevkinite(?).

Quartz Monzonites

This compositionally and texturally variable group of rocks is taken here to include quartz monzonite proper as well as small volumes of quartz syenite and monzonite. The rocks make up a large proportion of the hybrid suite, both in the southern and northern hybrid zones (cf. Whalen 1986). They are typically medium- to coarse-grained and vary from equigranular to porphyritic, white and pink to reddish, brown or, in rare cases, grey. The color index of samples from which modal data were obtained varies from 5 to 18 (J. Whalen, pers. comm. 1986). Where the mafic index is higher than 10, the mafic minerals are commonly heterogeneously distributed and may form bands (e.g., Fig. 3.2.6).

FIGURE 3.2. QUARTZ MONZONITE

1. Grain of perthitic K-feldspar (K) exhibiting local relict concentric zoning. Crossed polars. Scale bar = 0.5 mm. Quartz monzonite (MG63).

2. Amphibole (a) and biotite (b) in a recrystallized zone (along a fracture?) in unzoned plagioclase (P). Perthitic K-feldspar (K) forms a rim around the plagioclase. Crossed polars. Scale bar = 0.5 mm. Quartz monzonite (MG66).

3. Euhedral amphibole crystal exhibiting oscillatory zoning. Crossed polars. Scale bar = 0.5 mm. Quartz monzonite (MG44).

4. Clot of partly recrystallized plagioclase laths (P) with interstitial clinopyroxene (p) that is mantled by perthitic K-feldspar (k). Clinopyroxene is undergoing replacement by amphibole along its margins. Biotite and apatite are observed in the recrystallized areas of the plagioclase. Relict normal oscillatory zoning is preserved in one lath of plagioclase. Crossed polars. Scale bar = 1 mm. Plagioclase-phyric quartz monzonite (MG52).

5. Perthitic K-feldspar (K) exhibiting a rapakivi texture. Mantling plagioclase (P) is untwinned though some twinning is observed in plagioclase laths (e.g., p) included in the rim. The patchy extinction and fading of twin lamellae in the mantling plagioclase is a sign of recrystallization. A discontinuous thin rim of quartz lines the contact between the K-feldspar and mantling plagioclase. Crossed polars. Scale bar = 1 mm. Quartz monzonite porphyry (83-97).

6. Sample of banded contaminated K-feldspar-porphyritic granite(?) containing phenocrysts of perthitic K-feldspar exhibiting a well-developed rapakivi texture, plagioclase, quartz and amphibole in a groundmass of quartz, plagioclase, K-feldspar, amphibole, biotite and iron oxides. Quartz monzonite porphyry (83-61).

7. Recrystallized remnants of K-feldspar (k) rimmed by and intergrown with plagioclase (P). Mantling plagioclase also exhibits evidence of recrystallization. Crossed polars. Scale bar = 1 mm. Same sample as Fig. 3.2.6 (83-61).

8. Plagioclase phenocryst (p) containing an unzoned, rounded, apparently resorbed core. Crossed polars. Scale bar = 0.5 mm. Same sample as Fig. 3.2.6 (83-61).

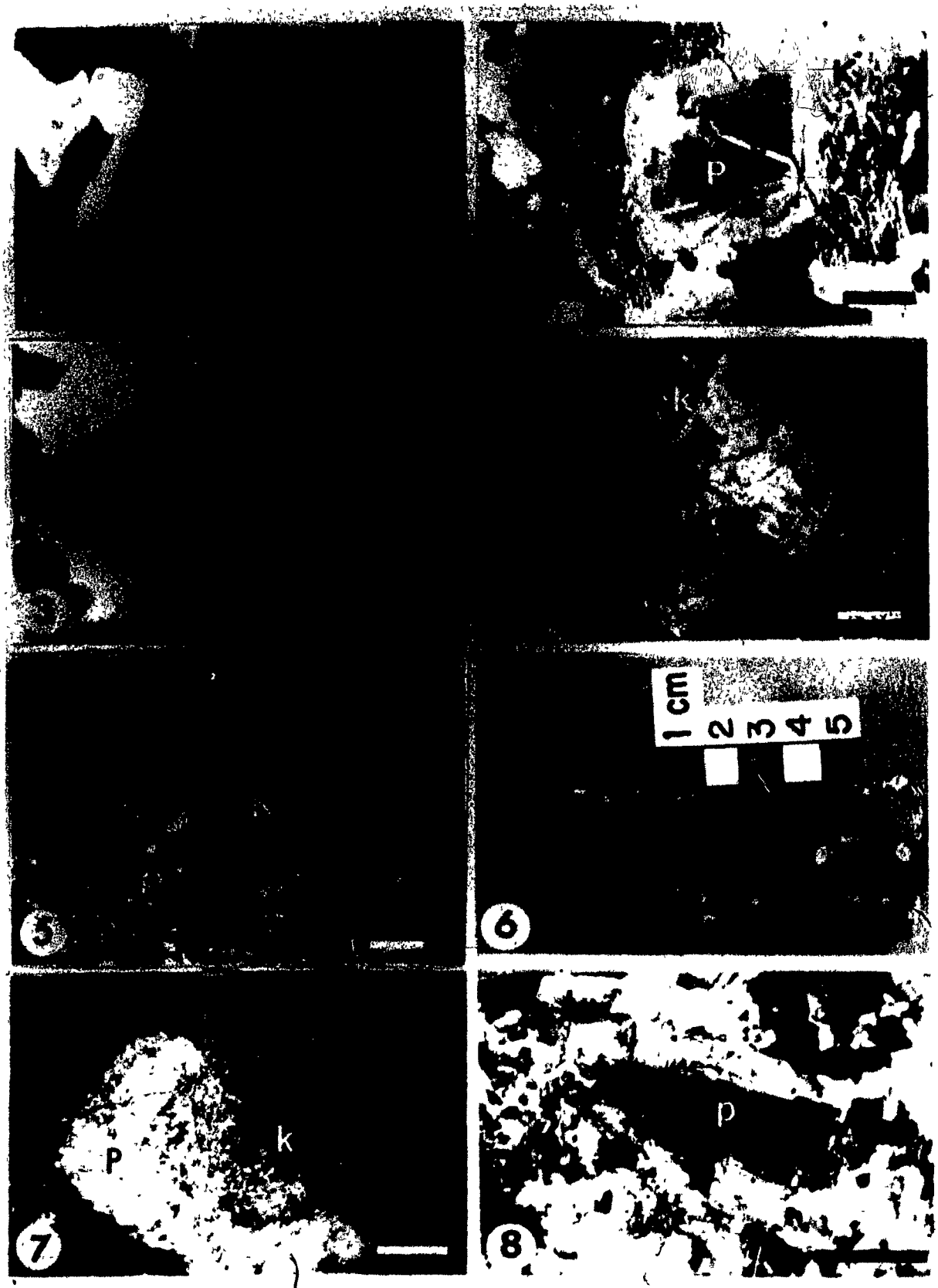
P
k
1 cm
2
3
4
5
6
P
k
7
p
8

In the field, the quartz monzonites are commonly closely associated with the granitic rocks. Both gradational and intrusive contacts are observed. In some areas (e.g., along the northern slope of mont Jacques-Cartier), the granite contains inclusions of both mesocratic and leucocratic quartz monzonite (which may in turn contain fine-grained mafic inclusions). The reverse relationship (inclusions of granite within quartz monzonite) is found at one locality (Chapter 4).

The more mafic inclusions within the quartz monzonites exhibit the same petrographic and field characteristics as those observed in the granitic rocks (Chapter 4).

The quartz monzonite varies from being plagioclase- to K-feldspar-dominant. Plagioclase forms dominantly subhedral, unzoned to strongly zoned (normal, oscillatory) laths or phenocrysts. Mantled plagioclase phenocrysts (up to 5 mm) are common in some samples of plagioclase-phyric quartz monzonite (e.g., MG52). Anhedral to subhedral, dominantly unzoned grains of plagioclase are common in the allotriomorphic- or hypidiomorphic-granular groundmass of many of the porphyritic samples.

K-feldspar forms anhedral to subhedral, commonly interstitial, weakly to strongly perthitic grains. In porphyritic samples, K-feldspar may form subhedral phenocrysts (up to 8 mm), and is the dominant mineral in the groundmass. Apparent zoning of the K-feldspar is observed in one sample (MG63, Fig. 3.2.1). Some samples of porphyritic quartz monzonite exhibit a well-developed rapakivi texture (Figs. 3.2.5, 3.2.7; Chapter 4).

Quartz forms anhedral, typically interstitial grains. Some of the porphyritic samples contain anhedral to rare subhedral phenocrysts of quartz.

Amphibole almost invariably predominates over biotite. Clinopyroxene is restricted to the more mafic, typically porphyritic samples (e.g., MG52). Observed primary accessory minerals are magnetite, ilmenite, pyrite, chalcopyrite, apatite, zircon, titanite (secondary?) and allanite.

MAJOR-ELEMENT GEOCHEMISTRY

Representative modes, whole-rock compositions and norms are given in Tables A3.2 and A4.2. No data are available for the alkali syenite. All the leucocratic intermediate rock types plot within the alkaline field of a $Na_2O + K_2O$ versus SiO_2 diagram (Whalen and Gariépy 1986). Both the syenitic and quartz monzonitic samples are predominantly metaluminous (A/CNK=0.93-1.03; C. Gariépy, pers. comm. 1985), exceptions being MG20 and MG63, which are slightly peraluminous (Table A4.2). The agpaitic index of the syenitic rocks varies from 0.83 to 0.95, whereas that of the quartz monzonites varies from 0.75 to 0.91. The plagioclase-phyric quartz monzonitic and syenitic samples (e.g., MG40, 52) are generally characterized by higher amounts of Ti, Fe, Mn, Mg, Ca and P, and lower Si and total alkalis than their nonporphyritic, more leucocratic counterparts (e.g., MG8, 44).

FELSIC MINERALOGY

Plagioclase

The plagioclase of the syenitic and quartz monzonitic rock types is typically white or grey and exhibits only minor

alteration to sericite. Detailed study was limited primarily to the moderately to strongly zoned laths and mantled phenocysts, as these are the grains most likely to be xenocrystic or contain a xenocrystic component (e.g., Hibbard 1981, Kuo and Kirkpatrick 1982).

Unmantled Zoned Laths of Plagioclase

The most complex zoning sequence is observed in the quartz monzonites; the most highly zoned grains commonly contain: 1) a relatively homogeneous core, 2) a zone exhibiting well-developed oscillatory zoning, and 3) a weakly zoned or unzoned rim.

Core compositions of these laths (Table A5.2) are relatively calcic, ranging up to An_{49} (calcic andesine). The core is typically anhedral, untwinned and sometimes shows slight diffuse zonation. Some grains contain a subhedral or euhedral core with diffuse remnant twinning. Alteration and fractures (often associated) are typically concentrated in the core. The core zone commonly is patchy (e.g., Vance 1965) and exhibits evidence of partial recrystallization (Chapter 2).

Evidence of partial resorption of the core (commonly including the surrounding oscillatory-zoned area) is widespread, resulting in the development of rounded or oval shapes (Fig. 3.2.8; in some grains the rim of the core may be less calcic than the outer rim). Resorption results from the reaction of plagioclase that is in compositional disequilibrium with the melt to form a mantle of plagioclase that is in equilibrium (Tsuchiyama 1985). Simple dissolution of the

plagioclase may also have occurred in some cases.

The unzoned to weakly zoned rim of these laths varies from albite to sodic oligoclase (An_{7-19}; Table A5.2).

Mantled Phenocrysts of Plagioclase

In many of the syenitic and some of the quartz monzonitic samples (e.g., MG40, 52), mantled phenocrysts (xenocrysts; see below) are common. Point counting of a plagioclase-phyric syenite (MG40, Table A3.1) indicates that 17% of this sample and 60 % of the total plagioclase content consist of mantled plagioclase phenocrysts. Mantled phenocrysts typically lack the unzoned or weakly zoned rim observed in unmantled ones. Analyses of mantled phenocrysts indicate relatively sodic compositions for the core, ranging up to An_{31} (sodic andesine; Table A5.2). This may indicate that they were derived from a more evolved source than that of the An-rich cores of the highly zoned plagioclase grains or that partial recrystallization has modified the calcic primary compositions. The rim of the mantled plagioclase exhibits an albite (An_{3-8}) composition.

The mantled plagioclase in the syenitic or quartz monzonitic rocks commonly exhibits evidence of a xenocrystic origin; this includes, 1) occurrence as medium- to coarse-grained clots or compound grains (Figs. 3.1.5, 3.2.4), in some cases with weakly to highly recrystallized mafic minerals or pseudomorphs that are themselves interpreted to have a xenocrystic origin (see below), and 2) common evidence of partial or complete recrystallization (e.g., Figs. 3.1.7, 3.1.8) and, therefore,

disequilibrium with the host magma, contrasting with the dominantly unrecrystallized groundmass plagioclase.

Whether mantling of the plagioclase occurs or not depends on whether one or two feldspars are on the liquidus during contamination by the plagioclase xenocrysts (e.g., Tuttle and Bowen 1958, McBirney 1979). The sole presence of K-feldspar on the liquidus is most likely in syenitic (or granitic) melts that are characterized by K-rich, An-poor compositions.

K-Feldspar

The K-feldspar of the syenites and quartz monzonites studied is typically reddish or brownish in color, weakly to strongly turbid and microperthitic. It predominantly occurs as vein perthite, but patch, interlocking, bleb, flame and rare braid perthite are also observed (terminology follows Smith 1974). Turbidity generally increases with degree and coarseness of perthite development. Nonturbid areas contain crystallographically-oriented rods and strings (Smith 1974) or are cryptoperthitic. Contacts between feldspars are commonly irregular, with many grains of K-feldspar, especially in the alkali syenite (84-23), exhibiting a rim of myrmekite or albite (may exhibit chessboard twinning).

Perthitic textures result from unmixing of the original homogeneous feldspar into K-rich and Na-rich phases below the solvus (Tuttle 1952). Whereas cryptoperthite develops upon simple cooling, the formation of microperthite requires the presence of a catalyst, usually assumed to be a water-rich volatile phase (Parsons 1978, 1980). Turbidity, due to a myriad

of submicroscopic fluid inclusions, also develops through interaction of the feldspar with a fluid (Folk 1955, Lalonde and Martin 1983). Hematite flakes on the walls of these fluid inclusions are probably responsible for the reddish color of the feldspar and indicate that the fluid causing recrystallization was oxidizing (Lalonde and Martin 1983); this is consistent with the oxidation of magnetite to hematite observed in many samples (e.g., MG10, 83-16, MG66).

Grid twinning is rare in the K-feldspar. It is predominantly developed around fractures, along coarse vein albite, grain margins or near sodium-metasomatized zones [i.e., where the feldspar has undergone the most extensive interaction with hydrothermal fluid(s)]. The scarcity of grid twinning is consistent with the cell-dimension data of the K-feldspar (Table A6.4). With the exception of the two most alkaline syenites (MG8, 84-23), the K-feldspar is monoclinic (orthoclase) to X rays. It exhibits a relatively wide range of Al-Si order ($2t_1$ varies between 0.81 and 0.91; Table A6.1, Fig. 3.3). Refinements of both orthoclase and intermediate microcline were obtained for MG8 (t_1O=0.46 and 0.87) and 84-23 (t_1O=0.42 and 0.78, respectively). The two different structures were refined using data from the same separate in the case of MG8. However, in the case of 84-23, two separates were analyzed, one being dominated by intermediate microcline and the other, by orthoclase, with only a trace of microcline. This suggests a heterogeneity in the degree of Al-Si order in this sample. The finer-grained areas of the sample seems to have undergone more extensive interaction with a fluid phase. The

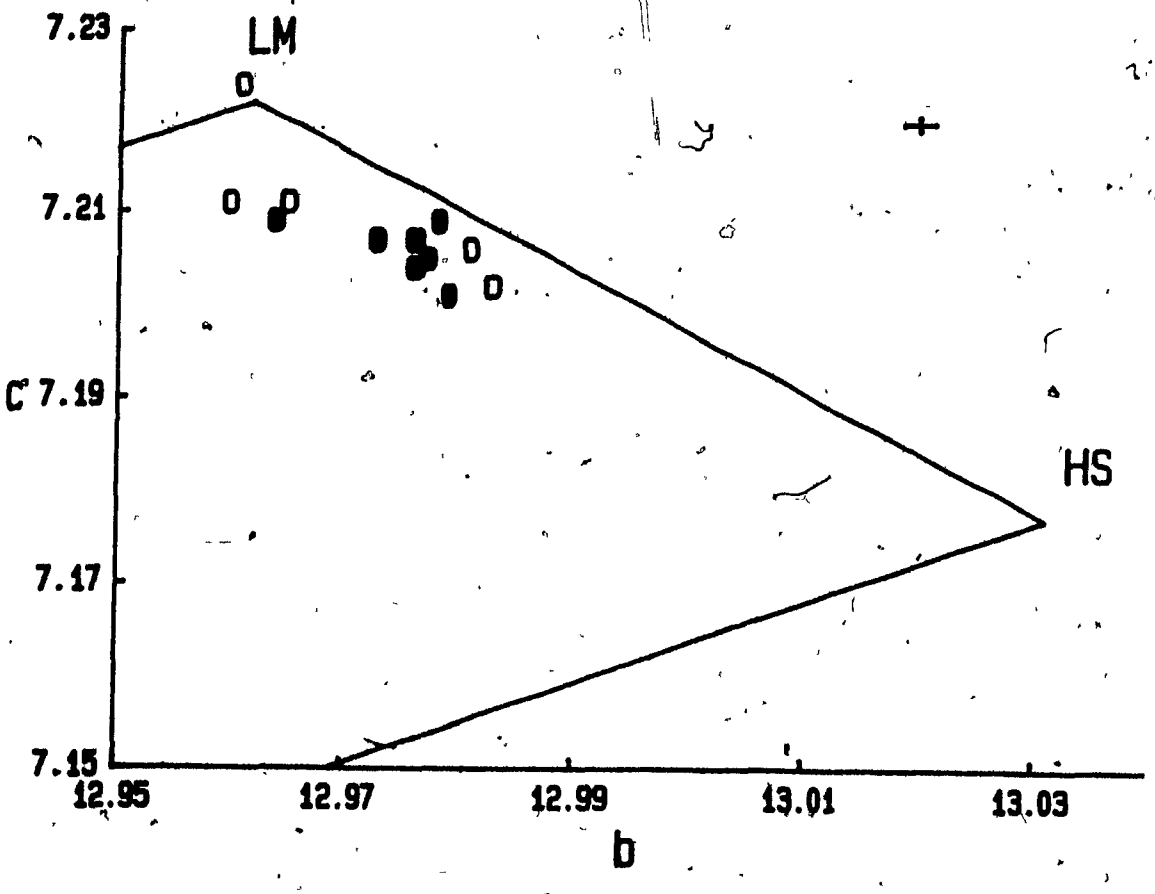

Figure 3.3. Plot of b versus c unit-cell dimensions for K-feldspar from the syenites and quartz monzonites. LM: low microcline, HS: high sanidine. Open circle: syenite, filled circle: quartz monzonite. Units: Å. Error bar is the average for the samples plotted.

general scarcity of grid twinning and the predominant monoclinic symmetry of K-feldspar indicate that interaction with a fluid must have occurred predominantly above the stability field of microcline (i.e., greater than 400°C; R. F. Martin, pers. comm. 1987).

The high Or content (Or_{92-98}) confirms that exsolution, possibly accompanied by alkali exchange with a vapor phase, has occurred (e.g., Orville 1963). The An content of the exsolved albite of the apparently hypersolvus syenites (e.g., MG8, 84-23; Table A6.2) varies from An_0 for the albite coexisting with intermediate microcline (84-23), to An_3 for that with orthoclase (84-23) and An_1 for that determined with both (MG8). This may indicate that some Ca loss from the perthite, i.e., albitization, occurred with ordering of the K-feldspar.

MAFIC MINERALOGY

Pyroxene

Clinopyroxene typically forms anhedral to subhedral prismatic grains that are commonly rimmed (e.g., Fig. 3.1.3) and, in some cases, completely replaced by amphibole, with or without biotite. Many grains exhibit textural evidence of recrystallization (e.g., intergrowth with other mafic minerals, uneven color, patchy extinction). In many of the quartz monzonites and some of the syenites, clinopyroxene is absent or occurs as rare colorless or pale green remnants.

Most, if not all, of the colorless, pale brown or pinkish brown and slightly pleochroic grains of (sodian) augite (Fig. 3.4; Table A7.3), that are most common within plagioclase-phyric syenites or quartz monzonites (e.g., MG10, 40, 52),

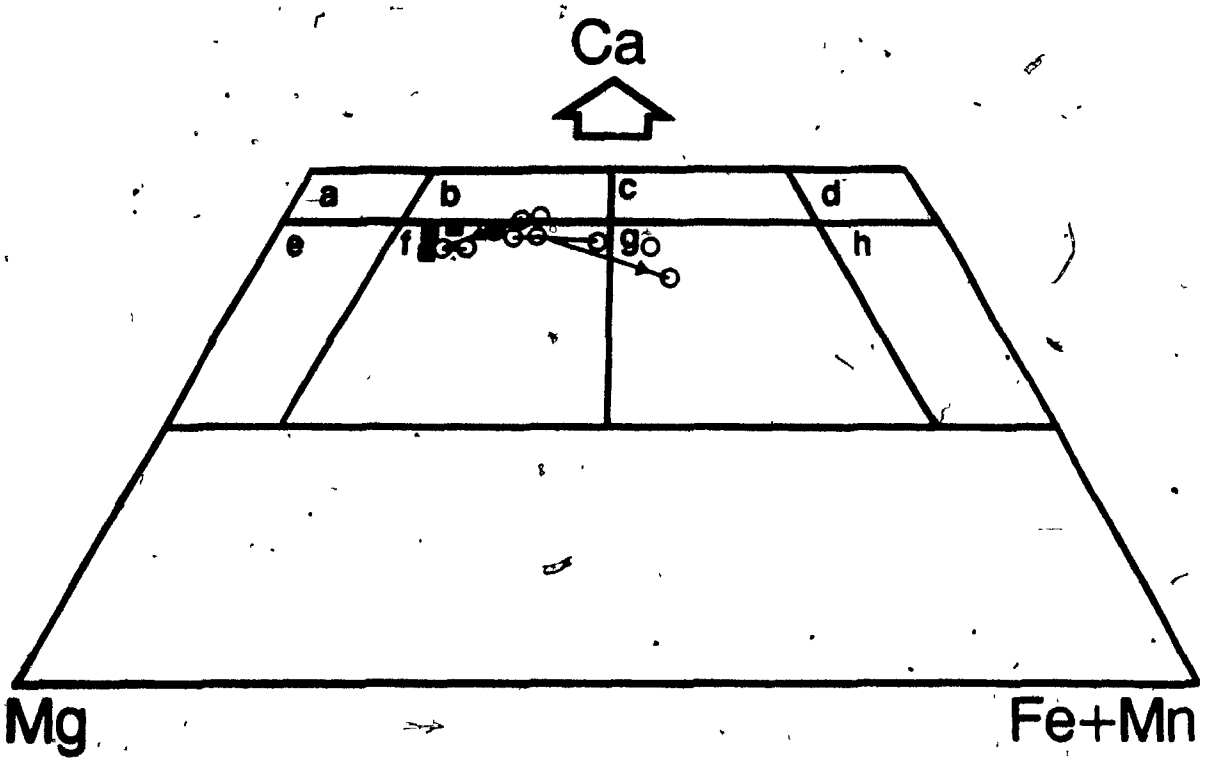

Figure 3.4. Selected average pyroxene compositions of the quartz-poor felsic rock types plotted in terms of cationic Ca-Mg-(Fe+Mn) in the "pyroxene quadrilateral". Compositional field are the same as in Figure 2.8. Filled square: monzodiorite, open circle: syenite, filled circle: quartz monzonite. Lines join compositions from the same sample; when present, arrow points toward the rim of zoned grains.

appear to be xenocrysts. Many form anhedral grains attached to the mantled plagioclase xenocrysts or occur as interstitial grains within mantled clots of plagioclase laths also interpreted to be xenocrystic (Fig. 3.2.4). Relative to the "primary" clinopyroxene of the mafic and mesocratic intermediate rock types (Table A7.1), the xenocrysts are characterized by a lower average Al (0.85-1.2 versus 3.5-8.9 wt. % Al_2O_3) and Ti (0.32-0.58 versus 1.3-5.2 wt. % TiO_2) and a generally lower X_{Mg} (0.54-0.69 versus 0.67-0.78). Therefore, the pyroxene xenocrysts are either derived from more evolved compositions than the primitive rocks from which pyroxene analyses were obtained (see below), or more likely, the pyroxene compositions have at least partly re-equilibrated with their host.

Excepting the alkali syenite (see below), zoning was only observed in one pyroxene grain from a plagioclase-phyric syenite (MG10; Fig. 3.1.3). This colorless grain is not attached to any plagioclase xenocrysts, in contrast to other colorless grains in the same sample. Significantly, the core $[Ca_{45.2}Mg_{35.1}(Fe+Mn)_{19.8}]$ of the zoned grain exhibits the most evolved composition obtained from this sample. The concentric zones around the core exhibit much more primitive compositions $[Ca_{42.3-42.9}Mg_{40.6-43.0}(Fe+Mn)_{14.7-16.8}]$ as well as higher Al (1.81-2.52 versus 1.47 wt. % Al_2O_3) and Ti (0.49-0.64 versus 0.37 wt. % TiO_2); these are the most primitive compositions obtained from any of the leucocratic intermediate syenitic samples studied. After an initial large increase in the zones immediately adjacent to the core, X_{Mg}, Ti and Al concentrations

display an irregular and less abrupt decrease toward the rim (Table A7.3). Although these compositional variations are interpreted to be primary, some recrystallization of the clinopyroxene (which is rimmed by amphibole) cannot be totally discounted. Examples of reversely zoned clinopyroxene (increasing X_{Mg} from core to rim) have been reported from several localities (e.g., Hewins 1974, Mørk 1984). Mørk (1984) attributed the increase in X_{Mg} of microphenocrysts from rhyolite to chemical contamination of the rhyolitic magma by basalt. As the plagioclase-phyric syenites exhibit abundant mineralogical and textural evidence of contamination by more primitive material at a relatively late stage, a similar explanation may account for the observed compositional variation within the zoned augite.

Within the alkali syenite (84-23), yellow-green to bright green pleochroic aegirine-augite commonly contains a colorless core of sodian augite. The augite exhibits an intermediate X_{Mg} (Table A7.3) and typically shows extensive replacement along the margin, fractures and cleavages by aegirine-augite (Fig. 3.1.2). The augite core may have undergone partial recrystallization, as indicated by its low Ti and proportion of others components.

A sample of monzonite (MG20) contains grains of pale green slightly pleochroic salite that exhibits a composition similar to the salite observed in the white granodiorite (No. 11, Table A7.2).

The most evolved average magmatic composition is $Ca_{42.6}Mg_{25.2}(Fe+Mn)_{32.2}$, for pale green to bright green

pleochroic sodian ferroaugite from syenite (MG8). The sodian ferroaugite is one of the few clinopyroxenes analyzed that definitively crystallized in equilibrium with its host. Relative to the other clinopyroxenes (excluding the probably subsolidus aegirine-augite), the sodian ferroaugite is relatively rich in sodium (Fig. 3.5), consistent with the high agpaitic index of the whole rock (Table A4.2).

In the pyroxene quadrilateral (Fig. 3.4), the clinopyroxene compositions from all the SiO_2-oversaturated rock types plot in a trend parallel to the diopside-hedenbergite join. However, as many of the samples show evidence of contamination and because many clinopyroxene grains are probably xenocrysts, the compositions cannot be considered to belong to a simple fractionation sequence. Instead they only demonstrate a general trend of clinopyroxene evolution. Ti and Al tend to be lower in the most evolved clinopyroxene, whereas Mn tends to be higher (with the notable exception of the salite in MG20).

A general trend of initially increasing hedenbergite component before subsequent acmite enrichment is typical of many silica-oversaturated alkaline complexes (Fig. 3.5; Stephenson and Upton 1982). However, the incipient sodium enrichment observed in the sodian ferroaugite suggests that it is unlikely that clinopyroxene in the McGerrigle suite reached hedenbergitic compositions. Further work will have to be carried out on the clinopyroxene of the alkali-feldspar granites to show this conclusively.

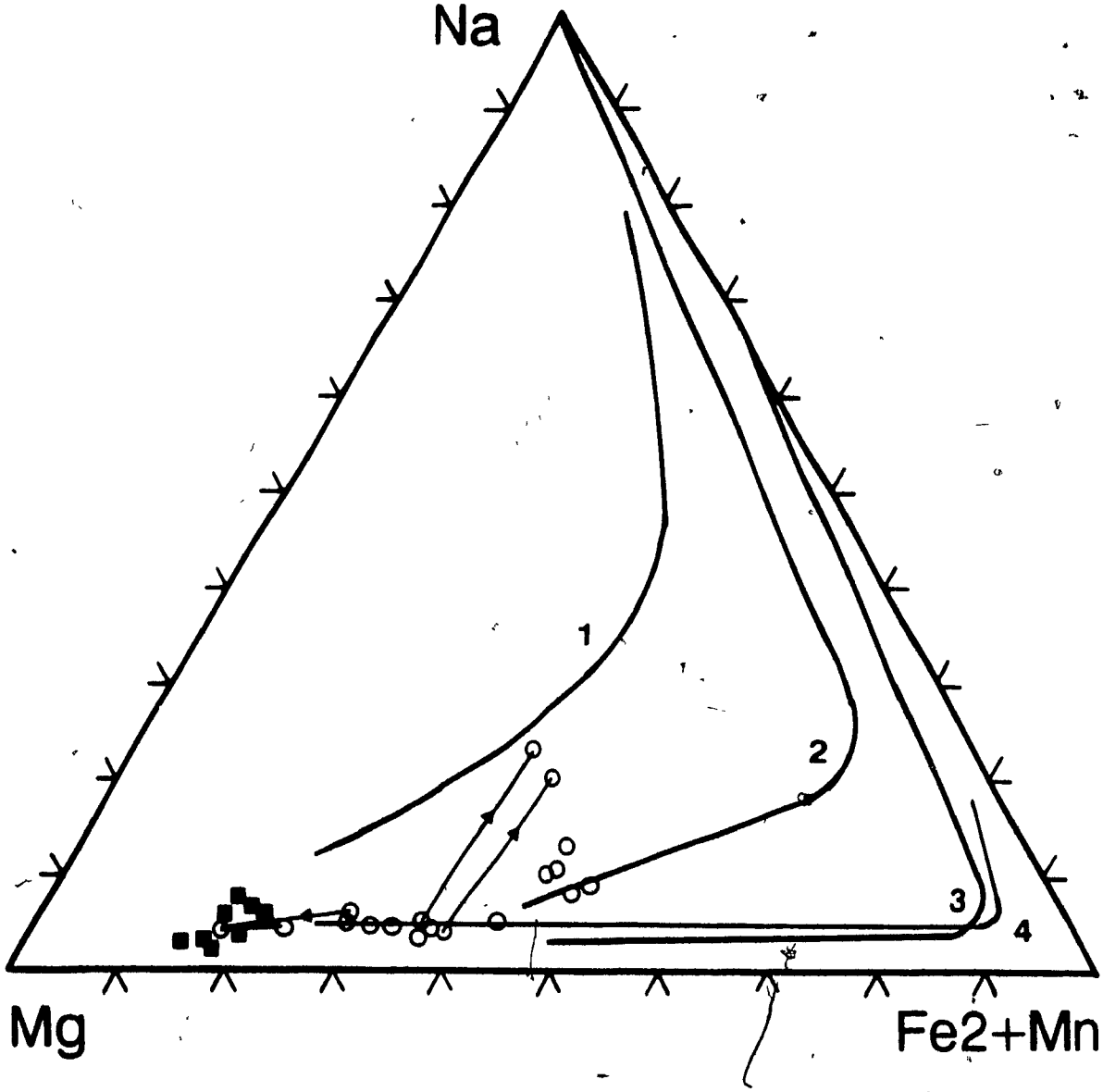

Figure 3.5: Selected pyroxene compositions plotted in terms of Na-Mg-Fe^{2+}+Mn. Same legend as Figure 3.4. Pyroxene compositional trends from other oversaturated alkaline suites: 1,2; Mulanje complex (Platt & Woolley 1986), 3) Coldwell ferroaugite syenites (Mitchell & Platt 1978), 4) Kûngnât Complex (Stephenson & Upton 1982). Lines join compositions from zoned grains with arrow pointing toward the rim.

Amphibole

In the syenites, amphibole predominantly occurs as anhedral, commonly interstitial, pale yellow-brown to brownish green pleochroic magnesio-hornblende (83-31), ferro-hornblende (MG40), actinolite and actinolitic hornblende (MG8) or ferro-actinolitic hornblende (MG10) [Table A8.3, Fig. 3.6.1]. Rare grains exhibit weak patchy or "sector" zoning or rims of slightly different composition; in all cases, however, compositional variations between zones are minor.

A plagioclase-phyric syenite (MG10) contains a subhedral grain of red-brown kaersutite (Chapter 2) that is undergoing recrystallization to green amphibole along its margin. The kaersutite is part of a mantled compound xenocryst with plagioclase, magnetite and recrystallized remnants of clinopyroxene (Fig. 3.1.5).

The alkali syenite (84-23) contains interstitial, pale greenish brown to olive green pleochroic and, in some cases, weakly zoned actinolite to winchite (Figs. 3.6.1, 3.6.3).

The samples of quartz monzonite typically contain subhedral, pale yellow-brown to brownish green pleochroic grains that vary in composition from actinolitic hornblende (MG63), magnesio-hornblende (MG52, MG66), to ferro-edenite (MG44) [Figs. 3.6.1, 3.6.2]. With the exception of MG44, where euhedral grains exhibit well-defined concentric zoning (Fig. 3.2.3), zoning is rarely observed and weakly developed.

The inclusion content in the amphibole grains is variable; opaque oxides and apatite are most common. Minor alteration to silicic amphibole, titanite or biotite is common, typically

Figure 3.6: Selected average amphibole compositions from the quartz-poor felsic rock types plotted in the classification diagrams from Leake (1978). Open circle: syenite, filled circle: quartz monzonite, star: alkali syenite. 3.6.1. Calcic amphiboles in which: $(Ca+Na)_{M4}>1.34$, 2) $Na_{M4}<0.67$, 3) $(Na+K)_{A}<0.5$ and 4) Ti<0.5 a.f.u. Compositional fields are the same as in Figure 2.11.2. 3.6.2. Calcic amphiboles in which: 1) $(Ca+Na)_{M4}>1.34$, 2) $Na_{M4}<0.67$, 3) $(Na+K)_{A}\geq 0.5$, 4) Ti<0.5 a.f.u., and 5) $Fe^{3+}>{}^{Vi}Al$. Compositional fields are the same as in Figure 2.11.3. Arrow points to rim. 3.6.3. Sodic-calcic amphiboles in which: 1) $(Ca+Na)_{M4}\geq 1.34$, 2) $0.67<Na_{M4}<1.34$ and 3) $(Na+K)_{A}<0.5$. a.f.u. a: winchite, b: barroisite, c: ferro-winchite, d: ferro-barroisite.

1.

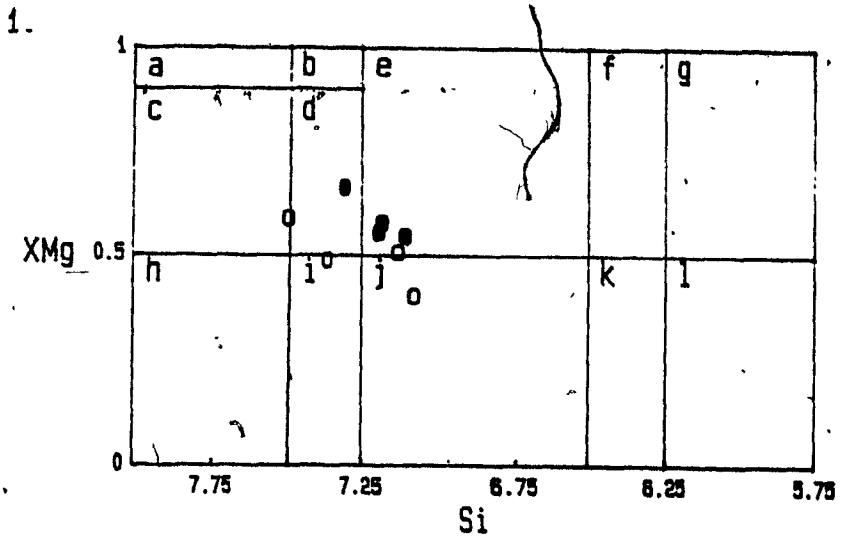
a
b
e
f
g
c
d
h
i
j
k
l
XMg
1
0.5
0
7.75
7.25
6.75
6.25
5.75
Si

2.

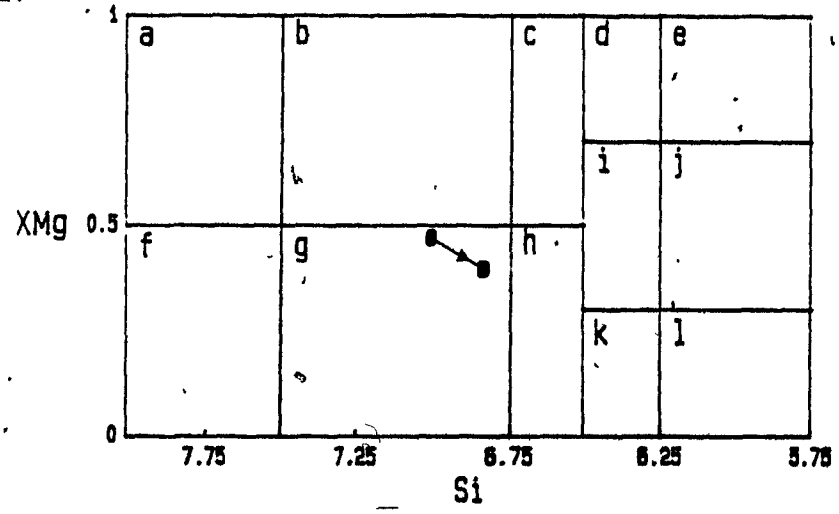
a
b
c
d
e
i
j
f
g
h
k
l
XMg
1
0.5
0
7.75
7.25
6.75
6.25
5.75
Si

3.

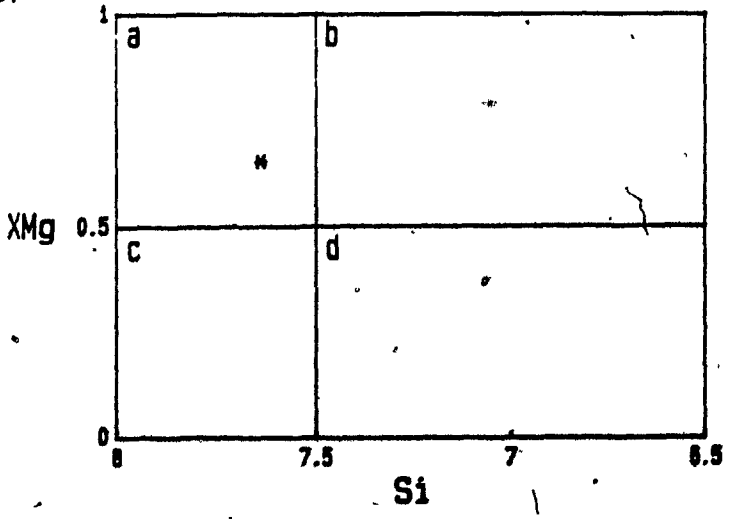
a
b
c
d
XMg
1
0.5
0
8
7.5
7
6.5
Si

along grain margins or fractures.

The compositional variations in amphibole among the syenites (Table A8.3) are complicated, and for the most part do not correlate with any parameter (e.g., X_{Fe}, Si). Fe^{3+} determinations by wet chemistry indicate a $X_{Fe}3+$ (Table 2.1) of 0.16 for the ferro-hornblende from a plagioclase-phyric syenite (MG40) and one of 0.19 to 0.20 for actinolite from a syenite (MG8). The variation in Ti [which is a function of T and $f(O_2)$; Helz 1973, Spear 1981] is complicated, being lower in Mg-rich than in Fe-rich calcic amphibole, and apparently independent of Si content.

The sodic-calcic amphibole winchite observed in the alkali syenite displays a low Al content and A-site occupancy, consistent with a low temperature of formation (Ernst 1968, Charles 1975).

The magnesio- and actinolitic hornblende of the quartz monzonites resembles that observed in the syenites and the plagioclase-dominant granites (Chapter 4). $X_{Fe}3+$ varies from 0.21 to 0.23 (including duplicate analyses) for the two samples analyzed (MG63, 66; Table 2.1).

Relative to the other felsic amphiboles the highly zoned ferroedenite of MG44 exhibits high Ti (1.4-2.1 wt. % TiO_2), Na (2.3-2.6 wt. % Na_2O) and A-site occupancy (0.534-0.705), a moderately high Al (6.1-7.1 wt. % Al_2O_3), K (0.7-0.93 wt. % K_2O) and X_{Fe} (0.549-0.631), and a low measured $X_{Fe}3+$ (0.08; Table 2.1). General trends of increasing Al, Ti, Mn, Fe, K and A-site occupancy, and decreasing Mg and Si, are observed from core to rim (Fig. 3.7.1-3.7.6). These trends, significantly

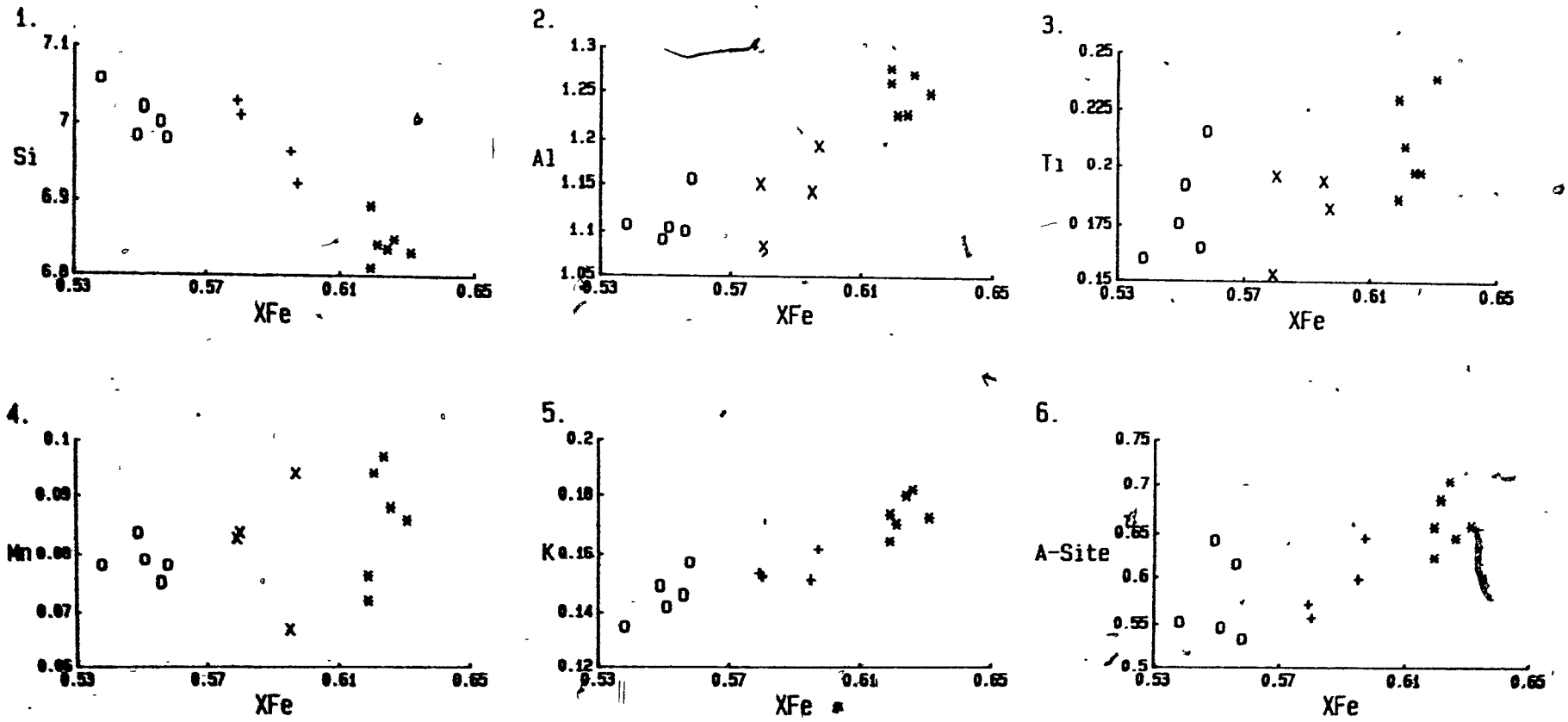

Figure 3.7. Compositional variations of zoned grains of amphibole from MG44 (quartz monzonite) with X_{Fe} (in atoms per 23 oxygen atoms). Circle: core composition, cross: intermediate zone composition, star: rim composition. 3.7.1. Si versus X_{Fe}, 3.7.2. Total Al versus X_{Fe}. 3.7.3. Ti versus X_{Fe}. 3.7.4 Mn versus X_{Fe}. 3.7.5 K versus X_{Fe}. 3.7.6 A-site occupancy versus X_{Fe}.

different from those observed in other zoned amphiboles (e.g., MG42, MG97), could be produced by either increasing temperature or decreasing $f(O_2)$ (Helz 1973, Spear 1981). The latter explanation is considered more probable given the limited evidence of mixing with a more mafic magma (rare fine-grained mafic clots up to 1 cm in size) in MG44.

F and Cl contents of amphibole are quite variable with average values ranging from 0.37 to 1.25 wt. % F and from 0.03 to 0.30 wt. % Cl, respectively (Table A8.3). No simple correlations among X_{Fe}, rock type and F- or Cl-content can be made; however, a good correlation between Cl and Si content is observed for the syenites (Fig. 3.8; see below).

Only A-site minus NaM4 versus ^{iv}Al exhibits a significant correlation in the hornblendes from the syenites (implying that edenite substitution is important). In all the hornblendes for which Fe^{3+} was determined, including the granites and a sample of monzodiorite (Tables A8.2, A8.3, A8.4), a significant imbalance (i.e, 0.21-0.48) between the amount of Na plus K in the A-site and R^{3+} plus Ti in the octahedral site on one hand, and the amount of Al (plus Fe^{3+}) in the tetrahedral site on the other is observed. Substitutions involving NaM4 (e.g., riebeckite, glaucophane or richterite; Table 2.2) may be chiefly responsible for balancing the excess charge; however, without H_2O determinations the possible significance of oxy-components (e.g., substitution 11, Table 2.2) cannot be evaluated. The high NaM4 values and low Al, Ti and A-site occupancies suggest that the winchite in the alkali syenite (84-23) contains a significant riebeckite component. Reasonably

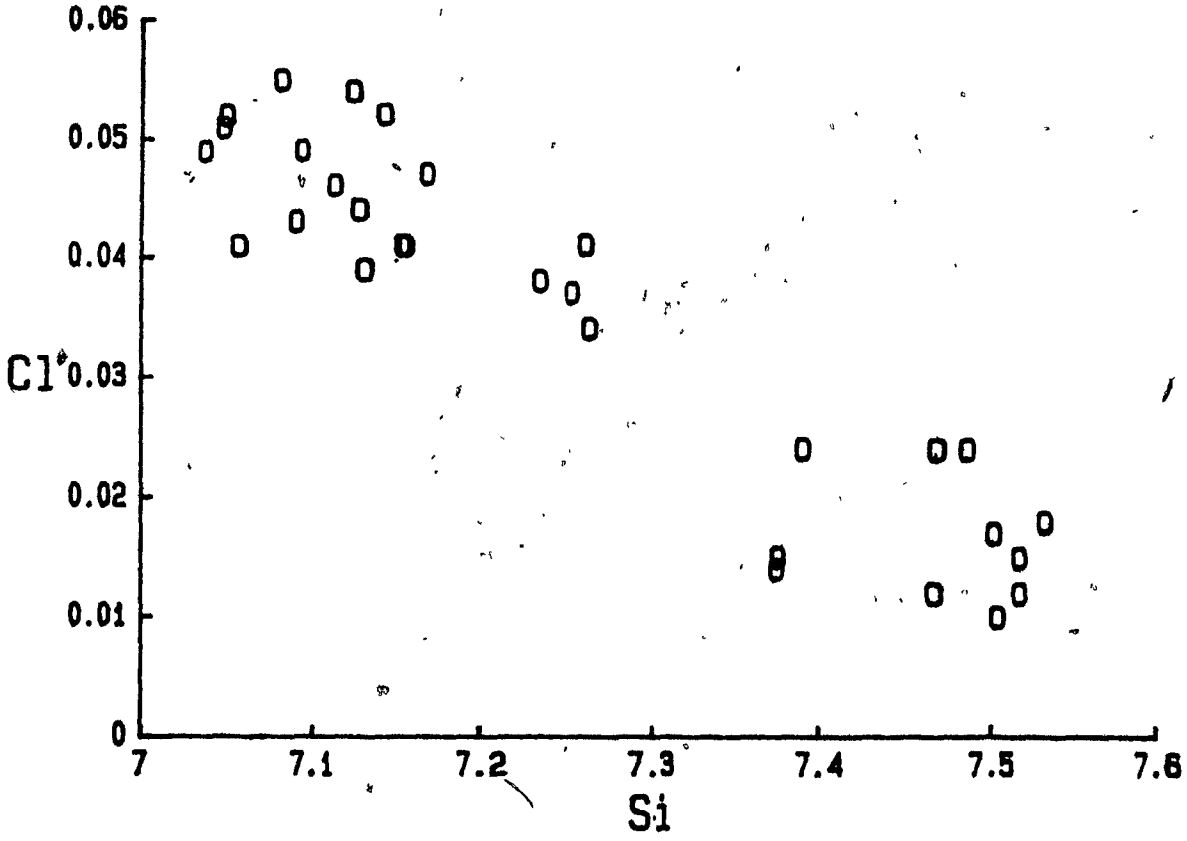

Figure 3.8. Cl versus Si content (in atoms per 23 oxygen atoms) for amphibole from the syenites.

good correlations between A-site minus NaM4 versus ^{iv}Al and NaM4 versus ^{vi}Al (Figs. 3.9.1, 3.9.2) suggest that both edenite and glaucophane substitutions occur in the zoned ferroedenite of MG44.

Biotite

Titaniferous biotite or titanbiotite occurs as light tan to dark brown pleochroic, anhedral or interstitial to subhedral grains. Inclusions are less abundant than in amphiboles, with apatite, opaque oxides and zircon most commonly observed. Minor incipient alteration to chlorite with or without titanite is visible in many samples.

The compositions (Table A9.2) plot close to the phlogopite-annite join (Fig. 3.10). Si+Al is almost invariably less than four requiring the presence of tetrahedral Fe^{3+}. The biotite from the quartz monzonites and especially from the syenites spans a large range in X_{Fe} (0.47-0.69). Though other elemental variations are observed (e.g., Ti, Al), no simple correlation with any single parameter is evident, probably reflecting the similar paragenesis (e.g., Czamanske et al. 1977) as well as the complex magmatic histories of the biotite population.

The measured $X_{Fe^{3+}}$ (Table 2.1) varies from 0.12 for iron-rich biotite from a plagioclase-phyric syenite (MG40) to 0.18 for a sample of quartz monzonite (MG66) (a duplicate of the MG66 biotite exhibits an unrealistically high value of 0.29; Chapter 4). In a Fe^{2+}-Fe^{3+}-Mg diagram (Fig. 2.15), MG40 plots just above the Ni-NiO buffer, whereas MG66 plots further toward the H-M buffer.

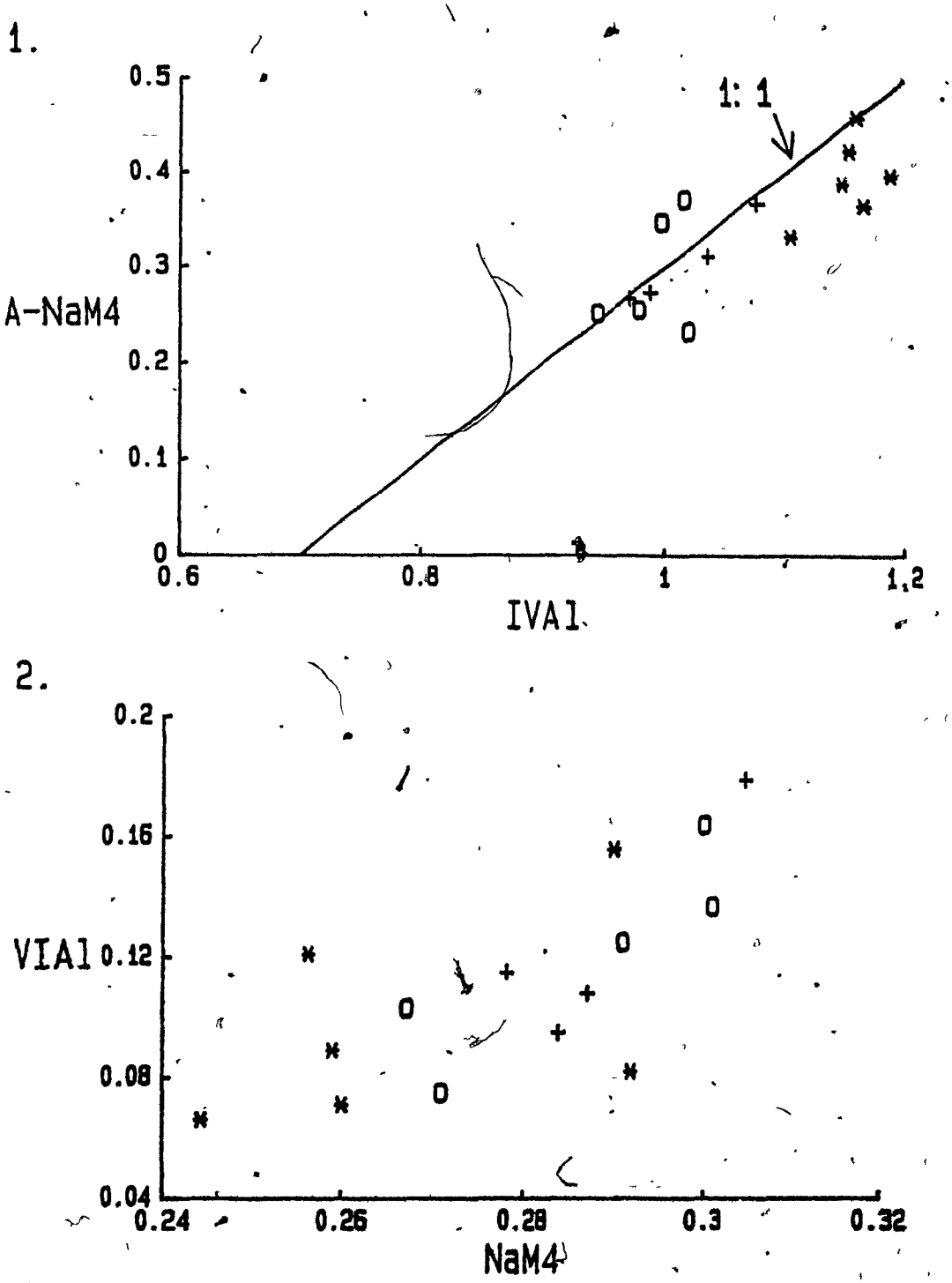

Figure 3.9. Compositional variations indicative of possible coupled substitutions occurring in the zoned grains of amphibole in MG44. Symbols are the same as in Figure 3.7. 3.9.1. Total A-site occupancy less Na in the M4 site versus tetrahedral Al. 3.9.2. Octahedral Al versus Na in the M4 site.

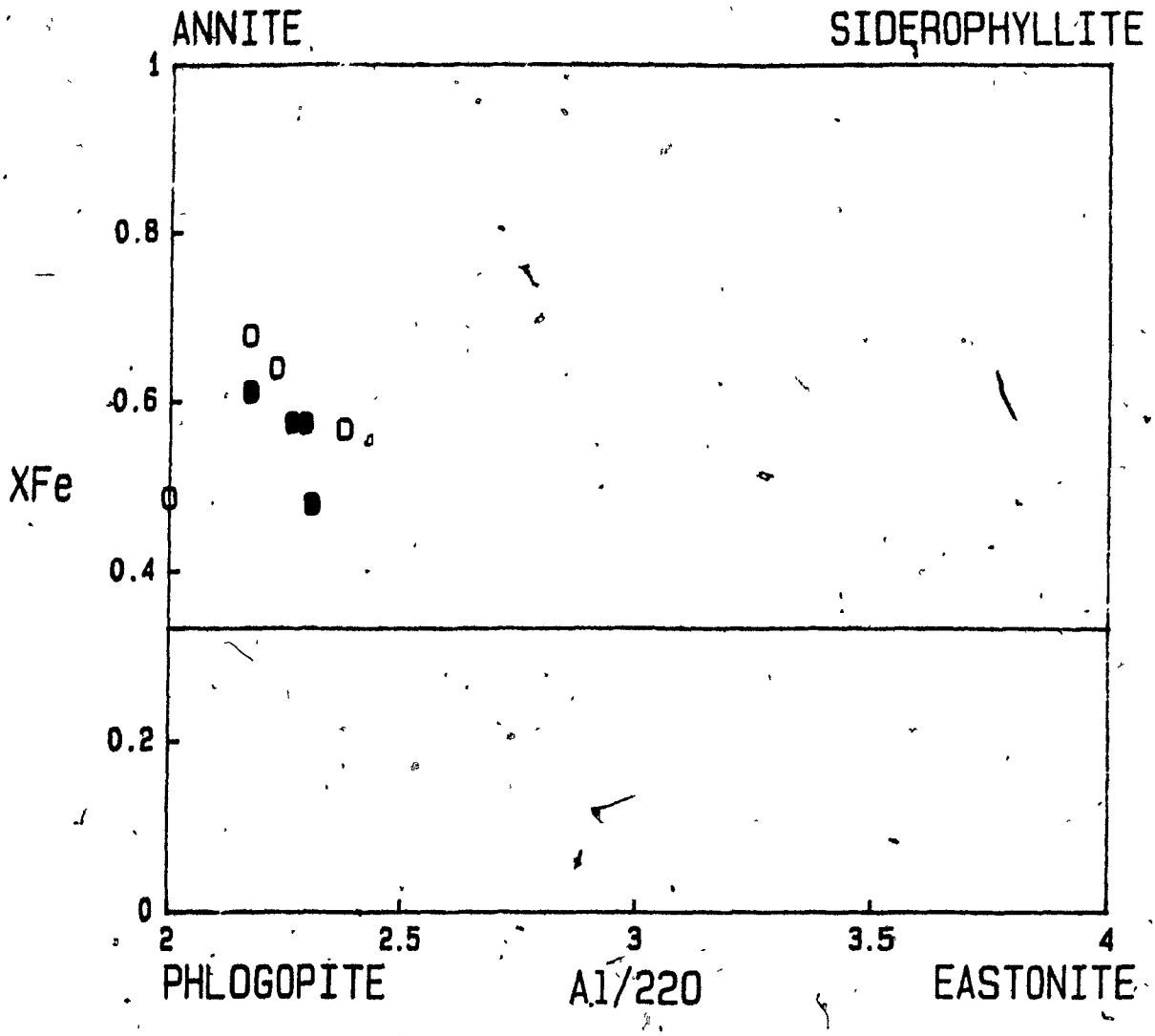

Figure 3.10. Average biotite compositions from the quartz-poor felsic rock types projected into the phlogopite-annite-eastonite-siderophyllite compositional field. Symbols are the same as in Figure 3.3, subfields as in Figure 2.14.

Average F and Cl contents for biotite range from 0.67 to 1.64 wt. % F and 0.07 to 0.46 wt. % Cl (Table A7.2) and, as in amphibole, overlap the range exhibited by the granites (Chapter 4).

Interrelations of the Mafic Silicates

The Fe-Mg distribution coefficient between clinopyroxene and amphibole varies between 2.07 and 3.87 (Table 3.1) for the pyroxene within the plagioclase-phyric syenites (MG10, 40). Whereas these high values do not in themselves demonstrate disequilibrium (cf. Helz 1973), the Mn partitioning between the two minerals does. As noted in Chapter 2, clinopyroxene should contain more Mn than amphibole; however, the K_DMnamph/cpx ratio is typically greater than one (0.87-3.21). The Fe-Mg distribution coefficient suggests disequilibrium between the early-formed sodian ferroaugite and the interstitial actinolite in the most evolved syenite studied (MG8); the K_DFe-Mg (0.44 or 0.76, depending on whether Fe^{3+} is included or not) is well below the values expected in igneous rocks (Helz 1973).

The K_D values between hornblende and biotite for Fe-Mg, Mn and Ti vary from 0.66 to 0.94, 2.53 to 3.52 and 0.26 to 0.38 for the syenites, and 0.70 to 0.91, 2.19 to 2.69 and 0.23 to 0.50 for the quartz monzonites, respectively. Similar values have been reported from other studies of felsic plutonic suites (e.g., Czamanske et al. 1977, Anderson 1980, Whalen 1985b).

The correlation between Cl and Si content of the amphibole is also reflected in the Clamph/Clbio ratio, which is lower for

			KDFe-Mg		Mn1/Mn2			Ti1/Ti2				
Sample	Unit	Amphibole	Cpx/Amph	Amph/Bio	Amph/Cpx	Bio/Cpx	Amph/Bio	Amph/Cpx	Bio/Cpx	Amph/Bio	FAmph/FBio	ClAmph/ClBio
MG8a	SYEN	Act.	0.44	0.66	0.72	0.26	2.8	6.18	22.55	0.27	1.28	0.29
MG8b	SYEN	Act.	1.74	-	1.35	0.48	-	1.94	7.09	-	-	-
MG10a	PSYN	Ferro-act. hbl.	2.39	0.72	1.98	0.86	3.52	3.68	13.91	0.26	0.55	0.26
MG10b	PSYN	Ferro-act. hbl.	3.87	-	3.21	0.91	-	1.98	7.46	-	-	-
84-23a	ALKS	Winchite	-	0.94	0.86	0.34	2.53	7.89	27.0	0.29	0.84	0.43
84-23b	ALKS	Winchite	-	-	1.41	0.56	-	17.00	60.75	-	-	-
MG40a	PSYN	Ferro-hbl.	3.49	0.84	1.27	0.49,	2.61	3.00	7.79	0.38	0.51	0.59
MG40b	PSYN	Ferro-hbl.	2.87	-	0.87	0.33	-	4.20	10.90	-	-	-
MG49*	QTMZ	Ferro-eden.	-	0.91	-	-	2.60	-	-	0.58	0.63	0.71
MG62	PQMZ	Mag.-hbl.	-	0.78	-	-	2.69	-	-	0.38	0.58	0.46
MG63	QTMZ	Act. hbl.	-	0.71	-	-	2.58	-	-	0.23	0.64	0.27
MG66	QTMZ	Mag.-hbl.	-	0.79	-	-	2.19	-	-	0.38	0.65	0.48

Table 3.1. Distribution coefficients (K_D) representing the co-distribution of Fe-Mg, Mn, Ti, F and Cl between the mafic minerals of the quartz-poor felsic rock types. Refer to Table 2.3 for the method of calculation. ALKS: alkali syenite, PQMZ: Plagioclase-phyric quartz monzonite. Other rock types as in Table 2.1. Clinopyroxene compositions used in the calculations are as follows; MG8a: sodian ferroaugite, MG8b: sodian augite (xenocryst), MG10a: sodian salite (core of zoned grain), MG10b: augite (toward rim of zoned grain), 84-23a: sodian augite (colorless core), 84-23b: aegirine-augite (bright green rim), MG40a: sodian augite (xenocryst), MG40b: sodian augite (partly recrystallized xenocryst?). *: average of all amphibole analyses used in the calculation.

the siliceous amphiboles (0.26-0.29) than for sub-siliceous amphiboles (0.46-0.71). The one exception, 84-23 (0.43) contains biotite that exhibits an exceptionally low Cl content (0.07 wt. % Cl). This implies that Cl has been preferentially lost by the siliceous amphiboles, most likely to a volatile phase (e.g., Chivas 1981), and that amphibole is more likely to lose Cl than biotite. In general the Famph/Fbio ratio is less than one, in agreement with the expected relationship (Troll and Gilbert 1972, Wones 1981); the actinolite observed in MG8 is a possible exception (Famph/Fbio=1.2) and could have been enriched in F under subsolidus conditions.

ACCESSORY MINERALOGY

Oxide Minerals

Magnetite forms anhedral to subhedral, partly interstitial, grains. Ilmenite is commonly associated with magnetite (cf. Chapter 2) or forms discrete anhedral to euhedral, rarely interstitial, grains that may exhibit alteration to titanite or, in rare cases, hematite.

As in the mesocratic intermediate and mafic lithologies (Chapter 2), all the magnetite grains of the leucocratic intermediate and syenitic rocks have undergone extensive subsolidus oxidation and diffusion. The primary and "exsolved" ilmenite commonly exhibits distinct chemical compositions (Table A10.2). In agreement with other studies (e.g., Neumann 1974, Mathison 1975), the "exsolved" ilmenite is enriched in Mn relative to the discrete "primary" grains. This occurs because down to about 600°C, Mn is partitioned among magnetite and both types of ilmenite. However, below this temperature, Mn is

preferentially partitioned into the "exsolved" phase that is in contact with the magnetite (D.H. Lindsley, pers. comm., 1986).

Compositions of ilmenite and magnetite from mafic clots do not differ significantly from those obtained elsewhere in the sample. This may indicate that partial re-equilibration of the oxides has occurred or that they formed in equilibrium with their host during the breakdown of the primary mafic xenocryst.

The range of Mn content in primary ilmenite is limited (2.3-6.0 wt. % MnO) and none exhibits the extreme enrichment in the pyrophanite ($MnTiO_3$) component reported from some other felsic intrusive bodies [up to 30.1 wt % MnO is reported for ilmenite from granites of the Finnmarka Complex by Czamanske and Mihalik (1972)].

Other Accessory Minerals

Apatite is ubiquitous and most abundant in the plagioclase-phyric samples (e.g.; MG40, 52). It typically forms acicular or prismatic grains (up to 0.6 mm long) that may exhibit a hollow core. Coarser, more equant grains (up to 0.6 x 0.4 mm) are also present in many samples (e.g., MG8, 10, 52) and may represent xenocrysts; in one case, a brown turbid core (No. 1, Table A11.2) is rimmed by colorless apatite (No. 2, Table A11.2) that also infills fractures within the core.

Zircon (No. 4, Table A11.2) is also ubiquitous, forming anhedral to euhedral, in some cases interstitial or skeletal, grains that may exhibit zoning (rarely with a metamict core).

Allanite (Nos. 3, 6; Table A11.2) is observed in many samples (e.g., MG8, 63), forming subhedral to euhedral, pale brown to

dark brown pleochroic grains that are commonly zoned. Hydration of the allanite to a pale yellow-brown to a glassy brown material is common.

Chevkinite (perrierite?) is observed (No. 5, Table A11.2) in several syenitic samples (e.g., MG40) that do not contain allanite. It forms red-brown pleochroic grains that, in some cases, are rimmed by a pale yellow alteration product, and may contain apatite inclusions. Chevkinite is chemically and structurally very similar to perrierite (Ito 1967, Calvo and Faggiani 1974), and the two minerals cannot be distinguished using the available data.

Titanite forms interstitial grains in some syenites (e.g., MG8, 84-23) and many quartz monzonites (e.g., MG44, 66). In many cases it results from alteration of oxide and mafic minerals and could be completely secondary (e.g., MG66).

DISCUSSION

Syenites

With the exception of the alkali-feldspar granites, the field relationships between the syenitic and granitic (quartz monzonitic) rocks are ambiguous. Relative to the quartz monzonites and the two-feldspar granites that dominate the pluton, the syenites show a high Na content (commonly greater than 6 wt. % Na_2O) and agpaitic index (0.83-0.95).

If the mantled xenocrysts observed in all syenites studied were ignored, many syenites (e.g., MG8) would be considered hypersolvus, i.e., they would contain no discrete grains of sodic plagioclase (Tuttle and Bowen 1958). Subsolvus syenites (i.e., containing discrete grains of albite and K-feldspar;

e.g., MG10, 4) commonly exhibit abundant evidence of contamination by more primitive material (see below) that undoubtedly resulted in Ca enrichment of the magma; an increase in Ca will result in the intersection of the feldspar solvus with the solidus and thereby result in the crystallization of two feldspars (Martin and Bonin 1976).

A hypersolvus mineralogy implies that the melt was Ca-poor [James and Hamilton (1969) concluded that at $P(H_2O)$=1 kbar, granitic liquids containing 3 wt. % or more normative An will precipitate two feldspars], relatively dry and crystallized at a low P(total) (Martin and Bonin 1976). It is interesting to note that the Ca-poor granites of the southern half of the pluton (C. Gariépy, pers. comm. 1985) are all subsolvus. This may reflect a lower water content of the syenitic magma (cf. Bonin and Martin 1976) as indicated by the late crystallization of amphibole, contrasting with the early crystallization of amphibole of similar composition in the granites (cf. Naney 1983). A more probable explanation, considering the shallow depth of intrusion (corresponding to approximately 2 kbar; de Römer 1977, Van Bosse 1985), may lie in the F-enriched character of the granites (Chapter 4); F lowers the pressure of intersection of the alkali feldspar solvus with the granite solidus by lowering the solidus (Weidner and Martin 1987).

Interpretation of the conditions of crystallization of the syenites is difficult owing to the limited data and the widespread evidence of extensive subsolidus recrystallization. This is especially evident in MG8, a syenite, where the silicic nature of the amphibole (e.g., Leake 1971) as well as its low

Cl content, the presence of significant amounts of microcline within the K-feldspar, and the disequilibrium among oxygen isotopes between quartz and K-feldspar (Chapter 6) all suggest that many of the constituent minerals have recrystallized to low temperatures in the presence of a deuteric fluid.

There is no evidence of a correlation between X_{Fe} of the biotite or amphibole and that of the whole rock (Fig. 3.11). This is consistent with the crystallization or equilibration of these minerals under variable $f(O_2)$ conditions (Czamanske and Wones 1973, Chivas 1981, Lalonde and Martin 1983). For example MG40, a plagioclase-phyric syenite, contains biotite and amphibole with higher X_{Fe} (0.68 and 0.64) and lower X_{Fe}^{3+} (0.11 and 0.16, respectively) than all other syenites. However, in MG8, a syenite characterized by a higher whole-rock X_{Fe} than MG40, the biotite and amphibole have a lower X_{Fe} (0.57 and 0.47), and amphibole exhibits a higher X_{Fe}^{3+} (0.19 to 0.20). These data, along with the presence of interstitial titanite (e.g., Haggerty 1976) in MG8 but not MG40, and the higher X_{Fe}^{3+} of the whole rock (0.51) versus MG40 (0.26), suggest that the amphibole and biotite in MG8 crystallized or equilibrated under conditions of a higher $f(O_2)$ than MG40.

The iron-rich nature of the early-forming clinopyroxene (X_{Fe}=0.54) in MG8 suggests that the high $f(O_2)$ indicated by the late-crystallizing biotite and amphibole may have developed at a late stage during this sample's magmatic history or even reflect subsolidus conditions. An apparent increase in the $f(O_2)$ at which the mafic minerals crystallized is commonly attributed to loss of H_2 via deuteric fluids at a magmatic

1.

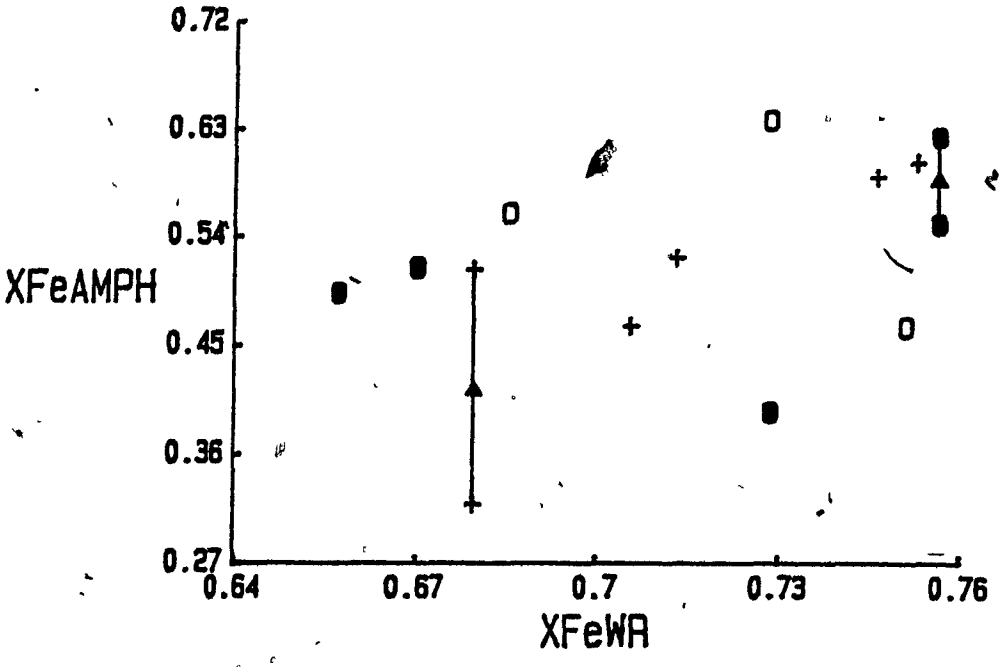

2.

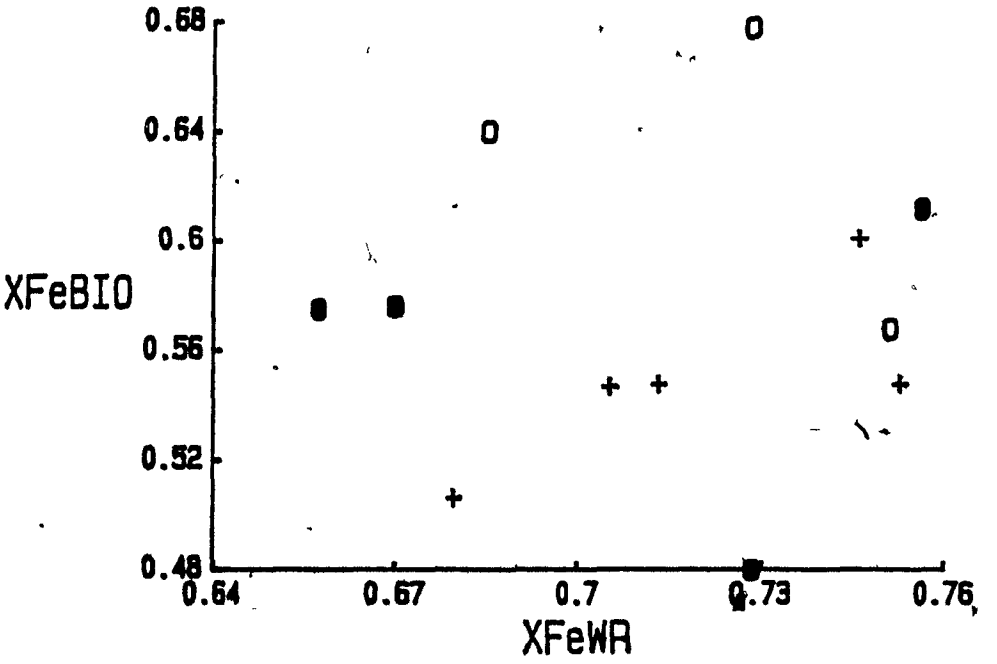

Figure 3.11. The relation of whole-rock and mineral compositions in terms of X_{Fe} (Fe/(Fe+Mg)). Symbols are the same as in Figure 2.15. 3.11.1. X_{Fe}Amphibole versus X_{Fe}Whole Rock. Line joins zoned grains, arrow points to the rim. 3.11.2. X_{Fe}Biotite versus X_{Fe}Whole Rock.

stage (e.g., Czamanske and Wones 1973) or (re)crystallization under subsolidus conditions in the presence of a fluid (Chivas 1981).

The composition of biotite in MG40 indicates a lower $f(O_2)$ than in the granites (Chapter 4) but similar to that observed in the more mafic samples (Chapter 2) and still above the Ni-NiO buffer. Another suggestion that the syenites were in general characterized by a relatively high intrinsic $f(O_2)$ (at least above the QFM buffer) is the lack of evidence that olivine was ever a stable phase. The degree of hedenbergite enrichment in the clinopyroxene is commonly related to oxygen fugacity (e.g., Larsen 1976, Stephenson and Upton 1982); the apparent lack of hedenbergite in the McGerrigle syenites is also consistent with their crystallization under a higher intrinsic $f(O_2)$ than many other silica-oversaturated alkaline suites (cf. Mitchell and Platt 1978, Stephenson and Upton 1982, Platt and Woolley 1986).

The textural and mineralogical evidence is most consistent with a hydrothermal rather than magmatic origin for the sodium-rich minerals of the alkali syenite (84-23). This evidence includes: 1) the control exerted by fractures and cleavages over the replacement of augite cores by aegirine-augite, 2) widespread textural evidence of albitization of K-feldspar along its margin, 3) heterogeneous development of both aegirine-augite and intermediate microcline, with many inclusions of clinopyroxene within K-feldspar exhibiting little or no evidence of being replaced by aegirine-augite, and 4) highly siliceous nature and low A-site occupancy of the

amphibole. The actual source of the metasomatizing fluid is unclear, as none of the other highly evolved syenites (e.g., MG8, 83-31) exhibits evidence of having generated an alkali-rich fluid. However, the similar textural and mineralogical characteristics of a suspected inclusion of alkali syenite within the miaskitic nepheline syenite (Chapter 5), suggest that a logical source of the metasomatizing fluids may be the miaskitic nepheline syenite. As 84-23 occurs on a ridge west of that on which the miaskitic nepheline syenite was mapped (Fig. 2.1), this could indicate a wider distribution of this type of nepheline syenite.

The relatively fine-grained texture of the majority of syenites indicates that they are unlikely to represent cumulates related to the granites. As syenitic melts occupy a thermal maximum relative to granitic melts (Morse 1968), they cannot be derived by fractionation of the latter. It is thus unlikely that the syenites and the volumetrically much more abundant quartz monzonites and two-feldspar granites are directly related. However, the small amounts of hypersolvus alkali-feldspar granite could have been derived through fractionation of a syenitic liquid (e.g., Abdel-Rahman and Martin 1987a), especially considering the close association of syenite and hypersolvus granite and their apparently gradational contacts.

Quartz Monzonites

In general the quartz monzonites commonly exhibit field, chemical and mineralogical evidence that they represent quartz-

poor or contaminated granites (see above, Chapter 4). Mineralogical compositions of the quartz monzonites and associated granites are typically very similar. For example, the magnesium-rich compositions of the mafic silicates in MG63, a white quartz monzonite (Tables A8.3, A9.2), are similar to those of the granodiorite (MG3, 68, 97; Table A8.4, A9.3) in gradational contact contact with MG63.

The exact relationship between the Fe^{3+}-content of amphibole and the $f(O_2)$ of the melt from which it crystallized, as well as the importance of other factors (e.g., T, composition), are not well understood (Gilbert et al. 1982). However, the agreement between the relative $f(O_2)$ indicated by the $X_{Fe}3+$ of the amphibole from the two syenites analyzed (MG8, 40) and that indicated by other data (see above) indicates that X_{Fe3+} can be qualitatively related to the $f(O_2)$. The limited experimental data available are consistent with this conclusion (e.g., Spear 1981, Thomas 1982). Two samples of quartz monzonite (MG63, 66) contain amphibole that exhibits similar $X_{Fe}3+$ to those of the granites (0.21-0.23 versus 0.21-0.25; Table 2.1), consistent with their crystallization or equilibration under analogous $f(O_2)$ conditions. The $X_{Fe}3+$ of the biotite from MG66 also indicates a similar $f(O_2)$ as those in the granites (Fig. 2.15), i.e., between the Ni-NiO and H-M buffers.

The composition [high Ti, Al, alkalis, A-site occupancy, X_{Fe} and low $X_{Fe}3+$ (0.08)] of the ferroedenite in quartz monzonite (MG44) are consistent with crystallization at a lower $f(O_2)$ than the other felsic rocks studied (Helz 1973, Spear 1981, Thomas 1982). A low $f(O_2)$ may also explain why a hastingsitic

amphibole is more stable in this sample than in the more alkali-rich syenites (e.g., MG8, 83-31; Thomas 1982).

Contamination of Syenites and Quartz Monzonites

Most quartz-poor felsic samples exhibit the following field, textural and mineralogical evidence of varying degrees of contamination: 1) textural heterogeneity and variable color index (e.g., 84-23, MG40, 52, 66), 2) the presence of mantled plagioclase xenocrysts (McBirney 1979, Hibbard 1981; e.g., MG8, 10, 83-16, MG40, 52) or moderately to strongly zoned laths with a resorbed or recrystallized core that may be An-rich (e.g., MG44, 63, 66), 3) occurrence of variably recrystallized, medium- to coarse-grained felsic clots dominated by plagioclase, or fine-grained mafic inclusions (e.g., MG8, 10, 83-16, 84-23, MG40, 44, 52), 4) occurrence of rare mafic xenocrysts that are typically attached to plagioclase or part of a felsic clot (e.g., MG8, 10, 40, 52), 5) presence of mafic pseudomorphs (e.g., MG10, 83-16, MG40, 52), and 6) presence of apparent apatite xenocrysts (e.g., MG8). These features tend to be best developed in the plagioclase-phyric samples that also exhibit the most primitive whole-rock compositions. In these samples the degree of contamination can be quite high; for example, as noted above, 17% of MG40 is made up of mantled plagioclase xenocrysts.

Contamination of a magma may occur either by mixing of solid materials with the magma (hybridization) or by mixing of magmas (cf. Whalen and Currie 1984). Several lines of evidence suggest that in most cases the source of the xenocrysts was highly

crystallized so that hybridization appears to have been more important than mixing: 1) abundance of xenocrysts or pseudomorphs after xenocrysts in many samples, 2) the presence of polycrystalline xenocrysts that may contain interstitial mafic minerals, and 3) the absence of dendritic or skeletal zones within or around plagioclase xenocrysts (cf. Hibbard 1981, Kuo and Kirkpatrick 1982). However, it is clear on the basis of field evidence that some magma mixing did occur (see above, Chapter 4).

The identity of the source of the contamination of the quartz-poor felsic rocks is still unclear. The limited field, mineralogical and petrographic data suggest that more than one contaminant was probably involved, and the type of inclusions that occur in a specific area may be a clue to their identity. Unfortunately, in many cases the xenocrysts have at least partly re-equilibrated with their host. However, the presence of kaersutite xenocrysts (MG10) and the An-rich (up to An_{49}) core of some plagioclase grains suggest that in many cases the contaminant was relatively primitive (e.g., gabbro or monzodiorite, cf. Chapter 2). On the other hand, the relatively evolved compositions of some apparently unrecrystallized augite xenocrysts (No. 12, Table A7.3) and mantled plagioclase xenocrysts in a plagioclase-phyric syenite (MG40) suggest that less primitive rocks have also been the source of some of the observed contamination (e.g., Sparks and Marshall 1986). Further work on the suspected xenocrysts is required to better constrain the identity of their source(s).

Chapter 4. FIELD RELATIONSHIPS, PETROGRAPHY AND MINERALOGY OF THE GRANITIC ROCKS

INTRODUCTION

This chapter presents a synthesis of the data obtained from all the granitic (quartz>20%) samples studied. Most of these were mapped as part of the granite suite (Fig. 2.1). The granites of the hybrid suite are included in view of their similarity to those in the granite suite as well as the generally ambiguous contact relationships between the two (Chapter 1).

Three major subdivisions were recognized in the field: 1) plagioclase-dominant granite (Unit 3a; Whalen 1986), 2) K-feldspar porphyritic granite (Unit 3c), 3) K-feldspar-dominant granite (Unit 3b).

FIELD RELATIONSHIPS AND PETROGRAPHY

Plagioclase-dominant Granite

The plagioclase-dominant granite occurs both in the northern and southern halves of the pluton (Whalen 1986). This unit is partly equivalent to the quartz monzonite and granodiorite "facies" of the granites described by de Römer (1977). The plagioclase-dominant granite exhibits a relatively broad range of compositional and textural variations, and the following description summarizes its general characteristics. Two texturally or compositionally distinct varieties are recognized that were not distinguished in the field and are described separately: 1) white granodiorite, and 2) granite porphyry (included in both units 3a and 3c of Whalen 1986).

Samples of plagioclase-dominant granite vary from fine- to

coarse-grained with an equigranular, seriate or porphyritic texture. Contacts with other types of granite in the southern half of the pluton seem gradational; however, the relatively sharp lithological changes observed on some traverses indicate that some intrusive contacts, especially with the K-feldspar-dominant granite, are possible as well.

Plagioclase typically forms subhedral, unzoned to moderately zoned laths or phenocrysts (up to 1 cm) which, in many cases, are highly recrystallized (Fig. 4.1.4). Some plagioclase phenocrysts form glomeroporphyritic clots. K-feldspar forms typically anhedral to subhedral, partly interstitial, grains that exhibit a weakly to well-developed perthitic texture. Rare rapakivi (in some cases as an internal rim of plagioclase) and granophyric textures are observed in some samples. Quartz forms anhedral to subhedral, commonly interstitial, grains.

Biotite is typically the dominant ferromagnesian mineral present. Pyroxene may occur as remnants in the core of amphibole grains. In one area (ridge east of mont McWhirter, cf. Whalen 1986), anhedral grains of pyroxene are the only ferromagnesian phase present; however, the pyroxene is not interpreted to be primary (Chapter 2). Primary accessory minerals observed include magnetite, ilmenite, pyrite, zircon, apatite, titanite (secondary?) and allanite.

White Granodiorite

The white (occasionally pink or brownish) granodiorite is restricted to the northern half of the pluton (e.g., near the Madeleine mine and at mont Ste-Anne) and is typically fine- to

FIGURE 4.1. GRANITE

1. K-feldspar (K) exhibiting a well-developed perthitic texture. Both crystallographically oriented string/rod and noncrystallographically oriented vein perthites are visible. Crossed polars. Scale bar = 0.5 mm. K-feldspar-dominant granite (84-526).

2. Biotite (B) forming pseudomorphs after amphibole. Scale bar = 0.5 mm. K-feldspar porphyritic granite (84-79).

3. Rapakivi feldspar with apparent replacement of perthitic K-feldspar (K) at its margins by plagioclase (P). Crossed polars. Scale bar = 1 mm. Same sample as Fig. 4.1.2 (84-79).

4. Highly recrystallized plagioclase lath (P) characterized by patchy extinction, fading or kinking of twin lamellae. Quartz (Q; white) and plagioclase (p) are present as inclusions in the lath. Crossed polars. Scale bar = 1 mm. Plagioclase-dominant granite (MG46).

5. Crystallographically-oriented inclusions of biotite outlining hexagonal growth-faces in quartz (Q). Crossed polars. Scale bar = 0.5 mm. White granodiorite (MG3).

6. K-feldspar porphyritic granite undergoing contamination by fine-grained mafic inclusions (M; black) resulting in the formation of a zone (grey) of intermediate grain size and composition. Dark zone at middle is a rust stain.

7. Complexly (oscillatory) zoned phenocryst of plagioclase (p). Alteration preferentially affects certain zones. Recrystallization resulting in the fading of twin lamellae and destruction of the primary zonation is concentrated in the core. Abrupt terminations of certain zones indicate partial reaction or resorption of the phenocryst. Crossed polars. Scale bar = 0.5 mm. Granite porphyry (MG51).

8. Fractured, weakly zoned plagioclase phenocryst (P) with a partially sericitized core and a recrystallized rim. The two halves of the phenocryst are separated by a second plagioclase lath (p). Crossed polars. Scale bar = 0.5 mm. Granite porphyry (MG42).


1
3
5
7
p
8

medium-grained and equigranular. Although most samples plot within the granodiorite field (Streckeisen 1976) some fall within the granite or tonalite fields. The relationship between this rock type and the other types of granite is ambiguous; the granodiorite appears to be cross-cut in places by the K-feldspar-dominant granite, but gradational contacts are also possible (cf. Girard 1971).

The granodiorite, in many areas, contains a large number of inclusions (e.g., north of mont Ste-Anne) and, in such cases, was mapped as part of the hybrid suite (Unit 2c, Whalen 1986).

Plagioclase forms dominantly subhedral, weakly to strongly zoned laths. K-feldspar is typically anhedral and commonly interstitial to plagioclase. Most samples studied are only weakly perthitic but exceptions are observed. Quartz forms anhedral to rare subhedral, partly interstitial, grains. In some samples, many of the quartz and plagioclase grains contain crystallographically-oriented biotite and apatite(?) inclusions (Fig. 4.1.5).

Biotite is generally the dominant (and in some samples the only) ferromagnesian mineral present. Biotite is subordinate to amphibole only in white granodiorite samples that contain abundant fine-grained, chilled mafic inclusions (e.g., MG97). Clinopyroxene is restricted to those samples that contain a high proportion of such inclusions and is commonly concentrated along the margin of the inclusion (Fig. 2.4.7). The pyroxene grains commonly exhibit varying degrees of replacement by amphibole, especially away from the inclusion margin. Observed primary accessory minerals include magnetite, ilmenite, pyrite,

apatite, zircon and allanite. Several samples (e.g., MG3) lack oxide minerals completely.

Granite Porphyry

A texturally distinct but volumetrically unimportant granite type is granite porphyry, which occurs in both the northern and southern halves of the pluton (e.g., eastern Cone) It is characterized by the presence of phenocrysts of feldspar, quartz and mafic minerals in a fine-grained matrix. Limited field data indicate that inclusions are not common; however, some outcrops exhibit evidence of contamination (i.e., textural heterogeneity, fine-grained mafic streaks; see below). This granite type is interpreted to represent either contaminated (e.g., MG42) or quenched (MG51) granite.

In the samples studied plagioclase is typically the dominant phenocryst phase, whereas K-feldspar dominates the generally allotriomorphic groundmass. Plagioclase phenocrysts are predominantly subhedral, unzoned to strongly zoned (4.1.7), and fractured in rare cases (Fig. 4.1.8). K-feldspar occurs as anhedral to nearly euhedral, typically strongly perthitic phenocrysts that may exhibit a rapakivi texture. Quartz phenocrysts are anhedral to subhedral and in some cases appear to exhibit a skeletal shape. In MG51 the quartz phenocrysts have undergone polygonization. Some samples (e.g., MG42) are heterogeneous, with clots of medium-sized grains (predominantly plagioclase) occurring without any interstitial groundmass present.

Amphibole and biotite occur mainly as phenocrysts, though

minor amounts also occur in the groundmass. Remnants of pyroxene were observed at the core of rare amphibole grains in one sample (MG42). Primary accessory minerals include magnetite, ilmenite, pyrite, chalcopyrite(?), zircon, apatite and allanite.

K-Feldspar Porphyritic Granite

The K-feldspar porphyritic granite is a relatively widespread unit. It occurs in both the northern and southern halves of the pluton (cf. Whalen 1986). This lithology can be considered to be partly equivalent to the granodiorite porphyry of de Römer (1977). It is typically medium- to coarse-grained and exhibits a well-developed porphyritic texture, with phenocrysts of K-feldspar up to at least 1.5 cm. In most cases, the K-feldspar porphyritic granite would be modally classified as a plagioclase-dominant granite; however, K-feldspar-dominant samples are also observed. Contacts between the K-feldspar porphyritic granite and K-feldspar-dominant granites appear to be generally gradational. However, apparent intrusive contacts with the K-feldspar-dominant granite were also observed (e.g., northeast of the summit of mont Jacques-Cartier; cf. Whalen 1986). Most outcrops show no or few inclusions except in areas close to the hybrid suite (e.g., north side of mont Jacques-Cartier).

Plagioclase forms predominantly unzoned to weakly zoned subhedral laths. K-feldspar typically forms anhedral, commonly porphyritic, grains that exhibit a well-developed perthitic and, locally, rapakivi texture. Quartz forms anhedral to rare

subhedral or euhedral, predominantly interstitial, grains.

Biotite and amphibole typically occur in approximately equal amounts. Amphibole is absent from only one sample, though pseudomorphs (Fig. 4.1.2) indicate that it was originally present. Primary accessory minerals observed are magnetite, ilmenite, pyrite, zircon, apatite, titanite (secondary?), allanite and chevkinite(?).

K-Feldspar-Dominant Granite

K-feldspar-dominant granite is the most abundant rock type in the pluton (cf. Whalen 1986). A modally and mineralogically distinct variant that was not distinguished in the field is alkali-feldspar granite (Streckeisen 1976), to be discussed separately (see below). The K-feldspar-dominant granite is generally equigranular; the grain size varies from fine to medium in the northern half (especially where associated with hybrid rocks) and in scattered areas in the southern half (typically close to the contact with the country rocks), to generally medium to coarse in the southern half. The coarser-grained rocks may exhibit a seriate texture, with crystals of K-feldspar up to 1.5 cm. At some outcrops miarolitic cavities, typically several centimetres across, are observed.

The K-feldspar-dominant granite is very abundant within the "hybrid" areas (included in Unit 2c, Whalen 1986) of the pluton where it contains numerous inclusions. At only one locality, north of mont Richardson, was the reverse relationship observed; there, oval inclusions of granite occur in a more mafic quartz monzonite, which also contains inclusions of less

evolved rock types.

K-feldspar occurs as anhedral to subhedral, locally partly interstitial, grains that commonly exhibit a well-developed perthitic texture. It may be mantled by or contain internal rims of plagioclase (rapakivi texture) or form a granophyric intergrowth with quartz. Plagioclase forms anhedral to subhedral laths that are typically unzoned to weakly zoned. Quartz forms anhedral to rarely subhedral, typically interstitial grains.

Biotite is present in all the samples studied and is commonly the dominant ferromagnesian mineral. In approximately one third of the samples, biotite is the only ferromagnesian mineral present; however, the presence of amphibole pseudomorphs indicates that, in at least some samples, the primary crystallization of amphibole was followed by its replacement by biotite. The primary accessory minerals present are magnetite, ilmenite, zircon, apatite, titanite, allanite and rare fluorite.

Alkali-Feldspar Granite

Areas of alkali-feldspar granite (forming bodies up to at least 100 by 500 m; Whalen 1986) have been identified in the northern half of the pluton (e.g., on ridge north of mont Passe). This rock type could only be distinguished from the K-feldspar-dominant granite in thin section or by staining, and its abundance may have been significantly underestimated in the present study. It is generally medium-grained, equigranular and exhibits the characteristics of a typical hypersolvus granite.

The alkali-feldspar granite and syenite show both gradational and intrusive contacts.

The K-feldspar is typically subhedral and exhibits a mesoperthitic texture. Plagioclase is relatively rare, occurring as anhedral, recrystallized, unzoned xenocrystic grains that are invariably mantled and replaced by K-feldspar. Quartz forms anhedral, typically interstitial grains.

Amphibole is the dominant ferromagnesian phase present. Clinopyroxene is observed in two of the three samples studied. Biotite, present in two samples, is subordinate to the other mafic minerals. Accessory minerals observed are opaque phases, apatite, zircon, titanite and allanite(?). No sample of this rock type was selected for detailed study.

Relationship Between Granite and its Inclusions

Inclusion types observed in the granites include monzonite (quartz), monzodiorite (quartz), diorite, gabbro, endoskarn (Fig. 2.6.1) and fine-grained mafic inclusions (Fig. 2.2.1, 2.2.2, 2.3.1). In the hybrid zones where they are abundant, the inclusions are generally less than 1 m across, but some exceed several tens of metres. Outside the hybrid areas of the pluton, especially within its southern half, inclusions are typically rare and less than two centimetres across. Some areas (e.g., north of mont Richardson) are dominated by a specific type of inclusion, whereas others (e.g., trail up mont Jacques-Cartier) are characterized by a large variety. In many cases the inclusions appear to represent older intrusive phases broken up almost <u>in situ</u> by the intruding granitic magma. On

the other hand, the fine-grained mafic inclusions exhibit both textural and field evidence that they coexisted as liquids with the granite melt (Chapter 2; Whalen 1985a).

Where the inclusion content is high, the quartz content of the granite commonly appears to decrease, so that it becomes more syenitic or monzonitic (probably reflecting the loss of Si to the inclusions; Chapter 2). However, contacts between the inclusion and the enclosing granite are typically sharp, with little or no visible evidence of contamination. Exceptions occur in hybrid zones of the pluton, where contamination of the granite is visible on a hand-specimen (Fig. 4.1.6) or outcrop scale, typically resulting in the formation of granite porphyry or porphyritic quartz monzonite. In situ contamination is visible where fine-grained mafic inclusions have gradational contacts with granite (Fig. 4.1.6) or where large fine-grained inclusions have disaggregated into smaller ones.

MAJOR-ELEMENT GEOCHEMISTRY

Selected modes, major-element compositions and norms are given in Tables A3.3 and A4.3. They are all marginally peraluminous, with A/CNK ratios between 1.0 and 1.05 and less than one weight per cent of normative corundum. Agpaitic indices vary from 0.57 to 0.85. In a Na_2O+K_2O versus SiO_2 diagram, the sample of white granodiorite (MG3) and one sample of granite porphyry (MG42) fall within the subalkaline field, while other granite samples plot in the alkaline field (cf. Whalen and Gariépy 1986). General trends of decreasing Al, Ti, Mg, Ca and Fe and increasing K, Si and X_{Fe} are found with increasing differentiation index (cf. Whalen and Gariépy 1986).

FELSIC MINERALOGY

Plagioclase

Plagioclase is typically white or grey and predominantly unaltered, except for minor sericitization of some grains. Laths exhibit variable degrees of recrystallization. Strongly zoned laths (e.g., Fig. 4.1.7) exhibit a similar sequence of zonation to those in quartz monzonite (cf. Chapter 3 for their detailed petrographic description).

All analyses of highly zoned plagioclase grains indicate a core more calcic than the rim. In the white granodiorite (MG3), core compositions range from sodic andesine to labradorite (An_{36-59}; Table A5.3) whereas the rim is oligoclase (An_{19-23}). In the plagioclase-dominant granite (MG46), the core ranges from sodic andesine to labradorite (An_{39-52}), with a rim of sodic oligoclase (An_{12-14}). In the granite porphyry (MG42), the core ranges from calcic oligoclase to labradorite (An_{28-50}), with a rim of sodic oligoclase (An_{13-14}). The K-feldspar porphyritic granite (MG83) contains a core of calcic oligoclase (An_{23-24}) and a rim of sodic oligoclase (An_{11-12}). The dominantly unzoned grains of the alkali feldspar granites were not analysed but limited optical data indicate an albite composition.

Several origins have been suggested for highly calcic plagioclase cores. They could represent: 1) residual grains derived from the source region of the granite (White and Chappell 1977, Scambos et al. 1986), 2) plagioclase crystallized under different physical conditions (e.g., higher T, P) or from a more primitive parental magma, from which the

granite was derived by fractional crystallization (Tuttle and Bowen 1958, McDowell 1978, Loomis and Welber 1982), 3) relict phenocrysts derived from a mafic end-member involved in magma mixing (Vernon 1983, Tsuchiyama 1985), or 4) xenocrysts derived through assimilation of mafic igneous rocks (McBirney 1979).

The origin of the highly calcic plagioclase cores (An greater than 40) cannot be determined on the basis of textural evidence alone. However, the presence of rare subhedral to euhedral cores, the preservation of relict twinning and zoning (Chapter 3), the high anorthite contents (up to An_{59}) and the identification of plagioclase xenocrysts in both the fine-grained mafic inclusions and the quartz-poor felsic rock types, are most compatible with either the third or fourth hypothesis (cf. Vernon 1983).

K-Feldspar

K-feldspar is typically brownish or reddish (rarely white), moderately to strongly turbid and microperthitic. It exhibits the same range of perthitic and other textures (e.g., Fig. 4.1.1) as the quartz-poor felsic samples (Chapter 3).

Extensive grid twinning in K-felspar is generally restricted to samples close to the outer contact of the pluton. In most samples grid twinning is relatively scarce (Chapter 3). This is consistent with the cell-dimension data for the K-feldspar (Table A6.5), as all the analyzed samples are monoclinic (orthoclase) to X rays. Traces of microcline were identified in some samples (e.g., MG57). The samples exhibit a relatively wide range in degree of Al-Si order ($2t_1$ is between 0.78 and

0.88; Table A6.1, Fig. 4.2) that is similar to the range exhibited by K-feldspar in the quartz-poor felsic samples (Chapter 3). The high Or content (Or_{91-95}) of the K-feldspar and the low An content of the exsolved albite (An_{0-4}; Table A6.2) are also analogous to those observed in the quartz-poor felsic rocks.

The petrographic, structural and compositional similarities of the K-feldspar in the granite and the quartz-poor felsic samples imply that the conclusions reached in Chapter 3 equally apply to the K-feldspar in the granites, i.e., they show evidence of widespread interaction with an oxidizing fluid at temperatures predominantly above 400°C.

Rapakivi textures (Figs. 4.1.3) are best developed within the K-feldspar-porphyritic granite and its contaminated equivalent. In the K-feldspar-porphyritic granite, few K-feldspar phenocrysts are mantled with sodic plagioclase, but typically all phenocrysts are mantled in the contaminated facies.

Generally the contact between the mantling plagioclase and the K-feldspar core is irregular and shows partial replacement of the K-feldspar (Fig. 4.1.3). This texture is especially well developed in contaminated granite; in some grains the K-feldspar also seems to have recrystallized to a complex intergrowth of K-feldspar and albite (Fig. 3.2.7). The absence or patchy development of twinning in the mantling plagioclase, especially in these samples of contaminated granite, also suggests recrystallization. In some cases the K-feldspar core is anhedral, exhibits planar contacts with the mantling

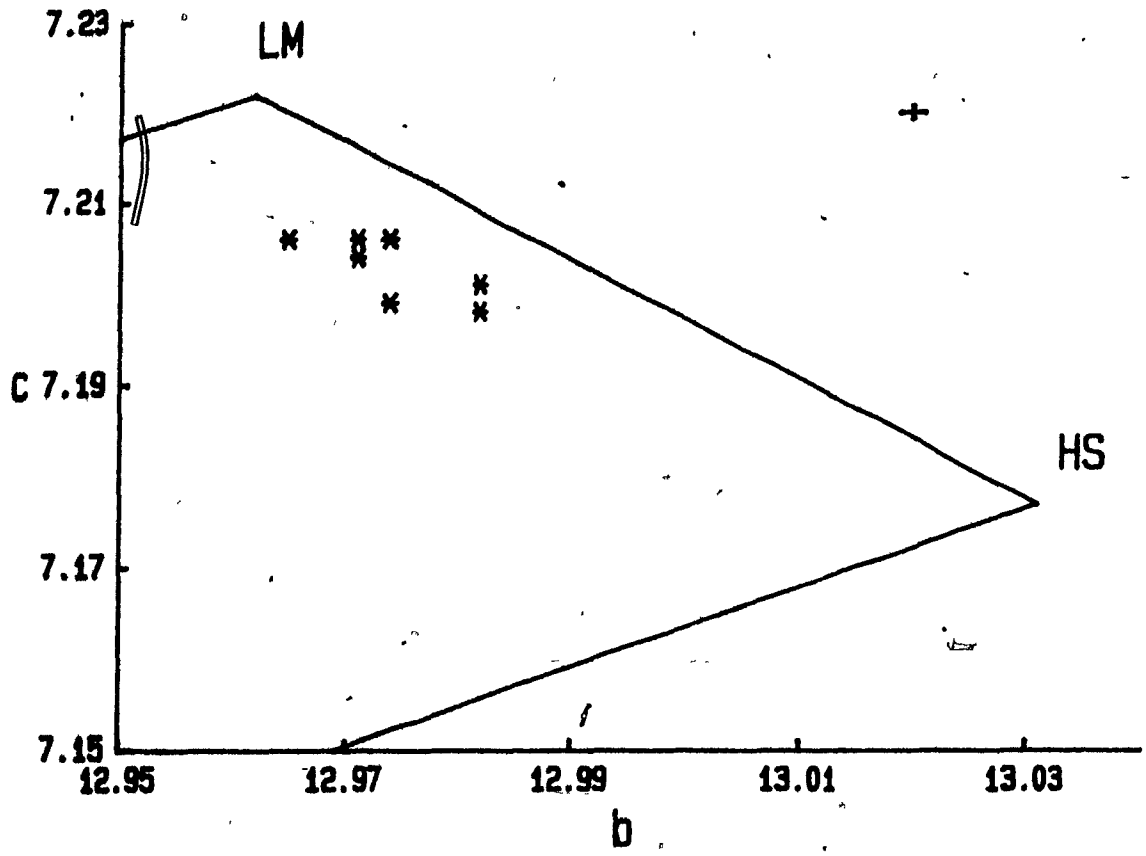

Figure 4.2. Plot of b versus c unit-cell dimensions for K-feldspar from the granites. LM: low microcline, HS: high sanidine. Units: Å. Error bar is the average for the samples plotted.

plagioclase and may have a intervening partial rim of quartz (Fig. 3.2.5). This texture is interpreted to represent partial resorption of the core, followed by later crystallization of the sodic plagioclase, possibly preceded by precipitation of quartz.

The most common model invoked to explain the origin of rapakivi textures involves changes in the physical conditions during crystallization [P, T, $f(H_2O)$] so that alkali feldspar is resorbed or replaced and overgrown by plagioclase (Tuttle and Bowen 1958, McDowell 1978, Cherry and Trembath 1978). Magma mixing (Hibbard 1981) is the mechanism favored to account for the rapakivi texture in the McGerrigle rocks as it best explains; 1) its abundance in some samples of contaminated granite (e.g., 83-61), and 2) the variable extent of recrystallization of the mantling plagioclase. Recrystallization could reflect progressive destabilization of the plagioclase mantle, as magma temperature increased (possibly due to mixing in of larger amounts of the mafic component?) during contamination.

MAFIC MINERALOGY

Amphibole

Where present, amphibole typically occurs as subhedral, prismatic, pale yellow-brown to brownish green or dark green pleochroic grains. Optical zonation is only rarely observed and typically weakly developed (darker rim than core). One exception is a sample of granite porphyry (MG42) in which phenocrysts are commonly zoned from a pale yellow-brown to brown pleochroic core to a brownish green rim. Inclusions (most

commonly biotite, oxides, apatite and zircon) are generally abundant. Most grains show minor alteration along fractures or at grain margins to actinolite, titanite and biotite.

The zoned phenocrysts in MG42 range from an edenitic hornblende core (Fig. 4.3.1) to a magnesio-hornblende rim (Fig. 4.3.2); slightly more iron-rich magnesio-hornblende occurs interstitially (Table A8.4). Amphibole from the white granodiorite (MG97), close to the contact of a chilled mafic inclusion, is dominantly actinolitic hornblende or actinolite, but one grain contains a core of magnesio-hornblende. Magnesio-hornblende is also present in samples of plagioclase-dominant granite (MG46) and granite porphyry (MG51). The K-feldspar porphyritic granite (MG83) contains ferro-hornblende, whereas ferro-hornblende and ferro-edenite occur in the K-feldspar-dominant granites (MG57, 83-55). Fe^{3+} determinations (Table 2.1) indicate a restricted range in $X_{Fe}3+$ values (0.21 to 0.25).

Three distinct "trends" of amphibole composition are observed. The first trend, considered to reflect the general magmatic evolution of the granites, is defined by unzoned amphibole (i.e., MG46, 51, 57, 83). Trends of increasing Mn, K and A-site occupancy with increasing X_{Fe} amphibole are observed (Figs. 4.4.1-4.4.3). These parallel the change in amphibole composition from magnesio-hornblende to ferro-hornblende and, finally, ferro-edenite.

The second trend is observed in the zoned phenocrysts and interstitial amphibole of MG42. The two zoned phenocrysts analyzed show a clear compositional gap between the brown

1.

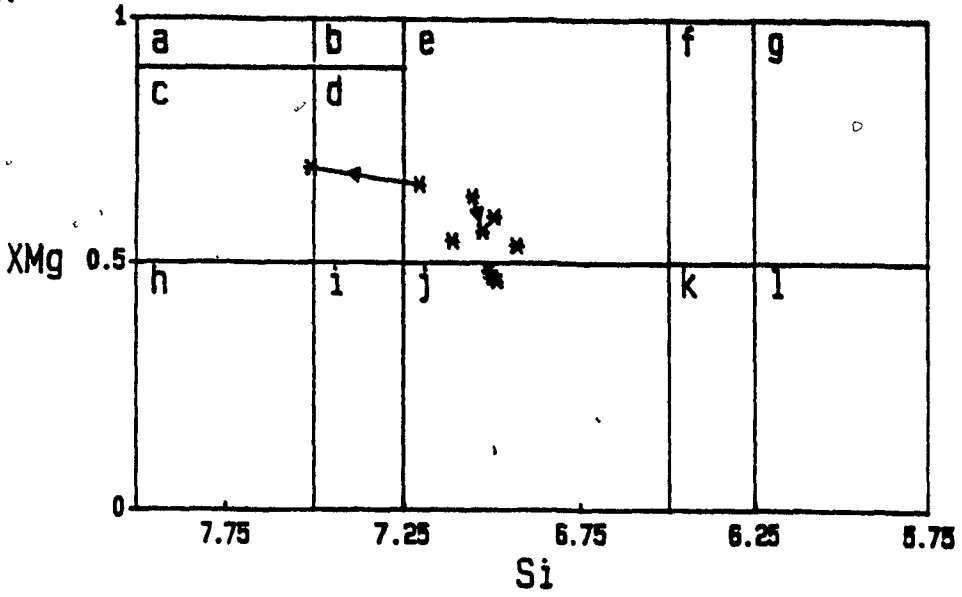

2.

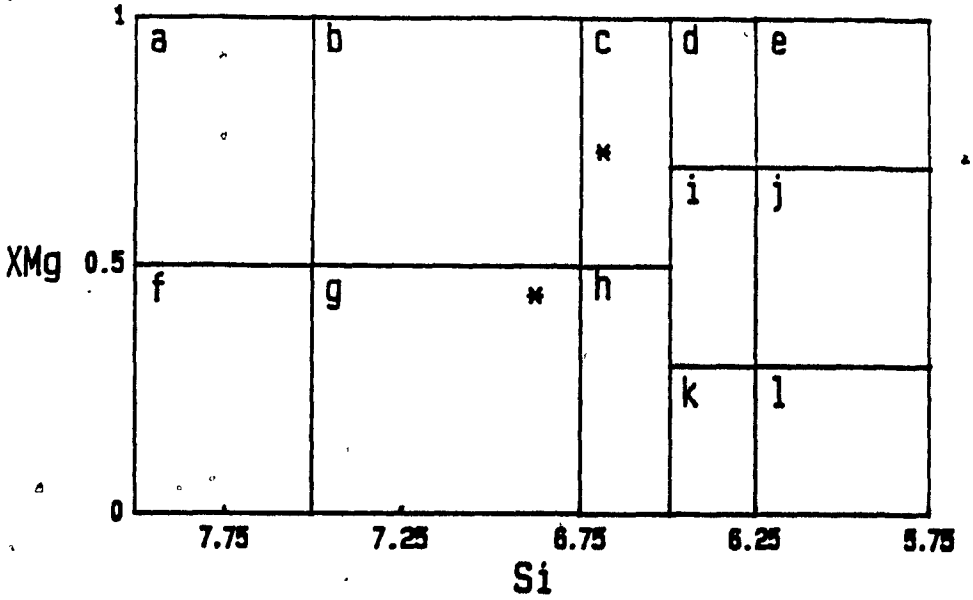

Figure 4.3. Selected average amphibole compositions from the granites plotted in the classification diagrams from Leake 1978. 4.3.1. Calcic amphiboles in which: 1) $(Ca+Na)_{M4} \geq 1.34$, 2) $Na_{M4} < 0.67$, 3) $(Na+K)_{M4} < 0.5$ and 4) Ti<0.5 a.f.u. Compositional fields are the same as in Figure 2.11.2. Lines join zoned grains with rim indicated by an arrow. 4.3.2. Calcic amphiboles in which: 1) $(Ca+Na)_{M4} > 1.34$, 2) $Na_{M4} < 0.67$, 3) $(Na+K)_{A} \geq 0.5$, 4) Ti<0.5 a.f.u. and 5) $Fe^{3+} > {}^{vi}Al$. Compositional fields are the same as in Figure 2.11.3.

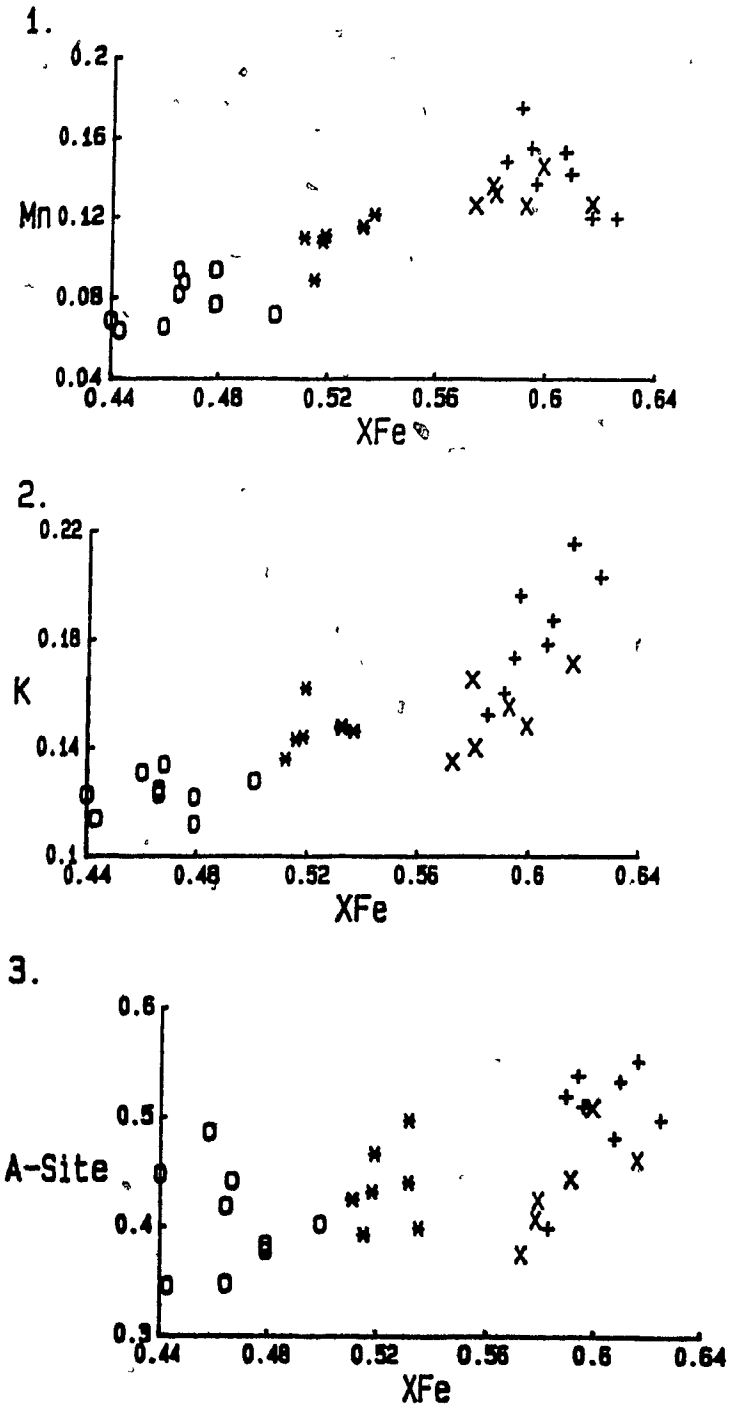

Figure 4.4. Compositional variations (in atoms per 23 oxygen atoms) of amphibole in granite with X_{Fe} (Fe/(Fe+Mg)). Open circle: plagioclase-dominant granite (MG46), star: granite porphyry (MG51), X: K-feldspar porphyritic granite (MG83), cross: K-feldspar-dominant granite (MG57). 4.4.1. Mn versus X_{Fe}. 4.4.2. K versus X_{Fe}. 4.4.3. A-site occupancy versus X_{Fe}.

edenitic hornblende core and the immediately surrounding magnesio-hornblende. This gap is widest (X_{Fe}=0.08) in the phenocryst with the best developed zoning and without textural evidence of core recrystallization. Significant gaps in Mn, K, Al, Cl, Si, Ti, Na_A and A-site occupancy are also observed. This grain shows oscillatory zoning for some elements (e.g., Ti, Si; Table A8.4); however, general trends of increasing Mn, K, Cl and Si, and decreasing Ti, Al (both ^{iv}Al and ^{vi}Al), Na_A and A-site occupancy with increasing X_{Fe} amphibole are observed (Fig. 4.5.1- 4.5.9).

The origin of the core of edenitic hornblende is unclear. Chemically it is characterized by the highest Al and lowest Mn, K and X_{Fe} of all the amphibole grains analyzed from the granites (Table A8.4). It also contains a high ^{vi}Al content and its X_{Fe} lies within the range exhibited by kaersutite of the mafic rock types (Chapter 2). These primitive chemical characteristics suggest a xenocrystic origin for the brown cores (e.g., Didier 1973, Vernon 1983), possibly derived from an intermediate magma. Unfortunately, all the amphibole grains in the intermediate inclusions (Chapter 2) have re-equilibrated with their more felsic hosts.

The third trend for amphiboles from the granites is best developed in a large grain from the white granodiorite (MG97). There is no optical evidence of zonation, but well-defined compositional variations occur from core to rim. These variations can be correlated with increasing silica and parallel a compositional change from magnesio-hornblende (core) to actinolite (rim) (Table A8.4). Trends of decreasing Ti , Al

4.5. Compositional variations of the amphibole from MG42 (granite porphyry) with X_{Fe} (in atoms per 23 oxygen atoms). Cross: brown core of zoned grains, star: green amphibole. 4.5.1. Si versus X_{Fe}. 4.5.2. Total Al versus X_{Fe}. 4.5.3. Octahedral Al versus X_{Fe}. 4.5.4. Ti versus X_{Fe}. 4.5.5. Mn versus X_{Fe}. 4.5.6. Na versus X_{Fe}. 4.5.7. K versus X_{Fe}. 4.5.8. A-site occupancy versus X_{Fe}. 4.5.9. Cl versus X_{Fe}.

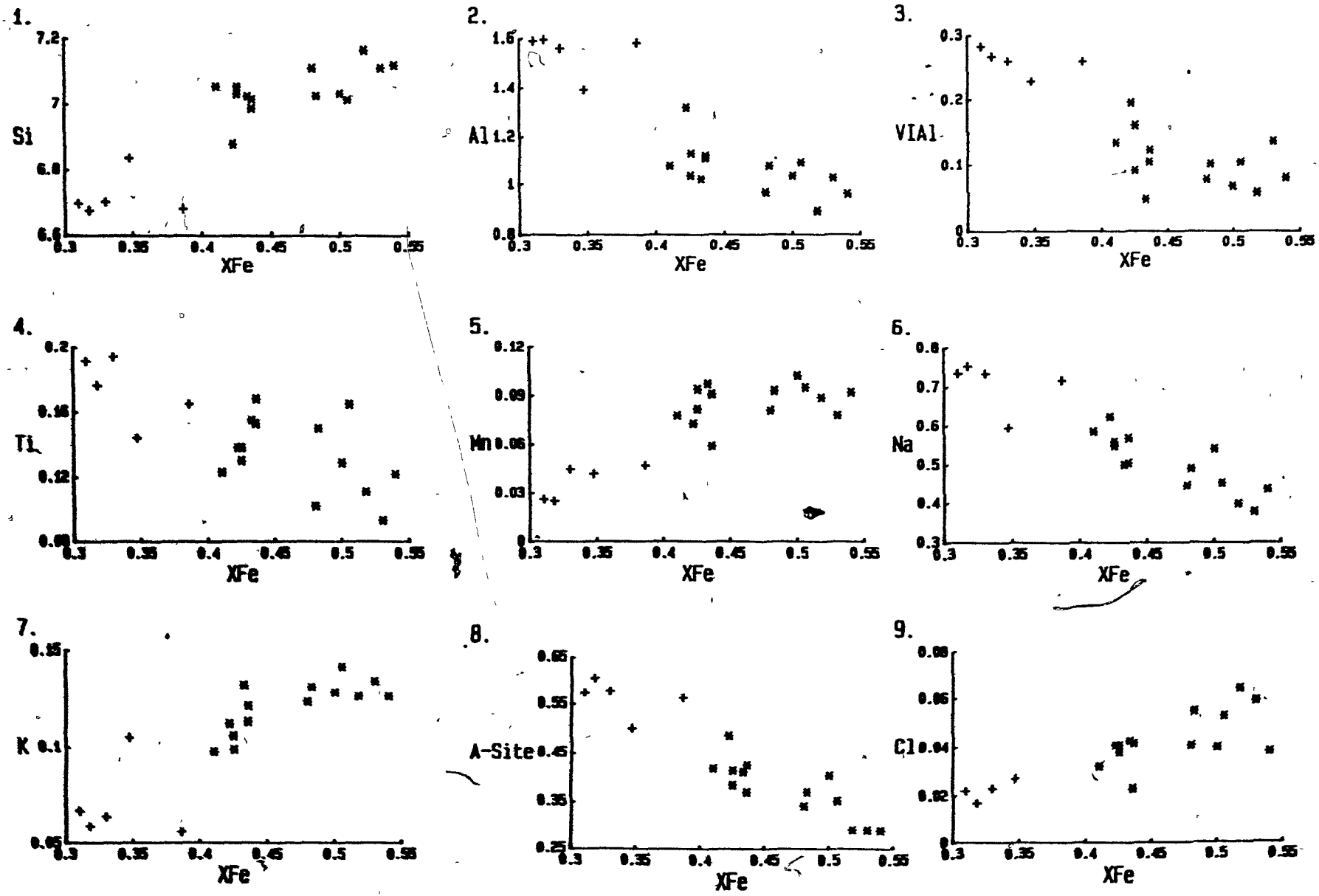
1.
Si
XFe
2.
Al
XFe
3.
VIAl
XFe
4.
Ti
XFe
5.
Mn
XFe
6.
Na
XFe
7.
K
XFe
8.
A-Site
XFe
9.
Cl
XFe

(principally ^{iv}Al), Fe, K, Na and A-site occupancy, and increasing Mg with increasing Si are probably the result of progressive re-equilibration of the amphibole at lower temperatures and higher $f(O_2)$ (Spear 1981). The trends are similar to those observed from zoned crystals that partly fill amygdular cavities and from the recrystallized groundmass amphibole in the fine-grained mafic inclusions (Chapter 2). Similar trends have also been reported from other felsic intrusive bodies (e.g., Czamanske and Wones 1973, Mason 1978, Chivas 1981). The siliceous character of the amphibole is unlikely to be of magmatic origin (Leake 1971, Gilbert et al. 1982) and probably results from progressive recrystallization under subsolidus conditions in the presence of a fluid phase.

The amphiboles generally contain more than 0.6 wt. % F and 0.15 wt. % Cl (Table A8.4). The highest values (averaging 1.69 wt. % F and 0.28 wt. % Cl) are found in a sample of K-feldspar-dominant granite (MG57); the lowest values are found in white granodiorite (MG97).

All three amphibole groups exhibit correlations between A-site minus NaM4 versus ^{iv}Al (Fig. 4.6.1), indicating that the edenite substitution is important. Analyses from MG42 show correlations between Ti and ^{iv}Al (Ti-tschermakite; Fig. 4.6.2) and ^{vi}Al versus ^{iv}Al (tschermakite; Fig. 4.6.3), suggesting that these substitutions also occur. Substitutions involving Na in the M4 site (e.g., riebeckite and richterite) probably also occur (Chapter 3).

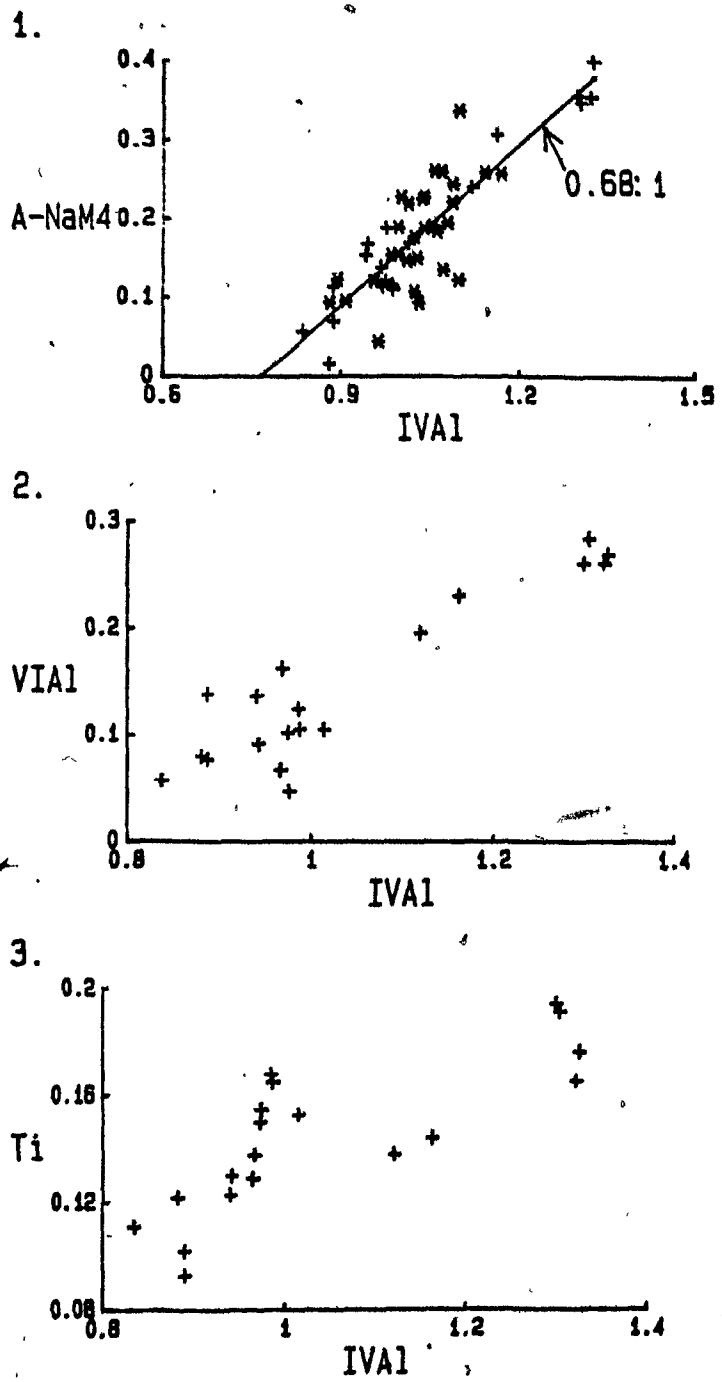

4.6. Compositional variations indicative of possible coupled substitutions. Star: selected granite amphibole analyses, cross: amphibole analyses from MG42 (granite porphyry). 4.6.1. Total A-site cations less Na in the M4 site versus tetrahedral Al. Line is a least-squares regression of the data from MG42 and has a slope of 0.68. 4.6.2. Octahedral Al versus tetrahedral Al. 4.6.3. Ti versus tetrahedral Al.

Biotite

Titaniferous biotite or titanbiotite typically forms anhedral to subhedral, commonly interstitial, light tan to dark brown pleochroic flakes. A sample of white granodiorite (MG3) also contains pale yellow to green pleochroic grains of biotite that, along with brown biotite, form crystallographically-oriented inclusions in quartz and plagioclase (Fig. 4.2.5). Inclusion content is variable, with oxides, apatite and zircon most commonly observed. Very minor incipient alteration to chlorite, with or without titanite or epidote, is common.

The compositions plot close to the phlogopite-annite join (Fig. 4.7) and span a relatively wide range of X_{Fe} content (0.42-0.60). As with the syenites and the quartz monzonites, Si+Al in biotite is commonly less than four. Although Al and Ti are generally lower and Mn is generally higher in the K-feldspar-dominant and K-feldspar porphyritic granites than in the plagioclase-dominant granites (Table A9.3), the data displays no clear trend.

The occurrence of the highest Al contents in the biotite from MG3 (white granodiorite), the only granitic sample analyzed in which no other mafic phases are present, is consistent with the observations of Nockolds (1947). These biotites also exhibit the lowest Ti contents (2.4-2.94 for the brown and 0.44-1.26 wt. % TiO_2 for the green) of all the grains analyzed and are probably not saturated with Ti. The absence of any Ti-rich phase such as ilmenite or titanite in this sample is consistent with this inference. The green color probably reflects both the low Ti content and a moderate to high Fe^{3+} content (Deer et

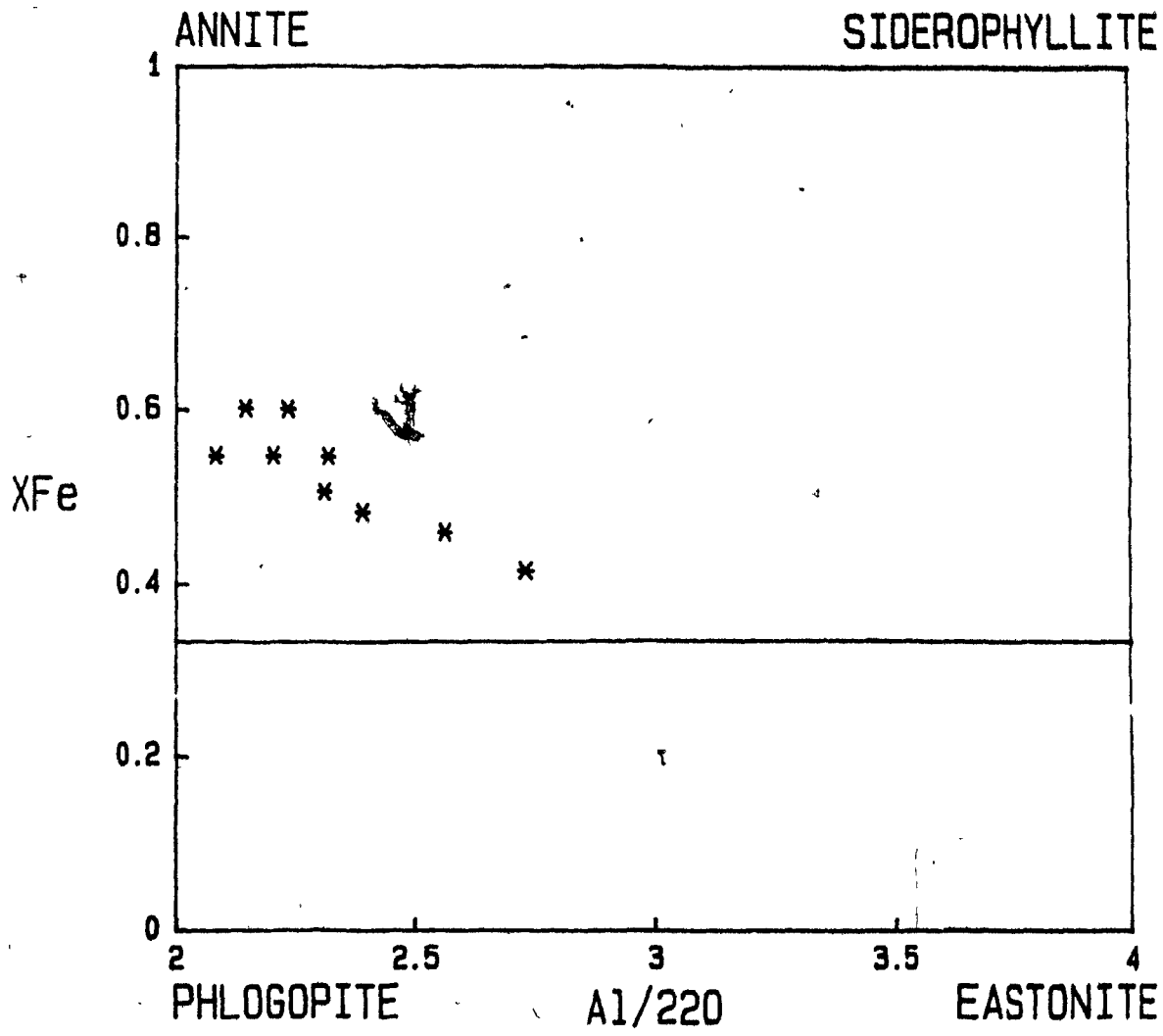

4.7. Average biotite compositions from the granites projected into the phlogopite-annite-eastonite-siderophyllite compositional field. Subfields as in Figure 2.14.

al. 1975). Relative to the brown biotite, the green variety is characterized by lower Ti, Mn and Fe, and higher Mg, Al and Si contents. Its origin is unclear; however, the more abundant brown biotite is likely to represent the equilibrium composition.

The X_{Fe}^{3+} obtained from different fractions of the same biotite separate may be very different (Table 2.1). When large discrepancies between the two determinations from the same separate are present, the higher value was discounted on the assumption that the X_{Fe}^{3+} of hornblende should be greater than that of the coexisting biotite (Dodge and Ross 1971, Stephenson 1977). Apart from minor amounts of chlorite, epidote and green biotite (adding to less than 5%), brown biotite is the only ferromagnesian mineral present in the white granodiorite studied (MG3); the X_{Fe}^{3+} of the biotite (0.19) is therefore taken to be that of the whole rock. The observed range of X_{Fe}^{3+} (0.17 to 0.20) is consistent with the limited range exhibited by the amphiboles (Table 2.1). In a plot of Fe^{2+}-Fe^{3+}-Mg (Wones and Eugster 1965), the compositions plot parallel to and about halfway between the Ni-NiO and H-M buffer curves (Fig. 2.15), suggesting a relatively high internally buffered $f(O_2)$. Biotite from I-type intrusive bodies of the Sierra Nevada batholith define a similar trend (Dodge et al. 1969).

Average F values are generally greater than 1.3 wt. % (Table A9.3) and exhibit a distribution similar to amphibole, i.e., highest in a sample of K-feldspar-dominant granite (MG57, 3.1 wt. %) and lowest in the white granodiorite (MG3, 68; 0.11-0.24 wt. % F). Average Cl contents are much less variable (0.34 to

0.44 wt. % Cl).

The most important controls of the halogen content of biotite are: 1) the activity of the halogen ion or acid present during crystallization, 2) the composition of the biotite, 3) the temperature of hydroxyl-halogen exchange, and 4) the effects of subsolidus leaching or enrichment due to hydrothermal fluids (Munoz 1984). The most important compositional control on the F-content is X_{Fe}, as Fe^{2+} prefers to form bonds with OH over F (Fe-F avoidance; Rosenberg and Foit 1977). Cl exhibits the reverse relationship, being concentrated in biotite with increasing X_{Fe} (Volfinger et al. 1985).

There is no evidence of a correlation between X_{Fe} and F-content (Fig. 4.8.1). This may reflect the importance of other factors [e.g., increasing f(HF)] or the large amount of analytical error inherent in the determination of F (Appendix I). The occurrence of highly F-enriched biotite (and amphibole) and the presence of fluorite in highly evolved samples of K-feldspar-dominant granite is consistent with a high f(HF), either in the magma or in the fluids derived from the magma (e.g., Munoz and Ludington 1974). The restricted variation exhibited by Cl with increasing X_{Fe} (Fig. 4.8.2) indicates that f(HCl) did not vary much and may even have decreased.

Interrelations of Mafic Silicates

Values of K_D between amphibole and biotite for both X_{Fe} and Mn are quite variable, ranging from 0.72 to 1.25 and 1.95 to 3.27 respectively (Table 3.1), whereas those for Ti exhibit a more limited range (0.30-0.39). These ranges overlap those

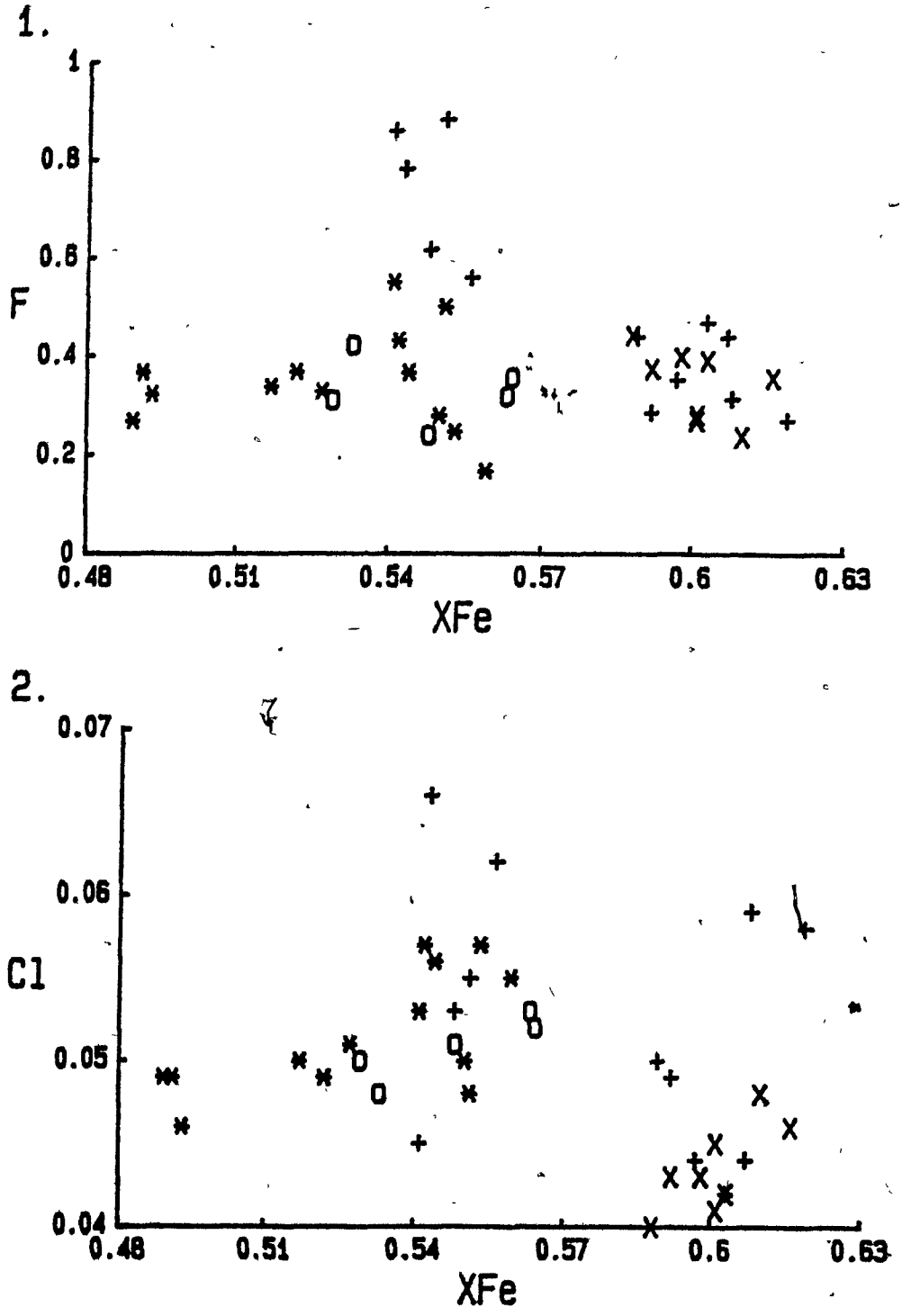

4.8. Variation of halogen content of biotite with X_{Fe} (in atoms per 23 oxygen atoms). Star: granite porphyry (MG42, 51), open circle: plagioclase-dominant granite (MG46), X: K-feldspar-porphyritic granite (MG83), cross: K-feldspar-dominant granite (83-55, MG57). 4.8.1. F versus X_{Fe}. 4.8.2. Cl versus X_{Fe}.

			KDFe-Mg		Mn1/Mn2			Ti1/Ti2				
Sample	Unit	Amphibole	Cpx/Amph	Amph/Bio	Amph/Cpx	Bio/Cpx	Amph/Bio	Amph/Cpx	Bio/Cpx	Amph/Bio	FAmph/FBio	ClAmph/ClBio
M642*	GP	Mag. hbl.	-	0.96	-	-	2.00	-	-	0.34	0.67	0.56
M646	PDGR	Mag.-hbl.	-	0.72	-	-	3.27	-	-	0.33	0.58	0.51
M661	GP	Mag.-hbl.	-	0.90	-	-	2.23	-	-	0.39	0.52	0.65
83-55	KFDG	Ferro-hbl.	-	0.90	-	-	1.95	-	-	0.32	0.52	0.55
M667	KFDG	Ferro-hbl.	-	1.25	-	-	2.63	-	-	0.31	0.54	0.64
M683	KFPG	Ferro-hbl	-	0.96	-	-	2.19	-	-	0.30	0.79	0.53

Table 4.1. Distribution coefficients (K_D) representing the co-distribution of Fe-Mg, Mn, Ti, F and Cl between the mafic minerals of the granites. Refer to Table 2.3 for the method of calculation. KFDG: K-feldspar-dominant granite. Other rock types as in Table 2.1. *: rim composition of a zoned amphibole phenocryst used in the calculation.

observed in the quartz-poor felsic rocks (Chapter 3). The Famph/Fbio values are all less than one, as expected, and fall within the range seen in the quartz-poor felsic rock types. A limited range of Clamph/Clbio values are observed, similar to those exhibited by quartz-poor felsic samples containing nonsilicic amphibole.

ACCESSORY MINERALOGY

Oxide Minerals

Both magnetite and ilmenite exhibit the same general textural and compositional characteristics as in the quartz-poor felsic rock types (Chapter 3). The primary ilmenite exhibits a range of Mn contents similar but even more restricted (3.9-5.2 wt. % MnO) than that of the quartz-poor felsic samples.

Other Accessory Minerals

Traces of apatite and subhedral to euhedral zircon (in some cases zoned) are ubiquitous, and are commonly associated with the mafic minerals. Allanite is observed in most samples (e.g., MG46, 51), forming anhedral or interstitial to subhedral, commonly zoned, pale yellow to dark brown pleochroic grains.

With one exception (MG3), interstitial or rare subhedral titanite is observed in all the granitic samples studied. In most cases, however, the titanite appears to be secondary, resulting from the breakdown of mafic and oxide minerals.

DISCUSSION

The mafic silicates, especially amphibole, can be used to aid in the classification of granites (e.g., Chappell and White 1974, Wones and Gilbert 1982). In A-type plutons, amphibole is

commonly alkali- and iron-rich, with the calcic amphiboles typically ranging from ferro-edenite to hastingsitic hornblende in composition (Czamanske et al. 1977, Anderson 1983). The observed compositional range of the amphibole within the McGerrigle granites (magnesio-hornblende to ferro-edenite) is more typical of I-type granite (e.g., Czamanske et al. 1981) and is consistent with the subalkaline to mildly alkaline whole-rock compositions.

On the other hand, the high F contents of the biotite and amphibole and the occurrence of minor accessory fluorite in the McGerrigle granites are more typical of A-type magmas, which are characterized by relatively high activities of fluorine (Loiselle and Wones 1979, Collins et al. 1982, Clemens et al. 1986). Fluorine affects both the chemical and physical properties of the melt as well as its evolution, by decreasing viscosity (Burnham 1979), and by increasing the stability of amphibole and the ability of the melt to retain large, highly charged cations such as Ga, Nb, Zr and REE (Collins et al. 1982). The F-enriched character of the granites may be inherited from their source, but could also be enhanced through magmatic evolution (e.g., Pichavant and Manning 1984).

In plagioclase-dominant samples the biotite and amphibole exhibit a limited range in $X_{Fe^{3+}}$ that correlates poorly with that of the whole rock (Fig. 4.9). However, a general trend of increasing X_{Fe} (amphibole or biotite) versus X_{Fe} whole rock is observed (Fig. 3.11). These granites therefore follow "Trend II" of Wones and Eugster (1965), indicating that the $f(O_2)$ of the magma was internally buffered, probably by the oxide

1.

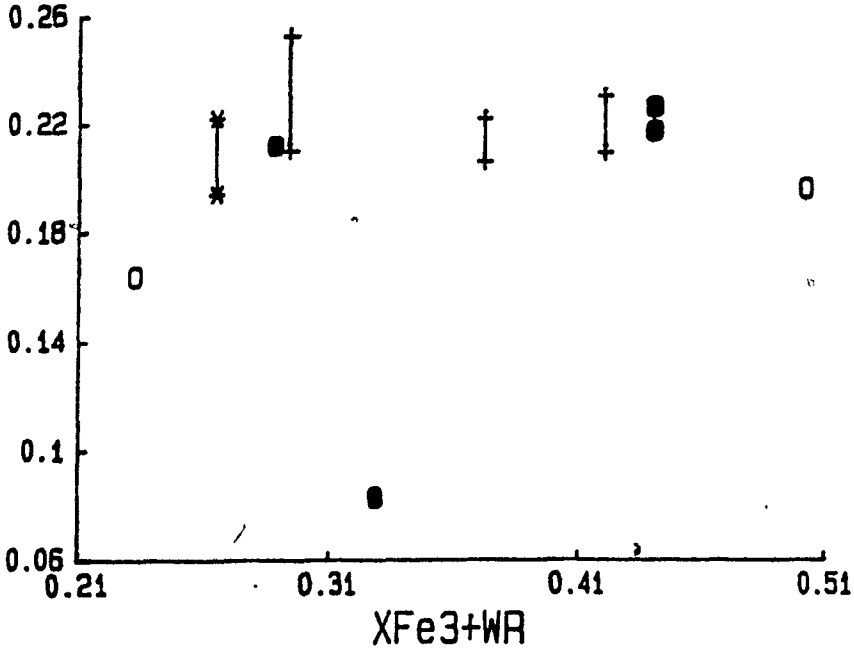

2.

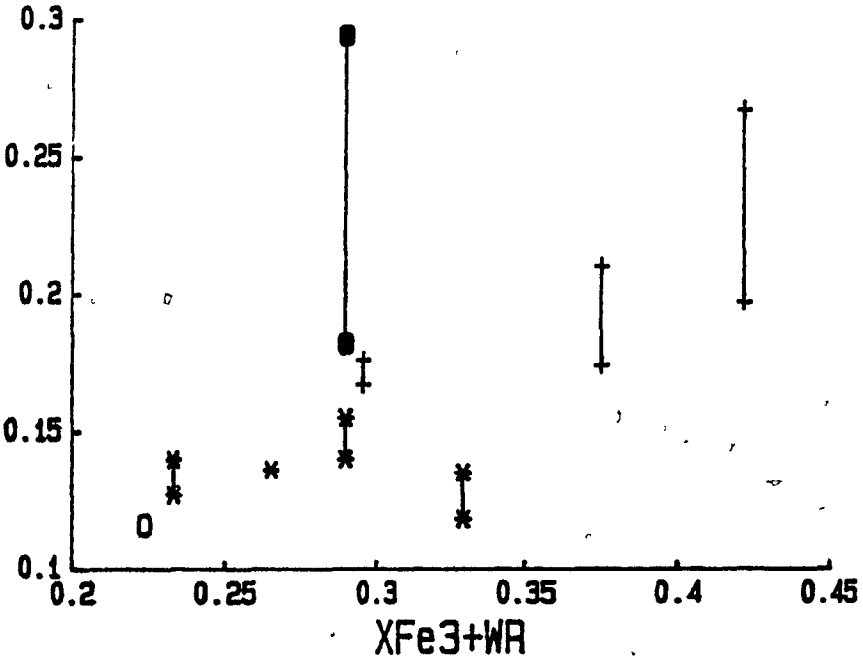

4.9. The relation of whole-rock and mineral compositions in terms of X_{Fe}^{3+} ($Fe^{3+}/(Fe^{3+}+Fe^{2+})$). Symbols are the same as in Figure 2.15. Lines join duplicate analyses of the same sample. 4.9.1. X_{Fe}^{3+}amphibole versus X_{Fe}^{3+}whole rock. 4.9.2 X_{Fe}^{3+}biotite versus X_{Fe}^{3+}whole rock.

minerals.

Data from the K-feldspar-dominant granite are more limited, as the generally poor condition of the mafic silicates in these rocks discouraged determination of redox ratios. The compositionally most evolved sample of K-feldspar-dominant granite studied (MG57) contains amphibole that plots on the continuation of the trend of the plagioclase-dominant granite (Fig. 3.11.1). Biotite, however, shows a lower X_{Fe} than expected. Significantly, the subhedral to nearly euhedral amphibole in this sample appears to have crystallized earlier than biotite, which is interstitial. This may indicate an increase in $f(O_2)$ between crystallization of amphibole and that of biotite (e.g., Wones and Eugster 1965, Czamanske and Wones 1973). The increase in $f(O_2)$ may reflect an increase in $f(H_2O)$ or loss of H_2 via a fluid phase during the crystallization history of this sample (e.g., Whitney 1972, Czamanske and Wones 1973). The limited evidence of local saturation by a fluid phase in the more evolved granites (e.g., miarolitic cavities, rare pegmatites) is also consistent with the latter possibility (e.g., Jahns and Burnham 1969). A more detailed study of the K-feldspar-dominant granite would be required to fully evaluate the role of fluid saturation during its crystallization.

No attempt has been made to quantify the conditions under which the granites crystallized. The $X_{Fe}3+$ of the biotite implies relatively oxidizing conditions, between the NNO and HM buffers (see above). Surprisingly, the $X_{Fe}3+$ of biotite from the white granodiorite (MG3), which contains no oxide minerals, plots parallel to that from the other granites (Fig. 2.15),

indicating that it crystallized at a similar $f(O_2)$.

The occurrence of interstitial titanite in many samples also indicates a relatively high $f(O_2)$ [Chapter 5], at least during late crystallization and early postmagmatic stages (Carmichael and Nicholls 1967, Czamanske and Wones 1973). The stability curve calculated for the assemblage titanite-magnetite-quartz-amphibole by Noyes et al. (1983) lies between the NNO and HM buffers.

The chemical characteristics (low K, Ti and Fe^{3+}, and high Mg and Ca) of the white granodiorite (MG3) are distinctive among the granites. These chemical characteristics, as well as trace-element data (C. Gariépy, unpubl. data), are consistent with large-scale exchange of chemical components between MG3 and the fine-grained mafic inclusions which represented coexisting mafic liquid (Chapter 2), found at the same outcrop. Similar associations have been ascribed to liquid immiscibility (e.g., Bender et al. 1982); though this is not considered to be the case in the McGerrigle Plutonic Complex, it is clear that the distribution of elements between the two liquids was in part controlled by liquid-liquid distribution coefficients analogous to those determined for immiscible liquids (Watson 1976, Ryerson and Hess 1978). For example, the lack of oxides within MG3 probably reflects the low Ti and Fe^{3+} content of the whole rock (cf. Carmichael et al. 1974). However, the composition of biotite indicates an $f(O_2)$ similar to that of the other granites (see above). Another possible explanation for the low abundance of these elements is the preferential partitioning of Fe (Fe^{3+}) and Ti into the mafic inclusion (liquids) through

diffusion (Yoder 1973, Ryerson and Hess 1978). The presence of ilmenite and magnetite in white granodiorite from the same outcrop but close to the contact with a chilled mafic inclusion is consistent with such a hypothesis.

The occurrence of highly recrystallized laths of plagioclase (MG42, 46, 51, 57, 83), zoned plagioclase with an An-rich core (MG3, 42, 46), rapakivi texture (MG83), rare mafic clots (MG42, 51) and amphibole xenocrysts (MG42) is consistent with variable amounts of contamination of the granitic liquid. These features are typically best developed in the plagioclase-dominated samples (e.g., MG42, 46, 51).

Apparent xenocrysts, especially of mafic minerals, are generally less abundant in the granites than the quartz-poor felsic rocks. The An-rich core compositions (up to An_{59}) of some of the zoned plagioclase laths from the plagioclase-dominant granites and the relatively primitive composition of the apparently xenocrystic brown amphibole (edenitic hornblende) of MG42 suggest relatively primitive source(s) of contamination (e.g., gabbro or monzodiorite, cf. Chapter 2).

The exact mechanism by which the contamination occurred is unclear. The rapakivi-textured grains are interpreted to result from magma mixing (see above, Hibbard 1981). However, samples containing abundant plagioclase xenocrysts, especially when present in compound grains, could just as easily be explained by contamination by previously crystallized material (i.e., hybridization). The predominance of plagioclase xenocrysts may reflect the settling out of mafic xenocrysts and aggregates owing to their higher density or the predominance of

plagioclase among the phenocryst phases in the contaminating magma.

CHAPTER 5. FIELD RELATIONSHIPS, PETROGRAPHY AND MINERALOGY OF THE NEPHELINE SYENITES

INTRODUCTION

The occurrence of small amounts of felsic undersaturated alkaline rocks in the McGerrigle Plutonic Complex is unique in the Gaspé area. This rock type was first identified by de Römer (1974, 1977), who interpreted it either as a recent hypabyssal intrusion or as xenoliths in granitic or syenitic hosts. De Römer (1977) also reported the existence of a relatively large area of nepheline syenite cross-cutting the granite and hybrid rocks just east of Les Cônes in the southern part of the complex. This was not substantiated in this study. A whole-rock chemical composition of such nepheline syenite (Anal. 99, Table 4; de Römer 1977) is almost identical to compositions of inclusions of endoskarn (Chapter 2), which are common in the same area (cf. Anal. 55, Table 2; Whalen and Gariépy 1986).

The nepheline syenites can be subdivided into two groups on the basis of differing chemical, mineralogical and field characteristics: 1) tinguaite dykes or sills (Sørensen 1974a, b), and 2) pods(?) of miaskitic nepheline syenite (that can also be classified as pulaskite). Together, both types of nepheline syenite make up less than 1 % of the exposed part of the complex. K-Ar dating carried out on a biotite separate from the miaskitic nepheline syenite (Whalen and Roddick 1987) indicates an age of 377±9 Ma, similar to that obtained from silica-oversaturated rocks of the hybrid suite.

FIELD RELATIONSHIPS AND PETROGRAPHY

Tinguaite

Tinguaite dykes and sills, up to 3 m across, were mapped at several localities in the northern half of the complex (cf. Whalen 1986). They are grey or dark green, typically porphyritic, with a very fine-grained to medium-grained groundmass. The tinguaite dykes or sills (occurring in pairs in some areas) typically cross-cut leucocratic intermediate rock types (syenites, quartz monzonites, etc.) and, at one locality, plagioclase-dominant granite (Whalen 1986). Chilled margins are commonly observed, with little or no evidence of metasomatism of the host rock at the contact.

The inclusions present in several of the tinguaites can be subdivided into two different types: 1) xenoliths, and 2) cognate inclusions. The first type occurs as rare angular to subangular metasomatized xenoliths of typically intermediate composition, up to 4 cm. These inclusions are more mafic than the wall rocks observed at the present level of exposure. The cognate inclusions occur as white to grey, fine- to coarse-grained, equigranular to porphyritic, round to elongate inclusions (e.g., MG98) ranging from less than one to over ten centimetres in size. Some of the larger cognate inclusions appear to be caught in the process of breaking up along their margins.

Within the bodies of tinguaite, K-feldspar occurs as subhedral to euhedral, pristine to moderately turbid perthitic laths or phenocrysts. Some phenocrysts exhibit a glomeroporphyritic texture (Fig. 5.1.1). The laths (both

FIGURE 5.1. TINGUAITES

1. Glomeroporphyritic perthitic K-feldspar phenocrysts in a fine-grained groundmass. Crossed polars. Scale bar = 0.5 mm. Sample from a peralkaline tinguaite sill (MG39).

2. Trachytic (pilotaxitic) texture formed by laths and phenocrysts of perthitic K-feldspar. Crossed polars. Scale bar = 0.5 mm. Sample from a tinguaite dyke (84-162).

3. A phenocryst of turbid perthitic K-feldspar (K) has undergone recrystallization (albitization?) to nonturbid secondary feldspar (r; light grey) principally along its margin. The phenocryst is characterized by a very patchy extinction. Scale bar = 1 mm. Sample from a peralkaline tinguaite dyke (84-105).

4. Recrystallized remnants (P) of feldspar (plagioclase?) at the core of a perthitic K-feldspar phenocryst (K). Crossed polars. Scale bar = 0.5 mm. Same sample as Fig. 5.1.1 (MG39).

5. Euhedral zoned aegirine crystal (Ae) containing a grass-green core and a blue-green titanian aegirine rim. Grain is cross-cut by fluorite (F). Scale bar = 0.1 mm. Sample from a peralkaline tinguaite dyke (MG37).

6. Euhedral phenocryst of arfvedsonite (A) coexisting with a phenocryst of aegirine (Ae). Scale bar = 0.25 mm. Same sample as Fig. 5.1.5 (MG37).

7. Remnants of sodic pyroxene (Ae) at the core of sodic amphibole (A). Crossed polars. Scale bar = 0.15 mm. Sample from a tinguaite dyke (84-149).

8. Zone dominated by grains of sodic pyroxene (Ae) is surrounded by grains of poikilitic amphibole (A) plus biotite which dominate the rest of the slide (with rare grains or remnants of alkali pyroxene). Scale bar = 1 mm. Same sample as 5.1.7 (84-149).


5
6
7
8

phenocrysts and in the groundmass) exhibit a weak to strong trachytic (pilotaxitic) texture (Fig. 5.1.2) that is typically best developed near the margin of the dyke (sill). In most samples the groundmass also contains (and in some cases is dominated by) allotriomorphic-granular, fine-grained patches of K-feldspar. Minor amounts of anhedral to subhedral albite are observed in the groundmass or as inclusions within K-feldspar phenocrysts. In one sample (MG39), highly recrystallized remnants of plagioclase(?) are visible in the core of some K-feldspar phenocrysts (Fig. 5.1.4).

Nepheline occurs in all samples as anhedral, commonly interstitial grains or, rarely, as anhedral to subhedral phenocrysts.

Clinopyroxene is the dominant mafic mineral in all the samples studied but one (84-149), in which amphibole is prominent. Biotite is ubiquitous, while amphibole occurs sporadically. The accessory mineralogy varies from dyke to dyke. Accessory minerals identified, some of which are secondary, include magnetite, ilmenite, pyrophanite, hematite, zircon, aenigmatite, sodalite, fluorite, pectolite, astrophyllite, apatite, titanite, pyrochlore, wohlerite and probable members of the eudialyte-eucolite(?) and rosenbushite-gotzenite(?) solid-solution series.

A white cognate inclusion (MG98) consists of an equigranular framework of moderately to strongly turbid perthitic laths of K-feldspar, with the rest of the minerals predominantly occurring as interstitial grains. Nepheline has apparently been completely replaced by secondary alteration products. Biotite

and clinopyroxene are the dominant mafic silicates, with subordinate amounts of amphibole also present. The accessory minerals identified, some of which are secondary, include magnetite, hematite, sodalite, apatite, titanite, zircon, calcite, fluorite, astrophyllite, pectolite(?) and cancrinite(?).

Miaskitic Nepheline Syenite

Pods(?) of miaskitic nepheline syenite are observed north of Mont Passe (cf. Whalen 1986). The poor outcrop coverage obscures the exact nature of the contact between the nepheline syenite and the surrounding rock types; however, it appears to intrude plagioclase-phyric syenite. The miaskitic nepheline syenite is grey, porphyritic with medium- to coarse-grained phenocrysts in a fine- to medium-grained groundmass. A highly metasomatized, irregularly-shaped mafic inclusion (approx. 10 cm long) was observed at one outcrop, whereas fine-grained cognate and possibly medium-grained alkali syenite inclusions occur at others. Beige or white, leucocratic "aplitic" rocks or veins cross-cut or are closely associated with the nepheline syenite at several outcrops.

K-feldspar forms anhedral to subhedral, pristine to strongly turbid, highly perthitic grains or phenocrysts. The elongate laths (either in groundmass or phenocrysts) commonly exhibit a trachytic texture. Rare anhedral to subhedral, twinned laths of albite are observed in the groundmass.

Nepheline forms anhedral, predominantly interstitial (occasionally poikilitic) to rare subhedral grains. It may be

intergrown with or included in K-feldspar phenocrysts.

Biotite is the dominant mafic mineral; it coexists with subordinate amounts of pyroxene. The accessory minerals are magnetite, apatite, zircon and titanite.

The "aplitic" samples exhibit an allotriomorphic-granular texture and consist almost entirely of mesoperthitic K-feldspar. Minor amounts of quartz (or, in some samples, nepheline), as well as titanite, pyroxene, biotite and opaque minerals are also present.

MAJOR-ELEMENT GEOCHEMISTRY

Selected modes, major-element compositions and norms are given in Tables A3.4 and A4.4. The miaskitic nepheline syenite has an agpaitic index (AI) of 0.93. The tinguaite dykes (sills) have an agpaitic index between 0.97 and 1.06 (C. Gariépy, pers. comm. 1985). Following Sørensen (1974b), the tinguaites would be classified as either intermediate (AI approximately equal to 1) or peralkaline (AI greater than 1).

Relative to the miaskitic nepheline syenite, the tinguaites contain greater amounts of Al, Fe, Mn, Na and incompatible trace elements (e.g., Zr, Nb, etc.) and lower amounts of Si, Ti, Mg, Ca, K, P and compatible trace elements (e.g., Sr, Ba, etc.; cf. Whalen and Gariépy 1986). Elemental variations between the different tinguaites do not reveal a simple relationship between chemical composition and agpaitic index. The intermediate tinguaite (MG94) studied is characterized by Ti, Fe, Mg, Ca, P and K contents nearly identical to those of the peralkaline tinguaites (Table 5.1). When the compatible trace elements are compared, MG94 contains lower amounts of Sr,

TABLE 5.1. A COMPARISON OF THE CHEMICAL COMPOSITION OF THREE TINGUAITES

Sample	MG37	MG39	MG94
SiO2 wt. %	59.56 (59.58)	59.97 (59.23)	60.77 (60.19)
TiO2	0.29 (0.29)	0.30 (0.23)	0.30 (0.30)
Al2O3	19.70 (19.31)	19.69 (19.33)	20.06 (19.70)
Fe2O3	3.05 (2.98)	3.64 (3.53)	2.51 (2.42)
FeO	0.90 (0.90)	0.40 (0.40)	1.40 (1.40)
FeOT	3.64 (3.58)	3.68 (3.57)	3.66 (3.58)
MgO	0.0 (0.07)	0.04 (0.03)	0.03 (0.04)
MnO	0.27	0.27	0.24
CaO	0.86 (0.90)	0.78 (0.78)	0.77 (0.78)
Na2O	9.35 (9.21)	9.28 (9.07)	8.78 (8.62)
K2O	5.05 (4.99)	5.13 (5.06)	5.05 (4.94)
P2O5	0.04 (0.09)	0.04 (0.08)	0.03 (0.09)
(Na+K)/Al	1.06	1.06	0.99
Rb ppm	186	183	175
Sr	27	71	9
Ba	70	87	77
Y	61	65	47
Pb	31	30	22
Zr	1803	1776	1348
Nb*	332	335	250
Ta*	17.9	-	16.2
Th*	59.4	61.0	35.2
La*	155.1	-	149.4
Ce*	248.5	-	233.7
Nd*	54.0	-	50.3
Sm*	9.39	-	8.47
Eu*	0.63	-	0.54
Tb*	1.38	-	1.16
Yb*	7.25	-	5.94
Lu*	1.22	-	1.03

Values in brackets and those marked by an asterisk were determined by Dr. C. Gariepy by XRF and neutron activation. Other values were determined at McGill University by XRF on a Philips PW1400 X-Ray spectrometer unit using either a fused pellet (predominantly major elements) or dry-pressed pellet (most trace elements).

similar Ba and lower amounts of Eu than the peralkaline tinguaites. Most incompatible elements (e.g., Zr, Nb, Y, Pb, Th and REE) are more abundant in the peralkaline tinguaites, whereas similar amounts of U, Rb and Ta are present in all three samples.

FELSIC MINERALOGY

K-feldspar

The K-feldspar is microperthitic; it varies from being weakly perthitic to mesoperthitic. The exsolved albite forms blebs, flames, patches, rims, braids or veins.

As in the other rock types grid twinning is only rarely developed and all the samples are monoclinic to X rays (Table A6.6). However, traces of microcline were identified in all spectra. The miaskitic nepheline syenite (MG16) contains orthoclase with the most ordered structure ($2t_1$=0.89). The tinguaites (MG37, 94) contain the most disordered K-feldspar sampled from the pluton, ranging from low sanidine to orthoclase ($2t_1$=0.72 to 0.79; Table A6.1). Both phenocrystic and groundmass K-feldspar were analyzed in MG94; the phenocrysts exhibit a lower degree of order. The data from the tinguaites are consistent with their occurrence as thin late-stage dykes that presumably cooled relatively rapidly, and experienced limited interaction with deuteric fluids.

In a b versus c plot (Fig. 5.2), the K-feldspar from the miaskitic nepheline syenite plots outside the quadrilateral of ideal cell-dimensions (Kroll and Ribbe 1983) for the alkali feldspars. Such deviations may result from the substitution of imperfectly-sized cations such as Rb and Fe^{3+} into the

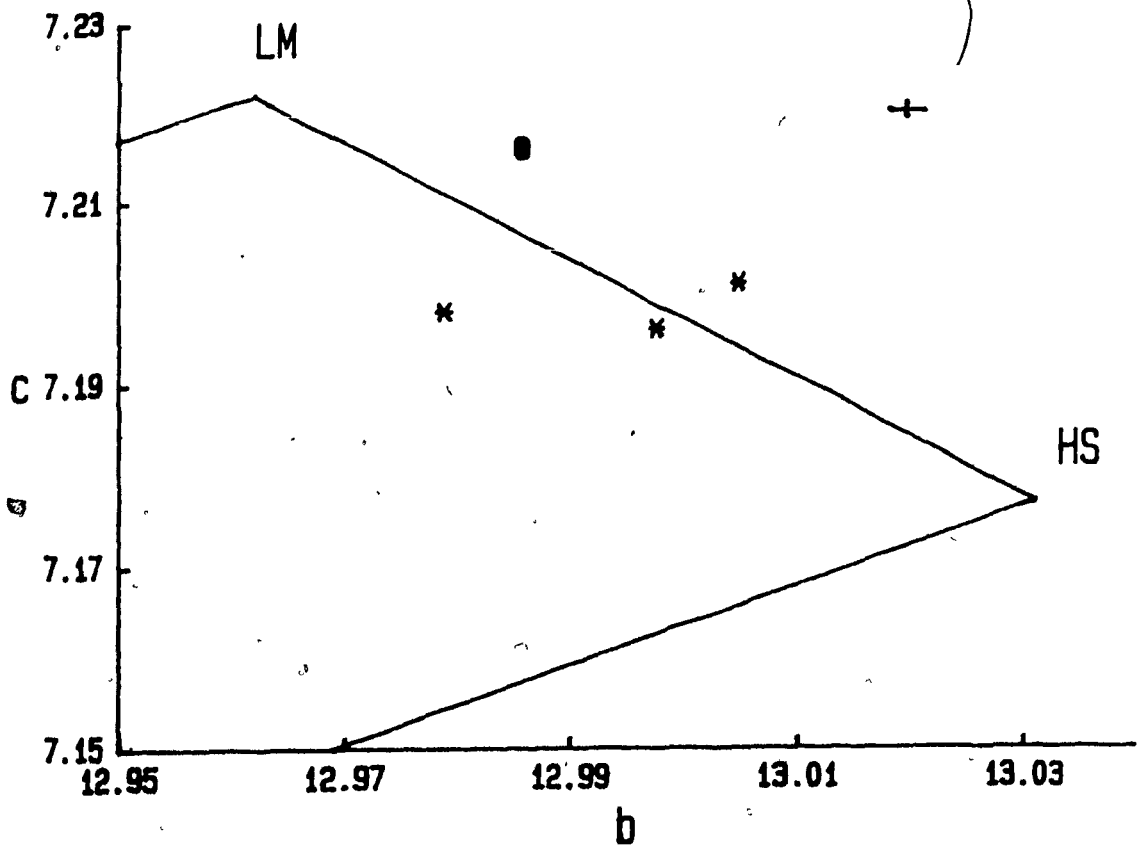

Figure 5.2. Plot of b versus c unit-cell dimensions for K-feldspar from the nepheline syenites. LM: low microcline, HS: high sanidine. Filled circle: miaskitic nepheline syenite, star: tinguaite. Units: Å. Error bar is the average for the samples plotted.

structure (e.g., Stevenson and Martin 1986).

Compositionally, the K-feldspar varies from Or_{94-100} (Table A6.1) indicating that extensive exsolution of albite has occurred. The exsolved albite in every sample has an estimated composition of An_0 (Table A6.2). The lower proportion of diffraction lines assigned unambiguously to K-feldspar than to albite (13 to 19 versus 31 to 54) suggests that the original homogeneous feldspar was albite-rich (e.g., White and Martin 1980). Although the feldspar in hypersolvus rocks commonly exhibits an Ab-rich bulk composition ($Or_{25-45}Ab_{70-50}An_{0-5}$; Sørensen 1974b), possible albite enrichment through metasomatism by a Na-rich fluid must also be considered. Petrographic evidence for such metasomatism is observed in some samples (Fig. 5.1.3). Such interaction must have occurred above the stability field of microcline (>400°C) and probably involved deuteric fluids generated during crystallization of the nepheline syenite. The presence of late-stage veinlets and veins cross-cutting the miaskitic nepheline syenites and some of the tinguaites (e.g., MG39) is consistent with the generation of such a fluid.

Feldspathoids

Nepheline is the most abundant feldspathoid. Average analyses (Table A5.4) exhibit low to moderate Ca (0-0.24 wt % CaO) and average Fe (0.19-0.72 wt. % Fe_2O_3). The observed discrepancies between Na+K+2Ca and $Al+Fe^{3+}$ (cation proportions) suggest some volatilization of the alkalis under the probe beam. The average nepheline compositions in the system nepheline-kalsilite-silica

(Table A5.4) plot near the ideal composition for plutonic nepheline ($Ne_{74.0}Ks_{22.1}Qtz_{3.9}$; Edgar 1984).

Sodalite is common in the peralkaline tinguaites, as interstitial grains or as anhedral to subhedral and, in some samples, possibly resorbed phenocrysts. However, it is typically absent or extremely rare in the miaskitic nepheline syenite and the intermediate tinguaites. The analyses of sodalite (Nos. 4, 7; Table A11.3) all indicate the ideal formula $Na_8(Al_6Si_6O_{24})Cl_2$, though the low Na contents (16.8-20.8 wt. % Na_2O) imply that significant loss of Na occurred during analysis. The compositions are characterized by low K and Ca and high Cl relative to sodalite data reported by Deer et al. (1963).

The agpaitic index of the magma does not appear to be a significant factor in determining sodalite stability as it is commonly reported from miaskitic rocks (e.g., Sørensen 1974b). Stormer and Carmichael (1971) concluded that the stability of sodalite is predominantly a function of silica activity; however, there is no evidence that the intermediate tinguaites were characterized by significantly higher activities of silica than the peralkaline ones. Rather, the scarcity of sodalite in the intermediate tinguaite studied (MG94) implies that other factors such as a lower Cl activity (e.g., Wellman 1970, Sood and Edgar 1970) were probably more important.

MAFIC MINERALOGY

Pyroxene

In the sample of miaskitic nepheline syenite studied, yellow-green to apple green pleochroic aegirine-augite (Table A7.4)

forms anhedral to subhedral, rarely interstitial, grains or phenocrysts. Rare grains exhibit slight normal or oscillatory zoning, with a rim typically darker than the core. In rare cases, remnants of colorless pyroxene are observed in the core. The grains that were analyzed, however, show an essentially uniform composition.

The tinguaites contain anhedral to euhedral, rarely interstitial prismatic grains or phenocrysts that vary from yellow-brown to deep green pleochroic aegirine-augite in the intermediate tinguaite (MG94), and yellow-green to grass green or deep green pleochroic aegirine in the peralkaline tinguaites (MG37,39) and the white cognate inclusion (MG98). In the peralkaline tinguaites, some grains have blue-green zones or, more typically, a rim of titanian aegirine (Fig. 5.1.5). A rare late-stage pale brown, slightly pleochroic rim of aegirine (No. 4, Table A7.4) is also observed on some grains of aegirine in one of the peralkaline tinguaites (MG37). In one sample (MG39), aegirine forms a mafic clot (Fig. 5.3.3) of nearly equigranular grains with minor amounts of biotite, magnetite and K-feldspar that may represent a pseudomorph.

Relative to sodic pyroxene compositions reported from alkaline undersaturated suites in the recent literature (e.g., Gomes et al. 1970, Larsen 1976, Brooks et al. 1982, Brousse and Rancon 1984), the McGerrigle pyroxenes are characterized by normal to moderately high Al contents (0.89-2.3 wt. % Al_2O_3), average to high Ti contents (0.36-4.0 wt. % TiO_2), low to moderately high Zr contents (0-1.8 wt. % ZrO_2) and average to moderately high Mn contents (0.30-2.4 wt. % MnO)

FIGURE 5.3. TINGUAITES

1. Poikilitic lepidomelane (b). Scale bar = 0.5 mm. Sample from an intermediate tinguaite dyke (MG94).

2. Remnants of Mg-rich biotite (b) at the core of an aegirine phenocryst (Ae). Scale bar = 0.15 mm. Sample from a peralkaline tinguaite sill (MG39).

3. Mafic clot consisting of approximately equigranular grains of aegirine (Ae) plus minor amounts of biotite, K-feldspar and magnetite. Scale bar = 0.5 mm. Same sample as Fig. 5.3.2 (MG39).

4. Pseudomorph after amphibole consisting of arfvedsonite (A), aegirine (Ae), pectolite (p) and minor fluorite. Scale bar = 0.5 mm. Sample from a peralkaline tinguaite dyke (Mg37).

5. Fibrous clump of astrophyllite (a), probably a pseudomorph after biotite; the black areas are aenigmatite. Scale bar = 0.5 mm. Sample from a peralkaline tinguaite dyke (84-105).

6. Zoned fluorite crystal (F). Scale bar = 0.1 mm. Medium-grained white cognate inclusion in a tinguaite dyke (MG98).

7. Wohlerite (w). Scale bar = 0.1 mm. Same sample as Fig. 5.3.1.

8. Pyrochlore (p). Scale bar = 0.1 mm. Same sample as Fig. 5.3.1.


1
3
5
W
7
8

The sodic pyroxene from the tinguaites is essentially silica-saturated (Si approximatly equal to 2.0); therefore, the majority of the aluminum is octahedrally coordinated, resulting in the presence of up to 10.1 mol. % jadeite component. Significant amounts of jadeite in low-pressure sodic pyroxenes are not uncommon in silica-undersaturated rock types (e.g., Popp and Gilbert 1972). The pale brown late-stage (possibly postmagmatic) aegirine overgrowths are the most enriched in the jadeite component, probably reflecting the increased stability of jadeite relative to nepheline and albite with decreasing temperature (Popp and Gilbert 1972, Rønsbo et al. 1977).

Whereas the Ti contents of the aegirine-augite in the miaskitic nepheline syenite and the intermediate tinguaite are uniformly low (0.38-0.55 wt. % TiO_2), the aegirine in the peralkaline tinguaites exhibits a wide range of values. The highest values are obtained from the blue-green rim, and the lowest are typically from the greenish core of both the groundmass and phenocrystic aegirine. Similar Ti-enriched aegirine in silica-undersaturated alkaline rocks has been reported at several other localities (e.g., Rønsbo et al. 1977, Ferguson 1977, Nielsen 1979). Since the aegirine is approximately silica-saturated, the component $CaTiAl_2O_6$, which controls titanium substitution in titansalite (Chapter 2), is not important in these pyroxenes. Rather, Ti incorporation is probably the result of the substitution of a $NaFM_{0.5}Ti_{0.5}Si_2O_6$ component (where $FM=Fe^{2+}$, Mg or Mn) into the pyroxene (Rønsbo et al. 1977, Ferguson 1977). The chief divalent cation involved is Fe^{2+}, as Mg and Mn are low in all cases and remain constant

or increase only slightly from the Ti-poor core to the Ti-rich rim in zoned aegirine (cf. Nos. 2, 3; Table A7.4). The presence of excess Na over calculated Fe^{3+} (or even total Fe) in all the grains analyzed from the tinguaites (but not in the miaskitic nepheline syenite) indicates that other Na-bearing components, such as jadeite and $NaFM_{0.5}Ti_{0.5}Si_2O_6$, must be present.

As Ti, Zr is concentrated in the blue-green rim of the titanian aegirine, even though both cations compete for the same site (M1; Larsen 1976). Zr probably enters the aegirine by substituting for Ti to form a $NaFM_{0.5}Zr_{0.5}Si_2O_6$ component (Ferguson 1977, Jones and Peckett 1980). Paradoxically, the lowest Zr values in the sodic pyroxene analyzed (commonly less than 0.1 wt. % ZrO_2) are also found in the peralkaline tinguaites, typically in cores of both groundmass and phenocrystic aegirine. The low Zr content of the core likely reflects the high solubility of zirconium in peralkaline melts (Watson 1979b). Zr enrichment in the pyroxene is therefore only observed when it crystallizes from late-stage residual liquids that are enriched in Zr (relative to the bulk rock).

The behavior of Mn mirrors that of Fe^{2+}; both elements are most abundant in the aegirine-augite of the intermediate tinguaite. Unlike biotite, the aegirine in MG39 is not highly enriched in Mg relative to that in MG37 (0.29-0.75 versus 0.23-0.47 wt. % MgO).

The compositional variation in sodic pyroxene can be illustrated in a plot of Na-Mg-Fe^{2+}+Mn (Fig. 5.4). The data points do not fall on a smooth trend, as has been reported for numerous other undersaturated alkaline complexes (e.g., Tyler

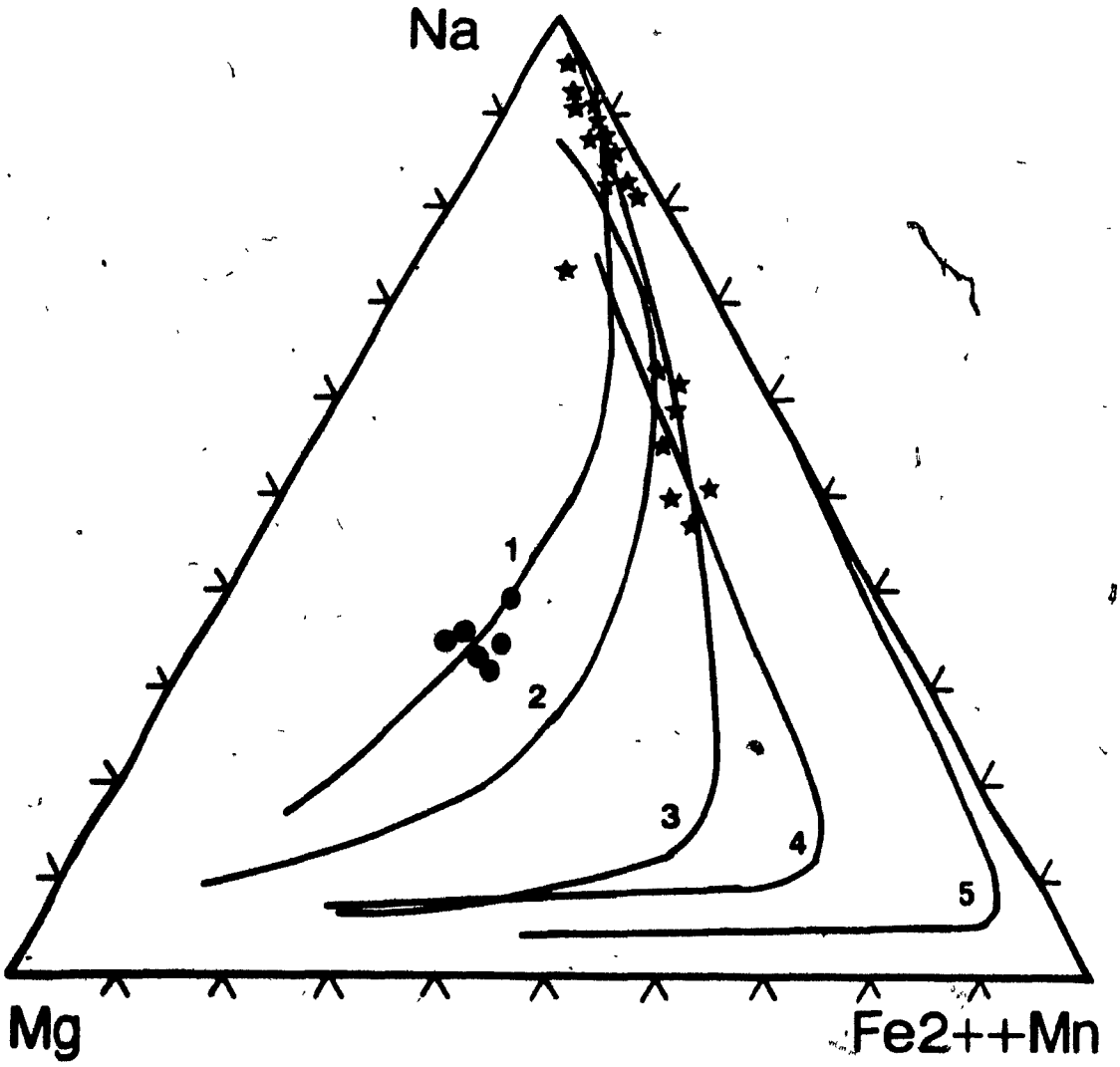

Figure 5.4. Selected pyroxene compositions plotted in terms of Na-Mg-Fe^{2+}+Mn. Symbols are the same as Figure 5.2. Pyroxene compositional trends from other silica-undersaturated alkaline suites: 1) Itapirapuã (Gomes et al. 1970), 2) Uganda (Tyler and King 1967), 3) South Qôroq (Stephenson 1972), 4) Coldwell nepheline syenites (Mitchell & Platt 1982), 5) Ilímaussaq (Larsen 1976).

and King 1967, Stephenson 1972). The reason is that the aegirine-augite from the miaskitic nepheline syenite is characterized by a much higher X_{Mg} than the aegirine-augite from the intermediate tinguaite dyke. A continuous compositional trend in this diagram is commonly interpreted in terms of consanguinity of the alkaline magmas from which the pyroxenes crystallized (e.g., Stephenson 1972, Nielsen 1979). The apparent lack of a smooth trend in the McGerrigle rocks does not disprove a genetic link between the tinguaites and the miaskitic nepheline syenites but indicates that processes or factors other than closed-system fractionation [e.g., variations of $f(O_2)$, $P(H_2O)$] must be partly responsible for the observed compositional variation.

Amphibole

Amphibole occurs in a minority of the tinguaites as anhedral to subhedral (rarely euhedral), commonly interstitial or poikilitic, unzoned grains or phenocrysts that exhibit a yellow-brown or brownish green to black or deep blue-green pleochroism. In one of the peralkaline tinguaites (MG37), amphibole also occurs in scarce fine-grained clots; it constitutes, with other minerals, an apparent pseudomorph after an amphibole xenocryst (Fig. 5.3.4).

Analyses from a peralkaline tinguaite (MG37) reveal a composition of manganoan potassian arfvedsonite (Table A8.5). Relative to arfvedsonite from other nepheline syenites (e.g., Larsen 1976, Ferguson 1977, Brooks et al. 1982) this one is characterized by high Mn (2.5-3.4 wt. % MnO) and K (2.1-3.3 wt.

% K_2O), and low Al (0.9-1.5 wt. % Al_2O_3), Mg (1.1-2.4 wt. % MgO) and Ca (0.7-1.7 wt. % CaO). Arfvedsonite is characteristic of the most highly evolved peralkaline rocks of alkaline undersaturated suites (Mitchell and Platt 1982).

Variable relationships between amphibole and sodic clinopyroxene are observed from one tinguaite to the next and even in thin section. In some cases one phase partly replaces the other (Fig. 5.1.7); however, examples where both appear to be at equilibrium are also observed (Fig. 5.1.6).

Biotite

Biotite is present in all the nepheline syenite samples studied; it is most abundant in the miaskitic nepheline syenite, where it forms light tan to dark greenish brown pleochroic, anhedral to euhedral, partly interstitial, flakes (up to 3 mm across) of manganiferous titaniferous biotite (Fig. 5.5; Table A9.4). It is less abundant in the tinguaite dykes. With one exception, these rocks contain anhedral to scarce subhedral or euhedral, commonly interstitial or poikilitic (Fig. 5.3.1) yellow-brown or orange, to dark brown or black pleochroic manganiferous titaniferous lepidomelane. The exception, a peralkaline tinguaite from a sill (MG39), contains anhedral, partly interstitial, flakes of pale brown to brown pleochroic manganiferous titaniferous Mg-rich biotite. In this sample, as well as in the white cognate inclusion studied (MG98), biotite also occurs as remnants in the core of aegirine grains (Fig. 5.3.2).

Relative to biotite compositions reported from other

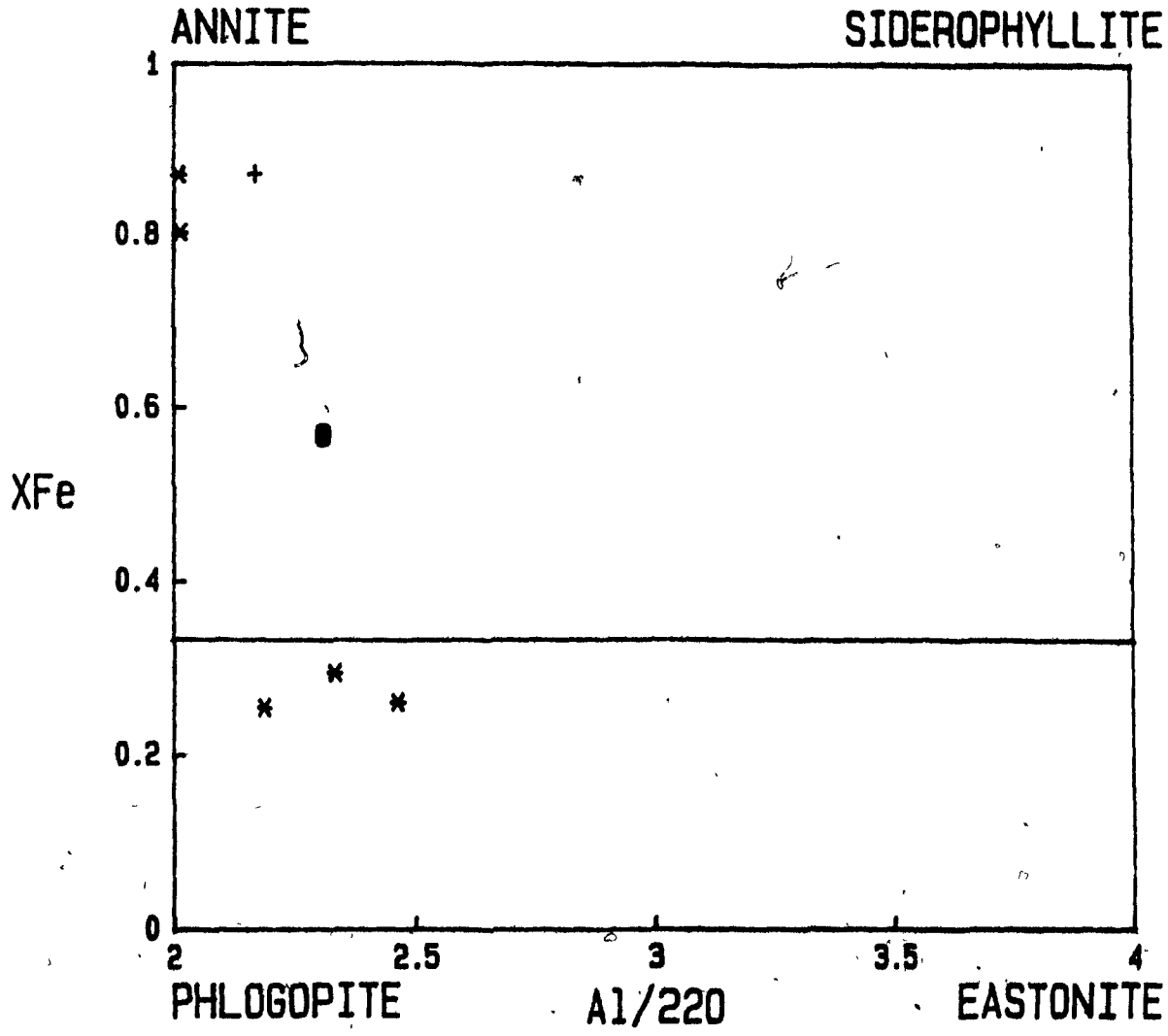

Figure 5.5. Selected biotite compositions from the nepheline syenites projected into the phlogopite-annite-eastonite-siderophyllite compositional field. Subfields as in Figure 2.14. Filled circle: miaskitic nepheline syenite, cross: intermediate tinguaite, star: peralkaline tinguaite.

nepheline syenite suites (e.g., Rock 1978, Mitchell and Platt 1982, Brooks et al. 1982), the McGerrigle examples are characterized by high Mn (1.6-4.8 wt. % MnO), moderate Ti (1.4-4.0 wt. % TiO_2) and low Na (0.03-0.18 wt. % Na_2O).

Biotite displays a large degree of compositional variation among the different samples of nepheline syenite. However, apart from a general trend of decreasing ^{iv}Al with increasing agpaitic index (Fig. 5.6.1), the observed compositional variations do not conform to a simple evolutionary sequence. Therefore, each type of biotite will be described separately.

The biotite from the miaskitic nepheline syenite is Mg-rich and Mn-poor relative to the lepidomelane of the tinguaites (Table A9.4). The lepidomelane is characterized by high Mn, variable Ti, low F and approximately constant X_{Fe}. The X-sites are typically completely filled in lepidomelane. The proportion of ^{vi}Al is very low in both the miaskitic biotite as well as the lepidomelanes, with Fe^{3+} required to occupy the tetrahedral site in some samples (e.g., MG94, 98).

The Mg-rich biotite observed in MG39 is characterized by a low X_{Fe}, high Mn and the presence of large amounts of ^{vi}Al. The low totals (91.6-94.0 wt. %) may indicate the presence of large amounts of Li; the high octahedral Al contents may reflect the substitution of $Li^{vi}Al$ for $2(Mg,Fe^{2+})$ (Vlasov 1966, Burt and Burton 1984).

The X_{Fe}^{3+} (Table 2.1) of the biotite from the miaskitic nepheline syenite (MG16) varies between 0.26 and 0.27, whereas one determination on lepidomelane (MG94) indicates an X_{Fe}^{3+} of 0.20. In terms of the Fe^{2+}-Fe^{3+}-Mg diagram (Fig. 2.15), the

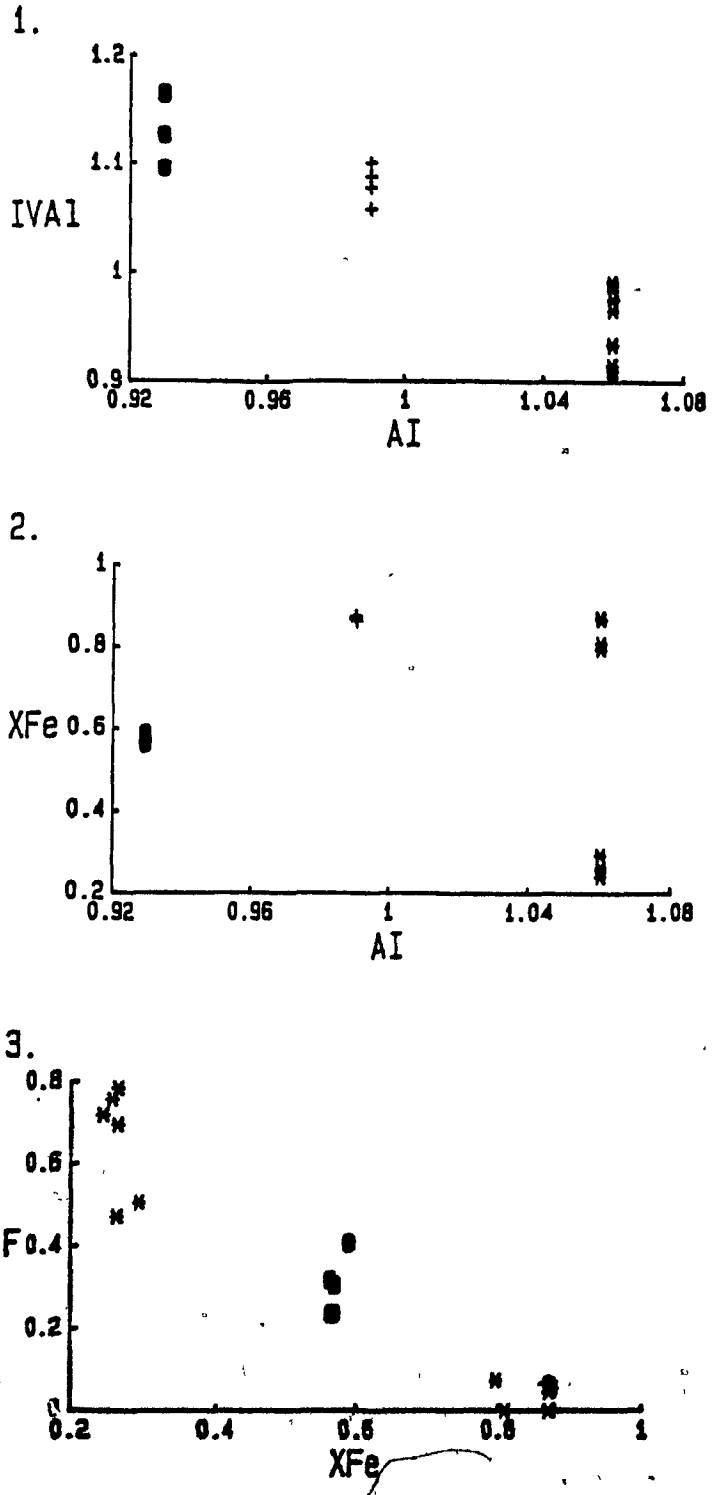

Figure 5.6. Compositional variations (in atoms per 11 oxygen atoms) of biotite in the nepheline syenites. Symbols are the same as in Figure 5.5. 5.6.1. Tetrahedral Al versus agpaitic index. 5.6.2. X_{Fe} versus agpaitic index. 5.6.3. F versus X_{Fe}.

biotite from the miaskitic nepheline syenite indicates $f(O_2)$ conditions above the hematite-magnetite buffer, whereas biotite from the intermediate tinguaite indicates a value between the Ni-NiO and Fe_3O_4-Fe_2O_3 buffers. However, the actual values are likely much lower, especially in the intermediate tinguaite, where the high Fe^{2+} (and Mn) and low Mg contents of the mica require the presence of appreciable amounts of Fe^{3+} to stabilize the structure even at low $f(O_2)$ conditions (Hazen and Wones 1972, Hewitt and Wones 1984).

The Mg-rich nature of the biotite from the miaskitic nepheline syenite and the peralkaline tinguaite (MG39) is consistent with a high $f(O_2)$ (cf. Wones and Eugster 1965). The presence of Mg-rich biotite is especially surprising in the peralkaline tinguaite where the whole-rock composition is very Mg-poor (0.04 wt. % MgO). The fact that the Mn content of the Mg-rich biotite of MG39 is almost identical to that of lepidomelane from another peralkaline tinguaite (MG37) of nearly identical whole-rock composition (cf. Table 5.1) indicates a close relationship between the two types of biotite. The shortage of Fe in the biotite can be related to the predominance of ferric over ferrous iron in the melt, as indicated by the high $X_{Fe^{3+}}$ of the whole rock (Table A4.4).

A decrease of F with increasing X_{Fe}(biotite) is observed (Fig. 5.6.3). Sodic amphibole in MG37 partitions F preferentially over biotite; this is the reverse of the typical relationship (e.g., Wones 1981). Both relationships reflect the Fe^{2+}-F avoidance rule (Chapter 4). Though the amphibole has a similar Fe content to the biotite, a large proportion of the

iron is probably located within the M2 site, which does not form direct bonds with an OH-site, unlike the M1 and M3 sites, or the M1 and M2 sites of biotite (Rosenberg and Foit 1977).

ACCESSORY MINERALOGY

Aenigmatite

Aenigmatite is observed in most peralkaline tinguaites studied (e.g., MG37); it forms red-brown to black pleochroic, anhedral to euhedral, partly interstitial, prismatic grains.

The aenigmatite (e.g., No. 2; Table A11.3) is characterized by low Al, Mg, Ca and calculated Fe^{3+}. The composition is therefore similar to that of end-member Ti-aenigmatite $Na_2Fe^{2+}_5TiSi_6O_{20}$ except for an extreme enrichment in Mn (4.6-5.9 wt. % MnO). The most Mn-enriched aenigmatite recorded so far (4.4 wt. % MnO) has been described from foyaite by Marsh (1975). The Fe^{3+}-poor nature of the aenigmatite is characteristic of that coexisting with arfvedsonite and aegirine, whereas its Ca- and Al-poor nature may reflect a relatively low temperature of crystallization (Larsen 1977). The lack of coexisting Fe-Ti oxide minerals is consistent with the existence of a no-oxide field where sodic pyroxene and aenigmatite coexist (Marsh 1975).

Oxide Minerals

The miaskitic nepheline syenite contains subhedral grains of magnetite that, in some cases, contain lamellae of pyrophanite (Table A10.4). The intermediate tinguaite (MG94) contains anhedral to rare subhedral, commonly interstitial, grains of magnetite as well as subhedral grains of ilmenite, that may

form clumps. Magnetite in MG94 invariably contains fine-trellis or sandwich intergrowths of Mn-rich ilmenite or pyrophanite (the width of the lamellae is smaller than the diameter of the probe beam used).

The aenigmatite-free peralkaline tinguaites (e.g., MG39) contain predominantly anhedral, in part interstitial, grains of magnetite that commonly exhibit replacement by hematite, pyrophanite or titanite.

The oxide minerals in the nepheline syenites are characterized by a high Mn content, as is commonly observed in other alkaline complexes (Neumann 1974, Brooks et al. 1982). The Mn enrichment of ilmenite lamellae or the presence of pyrophanite lamellae in magnetite reflect the preference of Mn for the rhombohedral over the spinel phase under low-temperature conditions of subsolidus "oxidation-exsolution" (e.g., Haggerty 1976). The Mn-rich compositions probably reflect the high Mn/Fe^{2+} ratio (0.112-0.667) of the parental magma, again reflecting their high $X_{Fe}3+$ values (Table A4.4).

Ilmenite is commonly absent from undersaturated rocks and magnetite is depleted in the ulvöspinel component (Haggerty 1976). In undersaturated magmas where a_{SiO2} is defined by the alkali feldspar - nepheline buffer (Carmichael et al. 1970) titanite is commonly the stable Ti-containing mineral. The stability of titanite can be related to $f(O_2)$ and a_{SiO2} as illustrated by the following reaction:

$3CaFeSi_2O_6 + 3FeTiO_3 + O_2 = 3CaTiSiO_5 + 2Fe_3O_4 + 3SiO_2$ (D. R. Wones, unpubl. manuscript)

that can be described by the following expression:

$$\log f(O_2) = G^{\circ}/RT + 3\log a_{CaTiSiO5} + 2\log a_{Fe3O4} + 3\log a_{SiO2} - 3\log a_{CaFeSi2O6} - 3\log a_{FeTiO3}$$

From this reaction it can be seen that titanite and magnetite would be favored by high $f(O_2)$ and low a_{SiO2} (at least above the titanite-perovskite buffer) if the activities of the other components are assumed to be constant.

In one of the peralkaline tinguaites (MG39), magnetite is not accompanied by an early-forming Ti-rich phase. The magnetite in these samples is characterized by exceptionally high Mn (8.3-9.3 wt. % MnO) and low Ti (0.06-0.16 wt. % TiO_2) and exhibits no petrographic evidence of having undergone "oxidation-exsolution" resulting in the formation of lamellae of a rhombohedral phase. As Mn should have been partitioned preferentially into any such lamellae, it appears unlikely that any major amounts of ilmenite was ever "exsolved" (though some Ti possibly diffused to the grain boundaries and formed secondary titanite during relatively high-temperature interaction with deuteric fluids; D. H. Lindsley, pers. comm. 1987). Therefore, the magnetite was probably initially highly depleted in titanium. Instead of forming a separate Ti-rich phase, the Ti appears to have been concentrated in aegirine (e.g., No. 5, Table A7.4) a situation consistent with a relatively high $f(O_2)$ in this tinguaite [e.g., Verhoogen 1962, Haggerty 1976]. The lack of primary titanite in these rocks may reflect a lower a_{CaO} in the tinguaites relative to the miaskitic nepheline syenite.

Other Accessory Minerals

The nepheline syenites, and especially the tinguaites, are characterized by a broad range of different accessory minerals, some of which have rarely been reported before in Canada (e.g., Traill 1980).

Titanite (No. 1, Table A11.3) crystallized early in the miaskitic nepheline syenite where it commonly forms rhomb-shaped or acicular grains, sometimes with a hollow core. In contrast, it commonly appears to be secondary in the tinguaites (with the possible exception of the white cognate inclusion), forming by deuteric alteration of the oxide phases.

Zircon is common in the miaskitic nepheline syenite and intermediate tinguaites, and typically exhibits textural evidence of a late crystallization [skeletal shape (poikilitic) or interstitial to K-feldspar]. Zircon is scarce or absent in the peralkaline tinguaites (MG39; No. 8, Table A11.3).

The zircon-free peralkaline tinguaites (e.g., MG37) contain a Na-Zr silicate (No. 5, Table A11.3) that forms predominantly interstitial, colorless to pale pink-brown, low-birefringent grains. This mineral is likely a member of the eudialyte-eucolite series $(Na,Ca,REE)_5(Fe^{2+},Mn)(Zr,Ti)[(Si_3O_9)_2](OH,Cl)$. The pale pink-brown zones may result from incipient alteration of the eudialyte-eucolite, as totals of analyses are invariably lower in those than in the colorless zones. The chief difference with previously reported compositions of eudialyte-eucolite minerals is the high Si (53.8-56.8 versus 46.1-53.4 wt. % SiO_2) and low Na (1.1-3.4 versus 11.4-15.7 wt. % Na_2O;

Deer et al. 1986). These discrepancies probably reflect Na loss through volatilization under the probe beam during analysis; similar analytical problems were reported by Carr et al. (1976).

The presence of zircon rather than a Na-Zr silicate in MG39 may appear anomalous as MG39 and MG37 are characterized by the same agpaitic index and near-identical whole-rock compositions (Table 5.1). Since MG39 exhibits petrographic evidence of contamination (e.g., Figs. 5.1.4, 5.3.3), the zircon could represent a xenocryst; however, no sign of resorption is visible. Since the formation of Na-Zr minerals depends on an excess of alkalis (Currie 1976), the presence of zircon in MG39 may be related to the higher Fe^{3+}/Fe^{2+} ratio of this rock. Watson (1979b) suggested that alkali complexing with Fe^{3+} (and Al) takes place in preference to alkali-zirconium silicate complexing; therefore, increasing the amount of Fe^{3+} in a melt will decrease the amount of alkalis available to complex with zirconium.

The intermediate tinguaite (MG94) also contains two other zirconium-rich minerals. The first occurs as colorless to yellow pleochroic, interstitial to rare subhedral grains (Fig. 5.3.7), some of which exhibit complex polysynthetic twinning. Its chemical composition (No. 10, Table A11.3) is similar to that of wohlerite ($NaCa_2(Zr,Nb)O[Si_2O_7]F$; Vlasov 1966). Colorless, low-birefringent, predominantly interstitial grains show a similar Ca/Na ratio, but lower totals (86.9-87.5 versus 92.3-93.5 wt. %; Table A11.3). They also show higher amounts of Ti (6.8-7.6 versus 1.1-1.2 wt. % TiO_2) and rare earths (e.g.,

0.73-1.0 versus 0.19-0.24 wt. % Ce_2O_3), and lower Zr (7.5-8.3 versus 13.7-14.2 wt. % ZrO_2) and Nb (1.2-1.5 versus 11.0-11.4 wt. % Nb_2O_3). This mineral may be a member of the rosenbushite-gotzenite series ($Ca_2Na(Zr,Ti)[Si_2O_7](O,OH,F)_2$; Deer et al. 1986) but this could not be confirmed by the available data.

The intermediate tinguaite also contains relatively rare pale yellow-green cubes of pyrochlore (Fig. 5.3.8; classified after Hogarth 1977), for which partial analytical data are given (No. 9, Table A11.3). The occurrence of pyrochlore is probably the result of both the high whole-rock Nb (250 ppm) and Ta (16.2 ppm) contents and the absence of large amounts of Ti- or Na-Zr-phases such as titanite, into which Nb and Ta could substitute (Gerasimovsky 1974).

Astrophyllite, $(K,Na)_3(Fe,Mn)_7Ti_2[Si_4O_{12}]_2(O,OH,F)_7$, forms prismatic or fibrous grains in many samples of peralkaline tinguaite (e.g., MG37). Incipient alteration of biotite to astrophyllite, mainly along cleavage planes, is observed in some samples. In one sample astrophyllite forms round, fibrous clumps (Fig. 5.3.5) that appear to represent pseudomorphs after biotite. Biotite being an aluminous mineral (Al greater or equal to Na+K), it is not surprising that it would become unstable in increasingly peralkaline melts and alter to astrophyllite, whose structure exhibits several similiarities with that of the trioctahedral micas (Woodrow 1967). The absence of astrophyllite in MG39 is consistent with the apparent antipathetic relationship between astrophyllite and Fe-Ti oxides phases reported by Marsh (1975), and implies that $f(O_2)$ of the magma influences in part the stability of

astrophyllite. The astrophyllite compositions are similar to those reported from other undersaturated suites (MacDonald and Saunders 1973); they exhibit high K/Na, Ca, Al and Mn contents.

Pectolite, $Ca_2NaH[SiO_3]_3$, forms anhedral to euhedral bladed grains in all the peralkaline tinguaites studied. It appears to be predominantly primary, but may be due to alteration of nepheline in the white cognate inclusion (MG98). The pectolite is characterized by relatively high Mn contents (3.38-5.64 wt % MnO) (Deer et al. 1978).

Like sodalite, fluorite is predominantly restricted to the peralkaline tinguaites, typically as a late-forming mineral occurring either interstitially or infilling late-stage microfractures. Rare subhedral zoned grains (Fig. 5.3.6) were also observed in the white cognate inclusion (MG98). The presence of fluorite indicates the importance of fluorine among the volatile constituents in the peralkaline tinguaites.

DISCUSSION

In general, the mineralogy of the different types of nepheline syenite indicates that they are unlikely to be related by simple closed-system fractionation, as the physical conditions of crystallization [principally $f(O_2)$ and probably $P(H_2O)$] vary from sample to sample.

The miaskitic nepheline syenite (MG16) appears to have crystallized under relatively highly oxidizing conditions, as indicated by the Mg-rich composition of both its biotite and clinopyroxene, the high Fe^{3+} content of the biotite, the lack of sodic amphibole and the presence of early-forming titanite coexisting with magnetite (Carmichael and Nicholls 1967,

Haggerty 1976). The best available estimate of $f(O_2)$ (from the Fe^{3+} content of the biotite) indicates conditions above the magnetite-hematite buffer. However, the presence of abundant magnetite implies that this estimate is higher than the actual value. The occurrence of metasomatized inclusions, abundant late-stage veins and aplite indicate that large amounts of deuteric fluid were probably evolved from the nepheline syenite at a late stage; this implies a relatively high initial $P(H_2O)$.

The conditions under which the intermediate tinguaite (MG94) crystallized are poorly constrained. As for the miaskitic nepheline syenite, estimates of $f(O_2)$ from the Fe^{3+} content of the biotite are likely grossly exaggerated. The occurrence of both ilmenite and magnetite, the late crystallization of both biotite and magnetite, and the more Fe-rich nature of the mafic silicates in the intermediate tinguaite are consistent with a lower $f(O_2)$ and probably $P(H_2O)$ than the miaskitic nepheline syenite. On the basis of experimental data, Bailey (1969) concluded that the presence of arfvedsonite indicates a maximum temperature of 700°C and a $f(O_2)$ in the range defined by the wüstite-magnetite and QFM buffers. Therefore, the lack of sodic amphibole in MG94 probably implies an $f(O_2)$ above the QFM buffer. The relatively disordered K-feldspar in this sample indicates limited interaction with deuteric fluids.

The assemblages in the peralkaline tinguaites containing aenigmatite and arfvedsonite (e.g., MG37) probably place the tightest constraints on the conditions of crystallization. Curtis and Currie (1981) concluded, on the basis of available thermodynamic data for the $f(O_2)$ buffering reaction:

$1/2O_2 + Na_3Fe_5Si_8O_{22}(OH)_2 + 2/3KAlSi_3O_8 + NaAlSiO_4 = 3NaFeSi_2O_6 + 2/3KAlFe_3Si_3O_{10}(OH)_2 + NaAlSi_3O_8 + 1/3H_2O$

that peralkaline magmas that coprecipitated sodic pyroxene and arfvedsonitic amphibole crystallized at temperatures that could not have been much above 650°C. They also concluded that these minerals indicate an oxygen fugacity well below the quartz-fayalite-magnetite buffer. Furthermore, end-member aenigmatite has been shown to be stable at temperatures below 800°C along the QFM buffer at $P(H_2O)$ above 1 kbar; the maximum stability of aenigmatite is probably limited to $f(O_2)$ values 1 log unit at most above the QFM buffer (D. H. Lindsley, pers. comm. 1987).

MG37 and MG39, which exhibit nearly identical whole-rock compositions (Table 5.1), and are closely associated in the field (Fig. 2.1), are probably derived from the same magma. However, their respective mineralogies are very different. The extreme Mg enrichment of the biotite, lack of sodic amphibole, presence of Ti-poor, Mn-rich magnetite rather than aenigmatite, lack of astrophyllite and Na-Zr silicates (and presence of zircon), as well as the high whole-rock $X_{Fe}3+$ of MG39 indicate that it crystallized under much more oxidized conditions than MG37.

The development of more oxidizing conditions in MG39 probably reflects the breakdown of the aegirine-arfvedsonite buffer (Larsen 1977, Curtis and Currie 1981) that may have controlled the $f(O_2)$ in MG37. If the $f(O_2)$ of MG39 was internally buffered (Carmichael and Nicholls 1967), it would have to involve equilibria between magnetite-biotite-acmite. Possible buffering reactions would be:

1) $2Fe_3O_4 + 3Na_2Si_2O_5(liquid) + 6SiO_2(liquid) + 1/2O_2 = 6NaFeSi_2O_6$,

2) $2KAlFe_3Si_3O_{10}(OH)_2 + 3Na_2Si_2O_5(liquid) + 6SiO_2(liquid) + 1.5O_2 = 6NaFeSi_2O_6 + 2KAlSi_3O_8 + 2H_2O$,

or a combination of the two. There is textural evidence (Fig. 5.3.2) for the second reaction. No field, chemical or textural evidence is found for saturation with a volatile phase. Rather, the presence of abundant fluorite-bearing microfractures in MG39 indicates that the volatiles remained in solution until the very late stages of crystallization, an inference consistent with the high solubilty of volatiles in alkaline magmas (Kogarko 1974, Burnham 1979). Therefore, there is no direct evidence that the $f(O_2)$ was externally controlled by the exsolution of a fluid phase (e.g., Larsen 1977). If the breakdown of the arfvedsonite-acmite buffer reflects an increase in $f(O_2)$, it could have been caused by the loss of H_2 from the thin sill (less than 2 m), presumably by diffusion.

The occurrence of Ti-rich aegirine in the two peralkaline tinguaites indicates that it can form under a relatively wide range of oxygen fugacities, and does not necessarily imply a highly oxidizing environment (e.g., Czamanske and Atkin 1985). The absence of a significant $NaMg_{0.5}Ti_{0.5}Si_2O_6$ component in the titanium-rich aegirine from MG39 is probably related to the low activity of MgO in the magma rather than low $f(O_2)$ [cf. Nielsen 1979]. Ti-enrichment of aegirine is dependent on the composition of the magma from which it crystallized (e.g., a_{TiO2} or a_{Na2O}; Nielsen 1979), which depends itself in part on the type and abundance of Ti-minerals that crystallized from

the magma. Since titanian aegirine typically occurs as a late-stage rim on Ti-poor aegirine, any early crystallizing or coprecipitating Ti-rich phase can only deplete the amount of Ti available to enter the aegirine. The stability and abundance of any Ti-mineral (e.g., titanite, aenigmatite) are partly dependent on $f(O_2)$, but the activities of other components (e.g., SiO_2, CaO, FeO) in the magma are also important.

Felsic undersaturated alkaline magmatism, especially involving agpaitic rock types in a continental setting, is typically associated with a tensional environment (e.g., Sørensen 1986). Examples include the Gardar Province (Upton 1974), the Oslo Alkaline Province (Neumann 1980) and the Monteregian Province of southern Quebec (Eby 1984, 1985). The alkaline magmatism within these provinces is attributed to rifting (e.g., Kumarapeli and Saull 1966, Bailey 1974) and is commonly localized around faults or areas of structural weakness (Kumarapeli 1970, Upton 1974, Bedard 1985).

The origin of felsic undersaturated rock types is generally ascribed to one of two models. The first involves differentiation of alkali basaltic, basanitic or nephelinitic magmas at low to high pressures (Coombs and Wilkinson 1969, Price et al. 1985, Sørensen 1986), whereas the second attributes their origin to partial melting of lower crustal rocks that may have undergone metasomatism by alkali- and rare element-rich volatiles derived from the mantle (Bailey 1974, Marsh 1987).

Several lines of evidence are consistent with the derivation of the McGerrigle nepheline syenites through differentiation of

a mafic parent. The analyzed alkaline mafic rocks of the pluton contain up to 6 wt. % normative nepheline (Chapter 2) and therefore could be representative of the parental magmas from which the nepheline syenites were derived (e.g., Kyle 1981). The observed depletion of Ca, Sr and Ba and well-developed Eu anomalies (Whalen and Gariépy 1986) are consistent with the occurrence of significant amounts of feldspar fractionation. Depletion of Cr, Ni, Sc and Mg indicates that fractionation of a mafic mineral(s) [clinopyroxene?; Chapter 2] probably also occurred. The observed enrichment in incompatible elements (e.g., Rb, Zr, Nb, Th, U, etc.; Whalen and Gariépy 1986) especially in the tinguaites, is consistent with their formation from highly fractionated residual liquids. The limited amounts of nepheline syenite observed is also consistent with a residual character.

The isotopic data, on the other hand, indicate a more complex picture, as the different samples exhibit a wide range of Pb isotopic values (C. Gariépy, pers. comm. 1985) and a moderate range of oxygen isotopic values (Chapter 6); in both cases the peralkaline tinguaites exhibit the highest values. La Rocque (1986) obtained a high initial $^{87}Sr/^{86}Sr$ ratio (between 0.7109 to 0.7115 depending on the model age used) for a tinguaite sample from the same locality and exhibiting a similar mineralogy to MG39. Such a high value indicates at least some interaction of the nepheline syenites with crustal rocks. Significantly, the presence of mafic pseudomorphs, recrystallized remnants of plagioclase at the core of K-feldspar phenocrysts and rare xenoliths (of basement?) also

suggest relatively late-stage contamination of the peralkaline tinguaites. Blaxland et al. (1978) attributed the $^{87}Sr/^{86}Sr$ enrichment of agpaitic syenites from the Ilímaussaq complex to preferential leaching of ^{87}Sr from the walls and roof of the magma chamber by highly reactive volatile-rich agpaitic magmas.

Another problem with a model involving fractional crystallization is the lack of observed intermediate members between the alkaline mafic and nepheline syenitic compositions. This may reflect the mechanism by which differentiation took place or the higher viscosity of the intermediate magmas relative to the high-temperature mafic and volatile-rich felsic magmas (e.g., MacDonald 1974, Philpotts 1982).

The miaskitic nepheline syenite is enriched in compatible elements (e.g., Ca, Mg, Sr, Ba, etc.) and depleted in incompatible elements (e.g., Zr, Nb, Th, etc.; Whalen and Garièpy 1986) relative to the tinguaites and could theoretically represent the parental magma from which they were derived. Since the molar fractions of $2CaO+K_2O+N_2O$ exceed that of Al_2O_3 in the miaskitic nepheline syenite, it could act as parent to peralkaline residual magmas through the "plagioclase effect" (the inability of pure albite to crystallize from a liquid containing Ca; Bowen 1945, Bailey and Schairer 1966). However, no anorthite component was identified in the K-feldspar. Rather, the Ca of the miaskitic nepheline syenites appears to be predominantly concentrated in the aegirine-augite (3.0 % of the rock, averaging 17 wt. % CaO) and titanite (1.9 % of the rock, 26 wt. % CaO). It therefore appears unlikely that the tinguaites formed through fractionation of the miaskitic

nepheline syenite unless the miaskitic nepheline syenite fractionated under different physicochemical conditions, for example at lower $f(O_2)$, which could favor the incorporation of Ca into the feldspar over titanite.

The chemical similarities of the tinguaites indicate that they are probably closely related and derived from the same parent. At least some of the intermediate tinguaites (e.g., MG94) exhibit compositions as evolved, or more so, than the peralkaline tinguaites with respect to many elements (e.g., Sr, Ba, Mg and Ca; Table 5.1). Therefore, the observed variation in agpaitic index (0.97-1.06) cannot be explained by a simple process of fractional crystallization. An alternative mechanism involves the loss of a Na-, Zr- and rare-element-rich volatile phase from an originally peralkaline magma (e.g., Larsen and Steenfelt 1974). This could explain why elements such as Na, Zr, Nb and REE, which would complex with volatile components, principally F and Cl, are depleted in MG94, whereas others (e.g., Ti, Mg, K) remain unchanged. The scarcity or absence of sodalite and fluorite within the intermediate tinguaites relative to the peralkaline ones, as well as their more primitive isotopic character, are also consistent with their formation from magmas characterized by a lower volatile content.

The above considerations suggest that although the nepheline syenites are probably derived from the same or very similar parents, their evolution cannot be explained in terms of a simple model of closed-system fractionation. Rather, processes involving crustal contamination and loss of volatiles must also

be responsible for the observed chemical, mineralogical and isotopic variations.

The most plausible model involves differentiation of undersaturated alkali basaltic or basanitic magma(s) at moderate pressures (i.e., within the crust but significantly below the current level of exposure) to form undersaturated felsic residua. During their rise to the present crustal level, the nepheline syenitic magmas were variably contaminated by crustal material and, in some cases, probably lost volatiles (possibly owing to decompression, due to a rapid rise toward the surface). Crustal contamination principally resulted in changes of the isotopic composition of the magma, whereas the loss of volatiles can account for at least some of the observed chemical variations between the different tinguaites. Other hypotheses, such as partial melting of metasomatized lower crust, cannot totally be discounted by the current data, but seem unnecessary to explain the observed compositional variations.

CHAPTER 6. PRELIMINARY STUDY OF THE OXYGEN ISOTOPE GEOCHEMISTRY OF THE MCGERRIGLE SUITE

INTRODUCTION

Oxygen isotopes have become one of the most important tools available to an igneous petrologist (cf. Valley et al. 1986). This approach has been used alone or in combination with other types of isotopic and geochemical data to determine: 1) the characteristics of the source from which the igneous magma was derived (e.g., O'Neil et al. 1977, O'Neil and Chappell 1977), 2) the degree to which crustal contamination of the melt has occurred (e.g., Taylor 1980, James 1981), and 3) the significance of fluid-rock interactions (e.g., Taylor 1977, Taylor and Forester 1979).

Mineral phases in isotopic equilibrium concentrate ^{18}O to varying degrees. The extent of fractionation is principally controlled by temperature and the chemical composition of the phases (O'Neil 1986); the degree of fractionation generally decreases with increasing temperature. In a common igneous mineral assemblage at equilibrium, quartz exhibits the highest ^{18}O content and magnetite, the lowest (Taylor and Epstein 1962). The primary whole-rock $\delta^{18}O$ value of an igneous rock will reflect the isotopic composition of the parent melt, that of the oxygen reservoir(s) that the melt was derived from or interacted with, the temperature at which the melt equilibrated with a given oxygen reservoir, and the extent to which igneous processes (such as crystal fractionation) have modified the value of the original magma (Taylor 1968). Secondary processes (e.g., interaction with hydrothermal fluids) taking place below

the solidus may result in isotopic exchange that modifies the primary $\delta^{18}O$ value of an igneous rock.

In plutonic rocks, the interpretation is complicated by the question of how closely the $\delta^{18}O$ of the whole rock reflects that of the magma from which it crystallized. Possible deviations may reflect the presence of a significant cumulate component and the probability that a fluid phase was evolved during crystallization (e.g., Taylor 1968; Kalamarides 1984). In this thesis, the $\delta^{18}O$ of the whole rock is assumed to approximate that of the magma from which it crystallized.

ANALYTICAL RESULTS

Whole-rock oxygen isotope data were obtained for representative samples of all the major rock types observed within the McGerrigle Plutonic Complex (Figs. 6.1, 6.2; Table 6.1). The observed $\delta^{18}O$ (whole rock) ranges from 5.6 to 7.9°/oo for the mafic and mesocratic intermediate samples, 5.8 to 6.3°/oo for the syenites, 6.6 to 7.5°/oo for the quartz monzonites, 6.0 and 9.3°/oo for the granites and 6.6 and 7.7°/oo for the nepheline syenites.

Data were also obtained for a limited number of quartz and K-feldspar separates (Table 6.1). The $\delta^{18}O$ value for quartz is lowest (6.4°/oo) in the syenite (MG8), highest (8.1°/oo) in the monzodiorite (MG23), and generally greater than 7.5°/oo. K-feldspar, on the other hand, is lowest (5.9°/oo) in the plagioclase-phyric syenite (MG40) and highest (7.4°/oo) in the monzodiorite (MG23). The corresponding Δ_{Q-F} range ($\delta^{18}O_{Quartz} - \delta^{18}O_{Feldspar}$) varies from -0.1 for the syenite (MG8) to 1.3 for the quartz monzonite (MG44).

Oxygen Isotope Composition of the McGerrigle Plutonic Complex

Sample	Rock Type	$\delta^{18}O_Q$	$\delta^{18}O_F$	Δ_{Q-F}	$\delta^{18}O_{WR}$ °/oo
MG8	SYEN	6.4	6.5	-0.1	6.3
MG9	DIOR				5.9
MG16	MIAS				6.7
MG23	MZDI	8.1	7.4	0.7	5.9
MG24	MAFI				7.9
MG28	KFDG				6.5
MG36	QTMZ				7.5
MG37	PTIN				7.7
MG40	PSYN	7.0	5.9	1.1	5.8
MG44	QTMZ	8.0	6.7	1.3	6.6
MG46	PDGR				6.0
MG51	GP				9.3
MG60	KFDG				6.9
MG63	QTMZ				6.6
MG64	GABB				5.6
MG66	QTMZ				7.4
MG83	KFPG	7.6	7.0	0.6	6.7
MG94*	ITIN				6.6
MG28*	KFDG				6.6
MG16*	MIAS				6.7
MG83*	KFPG				6.8
MG83*	KFPG				6.4

*: Replicate analyses. Q: quartz, F: K-feldspar, WR: whole rock. $\Delta_{Q-F} = \delta^{18}O_{quartz} - \delta^{18}O_{K\text{-}feldspar}$. All values in permil relative to SMOW. SYEN: syenite, DIOR: diorite, MIAS: miaskitic nepheline syenite, MZDI: monzodiorite, MAFI: fine-grained mafic inclusion, KFDG: K-feldspar-dominant granite, QTMZ: quartz monzonite, PTIN: peralkaline tinguaite, PSYN: plagioclase-phyric syenite, PDGR: plagioclase-dominant granite, GP: granite porphyry, GABB: gabbro, ITIN: intermediate tinguaite.

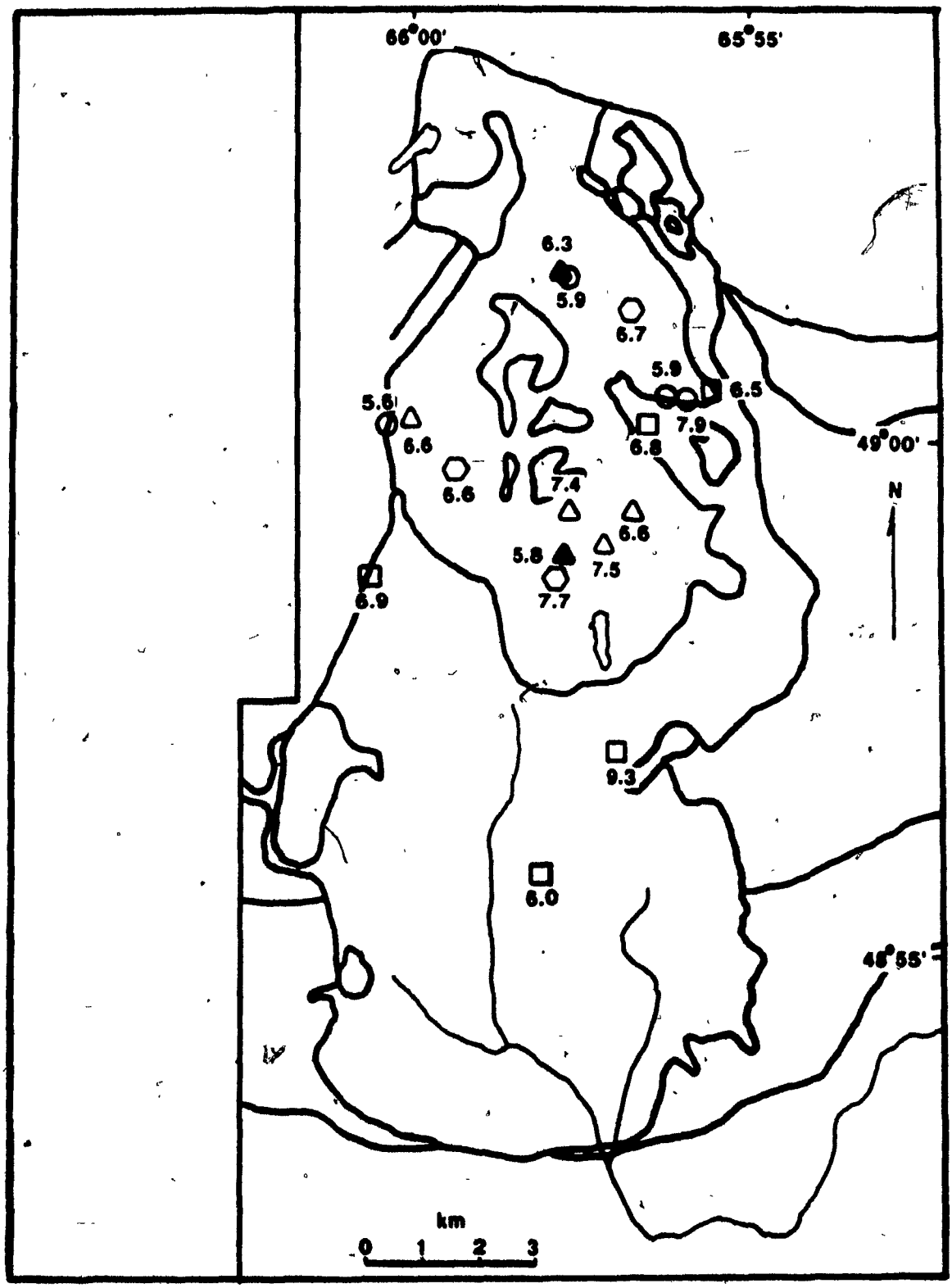

Figure 6.1. Sample location map showing the distribution of whole-rock $\delta^{18}O$ values. Symbols same as in Figure 2.1. Refer to Figure 1.2 for definition of the map units.

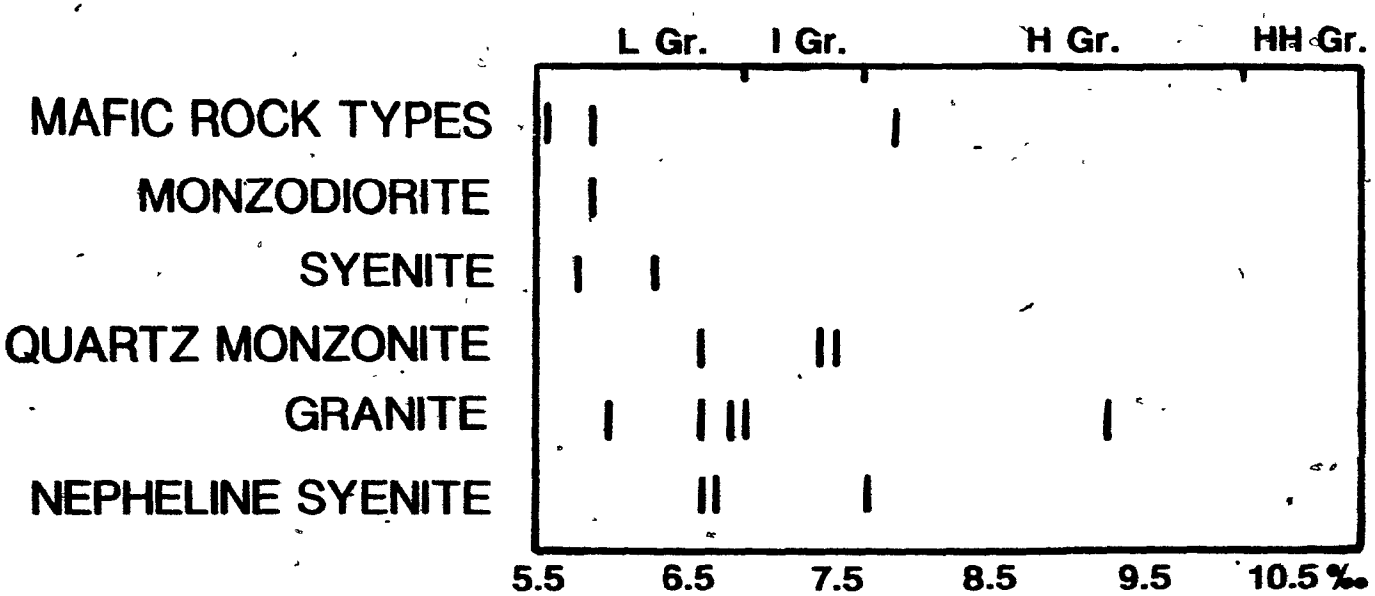

Figure 6.2. Range of values of the oxygen-isotope ratio of various rock types. L Gr.: L Group (5.5 to 6.9°/oo; Taylor 1968), I Gr.: I Group (7.0 to 7.7 °/oo), H Gr.: H Group (7.8 to 10.2 °/oo), HH Gr.: HH Group (≥10.3°/oo).

SIGNIFICANCE OF SUBSOLIDUS PROCESSES

An important consideration in evaluating the significance of whole-rock $\delta^{18}O$ values is the degree to which subsolidus processes have affected the primary values of the minerals. The degree of preservation of the primary $\delta^{18}O$ of the whole rock is especially difficult to assess in granites as they commonly exhibit evidence of a complex subsolidus history (e.g., Tuttle 1952). Subsolidus isotopic exchange will not affect the whole rock $\delta^{18}O$ if it occurs in a closed system and simply represents re-equilibration of the constituent minerals with each other with decreasing temperature (e.g., Giletti 1986). However, significant deviations of the whole-rock $\delta^{18}O$ value may occur if the rock interacts as a system open to an external isotopic reservoir (e.g., Taylor 1968, 1977).

One of the most sensitive tools available to judge the importance of open-system behavior is the fractionation factor between two different minerals (e.g., Gregory and Criss 1986). When isotopic exchange occurs under subsolidus conditions, different minerals are characterized by differing suceptibilities to isotopic re-equilibration (cf. Cole and Ohmoto 1986). When a mineral resistant to isotopic exchange (e.g., quartz or pyroxene) is compared to one of similar grain size and more susceptible to exchange (e.g., feldspar), nonequilibrium values commonly result if the rocks have undergone extensive interaction with an external reservoir of oxygen under subsolidus conditions. For example, abnormally large Δ_{Q-F} values (4 to 10‰ in granites at Skye, Mull and Ardnamurchan; Taylor 1968, Taylor and Forester 1971) have been

observed in epizonal granites that apparently exchanged with meteoric waters at moderate to high temperatures. $\delta^{18}O$ enrichment of feldspar relative to quartz may occur if the rock interacts with fluids characterized by a high $\delta^{18}O$ (e.g., "metamorphic" waters derived by devolatilization of isotopically heavy metasediments; Rumble et al. 1986) at moderate to high temperatures or with meteoric water at low temperatures (e.g., Wenner and Taylor 1976).

Interpretation of isotopic data is complicated by factors such as cooling rate, grain size and temperature which will determine for how long equilibrium between different minerals is maintained in the subsolidus environment (e.g., Giletti 1986). Under certain conditions (e.g., long cooling history or fine grain-size), isotopic equilibrium may be maintained throughout extensive subsolidus re-equilibration (e.g., Taylor 1971, Rumble et al. 1986). Therefore, it is premature to assume that no isotopic exchange has occurred with a fluid solely on the basis of the Δ_{Q-F} value. Furthermore, it should be noted that it is by no means clear that the normal range of Δ_{Q-F} in granites (i.e., between 0.8 and 1.5 °/oo; Criss and Taylor 1983) represents magmatic values. For example, the equations of Matsuhisa et al. (1979) suggested that these values correspond to a temperature range of approximately 400 to 500°C, whereas those of Bottinga and Javoy (1973) suggest a range of 500 to 800°C.

Mineralogical Evidence of Fluid-Rock Interactions

Taylor and Forester (1971), Criss and Taylor (1983), Ferry

(1985a,b) and Rumble et al. (1986), among others, have shown that mineralogical alteration of the granites is commonly accompanied by isotopic alteration.

The McGerrigle samples exhibit abundant mineralogical evidence of varying degrees of recrystallization and interaction with a hydrothermal fluid phase (Chapters 2-5). Possible fluids include deuteric fluids released during "closed-system" crystallization of the magma (e.g., Jahns and Burnham 1969, Parsons 1980) or an externally derived fluid forming part of an open system (e.g., Taylor 1968, Rumble et al. 1986).

In agreement with the observations of Ferry (1985b), K-feldspar appears to have been the phase most susceptible to mineralogical alteration. Evidence of K-feldspar recrystallization in the presence of a fluid includes: 1) the predominantly turbid appearance of the K-rich phase (Folk 1955, Lalonde and Martin 1983), 2) the predominance of microperthite over cryptoperthite (Parsons 1978, 1980), and 3) the moderate degree of order of the K-rich phase (orthoclase or, rarely intermediate microcline), as indicated by the X-ray data (Chapters 2-5). Ordering in K-feldspar requires the presence of water as a catalyst (Martin 1974) and probably occurs by the same mechanism as oxygen isotope exchange between feldspar and water (O'Neil and Taylor 1967), i.e., by very local steps of solution and reprecipitation. Since K-feldspar dominates many of the felsic samples analyzed, any isotopic exchange linked to its alteration should also be reflected in the whole-rock value.

The exact temperature at which recrystallization of the K-feldspar occurred is poorly constrained; however, as the majority of samples are monoclinic (orthoclase) to X rays, this suggests that temperatures were above 400°C (Chapters 2-5). The general lack of low-temperature alteration minerals (e.g., chlorite and uralitic amphibole) also suggests that the fluid-rock interactions occurred at relatively high temperatures (e.g., Taylor and Forester 1979).

Though quartz shows no direct evidence of recrystallization, many grains contain abundant fluid inclusions, commonly along microfractures. If quartz did exchange oxygen with a hydrothermal fluid, these microfractures may have lowered the effective grain size of the quartz, thereby facilitating the exchange (Forester and Taylor 1980, Cole et al. 1981).

In some samples (e.g, MG8, 63), the amphibole exhibits compositional evidence (including a high silica and low Cl contents; Chapters 2-4) of having undergone recrystallization in the presence of a fluid phase.

Isotopic Evidence of Fluid-Rock Interactions

Within the estimated analytical precision (±0.14 °/oo; Appendix 1), four of the five quartz-feldspar pairs fall within or close to the range (Fig. 6.3) expected for "normal" plutonic rocks. However, isotopic equilibration of the K-feldspar must have occurred concurrently with subsolidus recrystallization. This should be true even if recrystallization occurred in a closed system, as the subsolidus environment is characterized by lower temperatures than a magmatic one. If it is accepted

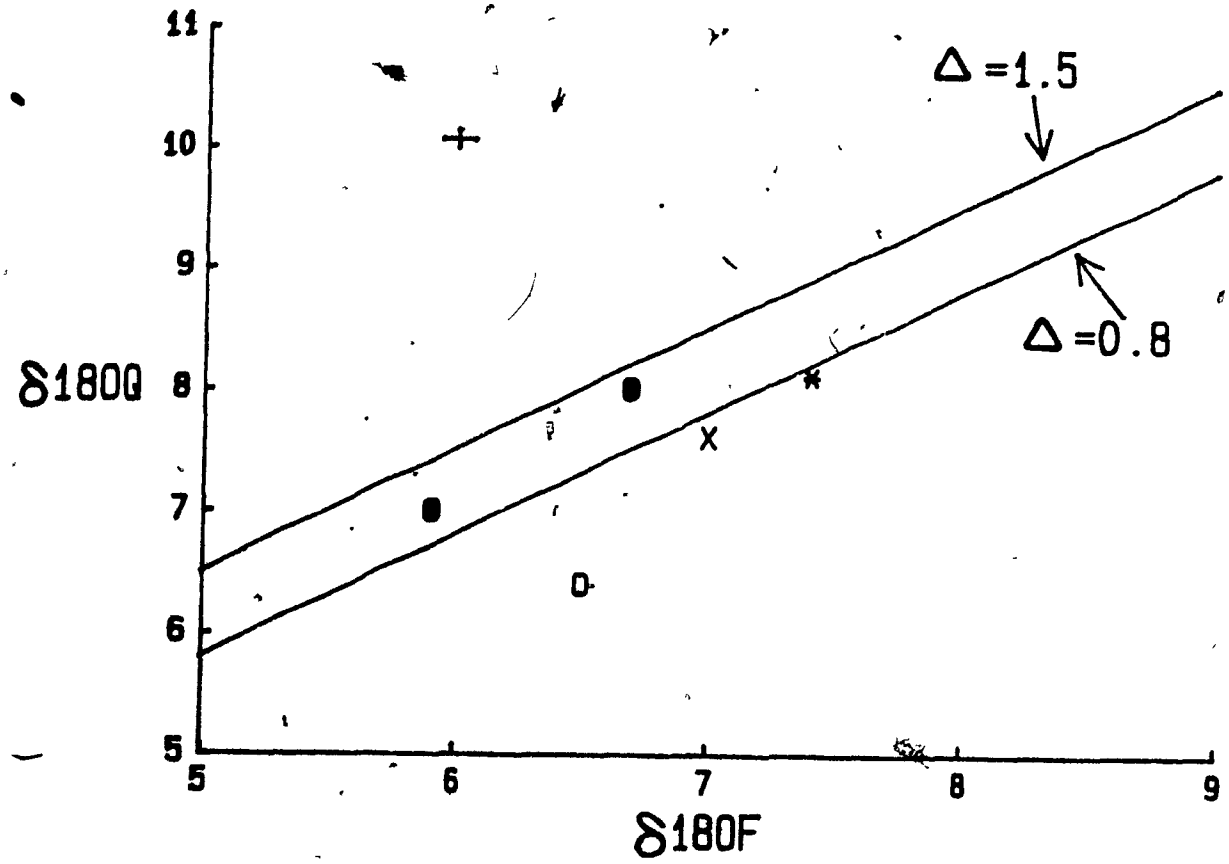

Figure 6.3. Oxygen isotopic compositions of coexisting quartz and K-feldspar for selected samples. Lines delimit the range of "normal" Δ-values expected for granites (Criss and Taylor 1983). Star: monzodiorite (MG23), open circle: syenite (MG8), filled circle: quartz monzonite (MG44, 66), X: K-feldspar porphyritic granite (MG83). Estimated analytical precision indicated in the upper left-hand corner of the diagram.

that K-feldspar did undergo recrystallization in the subsolidus, the low or negative Δ_{Q-F} values of some samples (e.g., MG8, 83) indicate that enrichment in ^{18}O of the feldspar relative to quartz must have occurred. As the mineralogical data suggest that this exchange occurred at moderately high temperatures (predominantly greater than 400°C), the process probably involved relatively ^{18}O-enriched fluids, such as deuteric or metamorphic waters (e.g., Sheppard 1986).

Since all the whole-rock $\delta^{18}O$ values fall within the range typical of "normal" igneous rocks (i.e., 5.5 to 11.0 °/oo; Taylor and Sheppard 1986) and K-feldspar exhibits no evidence of depletion relative to quartz, it is considered unlikely that interactions with meteoric waters were important in determining the whole-rock $\delta^{18}O$.

There is little compelling evidence to indicate for major re-equilibration of quartz, in agreement with other studies (e.g., Taylor 1968, Forester and Taylor 1980, Criss and Taylor 1983, Ferry 1985b). Temperatures calculated from the $\Delta_{quartz-whole\ rock}$ using simplified modes (quartz, feldspar, biotite, amphibole, ± pyroxene, ± magnetite) and the equations of Bottinga and Javoy (1973, 1975) define a range from 600 to 700°C. One exception, the syenite (MG8), exhibits an anomalously small Δ_{Q-WR} that probably reflects the ^{18}O enrichment of the K-feldspar, by far the most abundant mineral in this sample. An alternative explanation for the the low Δ_{Q-WR} as well as the low $\delta^{18}O$ value of the late-stage interstitial quartz may be loss of a fluid phase at the magmatic stage (at high temperatures a fluid phase will be

richer in ^{18}O than the coexisting melt; Taylor 1968). Furthermore, amphibole and biotite are late-stage minerals in this sample and show evidence that magmatic oxidation has occurred, possibly reflecting loss of hydrogen via a fluid phase (Chapter 3).

In conclusion, while the mineralogical data are consistent with significant amounts of recrystallization of K-feldspar and probably other minerals under subsolidus conditions in the presence of a fluid, the separates analysed do not show large-scale isotopic disequilibrium (with the one exception of MG8). However, the data do suggest that the "normal" Δ_{Q-F} range of granites reflects subsolidus rather than magmatic conditions. Some of the low Δ_{Q-F} values of the McGerrigle rocks may, however, simply be an artifact of ^{18}O enrichment of feldspar but not quartz through subsolidus interaction with a fluid phase. There is no evidence that the pluton has undergone extensive interaction with meteoric fluids. However, the possibility of limited interaction with ^{18}O-enriched fluids (possibly derived from the auréole) cannot totally be discounted (see below). If such open-system fluid-rock interactions have taken place, they must have occurred at relatively high temperatures, under conditions that enabled quartz and feldspar to remain approximately in equilibrium (cf. Rumble et al. 1986).

DISCUSSION

Mafic and Mesocratic Intermediate Rock Types

With one exception the mafic and mesocratic intermediate rock types have $\delta^{18}O$ whole-rock values that range from 5.6 to

5.9°/oo (Fig. 6.2). They plot at the lower end of the range of values reported from uncontaminated and unaltered continental alkali basalts (Kyser 1986), consistent with a proposal that they represent mantle-derived magmas, or their fractionation products, that have undergone little or no contamination by crustal materials that once resided on or near the Earth's surface (Taylor and Sheppard 1986). The exception (MG24), a value of 7.9°/oo from a chilled mafic pillow, may indicate contamination by such material though the process remains unclear. However, as MG24 comes from a small mafic inclusion, the high $\delta^{18}O$ may simply reflect equilibration of the inclusion with its felsic host and associated fluids, as has been reported in the case of dykes (e.g., Shieh and Taylor 1969, Turi and Taylor 1971). The low $\delta^{18}O$ values of the monzodiorites suggest that if they formed from alkali basalt through coupled fractionation and crustal assimilation (Chapter 2) or through magma mixing, the contaminant itself must have exhibited a low value of $\delta^{18}O$ (see below).

Syenites

The whole-rock $\delta^{18}O$ values obtained from the syenites (Fig. 6.2) are assumed to approximate those of the melts from which they crystallized, even though both analysed samples exhibit mineralogical and textural evidence of variable degrees of contamination by less evolved rock types (Chapter 3) that were presumably characterized by low values of $\delta^{18}O$ (probably between 5.6 and 6.0°/oo ; see above). Furthermore, the mineralogical data indicate that MG8 underwent extensive

interaction with hydrothermal fluids (see above, Chapter 3), which apparently resulted in an increase of the $\delta^{18}O$ of the K-feldspar (forming 60-70 % of the rock), and a parallel increase of the whole-rock $\delta^{18}O$. However, both samples exhibit $\delta^{18}O$ values at the low end of the "normal" values, within the range reported for syenites from other localities (Taylor and Sheppard 1986).

Interpretation of felsic rocks exhibiting a "normal" $\delta^{18}O$ value is less straightforward than for more extreme compositions (e.g., $\delta^{18}O$ greater than $+10.0^{o}/oo$ or less than $6.0^{o}/oo$; Taylor 1978). Possible models for the formation of felsic rocks at the low-^{18}O end of the spectrum (6.0 to $8.0^{o}/oo$) include: 1) differentiation from mantle-derived mafic magmas with little or no crustal assimilation (e.g., Taylor 1968, Foland et al. 1985), 2) partial melting of mantle-derived material (e.g., O'Neil and Chappell 1977) and 3) partial melting of deep-seated rocks of the lower crust (Taylor 1978). A more detailed study that couples other isotopic and geochemical data from the same samples will be required to evaluate which model is most appropriate for the McGerrigle syenites.

Granites and Quartz Monzonites

Both field and petrographic evidence (Chapter 3) indicates that the quartz monzonites are closely related to the granites; therefore, both lithologies are discussed together. The samples analyzed exhibit a larger range in $\delta^{18}O$ than all the other rock types put together (Fig. 6.2). The majority belong to Taylor's (1968) low-^{18}O group (5.5 to 6.9 $^{o}/oo$); however, samples

belonging to the intermediate- (7.0 to 7.7 °/oo) and high- (7.8 to 10.2 °/oo) ^{18}O groups are also present (e.g., MG66, 51). A similarly wide range of isotopic values has been reported for Pb (Whalen and Gariepy 1986) and Sr (La Rocque 1986). The limited data available indicate no correlation between the whole-rock geochemistry and isotopic composition; the granites exhibiting the highest (MG51) and lowest (MG46) $\delta^{18}O$ values are both of the plagioclase-dominant variety, exhibit similar differentiation indices (Table A4.3) and are found within the southern half of the pluton.

As noted above, $\delta^{18}O$ values greater or equal to 7.5 °/oo require contamination by ^{18}O-enriched material. A logical mechanism would be interaction with the shallow crust that overlies the Grenvillian basement and is represented by the Québec and Shickshock groups at the level of intrusion (cf. Seguin 1982). A wide variety of sedimentary rocks or their metamorphic equivalents (including shales, slates, sandstone and limestone; de Römer 1977, Van Bosse 1985) are observed in the aureole of the pluton. Therefore, the possibility that contamination occurred at the level of emplacement should also be considered as sedimentary rocks are characterized by generally high values of $\delta^{18}O$ (8 to 40 °/oo; Longstaffe 1987).

This contamination may occur through assimilation of the country rocks (or exchange, without assimilation) (e.g., Taylor 1980), or through subsolidus interaction with hydrothermal fluids derived by devolatilization of isotopically heavy metasediments (e.g., Turi and Taylor 1971, Rumble et al. 1986). Field evidence for assimilation is limited to rare country-rock

xenoliths that are up to several tens of metres in size and predominantly occur close to the margin of the pluton (this is especially true in the southern half of the pluton, where the largest isotopic variations are observed). No xenolith is present in any of the high-$\delta^{18}O$ rocks analyzed. Therefore, if contamination occurred at a magmatic stage by assimilation or exchange with the country rocks, it must have occurred below the current level of emplacement.

Whether or not the enrichment could have occurred through subsolidus interaction with ^{18}O-enriched fluids is unclear. As concluded above, the available mineralogical data indicates that high-temperature fluid-rock interactions did occur. Contamination of the margin of granitic plutons by fluids derived from the country rocks has been described by many authors (e.g., Shieh and Taylor 1969, Turi and Taylor 1971, Sisson 1984, Hill et al. 1986, Rumble et al. 1986). Evidence that such a fluid may have entered the pluton include: 1) the formation of an endoskarn (Chapter 2) that apparently underwent $^{87}Sr/^{86}Sr$ enrichment during metasomatism by fluids enriched in radiogenic strontium (La Rocque 1986), 2) mineralogical evidence that similar but less pronounced metasomatism has affected some granite samples, particularly around late-stage quartz veins (Chapter 2), and 3) the anomalously high $\delta^{34}S$ (27.5°/oo) exhibited by a sample of low-$\delta^{18}O$ granite (MG46), a finding that is best interpreted in terms of interaction with $\delta^{34}S$-rich fluids derived from the metasedimentary rocks of the aureole ($\delta^{34}S$ between 14.8 to 22.9°/oo; A. E. Williams-Jones, pers. comm. 1987).

The limited data from quartz monzonite and granite do not show a simple correlation between the $\delta^{18}O$ values and distance from the contact (Fig. 6.1). This lack of correlation may reflect the polyphase nature of the pluton, as well as the possibility that the exposed outcrop represents its roof zone (de Römer 1977). It may also be the result of preferential movement of hydrothermal fluids along fracture zones of limited width (e.g., Criss and Taylor 1986).

The low $\delta^{18}O$ values are assumed to be primary and are interpreted to reflect the source from which the bulk of the granites were derived, though some may in part reflect contamination by more primitive material (see above, Chapter 4). Even though some of the low-$\delta^{18}O$ samples may have interacted with fluids derived from the country rocks (e.g., MG46), the oxygen in these fluids had presumably equilibrated with the granites and, therefore, would not affect the primary $\delta^{18}O$ value (Turi and Taylor 1971). As previously noted, such values can be explained by several models.

Nepheline Syenites

Although no data on mineral separates were obtained for the nepheline syenites, the $\delta^{18}O$ values of the whole rock are interpreted to approximate those of the magmas from which they crystallized. All values fall within the range expected of "normal" igneous rocks (Fig. 6.2).

The relatively low values (6.6°/oo) of the miaskitic nepheline syenite and intermediate tinguaite (Chapter 5) are consistent with derivation through fractionation of mantle-

derived alkali basaltic or basanitic magmas without contamination by ^{18}O-rich crustal rocks.

The value of the peralkaline tinguaite (7.7°/oo) is slightly higher than expected for a magma derived simply through fractionation of a mantle-derived magma, and may indicate some contamination. Petrographic evidence (Chapter 5) and the high initial $^{87}Sr/^{86}Sr$ value obtained from a tinguaite (0.7107-0.7115 depending on what age is assumed; La Rocque 1986) are consistent with this conclusion. The degree of contamination, apparently extensive according to the Sr data, and relatively limited according to the oxygen data, can be explained in terms of the relative abundance of these elements. There is a very low concentration of Sr in the peralkaline tinguaites (27 to 71 ppm) and, therefore, the ratio of the amount of Sr in the melt to that present in any crustal contaminant is likely to be very small. On the other hand, almost all the rock-forming minerals and silicate melts have similar oxygen contents (45-50 wt. % O; Taylor 1980). Therefore, if the peralkaline tinguaite melt had interacted with a Sr-rich contaminant with a high initial $^{87}Sr/^{86}Sr$ value (old continental crust?), a large change in initial ratio of the tinguaite could be accompanied by a relatively limited change in $\delta^{18}O$ (cf. James 1981).

CHAPTER 7. SUMMARY AND CONCLUSIONS

SIGNIFICANCE OF MAGMA MIXING

While evidence for the coexistence of mafic and felsic magmas is well developed in the McGerrigle Plutonic Complex (Chapter 2, Whalen 1985a), the exact extent to which mixing occurred between these magmas is unclear. Many factors affect the degree to which magmas can mix: the physical and chemical properties of the magmas involved (e.g., T, latent heat of fusion, water content, etc.), their viscosity and the extent of crystallization at the temperature at which thermal equilibration occurred, the relative amounts and total volume of the magmas, and the cooling rate (Turner and Campbell 1986, Sparks and Marshall 1986, Frost and Mahood 1987). In general, magmas that have large compositional and temperature contrasts (e.g., basaltic and granitic magmas) are less likely to mix than those that have similar physical and chemical properties (Campbell and Turner 1986, Sparks and Marshall 1986).

The generally sharp contacts observed between mafic and mesocratic intermediate inclusions and their felsic hosts indicate that large-scale mixing did not occur at the present level of exposure. However, all rock types, including the fine-grained mafic inclusions, contain xenocrysts (Chapters 2-5), indicating varying amounts of contamination. The composition of most xenocrysts suggest that the contaminant was either a mafic or a relatively primitive intermediate (monzodiorite?) rock type or magma, though the possibility that some samples (e.g., MG40) may have undergone contamination by more evolved material cannot be ruled out (Chapters 2-4). The presence of

abundant xenocrysts implies that 1) large-scale mixing took place below the current level of exposure, in a zone where the proportion of mafic contaminant magma to silicic magma was high (Sparks and Marshall 1986) and in which the fluid dynamics favored mixing (e.g., close to a feeder of mafic magma; Turner and Campbell 1986), or that 2) hybridization (i.e., contamination of a magma by solid material) rather than magma mixing was the dominant process responsible for the presence of xenocrysts.

As discussed in Chapter 3, much of the textural evidence from the highly contaminated quartz-poor felsic rock types favors the latter mechanism. The wide range of rock types observed within the McGerrigle Plutonic Complex suggests a very complex system of magmatic plumbing. It is not unlikely that later pulses of magma rose through and were contaminated by products of previous ones (cumulates?). Significantly, the field and mineralogical data indicate that the most likely magma contaminants, i.e. the coarser-grained mafic and mesocratic intermediate rock types, typically predate their contaminated felsic hosts. Residual liquids may have been present within these contaminants, facilitating their assimilation and being available to mix with the host felsic magma. Even so, the chemical changes in the magma resulting from contamination may depend more on the ability of the host magma to react and equilibrate with xenocrysts derived from the contaminant (e.g., McBirney 1979) than on the efficiency of magma mixing.

In conclusion, evidence of small-scale mixing between magmas of different composition is not uncommon and may be important

in the genesis of small amounts of predominantly quartz monzonitic magmas (Chapters 3, 4). However, evidence for large-scale mixing (leading to formation of the monzodiorites?) is typically absent. If such mixing did occur, it must have taken place below the current level of exposure (e.g., Vernon 1983). If this was the case the chemical effects of other processes (e.g., fractional crystallization, assimilation) have probably been superimposed on any such hybrid magmas (e.g., Whalen and Currie 1984).

THE ORIGIN OF THE SYENITES AND GRANITES

One of the principal models suggested for the derivation of intermediate and felsic rocks in some anorogenic complexes is simple fractional crystallization of a mafic magma (e.g., Upton and Thomas 1980, Neumann 1980, Foland et al. 1985). Though the $\delta^{18}O$ values of syenites and most granites of the McGerrigle plutonic complex do not rule out this model (Chapter 6), such a scheme of fractionation is unlikely to have occurred without crustal assimilation because: 1) all the relatively pristine mafic rocks observed in the pluton are silica-undersaturated, requiring that the thermal barrier separating silica-undersaturated from silica-oversaturated melts be crossed (Chapter 2), 2) fractionation of the apparent liquidus or near-liquidus phases (plagioclase and clinopyroxene) of these mafic magmas is more likely to result in the formation of silica-undersaturated residua (Chapters 2, 5), 3) if the higher $\delta^{18}O$ values exhibited by some granites accurately reflect those of the magma from which they crystallized (cf. Chapter 6), these magmas must have undergone contamination by ^{18}O-rich crustal

material, and 4) the wide range in initial Pb-isotope compositions of clear K-feldspar grains also indicates variable degrees of crustal involvement (C. Gariépy, pers. comm. 1987).

Therefore, a more complex model, such as the reaction-melting model of Barker et al. (1975), is probably more appropriate. In this model, an alkali basaltic magma collects at or near the base of the crust, where it begins to crystallize, releasing heat that causes partial melting of the lower-crust granulites, resulting in contamination of the mafic magma and, ultimately, formation of a syenitic fraction. Further differentiation (in part by "classical" crystal fractionation), partial melting and contamination at higher levels in the crust result in the formation of the granites (e.g., Collerson 1982). This scenario can be further complicated if contamination of the individual magmas through magma mixing or hybridization occurs (e.g., Whalen and Currie 1984).

A similar model could account for the close relationship between felsic and mafic magmatism in the McGerrigle plutonic complex, reflected in the complicated field relationships; these indicate that mafic magmatism predated, was contemporaneous with and, in part, postdated felsic magmatism (Chapter 2). Furthermore, the presence of syenites and intermediate rock types (i.e., monzodiorite and quartz monzodiorite; Chapter 2) is consistent with the above "reaction-melting"-fractionation model.

Unfortunately, it is impossible, on the basis of the available data, to evaluate the relative importance of contamination of a fractionating mantle-derived magma (e.g.,

DePaolo 1981) and simple partial melting of a crustal source in which the mafic liquids act only as a heat source (e.g., Clemens et al. 1986). However, some constraints can be placed on the possible crustal sources involved. The low values of $\delta^{18}O$ exhibited by the syenites and most granites (Chapter 6) and the low initial $^{87}Sr/^{86}Sr$ ratio (down to as low as 0.7031) obtained for many of the felsic samples studied by La Rocque (1986) suggest that any crustal material involved was geochemically primitive and most likely mantle-derived. Considering the present knowledge of the crustal section beneath the McGerrigle Plutonic Complex (Chapter 1; cf. Seguin 1982), this source most likely lies within the Precambrian basement. The low initial $^{87}Sr/^{86}Sr$ values imply that the source must have been depleted in Rb, ruling out the possibility of major involvement of the upper crust in the generation of these magmas (R. Doig, pers. comm. 1987). Possible Rb-depleted sources include mafic or felsic granulites (e.g., Leeman et al. 1985).

The relatively F-enriched (Chapter 4) and transitional anorogenic character (La Rocque 1986, Whalen and Garlepy 1986) of the granitic magmas (Chapter 4) presumably reflects interaction with or derivation from a crustal source (e.g., Christiansen & Lee 1986), and may further constrain the type of crust involved. Clemens et al. (1986) concluded that A-type magmas are derived from an anhydrous but not necessarily F-enriched lower crustal source, where melting most likely involves fluid-absent breakdown of residual, halogen-enriched micas and amphiboles. Hypothesized lower crustal sources

include felsic granulite that has undergone a previous melting event (e.g., Collins et al. 1982) or a tonalitic to granodioritic meta-igneous source (Anderson 1983). Note that lower to middle crustal Grenville granulites exposed north of the study area (across the St. Lawrence River) do contain F-enriched biotite (Perrault 1986). An alternative model for the generation of A-type magmas invokes enrichment in F and other trace elements of the lower crust by metasomatism (e.g., Abdel-Rahman and Martin 1987b). An explanation of the intermediate I- to A-type character of the McGerrigle pluton (La Rocque 1986) may lie in the lack of evidence for a previous melting event of the lower-crust source; most A-type igneous rocks occur late in the intrusive cycle, after the generation of an I-type granitic melt (Collins et al. 1982).

The high values of $\delta^{18}O$ exhibited by some granites and quartz monzonites are consistent with contamination by or derivation from ^{18}O-enriched crustal material (Chapter 6). Similarly, high values of $^{87}Sr/^{86}Sr$ initial ratio (up to 0.7143) were obtained for many of the samples of southern granites analyzed by La Rocque (1986). Unfortunately, it is not clear at which stage the contamination occurred. The poor correlation among ^{18}O, geochemical and Pb-isotope data from the same samples (C. Gariépy, pers. comm. 1987) may reflect the role of late-stage, (i.e., subsolidus) processes in the development of these high values (cf. Chapter 6).

In conclusion, a model of simple fractionation of mantle-derived magmas to form the syenites and granites appears to be ruled out by the available data. A more complicated model, such

as the reaction-melting model of Barker et al. (1975), appears to be more appropriate and better explains the wide range of rock types observed in the McGerrigle Plutonic Complex. The bulk of the available isotopic data and the relatively F-enriched nature of the magmas appears to favor the lower crust as a source or contaminant (e.g., Collins et al. 1982, Anderson 1983, Clemens et al. 1986). The relative importance of mantle- and crust-derived components within these magmas may be in part resolved by geochemical and isotopic studies presently under way (cf. Whalen and Gariépy 1986).

GENERAL CONCLUSIONS

This project was carried out to identify and characterize the rock types present within the McGerrigle Plutonic Complex, to determine their interrelationships and to establish constraints on their petrogenesis. This was done using field relations, petrography, mineral chemistry, degree of Al-Si order of the feldspars and oxygen isotope geochemistry. The major findings of this study can be summarized as follows:

1. Labradorite (up to An_{67}) is the most primitive plagioclase composition found in the complex. The plagioclase of the mafic and mesocratic intermediate rock types is variably recrystallized to a more sodic composition; recrystallization in some samples has almost destroyed the primary plagioclase. The more felsic rock types commonly contain recrystallized laths, an An-rich core (up to An_{59}) or mantled plagioclase phenocrysts that are interpreted to be xenocrysts. Whereas most oversaturated felsic magmas crystallized both plagioclase and

K-feldspar (i.e, were subsolvus or were generally too calcic to be otherwise), some low-Ca syenitic and granitic magmas are interpreted to have crystallized only one feldspar (i.e, are hypersolvus).

2. The K-feldspar is predominantly orthoclase in all rock types; it exhibits a limited compositional range (i.e., Or_{90-100}) that is consistent with the presence of an exsolved albitic phase. Its variably turbid nature and the non-crystallographically oriented perthitic lamellae indicate that the K-feldspar underwent recrystallization in the presence of a fluid phase. The characteristic reddish color of the K-feldspar in the oversaturated felsic rock types indicates that these rocks interacted with an oxidizing fluid. The predominance of orthoclase over microcline, especially in the volumetrically dominant granites, is anomalous for a pluton this size. The fluid-rock interactions that are responsible for K-feldspar ordering predominantly occurred above the stability field of microcline (i.e., above 400°C). This may indicate that most of the circulation of hydrothermal fluids through the granites occurred at relatively high temperatures, as suggested by the generally pristine condition of the mafic minerals and the low abundance of secondary minerals (e.g., Taylor and Forester 1979, Norton and Taylor 1979). A rapakivi texture observed in some granites and their contaminated equivalents is interpreted to result from magma mixing.

3. The primary clinopyroxene of the mafic and mesocratic intermediate rock types is Ti-rich [i.e., titaniferous salite or titansalite (augite)] consistent with the alkaline character

of these rocks. The principal substitution of $TiAl_2$ for $(Mg,Fe^{2+})Si_2$ is coupled with the substitution of Fe^{2+} for Mg. Secondary (sodian) salite commonly coexists with (or results from the recrystallization of) the primary clinopyroxene in the mafic and mesocratic intermediate inclusions.

Among the oversaturated felsic rock types clinopyroxene is relatively common in some syenites but is rare in the granites and most quartz monzonites. Sodian ferroaugite is the most evolved clinopyroxene that crystallized from an oversaturated felsic melt. Grains of (sodian) augite in the quartz-poor felsic rock types commonly are interpreted to represent xenocrysts derived from more primitive rock types. Compositional zoning in one grain of augite from a plagioclase-phyric syenite may record the effect of magma mixing on the composition of the syenitic melt.

The clinopyroxene from the nepheline syenites varies from aegirine-augite to aegirine; titanian aegirine occurs as a late-stage rim in the peralkaline tinguaites and reflects the buildup of the component $NaFe^{2+}_{0.5}Ti_{0.5}SiO_6$ into the clinopyroxene. Whether Ti-enrichment of aegirine occurs or not depends on the type, sequence of crystallization and abundance of Ti-bearing minerals that precipitated from the magma. In the peralkaline tinguaites studied, Ti-rich aegirine appears to have formed both under conditions of relatively low (MG37) and high (MG39) $f(O_2)$.

4. Primary kaersutite occurs as a relatively late-stage mineral in the mafic rock types. In the fine-grained mafic, and mesocratic intermediate inclusions, hornblende has re-

equilibrated with the more felsic hosts. One exception, a chilled fine-grained mafic inclusion (MG97) in contact with white granodiorite, still preserves remnants of magnesian hastingsite, apparently ruling out the possibility that the mafic inclusion and granodiorite represent immiscible liquids. Compositional trends of the recrystallized amphiboles in the inclusions can be explained in terms of recrystallization at a subsolidus stage, presumably in the presence of a fluid, under conditions of generally decreasing temperature and increasing $f(O_2)$.

In the oversaturated syenites, amphibole is predominantly interstitial and varies from hornblende to actinolite in composition; alkali syenite (84-23) contains winchite. The more silicic amphiboles tend to be depleted in Cl relative to their less silicic counterparts. One plagioclase-phyric syenite (MG10) contains a compound xenocryst with kaersutite. Hornblende is also characteristic of the quartz monzonites. The one exception (MG44) contains zoned ferroedenite that apparently crystallized under conditions of low and decreasing $f(O_2)$.

In granite, the magmatic evolutionary trend of amphibole appears to be: magnesio-hornblende ⇒ ferro-hornblende ⇒ ferroedenite, paralleling the progressively more evolved chemical characteristics of their hosts. Brown cores of edenitic hornblende observed in the granite porphyry (MG42) are interpreted to be xenocrysts, possibly derived from a mesocratic intermediate rock type. Grains of amphibole zoned from magnesio-hornblende to actinolite in white granodiorite

are interpreted in the same way as the recrystallized amphiboles of the mafic recrystallized inclusions.

Manganoan potassium arfvedsonite is present in a minority of the tinguaite dykes.

Many different types of coupled substitutions appear to be operating in the amphiboles of the McGerrigle Plutonic Complex. Direct evidence is most commonly observed for the edenite substitution; however, evidence for the Ti-tschermak, tschermak, glaucophane and riebeckite substitutions is also observed.

5. With the exception of the nepheline syenites, titaniferous biotite or titanbiotite is present in all of the rock types studied. Biotite has re-equilibrated in most of the mafic and mesocratic intermediate inclusions with their more felsic hosts. The biotite of the felsic rock types spans a wide range in X_{Fe} (0.44-0.69) and is typically characterized by relatively high F contents (up to 3.1 wt. % F). Manganiferous titaniferous biotite (lepidomelane) is present in the nepheline syenites.

Fe^{3+} determinations all indicate an $f(O_2)$ higher than the Ni-NiO buffer for all rock types (higher than the MH buffer for the miaskitic nepheline syenite). The presence of kaersutite in the gabbro (MG64) and magnetite in the miaskitic nepheline syenite (MG16) suggests that the magmatic $f(O_2)$ may have been lower than indicated by the biotite. The anomalously Mg-rich nature of the biotite in a highly evolved peralkaline tinguaite (MG39) is interpreted to reflect the high $f(O_2)$ of the magma from which it crystallized.

6. The distribution coefficients (K_D) for Fe-Mg, Mn and Mg

between primary clinopyroxene and amphibole suggest that these minerals never crystallized in equilibrium, consistent with the textural data. Kaersutite and biotite in the gabbro (MG64) are also not in equilibrium. The K_D values of amphibole and biotite in the felsic rock types exhibit a range similar to that reported from other felsic suites. The range in K_D values for Fe-Mg, Mn and Ti shown by hornblende and biotite in the mafic and mesocratic intermediate inclusions overlap those observed in the felsic rock types. In samples where siliceous amphibole is present, their Cl depletion relative to biotite, suggests that amphibole may be more susceptible to recrystallization in the presence of a fluid than biotite.

7. With rare exceptions, magnetite and ilmenite are ubiquitous. Magnetite has invariably undergone granular exsolution in the subsolidus and, therefore, cannot be used directly for geothermometry (oxybarometry). In the felsic rock types, primary ilmenite can be distinguished from "exsolved" ilmenite by its lower Mn content; however, this distinction disappears in the more mafic rocks, probably because of the lower initial Mn content of their titaniferous magnetite. The Mn-contents of magnetite and ilmenite are highest in the nepheline syenites, reflecting the high values of the Mn/Fe^{2+} ratio of this rock type; pyrophanite is observed as lamellae in magnetite and apparently as a secondary mineral.

Instead of Fe-Ti oxides, aenigmatite is present in the majority of the peralkaline tinguaites, consistent with the presence of a no-oxide field in which aenigmatite and sodic pyroxene coexist. The aenigmatite exhibits a composition that,

apart from its high Mn-content, is near end-member Ti-aenigmatite.

8. Primary accessory minerals in the mafic and mesocratic intermediate rock types include pyrite, chalcopyrite, pyrrhotite, apatite, zircon, and allanite(?). The silica-oversaturated felsic rock types contain pyrite, pyrrhotite, chalcopyrite, apatite, zircon, titanite, allanite, chevkinite(?) and fluorite. Fluorite is restricted to the most evolved granite samples. Some of the apatite in the felsic samples appears to be xenocrystic. Titanite commonly appears to be secondary; primary titanite was only positively identified in some of the more evolved felsic samples.

The widest variety of accessory minerals is observed in the nepheline syenites: apatite, zircon, titanite, sodalite, aenigmatite, fluorite, astrophyllite, pyrochlore, wohlerite, pectolite and probable members of the eudialyte-eucolite and rosenbushite-gotzenite series were identified. The assemblage of accessory minerals varies from sample to sample; in addition to a dependence on whole-rock chemistry, it appears to be strongly affected by the $f(O_2)$ of the magma. For example, the presence of Na-Zr silicates and astrophyllite in one peralkaline tinguaite (MG37) but not in another that has a identical agpaitic index and a similar whole-rock composition (MG39) [and which contains zircon] is consistent with the higher $f(O_2)$ inferred for the latter.

9. The observed range in $\delta^{18}O$ (whole rock) is 5.6 to 7.9°/oo for the mafic and mesocratic intermediate samples, 5.8 to 6.3°/oo for the syenites, 6.0 to 9.3°/oo for the quartz

monzonites and granites, and 6.6 to 7.7°/oo for the nepheline syenites. The fractionation values for quartz - K-feldspar (Δ) suggest that in some samples K-feldspar has been enriched in ^{18}O relative to quartz; however, for the most part, equilibrium between the two minerals is approximately preserved. Mineralogical evidence suggests that this equilibrium reflects subsolidus rather than magmatic conditions. Therefore, the possibility that some of the higher $\delta^{18}O$ values (whole rock) reflect fluid-rock interactions cannot be ruled out on the basis of the available data. However, there is no evidence of extensive interaction with meteoric water. Most of the samples analyzed exhibit low $\delta^{18}O$ values, which suggest little or no contamination by crustal materials that once resided on or near the Earth's surface. The samples exhibiting values greater than 7.5°/oo require contamination by such material. The exact source and timing of this contamination are unclear; however, the presence of abundant metasedimentary rocks in the aureole of the pluton, the limited development of endoskarn and the anomalously high $\delta^{34}S$ exhibited by one granite (MG46) suggest that this contamination may have occurred at a late, possibly subsolidus stage.

10. Silica-undersaturated mafic magmatism preceded, was contemporaneous with and, in part, postdated felsic magmatism. The mafic rocks contain primary minerals (i.e., labradorite, titansalite and kaersutite) that are characteristic of alkali basaltic rocks. Labradorite and titansalite are the only liquidus or near-liquidus phases positively identified; fractionation of these phases would most likely result in the

formation of a more silica-undersaturated residua (represented by the nepheline syenites?). Some of the fine-grained mafic inclusions contain apparent xenocrysts of labradorite and titansalite (titaniferous salite) that, at least in some cases, crystallized at relatively high pressures and were probably derived from cumulates formed at greater depths. The gabbro studied in detail crystallized at a temperature greater than 950°C, at moderate $f(O_2)$ [i.e., between the QFM and Ni-NiO buffers], and at a relatively high $f(H_2O)$. The alkali basaltic dyke studied probably crystallized at a lower $f(O_2)$ [possibly below the QFM buffer].

11. Mesocratic intermediate rock types, including diorite, monzodiorite and quartz monzodiorite, occur as inclusions within more felsic hosts. Of the mafic minerals present in these rocks, only rare grains of clinopyroxene have not undergone re-equilibration with their more felsic host. The diorites probably represent recrystallized equivalents of the gabbros. A few monzodiorites exhibit excellent evidence that they crystallized from hybrid magmas; however, in general evidence of an origin through magma mixing is lacking. An equally attractive model for many of the samples involves assimilation coupled with fractional crystallization of an alkali basaltic magma.

12. Inclusions of endoskarn are observed in hybrid zones close to the contact with the country rocks in the southern half of the pluton. Endoskarn material generally represents mafic or mesocratic intermediate rock types that have undergone Ca-metasomatism, resulting in the formation of a plagioclase-

diopside-titanite (±rutile) assemblage. The major chemical changes during metasomatism include a large increase in Ca and decreases in K, Fe^{3+} and Fe^{2+}. Similar chemical changes at temperatures greater than 500-550°C affect the highest-grade calcareous rocks of the aureole (Van Bösse 1985). The metasomatizing fluid is believed to have passed through part of the aureole before circulating back into the pluton.

13. The suite of syenitic rocks is interpreted to have an origin distinct from that of the two-feldspar granites (including a majority of the K-feldspar-dominant granites). They are characterized by low amounts of quartz (less than 5%), a generally high Na content and agpaitic index, presence of interstitial amphibole, and a hypersolvus character in the more evolved samples. Rare samples contain alkali amphibole (winchite) and clinopyroxene (aegirine-augite); however, these minerals are interpreted to have formed in the subsolidus as a result of the interaction of the host rock with hydrothermal fluids that were possibly derived from the miaskitic nepheline syenite. All the samples studied exhibit varying degrees of contamination by more primitive material, most likely through hybridization. Mineralogical evidence suggests that the syenites all crystallized at relatively high $f(O_2)$ [i.e., above the QFM buffer] and that the $f(O_2)$ varied from sample to sample. Some samples (e.g., MG8, 83-31) may have undergone magmatic oxidation, reflecting the loss of H_2 via a fluid phase during the final stages of crystallization. The available isotopic and geochemical data suggest that the syenites were formed from a mantle-derived magma that underwent fractional

crystallization - assimilation in the lower crust. However, a model for their derivation through simple melting of a (metasomatized?) lower crust material, as proposed by Morogan & Martin (1985), cannot be ruled out on the basis of the available data.

14. The quartz monzonites appear to be closely related to the granites. Some samples (e.g., MG52) apparently resulted from contamination of a granitic magma by more primitive material; others may be "cumulates" derived from a granitic melt or as a result of the loss of Si from the granitic magma to the abundant mafic and mesocratic intermediate inclusions that are typically present in the hybrid zones of the pluton. With one exception (MG44), the mineral chemistry of the quartz monzonites is consistent with their crystallization under conditions similar to those that governed the two-feldspar granites.

15. A relatively large range of compositionally or texturally (but not necessarily genetically) distinct varieties of granite are recognized in the pluton: K-feldspar-dominant granite, alkali-feldspar (hypersolvus) granite, K-feldspar porphyritic granite, plagioclase-dominant granite, white granodiorite and granite porphyry. All granitic samples studied contain a xenocrystic component (principally plagioclase) derived from more primitive rock types; xenocrysts are most common in the least evolved granites (e.g., MG3, 42, 46). The granites studied crystallized at a relatively high, internally buffered $f(O_2)$ [probably above the Ni-NiO buffer]. However, limited evidence from the K-feldspar-dominant granites suggests that

magmatic oxidation, possibly due to the loss of H_2 via a fluid phase, may have been at least locally important in this rock type. The mineralogy of the granites is consistent with the transitional I- to A-type character indicated by the whole-rock geochemistry (La Rocque 1986). The distinct chemical characteristics of some samples of white granodiorite may in part reflect the partitioning of elements between the granodioritic melt and coexisting mafic liquids. The majority of the available data could be explained by contamination of a mantle-derived magma by material from the lower crust or by direct derivation of the granite through partial melting of isotopically primitive lower crust. The presence of granites (and quartz monzonites) that do exhibit relatively high $\delta^{18}O$ values (up to 9.3°/oo) requires that some ^{18}O-enriched material be involved in their genesis; however, the exact stage at which the granites acquired these high values is not clear. The small amounts of alkali-feldspar (hypersolvus) granite were probably derived through fractionation of a syenitic magma.

16. Two varieties of nepheline syenite are recognized in the northern half of the McGerrigle plutonic complex: pods(?) of miaskitic nepheline syenite and intermediate to peralkaline tinguaite dykes or sills. The variability in the mineral assemblages exhibited by the different nepheline syenites indicates that the physical conditions of crystallization (e.g., T, $f(O_2)$...) varied from sample to sample. The miaskitic nepheline syenite crystallized under relatively high $f(O_2)$ conditions (possibly close to the M-H buffer). The tinguaites appear to have crystallized under a range of $f(O_2)$ conditions

(probably both below and above the QFM buffer) and, at least in some cases, at temperatures around 650°C. The $f(O_2)$ of one sample of peralkaline tinguaite (MG37) was probably buffered by the aegirine-arfvedsonite assemblage, whereas that of the other (MG39) was probably buffered by one or more reaction(s) involving magnetite, biotite and aegirine. Some tinguaites exhibit textural evidence of contamination, including pseudomorphs of mafic phases, feldspar remnants and rare country-rock xenoliths. The nepheline syenites most likely represent residua derived through fractionation of an alkali basaltic magma(s). Their whole-rock isotopic variations are attributed to varying degrees of crustal contamination as the magmas rose to the level of emplacement. The mineralogical data indicate that the miaskitic nepheline syenite is unlikely to represent the parent of the more evolved tinguaites. The chemical similarities between the intermediate and peralkaline tinguaites studied are considered principally to reflect their derivation from the same magma; their differences may reflect the loss of an Na-, Zr- and rare-element-rich volatile phase.

REFERENCES

Abdel-Rahman, A. M. & Martin, R. F. (1987a): The Deloro anorogenic igneous complex, Madoc, Ontario. 1. Geochemistry and feldspar mineralogy of the felsic plutonic rocks. Can. Mineral. **25**, 321-336.

Abdel-Rahman, A. M. & Martin, R. F. (1987b): Lithospheric metasomatism and within-plate magmatism in northeastern Egypt. Geol. Soc. Amer. Abstr. Program **19**, 566.

Akasaka, M. & Onuma, K. (1980): The join $CaMgSi_2O_6$-$CaFeAlSiO_6$-$CaTiAl_2O_6$ and its bearing on the Ti-rich fassaitic pyroxenes. Contr. Mineral. Petrology **71**, 301-312.

Akella, J. & Boyd, F. R. (1973): Partitioning of Ti and Al between coexisting silicates, oxides, and liquids. Proc. 4th Lunar Sci. Conf. (Supp. 4, Geochim. Cosmochim. Acta), **1**, 1049-1059.

Anderson, J. L. (1980): Mineral equilibria and crystallization conditions in the Late Precambrian Wolf River rapakivi massif, Wisconsin. Amer. J. Sci. **280**, 289-332.

Anderson, J. L. (1983): Proterozoic anorogenic granite plutonism of North America. In Proterozoic Geology: Selected Papers from an International Proterozoic Symposium (L. G. Medaris, Jr., C. W. Byers, D. M. Mickelson & W. C. Shanks, eds.). Geol. Soc. Amer. Mem. **161**, 133-154.

Appleman, D. E. & Evans, H. T., Jr. (1973): Job 9214: Indexing and least-squares refinement of powder diffraction data. U. S. Geol. Surv., Comp. Contr. **20**.

Bailey, D. K. (1969): The stability of acmite in the presence of H_2O. Amer. J. Sci. **267-A**, 1-16.

Bailey, D. K. (1974): Melting in the deep crust. In The Alkaline Rocks (H. Sørensen, ed.). John Wiley & Sons, New York, 436-442.

Bailey, D. K. & Schairer, J. F. (1966): The system Na_2O-Al_2O_3-Fe_2O_3-SiO_2 at 1 atmosphere, and the petrogenesis of alkaline rocks. J. Petrology **7**, 114-170.

Barker, F., Wones, D. R., Sharp, W. N. and Desborough, G. A. (1975): The Pikes Peak batholith, Colorado Front Range, and a model for the origin of the gabbro-anorthosite-syenite-potassic granite suite. Precamb. Res. **2**, 97-160.

Beaudin, J. (1980): Région du Mont Albert et du Lac Cascapédia. Ministère de l'Energie et des Ressources, Québec, Rapport Final, DPV-705.

Bédard, J. H. (1985): The opening of the Atlantic, the Mesozoic

New England igneous province, and mechanisms of continental breakup. Tectonophys. **113**, 209-232.

Bédard, J. H. (1986): Pre-Acadian magmatic suites of the southeastern Gaspé Peninsula. Geol. Soc. Amer. Bull. **97**, 1177-1191.

Bédard, J. H., Ludden, J. N. & Francis, D. M. (1987): The Mégantic intrusive complex, Québec: a study of the derivation of silica-oversaturated anorogenic magmas of alkaline affinity. J. Petrology **28**, 355-388.

Béland, J. (1969): The geology of Gaspé. Can. Inst. Mining Trans. **72**, 213-220.

Béland, J. (1974): La tectonique des Appalaches du Québec. Geosc. Canada **1**, 4, 26-32.

Béland, J. (1982): Geology of the Quebec Appalachians. In Guidebook to Excursion 7B: Paleozoic Continental Margin Sedimentation in the Quebec Appalachians (R. Hesse, G. V. Middleton & B. R. Rust, eds.). McMaster University, Hamilton, 11-23.

Bender, J. F., Hanson, G. N. & Bence, A. E. (1982): The Cortlandt complex: evidence for large-scale liquid immiscibility involving granodiorite and diorite magmas. Earth Planet. Sci. Lett. **58**, 330-344.

Bird, D. K., Schiffman, P., Elders, W. A., Williams, A. E. & McDowell, S. D. (1984): Calc-silicate mineralization in active geothermal systems. Econ. Geol. **79**, 671-695.

Bird, J. M. & Dewey, J. F. (1970): Lithosphere plate - continental margin tectonics and the evolution of the Appalachian orogen. Geol. Soc. Amer. Bull. **81**, 1031-1060.

Blasi, A. (1977): Calculation of T-site occupancies in alkali feldspar from refined lattice constants. Mineral. Mag. **41**, 525-526.

Blaxland, A. B., van Breemen, O., Emeleus, C. H. and Anderson, J. G. (1978): Age and origin of the major syenite centers in the Gardar province of south Greenland: Rb-Sr studies. Geol. Soc. Amer. Bull. **89**, 231-244.

Bonin, B. & Giret, A. (1984): The plutonic alkaline series: the problem of their origin and differentiation, the role of their mineralogical assemblages. Phys. Earth Planet. Inter. **35**, 212-221.

Bottinga, Y. & Javoy, M. (1973): Comments on oxygen isotope geothermometry. Earth Planet. Sci. Lett. **20**, 250-265.

Bottinga, Y. & Javoy, M. (1975): Oxygen isotope partitioning

among the minerals in igneous and metamorphic rocks. Rev. Geophys. Space Phys. 13, 401-418.

Bourque, P. A., Laurent, R. & St.-Julien, P. (1985): Acadian wrench faulting in southern Gaspé Peninsula, Québec Appalachians. Geol. Assoc. Can.-Mineral. Assoc. Can. Program Abstr. 10, A6.

Bowen, N. L. (1945): Phase equilibria bearing on the origin and differentiation of alkaline rocks. Amer. J. Sci. 243A, 75-89.

Bradley, D. C. (1983): Tectonics of the Acadian orogeny in New England and adjacent Canada. J. Geol. 91, 381-400.

Brooks, C. K., Engell, J. Larsen, L. M. & Pedersen A. K. (1982): Mineralogy of the Werner Bjerge alkaline complex, East Greenland. Meddr. Grønland Geoscience 7.

Brousse, R. & Rançon, J. PH. (1984): Crystallization trends of pyroxenes from agpaitic phonolites (Cantal, France). Mineral. Mag. 48, 39-45.

Brown, P. E. & Becker, S. M. (1986): Fractionation, hybridisation and magma-mixing in the Kialineq centre, east Greenland. Contr. Mineral. Petrology 92, 57-70.

Buddington, A. F. & Lindsley, D. H. (1964): Iron-titanium oxide minerals and synthetic equivalents. J. Petrology 5, 310-357.

Burnham, C. W. (1979): The importance of volatile constituents. In The Evolution of the Igneous Rocks: Fiftieth Anniversary Perspectives (H. S. Yoder, ed.), Princeton University Press, Princeton, 439-482.

Burt, D. M. & Burton, J. H. (1984): Vector representation of lithium and other mica compositions using exchange operators. Geol. Soc. Amer. Abstr. Program 16, 460.

Calvo, C. & Faggiani, R. (1974): A re-investigation of the crystal structure of chevkinite and perrierite. Amer. Mineral. 59, 1277-1285.

Cameron, M. & Papike, J. J. (1981): Structural and chemical variations in pyroxenes. Amer. Mineral. 66, 1-50.

Campbell, I. H. & Borley, G. D. (1974): The geochemistry of pyroxenes from the lower layered series of the Jimberlana Intrusion, Western Australia. Contr. Mineral. Petrology 47, 281-297.

Campbell, I. H. & Turner, J. S. (1986): The influence of viscosity on fountains in magma chambers. J. Petrology 27, 1-30.

Carmichael, I. S. E. (1967): The iron-titanium oxides of salic

volcanic rocks and their associated ferromagnesian silicates. Contr. Mineral. Petrology 14, 36-64.

Carmichael, I. S. E. & Nicholls, J. (1967): Iron-titanium oxides and oxygen fugacities in volcanic rocks. J. Geophys. Res. 72, 4665-4687.

Carmichael I. S. E., Nicholls, J. & Smith, A. L. (1970): Silica activity in igneous rocks. Amer. Mineral. 55, 246-263.

Carmichael, I. S. E., Turner, F. J. & Verhoogen, J. (1974): Igneous Petrology. McGraw-Hill Book Company, New York.

Carr, G. R., Phillips, E. R. & Williams, P. R. (1976): An occurrence of eudialyte and manganoan pectolite in a phonolite dyke from south-eastern Queensland. Mineral. Mag. 40, 853-856.

Cavarretta, G., Gianelli, G. & Puxeddu, M. (1982): Formation of authigenic minerals and their use as indicators of the physicochemical parameters of the fluid in the Larderello-Travale geothermal field. Econ. Geol. 77, 1071-1084.

Cawthorn, R. G. (1976): Some chemical controls on igneous amphibole compositions. Geochim. Cosmochim. Acta 40, 1319-1328.

Chappell, B. W. & White, A. J. R. (1974): Two contrasting granite types. Pacific Geol. 8, 173-174.

Charles, R. W. (1975): The phase equilibria of richterite and ferrorichterite. Amer. Mineral. 60, 367-374.

Cherry, M. E. & Trembath, L. T. (1978): The pressure quench formation of rapakivi texture. Contr. Mineral. Petrology 68, 1-6.

Chivas, A. R. (1981): Geochemical evidence for magmatic fluids in porphyry copper mineralization. 1. Mafic silicates from the Koloula igneous complex. Contr. Mineral. Petrology 78, 389-403.

Christiansen, E. H. & Lee, D. E. (1986): Fluorine and chlorine in granitoids from the Basin and Range province, western United States. Econ. Geol. 81, 1484-1494.

Clayton, R. N. & Mayeda, T. K. (1963): The use of bromine pentafluoride in the extraction of oxygen from oxides and silicates for isotopic analysis. Geochim. Cosmochim. Acta 27, 43-52.

Clemens, J. D., Holloway, J. R. & White, A. J. R. (1986): Origin of an A-type granite: experimental constraints. Amer. Mineral. 71, 317-324.

Coish, R. A. & Taylor, L. A. (1979): The effects of cooling rate on texture and pyroxene chemistry in DSDP Leg 34 basalt: A microprobe study. Earth Planet. Sci. Lett. **42**, 389-398.

Cole, D. R. & Ohmoto, H. (1986): Kinetics of isotopic exchange at elevated temperatures and pressures. In Stable Isotopes in High Temperature Geological Processes (J. W. Valley, H. P. Taylor, Jr. & J. R. O'Neil, eds.). Mineral. Soc. Amer., Rev. Mineral. **16**, 41-90.

Cole, D. R., Ohmoto, H. & Lasaga, A. C. (1981): Rates of oxygen and hydrogen isotopic exchange in mineral-fluid systems; surface exchange versus diffusion. Geol. Soc. Amer. Abstr. Program **13**, 428.

Collerson, K. D. (1982): Geochemistry and Rb-Sr geochronology of associated Proterozoic peralkaline and subalkaline anorogenic granites from Labrador. Contrib. Mineral. Petrology **81**, 126-147.

Collins, W. J., Beams, S. D., White, A. J. R. & Chappell, B. W. (1982): Nature and origin of A-type granites with particular reference to southeastern Australia. Contr. Mineral. Petrology **80**, 189-200.

Coombs, D. S. & Wilkinson, J. F. G. (1969): Lineages and fractionation trends in undersaturated volcanic rocks from the East Otago volcanic province (New Zealand) and related rocks. J. Petrology **10**, 440-501.

Criss, R. E. & Taylor, H. P., Jr. (1983): An $^{18}O/^{16}O$ and D/H study of Tertiary hydrothermal systems in the southern half of the Idaho batholith. Geol. Soc. Amer. Bull. **94**, 640-663.

Criss, R. E. & Taylor, H. P., Jr. (1986): Meteoric-hydrothermal systems. In Stable Isotopes in High Temperature Geological Processes (J. W. Valley, H. P, Taylor, Jr. & J. R. O'Neil, eds.). Mineral. Soc. Amer., Rev. Mineral. **16**, 373-424.

Currie, K. L. (1976): The alkaline rocks of Canada. Geol. Surv. Can. Bull. **239**.

Curtis, L. W. & Currie, K. L. (1981): Geology and petrology of the Red Wine alkaline complex, central Labrador. Geol. Surv. Can. Bull. **294**.

Czamanske, G. K. & Atkin, S. A. (1985): Metasomatism, titanian acmite, and alkali amphiboles in lithic-wacke inclusions within the Coyote Peak diatreme, Humboldt County, California. Amer. Mineral. **70**, 499-516.

Czamanske, G. K., Ishihara, S. & Atkin, S. A. (1981): Chemistry of rock-forming minerals of the Cretaceous-Paleocene batholith in southwestern Japan and implications for magma genesis. J. Geophys. Res. **86**, B11, 10431-10469.

Czamanske, G. K. & Mihálik, P. (1972): Oxidation during magmatic differentiation. Finnmarka complex, Oslo area, Norway. 1. The opaque oxides. J. Petrology **13**, 493-509.

Czamanske, G. K. & Wones, D. R. (1973): Oxidation during magmatic differentiation, Finnmarka complex, Oslo area, Norway. 2. The mafic silicates. J. Petrology **14**, 349-380.

Czamanske, G. K., Wones, D. R. & Eichelberger, J. C. (1977): Mineralogy and petrology of the intrusive complex of the Pliny Range, New Hampshire. Amer. J. Sci. **277**, 1073-1123.

Deer, W. A., Howie, R. A. & Zussman, J. (1963): Rock-Forming Minerals. 4. Framework Silicates. Longmans, Green and Co. Ltd., London.

Deer, W. A., Howie, R. A. & Zussman, J. (1975): An Introduction to the Rock-Forming Minerals. Longman Group Limited, London.

Deer, W. A., Howie, R. A. & Zussman, J. (1978): Rock-Forming Minerals. 2A. Single-Chain Silicates (2nd edition). Longman Group Limited, London.

Deer, W. A., Howie, R. A. & Zussman, J. (1986): Rock-Forming Minerals. 1B. Disilicates and Ring Silicates (2nd edition). John Wiley & Sons, New York.

DePaolo, D. J. (1981): Trace element and isotopic effects of combined wallrock assimilation and fractional crystallization. Earth Planet. Sci. Lett. **53**, 189-202.

de Römer, H. S. (1974): Geology and age of some plutons in north-central Gaspé, Canada. Can. J. Earth Sci. **11**, 570-582.

de Römer, H. S. (1977): Région des Monts McGerrigle. Ministère des Richesses Naturelles, Québec, Rapport Géologique **174**.

Didier, J. (1973): Granites and their Enclaves. Elsevier Scientific Publishing Company, New York.

Didier, J. (1987): Contribution of enclave studies to the understanding of origin and evolution of granitic magmas. Geologische Rundschau **76**, 41-50.

Dodge, F. C. W. & Ross, D. C. (1971): Coexisting hornblendes and biotites from granitic rocks near the San Andreas fault, California. J. Geol. **79**, 158-172.

Dodge, F. C. W., Smith, V. C. & Mays, R. E. (1969): Biotites from granitic rocks of the central Sierra Nevada batholith, California. J. Petrology **10**, 250-271.

Dolfi, D. & Trigila, R. (1983): Clinopyroxene solid solutions and water in magmas: results in the system phonolitic tephrite-H_2O, Mineral. Mag. **47**, 347-351.

Downes, M. J. (1974): Sector and oscillatory zoning in calcic augites from M. Etna, Sicily. Contr. Mineral. Petrology **47**, 187-196.

Dowty, E. (1976): Crystal structure and crystal growth. II. Sector zoning in minerals. Amer. Mineral. **61**, 460-469.

Duquette, G., Lachance, S. & Morin, R. (1984): Géologie et forages stratigraphiques: Mont Vallières-de-Saint-Réal. Ministère de l'Energie et des Ressources, Québec, **ET83-10**.

Eby, G. N. (1984): Monteregian Hills. I. Petrography, major and trace element geochemistry and strontium isotopic chemistry of the western intrusions: Mounts Royal, St. Bruno, and Johnson. J. Petrology **25**, 421-452.

Eby, G. N. (1985): Monteregian Hills. II. Petrography, major and trace element geochemistry and strontium isotopic chemistry of the eastern intrusions: Mounts Shefford, Brome and Megantic. J. Petrology **26**, 418-448.

Edgar, A. D. (1984): Chemistry, occurrence and paragenesis of feldspathoids: a review. In Feldspars and Feldspathoids-Structures, Properties and Occurrences. D. Reidel Publishing Company, Dordrecht, 501-532.

Eichelberger, J. C. (1980): Vesiculation of mafic magma during replenishment of silicic magma reservoirs. Nature **288**, 446-450.

Einaudi, M. T. & Burt, D. M. (1982): A special issue devoted to skarn deposits: Introduction - terminology, classification and composition of skarn deposits. Econ. Geol. **77**, 745-754.

Ernst, W. G. (1968): Amphiboles: Crystal Chemistry, Phase Relations and Occurrence. Springer-Verlag, New York.

Exley, R. A. (1980): Microprobe studies of REE-rich accessory minerals: implications for Skye granite petrogenesis and REE mobility in hydrothermal systems. Earth Planet. Sci. Lett. **48**, 97-110.

Fabriès, J., Conquéré, F. & Arnaud, J. (1984): The mafic silicates in the Saint Quay-Portrieux gabbro-diorite intrusion: crystallization conditions of a calc-alkaline pluton. Bull. Minéral. **107**, 715-736.

Ferguson, A. K. (1977): The natural occurrence of aegirine-neptunite solid solution. Contr. Mineral. Petrology **60**, 247-253.

Ferry, J. M. (1985a): Hydrothermal alteration of Tertiary igneous rocks from the Isle of Skye, northwest Scotland. I. Gabbros. Contr. Mineral. Petrology **91**, 264-282.

Ferry, J. M. (1985b): Hydrothermal alteration of Tertiary igneous rocks from the Isle Of Skye, northwest Scotland. II. Granites. Contr. Mineral. Petrology **91**, 283-304.

Fodor, R. V., Keill, K. & Bunch, T. E. (1975): Contributions to the mineral chemistry of Hawaiian rocks. IV. Pyroxenes in rocks from the Haleakala and West Maui volcanoes, Maui, Hawaii. Contr. Mineral. Petrology **50**, 173-195.

Foland, K. A., Henderson, C. M. B. & Gleason, J. (1985): Petrogenesis of the magmatic complex at Mount Ascutney, Vermont, USA. I. Assimilation of crust by mafic magmas based on Sr and O isotopic and major element relationships. Contr. Mineral. Petrology **90**, 331-345.

Folk, R. L. (1955): Note on the significance of "turbid" feldspars. Amer. Mineral. **40**, 356-357.

Forester, R. W. & Taylor, H. P., Jr. (1980): Oxygen, hydrogen and carbon isotope studies of the Stony Mountain Complex, Western San Juan Mountains, Colorado. Econ. Geol. **75**, 362-383.

Frost, T. P. & Mahood, G. A. (1987): Field, chemical, and physical constraints on mafic-felsic magma interaction in the Lamarck Granodiorite, Sierra Nevada, California. Geol. Soc. Amer. Bull. **99**, 272-291.

Gagnon, Y. D. & Jamieson, R. A. (1985): Geology of the Mont Albert region, Gaspé Peninsula, Quebec. In Current Research, Part A. Geol. Surv. Can. Pap. **85-1A**, 783-788.

Gerasimovsky, V. I. (1974): Trace elements in selected groups of alkaline rocks. In The Alkaline Rocks (H. Sørensen, ed.). John Wiley & Sons, New York, 402-412.

Gibb, F. G. F. (1973): The zoned clinopyroxenes of the Shiant Isles sill, Scotland. J. Petrology **14**, 203-230.

Gilbert, M. C., Helz, R. T., Popp, R. K. & Spear, F. S. (1982): Experimental studies of amphibole stability. In Amphiboles: Petrology and Experimental Phase Relations (D. R. Veblen & P. H. Ribbe, eds.). Mineral. Soc. Amer., Rev. Mineral. **9B**, 229-353.

Giletti, B. J. (1986): Diffusion effects on oxygen isotope temperatures of slowly cooled igneous and metamorphic rocks. Earth Planet. Sci. Lett. **77**, 218-228.

Girard, P. (1967): Géologie de la région du Mont Richardson. Ministère Richesses Naturelles, Québec, Rapport Préliminaire **563**.

Girard, P. (1969): Geology of the Madeleine mines deposit. Can. Inst. Mining Trans. **72**, 239-247.

Girard, P. (1971): The Madeleine copper mine, Gaspé, Quebec: a hydrothermal deposit. Ph.D. thesis, McGill University, Montreal, Quebec.

Girardeau, J. & Mevel, C. (1982): Amphibolitized sheared gabbros from ophiolites as indicators of the evolution of the oceanic crust: Bay of Islands, Newfoundland. Earth Planet. Sci. Lett. **61**, 151-165.

Giret, A., Bonin, B. & Leger, J.-M. (1980): Amphibole compositional trends in oversaturated and undersaturated alkaline plutonic ring-complexes. Can. Mineral. **18**, 481-495.

Gomes, C. de B., Moro, S. L. & Dutra, C. V. (1970): Pyroxenes from the alkaline rocks of Itapirapuã, São Paulo, Brazil. Amer. Mineral. **55**, 224-230.

Gorbatschev, R. (1977): The influence of some compositional relations on the partition of Fe and Mg between biotite and Ca-amphibole. Neues. Jahrb. Mineral. Abh. **130**, 3-11.

Greenland, L. P., Gottfried, D. & Tilling, R. I. (1968): Distribution of manganese between coexisting biotite and hornblende in plutonic rocks. Geochim. Cosmochim. Acta **32**, 1149-1163.

Gregory, R. T. & Criss, R. E. (1986): Isotopic exchange in open and closed systems. In Stable Isotopes in High Temperature Geological Processes (J. W. Valley, H. P. Taylor, Jr. & J. R. O'Neil, eds.). Mineral. Soc. Amer., Rev. Mineral. **16**, 91-127.

Gupta, A. K., Onuma, K., Yagi, K. & Lidiak, E. G. (1973): Effect of silica concentration on the diopsidic pyroxenes in the system diopside-$CaTiAl_2O_6$-SiO_2. Contr. Mineral. Petrology **41**, 333-344.

Haggerty, S. E. (1976): Opaque mineral oxides in terrestrial igneous rocks. In Oxide Minerals (D. Rumble III, ed.). Mineral. Soc. Amer., Rev. Mineral. **3**, Hg101-Hg300.

Harris, N. B. and Einaudi, M. T. (1982): Skarn deposits in the Yerington district, Nevada: metasomatic skarn evolution near Ludwig. Econ. Geol. **77**, 877-898.

Hazen, R. M. & Wones, D. R. (1972): The effect of cation substitutions on the physical properties of trioctahedral micas. Amer. Mineral. **57**, 103-129.

Helz, R. T. (1973): Phase relations of basalts in their melting range at $P(H_2O)$=5 kb as a function of oxygen fugacity. 1. Mafic phases. J. Petrology **14**, 249-302.

Hewins, R. H. (1974): Pyroxene crystallization trends and contrasting augite zoning in the Sudbury Nickel Irruptive. Amer. Mineral. **59**, 120-126.

Hewitt, D. A. & Abrecht, J. (1986): Limitations on the interpretation of biotite substitutions from chemical analyses of natural samples. Amer. Mineral. **71**, 1126-1128.

Hewitt, D. A. & Wones, D. R. (1984): Experimental phase relations of the micas. In Micas (S. W. Bailey, ed.). Mineral. Soc. Amer., Rev. Mineral. **13**, 201-256.

Hibbard, M. J. (1981): The magma mixing origin of mantled feldspars. Contr. Mineral. Petrology **76**, 158-170.

Hill, R. I., Silver, L. T. & Taylor, H. P., Jr. (1986): Coupled Sr-O isotope variations as an indicator of source heterogeneity for the northern Peninsular Ranges batholith. Contr. Mineral. Petrology **92**, 351-361.

Himmelberg, G. R. & Ford, A. B. (1977): Iron-titanium oxides of the Dufek intrusion, Antartica. Amer. Mineral. **62**, 623-633.

Hogarth, D. D. (1977): Classification and nomenclature of the pyrochlore group. Amer. Mineral. **62**, 403-410.

Hollister, L. S. & Gancarz, A. J. (1971): Compositional sector-zoning in clinopyroxene from the Narce area, Italy. Amer. Mineral. **56**, 959-979.

Huppert, H. E., Sparks, R. S. J. & Turner, J. S. (1982): Effects of volatiles on mixing in calc-alkaline magma systems. Nature **297**, 554-557.

Irvine, T. N. & Baragar, W. R. A. (1971): A guide to the chemical classification of the common volcanic rocks. Can. J. Earth Sci. **8**, 523-548.

Islam, S., Hesse, R. & Chagnon, A. (1982): Zonation of diagenesis and low-grade metamorphism in Cambro-Ordovician flysch of Gaspé Peninsula, Quebec Appalachians. Can. Mineral. **20**, 155-167.

Ito, J. (1967): A study of chevkinite and perrierite. Amer. Mineral. **52**, 1094-1104.

Jahns, R. H. & Burnham, C. W. (1969): Experimental studies of pegmatite genesis. I. A model for the derivation and crystallization of granitic pegmatites. Econ. Geol. **64**, 843-864.

James, D. E. (1981): The combined use of oxygen and radiogenic isotopes as indicators of crustal contamination. Ann. Rev. Earth Planet. Sci. **9**, 311-344.

James, R. S. & Hamilton, D. L. (1969): Phase relations in the system $NaAlSi_3O_8$-$KAlSi_3O_8$-$CaAl_2Si_2O_8$-SiO_2 at 1 kilobar water vapour pressure. Contr. Mineral. Petrology **21**, 111-141.

Jones, A. P. & Peckett, A. (1980): Zirconium-bearing aegirines from Motzfeldt, south Greenland. Contr. Mineral. Petrology **75**, 251-255.

Jones, I. W. (1933): The Tabletop map-area, Gaspé Peninsula. Service des Mines, Québec, annual report for the calendar year 1932, part D, 3-32.

Kalamarides, R. I. (1984): Kiglapait geochemistry. VI. Oxygen isotopes. Geochim. Cosmochim. Acta **48**, 1827-1836.

Keppie, J. D., St.-Julien, P., Hubert, C., Béland, J., Skidmore, B., Fyffe, L. R., Ruitenberg, A. A., McCutcheon, S. R., Williams, H. & Bursnall, J. (1980): Times of deformation in the Canadian Appalachians. In Regional Trends in the Geology of the Appalachian-Caledonian-Hercynian-Mauritanide Orogen (P. E. Schenk, ed.). D. Reidel Publishing Company, Dordrecht, 307-313.

Kogarko, L. N. (1974): Role of volatiles. In The Alkaline Rocks (H. Sørensen, ed.). John Wiley & Sons, New York, 474-487.

Kretz, R. (1960): The distribution of certain elements among coexisting calcic pyroxenes, calcic amphiboles and biotites in skarns. Geochim. Cosmochim. Acta **20**, 161-191.

Kroll, H. & Ribbe, P. H. (1983): Lattice parameters, composition and Al, Si order in alkali feldspars. In Feldspar Mineralogy (P. H. Ribbe, ed.). Mineral. Soc. Amer., Rev. Mineral. **2** (2nd edition), 57-99.

Kumarapeli, P. S. (1970): Monteregian alkalic magmatism and the St. Lawrence Rift System in space and time. Can. Mineral. **10**, 421-431.

Kumarapeli, P. S. & Saull, V. A. (1966): The St. Lawrence Valley system: a North American equivalent of the East African Rift Valley system. Can. J. Earth Sci. **3**, 639-658.

Kuo, L.-C. & Kirkpatrick, R. J. (1982): Pre-eruption history of phyric basalts from DSDP Legs 45 and 46: evidence from morphology and zoning patterns in plagioclase. Contr. Mineral. Petrology **79**, 13-27.

Kushiro, I. (1960): Si-Al relation in clinopyroxenes from igneous rocks. Amer. J. Sci. **258**, 548-554.

Kushiro, I. (1969): Clinopyroxene solid solutions formed by reactions between diopside and plagioclase at high pressures. Mineral. Soc. Amer. Spec. Pap. **2**, 179-191.

Kyle, P. R. (1981): Mineralogy and geochemistry of a basanite to phonolite sequence at Hut Point Peninsula, Antarctica, based on core from Dry Valley drilling project drillholes 1, 2 and 3. J. Petrology **22**, 451-500.

Kyser, T. K. (1986): Stable isotope variations in the mantle. In Stable Isotopes in High Temperature Geological Processes (J. W. Valley, H. P. Taylor, Jr. & J. R. O'Neil, eds.). Mineral. Soc. Amer., Rev. Mineral. 16, 141-164.

Lachance, S. & Duquette, G. (1977): Région de Boisbuisson (NW). Ministère des Richesses Naturelles, Québec, Rapport Géologique 187.

Laird, J. & Albee, A. L. (1981): High-pressure metamorphism in mafic schist from northern Vermont. Amer. J. Sci. 281, 97-126.

Lalonde, A. E. & Martin, R. F. (1983): The Baie-des-Moutons syenitic complex, La Tabatière, Québec. 1. Petrography and feldspar mineralogy. Can. Mineral. 21, 65-79.

La Rocque, C. (1986): Geochronology and Petrology of North-Central Gaspé Igneous Rocks, Quebec. M.Sc. thesis, McGill University, Montreal, Quebec.

La Rocque, C. & Doig, R. (1984): Geochemistry and geochronology of York River Formation volcanic rocks and associated intrusive of the Gaspe Peninsula, Quebec. Maritime Sediments and Atlantic Geology 20, 114-115.

Larsen, L. M. (1976): Clinopyroxenes and coexisting mafic minerals from the alkaline Ilímaussaq intrusion, south Greenland. J. Petrology 17, 258-290.

Larsen, L. M. (1977): Aenigmatites from the Ilímaussaq intrusion, south Greenland: chemistry and petrological implications. Lithos 10, 257-270.

Larsen, L. M. & Steenfelt, A. (1974): Alkali loss and retention in an iron-rich peralkaline phonolite dyke from the Gardar province, south Greenland. Lithos 7, 81-90.

Leake, B. E. (1971): On aluminous and edenitic hornblendes. Mineral. Mag. 38, 389-407.

Leake, B. E. (1978): Nomenclature of amphiboles. Can. Mineral. 16, 501-520.

Le Bas, M. J. (1962): The role of aluminum in igneous clinopyroxenes with relation to their parentage. Amer. J. Sci. 260, 267-288.

Lebel, D. & Hubert, C. (1986): Acadian wrench tectonics in the Rimouski-Matapedia area of the Québec Appalachians: a model. Geol. Assoc. Can.-Mineral. Assoc. Can. Program Abstr. 11, A94.

Leeman, W. P., Menzies, M. A., Matty, D. J. & Embree, G. F. (1985): Strontium, neodymium and lead isotopic compositions

of deep crustal xenoliths from the Snake River Plain: evidence for Archean basement. Earth Planet. Sci. Lett. 75, 354-368.

Leung, I. S. (1974): Sector-zoned titanaugites: morphology, crystal chemistry and growth. Amer. Mineral. 59, 127-138.

Loiselle, M. C. & Wones, D. R. (1979): Characteristics and origin of anorogenic granites. Geol. Soc. Amer. Abstr. Program 11, 468.

Longstaffe, F. J. (1987): Stable isotope studies of diagenetic processes. In Stable Isotope Geochemistry of Low Temperature Processes (T. K. Kyser, ed.). Mineral. Assoc. Can., Short-Course Handbook 13, 187-257.

Loomis, T. P. & Welber, P. W. (1982): Crystallization processes in the Rocky Hill granodiorite pluton, California: an interpretation based on compositional zoning of plagioclase. Contr. Mineral. Petrology 81, 230-239.

Low, A. P. (1885): Report on explorations and surveys in the interior of the Gaspé Peninsula. Geol. Surv. Can.; report of progress for 1882-83-84.

MacDonald, R. (1974): The role of fractional crystallization in the formation of the alkaline rocks. In The Alkaline Rocks (H. Sørensen, ed.). John Wiley & Sons, New York, 442-459.

MacDonald, R. & Saunders, M. J. (1973): Chemical variation in minerals of the astrophyllite group. Mineral. Mag. 39, 97-111.

MacKenzie, W. S., Donaldson, C. H. and Guilford, C. (1984): Atlas of igneous rocks and their textures. Longman Group Limited, Burnt Mill, Harlow, England.

Manning, C. E. & Bird, D. K. (1986): Hydrothermal clinopyroxenes of the Skaergaard intrusion. Contr. Mineral. Petrology 92, 437-447.

Marsh, J. S. (1975): Aenigmatite stability in silica-undersaturated rocks. Contr. Mineral. Petrology 50, 135-144.

Marsh, J. S. (1987): Evolution of a strongly differentiated suite of phonolites from the Klinghardt Mountains, Namibia. Lithos 20, 41-58.

Marshall, L. A. & Sparks, R. S. J. (1984): Origin of some mixed-magma and net-veined ring intrusions. J. Geol. Soc. London 141, 171-182.

Martin, R. F. (1974): Controls of ordering and subsolidus phase relations in the alkali feldspars. In The Feldspars (W. S. MacKenzie & J. Zussman, eds.). Manchester University Press,

Manchester, 313-336.

Martin, R. F. & Bonin, B. (1976): Water and magma genesis: the association hypersolvus granite - subsolvus granite. Can. Mineral. **14**, 228-237.

Mason, D. R. (1978): Compositional variations in ferromagnesian minerals from porphyry copper-generating and barren intrusions of the Western Highlands, Papua New Guinea. Econ. Geol. **73**, 878-890.

Mathison, C. I. (1975): Magnetites and ilmenites in the Somerset Dam layered basic intrusion, southeastern Queensland. Lithos **8**, 93-111.

Matsuhisa, Y., Goldsmith, J. R. & Clayton, R. N. (1979): Oxygen isotopic fractionation in the system quartz-albite-anorthite-water. Geochim. Cosmochim. Acta **43**, 1131-1140.

McBirney, A. R. (1979): Effects of assimilation. In The Evolution of the Igneous Rocks: Fiftieth Anniversary Perspectives (H. S. Yoder, ed.), Princeton University Press, Princeton, 307-338.

McBirney, A. R., Baker, B. H. & Nilson, R. H. (1985): Liquid fractionation. 1. Basic principles and experimental simulations. J. Volc. Geotherm. Res. **24**, 1-24.

McDowell, S. D. (1978): Little Chief granite porphyry: feldspar crystallization history. Geol. Soc. Amer. Bull. **89**, 33-49.

McGerrigle, H. W. & Skidmore, W. D. (1967): Geological Map, Gaspé Peninsula. Ministère Richesses Naturelles, Québec, Map **1642**.

Mitchell, R. H. & Platt, R. G. (1978): Mafic mineralogy of ferroaugite syenite from the Coldwell alkaline complex, Ontario, Canada. J. Petrology **19**, 627-651.

Mitchell, R. H. & Platt, R. G. (1982): Mineralogy and petrology of nepheline syenites from the Coldwell alkaline complex, Ontario, Canada, J. Petrology **23**, 186-214.

Mørk, M. B. E. (1984): Magma mixing in the post-glacial Veidivötn fissure eruption, southeast Iceland: a microprobe study of mineral and glass variations. Lithos **17**, 55-75.

Morogan, V. & Martin, R. F. (1985): Mineralogy and partial melting of fenitized crustal xenoliths in the Oldoinyo Lengai carbonatitic volcano, Tanzania. Amer. Mineral. **70**, 1114-1126.

Morse, S. A. (1968): Syenites. Carnegie Inst. Washington Year Book **67**, 112-120.

Munoz, J. L. (1984): F-OH and Cl-OH exchange in micas with

applications to hydrothermal ore deposits. In Micas (S. W. Bailey, ed.). Mineral. Soc. Amer., Rev. Mineral. 13, 469-493.

Munoz, J. L. & Ludington, S. D. (1974): Fluoride-hydroxyl exchange in biotite. Amer. J. Sci. 274, 396-413.

Maney, M. T. (1983): Phase equilibria of rock-forming ferromagnesian silicates in granitic systems. Amer. J. Sci. 283, 993-1033.

Neumann, E.-R. (1974): The distribution of Mn^{2+} and Fe^{2+} between ilmenites and magnetites in igneous rocks. Amer. J. Sci. 274, 1074-1088.

Neumann, E.-R. (1980): Petrogenesis of the Oslo region larvikites and associated rocks. J. Petrology 21, 499-531.

Neumann, E.-R., Larsen, B. T. & Sundvoll, B. (1985): Compositional variations among gabbroic intrusions in the Oslo rift. Lithos 18, 35-59.

Nielsen, T. F. D. (1979): The occurrence and formation of Ti-aegirines in peralkaline syenites. An example from the Tertiary ultramafic alkaline Gardiner Complex, east Greenland. Contr. Mineral. Petrology 69, 235-244.

Nockolds, S. R. (1947): The relation between chemical composition and paragenesis in the biotite micas of igneous rocks. Amer. J. Sci. 245, 401-420.

Norton, D. & Taylor, H. P., Jr. (1979): Quantitative simulation of the hydrothermal systems of crystallizing magmas on the basis of transport theory and oxygen isotope data: an analysis of the Skaergaard intrusion. J. Petrology 20, 421-486.

Noyes, H. J., Wones, D. R. & Frey, F. A. (1983): A tale of two plutons: petrographic and mineralogical constraints on the petrogenesis of the Red Lake and Eagle Peak plutons, central Sierra Nevada, California. J. Geol. 91, 353-379.

O'Neil, J. R. (1986): Theoretical and experimental aspects of isotopic fractionation. In Stable Isotopes in High Temperature Geological Processes (J. W. Valley, H. P. Taylor, Jr. & J. R. O'Neil, eds.). Mineral. Soc. Amer., Rev. Mineral. 16, 1-40.

O'Neil, J. R. & Chappell, B. W. (1977): Oxygen and hydrogen isotope relations in the Berridale batholith. J. Geol. Soc. Lond. 133, 559-571.

O'Neil, J. R., Shaw, S. E. & Flood, R. H. (1977): Oxygen and hydrogen isotope compositions as indicators of granite genesis in the New England batholith, Australia. Contr. Mineral. Petrology 62, 313-328.

O'Neil, J. R. & Taylor, H. P. (1967): The oxygen isotope and cation exchange chemistry of feldspars. Amer. Mineral. 52, 1414-1437.

Orville, P. M. (1963): Alkali ion exchange between vapor and feldspar phases. Amer. J. Sci. 261, 201-237.

Osberg, P. H. (1978): Synthesis of the geology of the northeastern Appalachians, U.S.A. Geol. Surv. Can. Pap. 78-13, 137-147.

Otten, M. T. (1984): The origin of brown hornblende in the Artfjället gabbro and dolerites. Contr. Mineral. Petrology 86, 189-199.

Otten, M. T. (1985): The subsolidus history of the Artfjället gabbro: a TEM study of olivine, augite and orthopyroxene. J. Petrology 26, 488-514.

Parsons, I. (1978): Feldspars and fluids in cooling plutons. Mineral. Mag. 41, 1-17.

Parsons, I. (1980): Alkali-feldspar and Fe-Ti oxide exsolution textures as indicators of the distribution and subsolidus effects of magmatic "water" in the Klokken layered syenite intrusion, south Greenland. Roy. Soc. Edinb. Trans., Earth Sci. 71,1-12.

Payette, S. & Boudreau, F. (1984): Evolution postglaciaire des hauts sommets alpins et subalpins de la Gaspésie. Can. J. Earth Sci. 21, 319-335.

Perrault, S. (1987): Géothermométrie, géobarométrie et nature des fluides métamorphiques dans les gneiss à cordiérite de la région de Saint-Augustin de Saguenay, Province de Grenville, Québec. Mémoire de maitrise, Université de Montréal, Montréal, Québec.

Phillips, E. R. & Rickwood, P. C. (1975): The biotite-prehnite association. Lithos 8, 275-281.

Philpotts, A. R. (1982): Compositions of immiscible liquids in volcanic rocks. Contr. Mineral. Petrology 80, 201-218.

Pichavant, M. & Manning, D. (1984): Petrogenesis of tourmaline granites and topaz granites; the contribution of experimental data. Phys. Earth Planet. Int. 35, 31-50.

Platt, R. G. & Woolley, A. R. (1986): The mafic mineralogy of the peralkaline syenites and granites of the Mulanje complex, Malawi. Mineral. Mag. 50, 85-99.

Poldervaart, A. & Hess, H. H. (1951): Pyroxenes in the crystallization of basaltic magma. J. Geol. 59, 472-489.

Popp, R. K. & Gilbert, M. C. (1972): Stability of acmite-jadeite pyroxenes at low pressure. Amer. Mineral. 57, 1210-1231.

Presnall, D. C., Dixon, S. A., Dixon, J. R., O' Donnell, T. H., Brenner, N. L., Schrock, R. L. & Dycus, D. W. (1978): Liquidus phase relations on the join diopside-forsterite-anorthite from 1 atm to 20 kbar: their bearing on the generation and crystallization of basaltic magma. Contr. Mineral. Petrology 66, 203-220.

Price, R. C., Johnson, R. W., Gray, C. M. and Frey, F. A., (1985): Geochemistry of phonolites and trachytes from the summit region of Mt. Kenya. Contr. Mineral. Petrology 89, 394-409.

Reid, J. B., Evans, O. C. & Fates, D. G. (1983): Magma mixing in granitic rocks of the central Sierra Nevada, California. Earth Planet. Sci. Lett. 66, 243-261.

Richardson, J. (1859): On a portion of the Gaspé Peninsula, including an examination of the coast from Marsoui river to Rivière du Loup. Geol. Surv. Can.; report of progress for the year 1858, 102-170.

Robert, J. L. (1966): Geology of Mount Vallières-de-Saint-Réal area, Gaspé-North county. Ministère Richesses Naturelles, Québec, Preliminary Report 549.

Robert, J. L. (1967): Geology of Lesseps Creek area. Gaspé-North county. Ministère Richesses Naturelles, Québec, Rapport Préliminaire 562.

Robinson, P. (1980): The composition space of terrestrial pyroxenes-internal and external limits. In Pyroxenes (C. T. Prewitt, ed.). Mineral. Soc. Amer., Rev. Mineral. 7, 419-494.

Rock, N. M. S. (1978): Petrology and petrogenesis of the Monchique alkaline complex, southern Portugal. J. Petrology 19, 171-214.

Rock, N. M. S. (1982): Chemical mineralogy of the Monchique alkaline complex, southern Portugal. Contr. Mineral. Petrology 81, 64-78.

Roksandic, M. M. & Granger, B. (1981): Structural styles of Anticosti Island, Gaspé passage and eastern Gaspé Peninsula inferred from reflection seismic data. In IUGS Subcommision on Silurian Stratigraphy; Ordovician-Silurian Boundary Working Group. Vol. II: Stratigraphy and Paleontology (P. J. Lesperance, ed.), 211-221.

Rønsbo, J. G., Pedersen, A. K. & Engell, J. (1977): Titan-aegirine from early Tertiary ash layers in northern Denmark. Lithos 10, 193-204.

Rosenberg, P. E. & Foit, F. F. (1977): Fe^{2+}-F avoidance in silicates. Geochim. Cosmochim. Acta **41**, 345-346.

Rumble, D., Ferry, J. M. & Hoering, T. C. (1986): Oxygen isotope geochemistry of hydrothermally-altered synmetamorphic granitic rocks from south-central Maine, USA. Contr. Mineral. Petrology **93**, 420-428.

Rust, B. R. (1981): Alluvial deposits and tectonic style: Devonian and Carboniferous sucessions in eastern Gaspé. In Sedimentation and Tectonics in Alluvial Basins (A. D. Miall, ed.). Geol. Assoc. Can. Spec. Pap. **23**, 49-76.

Ryerson, F. J. & Hess, P. C. (1978): Implications of liquid-liquid distribution coefficients to mineral-liquid partioning. Geochim. Cosmochim. Acta **42**, 921-932.

Sack, R. O. & Carmichael, I. S. E. (1984): $Fe^{2+} \rightleftharpoons Mg^{2+}$ and $TiAl_2 \rightleftharpoons MgSi_2$ exchange reactions between clinopyroxenes and silicate melts. Contr. Mineral. Petrology **85**, 103-115.

St.-Julien, P. & Hubert, C. (1975): Evolution of the Taconian orogen in the Quebec Appalachians. Amer. J. Sci. **275A**, 337-362.

St.-Julien, P. & Béland, J. (editors) (1982): Major structural zones and faults of the northern Appalachians, Geol. Assoc. Can. Spec. Pap. **24**.

Scambos, T. A., Loiselle, M. C. & Wones, D. R. (1986): The Center Pond pluton: the restite of the story (phase separation and melt evolution in granitoid genesis). Amer. J. Sci. **286**, 241-280.

Schweitzer, E. L., Papike, J. J. & Bence, A. E. (1979): Statistical analysis of clinopyroxenes from deep-sea basalts. Amer. Mineral. **64**, 501-513.

Seguin, M. K. (1982): Geophysics of the Quebec Appalachians. Tectnophys. **81**, 1-50.

Sheppard, S. M. F. (1986): Characterization and isotopic variations in natural waters. In Stable Isotopes in High Temperature Geological Processes (J. W. Valley, H. P. Taylor, Jr. & J. R. O'Neil, eds.). Mineral. Soc. Amer., Rev. Mineral. **16**, 165-183.

Shieh, Y. N. & Taylor, H. P. (1969): Oxygen and hydrogen isotope studies of contact metamorphism in the Santa Rosa range, Nevada, and other areas. Contr. Mineral. Petrology **20**, 306-356.

Sisson, V. B. (1984): Sources of hydrothermal fluid associated with the Ponder pluton, Coast Plutonic Complex, British Columbia, Canada. Geol. Soc. Amer. Abstr. Program **16**, 658.

Smith, D. (1970): Mineralogy and petrology of the diabasic rocks in a differentiated olivine diabase sill complex, Sierra Ancha, Arizona. Contr. Mineral. Petrology **27**, 95-113.

Smith, J. V. (1974): Feldspar Minerals. 1. Crystal Structure and Physical Properties. 2. Chemical and Textural Properties. Springer-Verlag, New York.

Sood , M. K. & Edgar, A. D. (1970): Melting relations of undersaturated alkaline rocks from the Ilímaussaq intrusion and Grønnedal-Ika Complex south Greenland, under water vapour and controlled partial oxygen pressure. Meddr. Grønland **181**, No. 12.

Sørensen, H. (1974a): Alkali syenites, feldspathoidal syenites and related lavas. In The Alkaline Rocks (H. Sørensen, ed.). John Wiley & Sons, New York, 22-52.

Sørensen, H. (1974b): Simplified modal classification of alkaline igneous rocks. In The Alkaline Rocks (H. Sørensen, ed.). John Wiley & Sons, New York, 20-21.

Sørensen, H. (1986): The alkaline rocks - a review. Fortschr. Mineral. **64**, 63-86.

Sparks, R. S. J. & Marshall, L. A. (1986): Thermal and mechanical constraints on mixing between mafic and silicic magmas. J. Volc. Geotherm. Res. **29**, 99-124.

Spear, F. S. (1981): An experimental study of hornblende stability and compositional variability in amphibolite. Amer. J. Sci. **281**, 697-734.

Speer, J. A. (1984): Micas in igneous rocks. In Micas (S. W. Bailley ed.). Mineral. Soc. Amer., Rev. Mineral. **13**, 299-356.

Stephenson, D. (1972): Alkali clinopyroxenes from nepheline syenites of the South Qôroq centre, south Greenland. Lithos **5**, 187-201.

Stephenson, D. & Upton, B. G. J. (1982): Ferromagnesian silicates in a differentiated alkaline complex: Kûngnât Fjeld, south Greenland. Mineral. Mag. **46**, 283-300.

Stephenson, N. C. N. (1977): Coexisting hornblendes and biotites from Precambrian gneisses of the south coast of Western Australia. Lithos **10**, 9-27.

Stevenson, R. K. & Martin, R. F. (1986): Implications of the presence of amazonite in the Broken Hill and Geco metamorphosed sulfide deposits. Can. Mineral. **24**, 729-745.

Stormer, J. C. and Carmichael, I. S. E. (1971): The free energy of sodalite and the behavior of chloride, fluoride and sulfate in silicate magmas. Amer. Mineral. **56**, 292-306.

Streckeisen, A. (1976): To each plutonic rock its proper name. Earth-Sci. Rev. **12**, 1-33.

Sturchio, N. C. & Muehlenbachs, K. (1985): Origin of low-^{18}O metamorphic rocks from a late Proterozoic shear zone in the Eastern Desert of Egypt. Contr. Mineral. Petrology **91**, 188-195.

Taylor, H. P., Jr. (1968): The oxygen isotope geochemistry of igneous rocks. Contr. Mineral. Petrology **19**, 1-71.

Taylor, H. P., Jr. (1971): Oxygen isotope evidence for large-scale interaction between meteoric ground waters and Tertiary granodiorite intrusions, western Cascade Range, Oregon. J. Geophys. Res. **76**, 7855-7874.

Taylor, H. P., Jr. (1977): Water/rock interactions and the origin of H_2O in granitic batholiths. J. Geol. Soc. Lond. **133**, 509-558.

Taylor, H. P., Jr. (1978): Oxygen and hydrogen isotope studies of granitic rocks. Earth. Planet. Sci. Lett. **38**, 175-210.

Taylor, H. P., Jr. (1980): The effects of assimilation of country rocks by magmas on $^{18}O/^{16}O$ and $^{87}Sr/^{86}Sr$ systematics in igneous rocks. Earth Planet. Sci. Lett. **47**, 243-254.

Taylor, H. P., Jr. & Epstein, S. (1962): Relationship between O^{18}/O^{16} ratios in coexisting minerals of igneous and metamorphic rocks. 1. Principles and experimental results. Geol. Soc. Amer. Bull. **73**, 461-480.

Taylor, H. P., Jr. & Forester, R. W. (1971): Low-O^{18} igneous rocks from the intrusive complexes of Skye, Mull and Ardnamurchan, western Scotland. J. Petrology **12**, 465-497.

Taylor, H. P., Jr. & Forester, R. W. (1979): An oxygen and hydrogen isotope study of the Skaergaard intrusion and its country rocks: a description of a 55-M. Y. old fossil hydrothermal system. J. Petrology **20**, 355-419.

Taylor, H. P., Jr. & Sheppard, S. M. F. (1986): Igneous rocks: I. Processes of isotopic fractionation and isotope systematics. In Stable Isotopes in High Temperature Geological Processes (J. W. Valley, H. P. Taylor, Jr. & J. R. O'Neil, eds.). Mineral. Soc. Amer., Rev. Mineral. **16**, 227-271.

Thomas, W. M. (1982): Stability relations of the amphibole hastingsite. Amer. J. Sci. **282**, 136-164.

Thompson, R. N. (1974): Some high-pressure pyroxenes. Mineral. Mag. **39**, 768-787.

Tracy, R. J. & Robinson, P. (1977): Zoned titanian augite in

alkali olivine basalt from Tahiti and the nature of titanium substitutions in augite. Amer. Mineral. 62, 634-645.

Traill, R. J. (1980): Catalogue of Canadian minerals. Geol. Surv. Can. Pap. 80-18.

Troll, G. & Gilbert, M. C. (1972): Fluorine-hydroxyl substitution in tremolite. Amer. Mineral. 57, 1386-1403.

Tsuchiyama, A. (1985): Dissolution kinetics of plagioclase in the melt of the system diopside-albite-anorthite and the origin of dusty plagioclase in andesites. Contr. Mineral. Petrology 89, 1-16.

Tulloch, A. J. (1979): Secondary Ca-Al silicates as low-grade alteration products of granitoid biotite. Contr. Mineral. Petrology 69, 105-117.

Turi, B. & Taylor, H. P., Jr. (1971): An oxygen and hydrogen isotope study of a granodiorite pluton from the Southern California batholith. Geochim. Cosmochim. Acta 35, 383-406.

Turner, J. S. & Campbell, I. H. (1986): Convection and mixing in magma chambers. Earth-Sci. Rev. 23, 255-352.

Tuttle, O. F. (1952): Origin of the contrasting mineralogy of extrusive and plutonic salic rocks. J. Geol. 60, 107-124.

Tuttle, O. F. & Bowen, N. L. (1958): Origin of granite in the light of experimental studies in the system $NaAlSi_3O_8$-$KAlSi_3O_8$-SiO_2-H_2O. Geol. Soc. Amer. Mem. 74.

Tyler, R. C. & King, B. C. (1967): The pyroxenes of the alkaline igneous complexes of eastern Uganda. Mineral. Mag. 36, 5-21.

Upton, B. G. J. (1974): The alkaline province of south-west Greenland. In The Alkaline Rocks (H. Sørensen, ed.). John Wiley & Sons, New York, 221-238.

Upton, B. G. J. & Thomas, J. E. (1980): The Tugtutoq younger giant dyke complex, south Greenland: fractional crystallization of transitional olivine basalt magma. J. Petrology 21, 167-198.

Valley, J. W., Taylor, H. P., Jr. & O'Neil, J. R. (editors)(1986): Stable Isotopes in High Temperature Geological Processes. Mineral. Soc. Amer., Rev. Mineral. 16.

Van Bosse, J. Y. (1985): Metamorphism and Alteration in the Thermal Aureole of the McGerrigle Mountains Pluton, Gaspé, Quebec. M.Sc. thesis, McGill University, Montreal, Quebec.

Vance, J. A. (1965): Zoning in igneous plagioclase: patchy zoning. J. Geol. 73, 636-651.

Verhoogen, J. (1962): Distribution of titanium between silicates and oxides in igneous rocks. Amer. J. Sci. **260**, 211-220.

Vernon, R. H. (1983): Restite, xenoliths and microgranitoid enclaves in granites. J. Proc. R. Soc. New South Wales **116**, 77-103.

Vlasov, K. A. (editor) (1966): Geochemistry and Mineralogy of Rare Elements and Genetic Types of their Deposits. 2. Mineralogy of Rare Elements. Israel Program for Scientific Translations Ltd., Jerusalem.

Vogel, T. A. (1982): Magma mixing in the acidic-basic complex of Ardnamurchan: implications on the evolution of shallow magma chambers. Contr. Mineral. Petrology **79**, 411-423.

Volfinger, M., Robert, J. L., Vielzeuf, D. & Neiva, A. M. R. (1985): Structural control on the chlorine content of OH-bearing silicates (micas and amphiboles). Geochim. Cosmochim. Acta **49**, 37-48.

Walker, G. P. L. & Skelhorn, R. R. (1966): Some associations of acid and basic igneous rocks. Earth-Sci. Rev. **2**, 93-109.

Walker, K. R., Ware, N. G. & Lovering, J. F. (1973): Compositional variations in the pyroxenes of the differentiated Palisades Sill, New Jersey. Bull. Geol. Soc. Am. **84**, 89-110.

Wanless, R. K., Stevens, R. D., Lachance, G. R. & Delabio, R. N. (1973): Age determinations and geological studies, K-Ar isotopic ages, Report 11. Geol. Surv. Can. Pap. **73-2**.

Wares, R. (1983): Synthèse métallogénique du Gîte Sullipek et de ses environs. Ministère de l'Energie et des Ressources, Québec, **DP83-02**.

Wass, S. Y. (1973): The origin and petrogenetic significance of hour-glass zoning in titaniferous clinopyroxenes. Mineral. Mag. **39**, 133-144.

Wass, S. Y. (1979): Multiple origins of clinopyroxenes in alkali basaltic rocks. Lithos **12**, 115-132.

Watson, E. B. (1976): Two-liquid partition coefficients: experimental data and geochemical implications. Contr. Mineral. Petrology **56**, 119-134.

Watson, E. B. (1979a): Apatite saturation in basic to intermediate magmas. Geophys. Res. Lett. **6**, 937-940.

Watson, E. B. (1979b): Zircon saturation in felsic liquids: experimental results and applications to trace element geochemistry. Contr. Mineral. Petrol. **70**, 407-419.

Weidner, J. R. & Martin, R. F. (1987): Phase equilibria of a fluorine-rich leucogranite from the St. Austell pluton, Cornwall. Geochim. Cosmochim. Acta **51**, 1591-1597.

Wellman, T. R. (1970): The stability of sodalite in a synthetic syenite plus aqueous chloride fluid system. J. Petrology **11**, 49-71.

Wenner, D. B. & Taylor, H. P. (1976): Oxygen and hydrogen isotope studies of a Precambrian granite-rhyolite terrane, St. Francois Mountains, southeastern Missouri. Geol. Soc. Amer. Bull. **87**, 1587-1598.

Whalen, J. B. (1985a): The McGerrigle plutonic complex, Gaspé, Québec: evidence of magma mixing and hybridization. In Current Research, Part A. Geol. Surv. Can. Pap. **85-1A**, 795-800.

Whalen, J. B. (1985b): Geochemistry of an island-arc plutonic suite: the Uasilau - Yau Yau intrusive complex, New Britain, P. N. G. J. Petrology **26**, 603-632.

Whalen, J. B. (1986): Geology of the McGerrigle Mountains plutonic complex, Gaspé, Québec: 1:25,000 scale map and marginal notes. Geol. Surv. Can. Open File **1284**.

Whalen, J. B. & Currie, K. L. (1984): The Topsails igneous terrane, western Newfoundland: evidence for magma mixing. Contr. Mineral. Petrology **87**, 319-327.

Whalen, J. B. & Garispy, C. (1986): Petrogenesis of the McGerrigle plutonic complex, Gaspé, Québec: a preliminary report. In Current Research, Part A. Geol. Surv. Can. Pap. **86-1A**, 265-274.

Whalen, J. B. & Roddick, J. C. M. (1987): K-Ar geochronology of the McGerrigle plutonic complex, Gaspésie Peninsula, Québec. In Current Research, Part A. Geol. Surv. Can. Pap. **87-1A**, 375-380.

White, A. J. R. & Chappell, B. W. (1977): Ultrametamorphism and granitoid genesis. In Experimental Petrology Related to Extreme Metamorphism (D. H. Green, ed.). Tectonophys. **43**, 7-22.

White, M. V. W. & Martin, R. F. (1980): The metasomatic changes that accompany uranium mineralization in the nonorogenic rhyolites of the Upper Aillik Group, Labrador. Can. Mineral. **18**, 459-479.

Whitney, J. A. (1972): The effect of reduced H_2O fugacity on the buffering of oxygen fugacity in hydrothermal experiments. Amer. Mineral. **57**, 1902-1908.

Wilkinson, J. F. G. (1956): Clinopyroxenes of alkali basalt magma. Amer. Mineral. **41**, 724-743.

Williams, H. (1979): Appalachian orogen in Canada. Can. J. Earth Sci. **16**, 792-807.

Williams, H. & Hatcher, R. D., Jr. (1983): Appalachian suspect terranes. In Contributions to the Tectonics and Geophysics of Mountain Chains (R. D. Hatcher, Jr., H. Williams & I. Zietz, eds.). Geol. Soc. Amer. Mem. **158**, 33-53.

Williams-Jones, A. E., Samson, I. M. & Linnen, R. L. (1986): Preliminary results of a study of the ores, wall-rock alteration, and fluid inclusions at the Madeleine copper mine, Gaspé, Québec. In Current Research, Part A. Geol. Surv. Can. Pap. **86-1A**, 239-249.

Wones, D. R. (1981): Mafic silicates as indicators of intensive variables in granitic magmas. Mining Geol. **31**, 191-212.

Wones, D. R. & Eugster, H. P. (1965): Stability of biotite: Experiment, theory, and application. Amer. Mineral. **50**, 1228-1272.

Wones, D. R. & Gilbert, M. C. (1982): Amphiboles in the igneous environment. In Amphiboles: Petrology and Experimental Phase Relations (D. R. Veblen & P. H. Ribbe, eds.). Mineral. Soc. Amer., Rev. Mineral. **9B**, 355-390.

Woodrow, P. J. (1967): The crystal structure of astrophyllite. Acta Cryst. **22**, 673-678.

Wyllie, P. J., Cox, K. G. & Biggar, G. M. (1962): The habit of apatite in synthetic systems and igneous rocks. J. Petrology **3**, 238-243.

Yoder, H. S., Jr. (1973): Contemporaneous basaltic and rhyolitic magmas. Amer. Mineral. **58**, 153-171.

Yoder, H. S., Jr. & Tilley, C. E. (1962): Origin of basalt magmas: an experimental study of natural and synthetic rock systems. J. Petrology **3**, 342-532.

APPENDIX I. ANALYTICAL PROCEDURES

Electron Microprobe analysis

Analyses of minerals mounted on polished thin sections were made on a Cameca Microbeam Model MB-1 electron microprobe with four wavelength-dispersive sequential spectrometers. An accelerating voltage of 15 kV and a current of 7 nA were used. Counting times of 25 seconds were used for all elements with the exception of Fe, for which a period of 35 seconds was used. Different standards were used for different minerals. For clinopyroxene, olivine (Fe), diopside (Si, Ca, Mg), $MnTiO_3$ (Mn, Ti), albite (Na, Al), Cr_2O_3 (Cr), spessartine (Mn) and zircon (Zr) were used. For the feldspars and feldspathoids, andradite (Fe, Ca), albite (Na), orthoclase (Si, Al, K), $MnTiO_3$ (Ti) and MgO (Mg) were used. For amphibole and biotite, andradite (Fe), $MnTiO_3$ (Mn, Ti), LiF (F), vanadinite (Cl), orthoclase (Si, Al, K), diopside (Ca, Mg) and albite (Na) were used. For the iron oxides, $MnTiO_3$ (Mn, Ti), hematite (Fe), MgO (Mg), Al_2O_3 (Al), vanadinite (V), NiO (Ni) and Cr_2O_3 (Cr) were used. For the accessory minerals, andradite (Fe, Ca), $MnTiO_3$ (Mn, Ti), albite (Na), orthoclase (Si, Al, K), vanadinite (Cl), MgO (Mg), LiF (F), celestite (Sr), zircon (Zr), Nb, apatite (P) and a rare-earth glass standard (Ce, La) were used. An example of the calculated analytical precision based on counting statistics for different elements from an amphibole analysis is given below. The results should be considered to represent the minimum value for most elements as many other factors must be considered such as degree of polish, quality of standards used, volatilization, etc.

Element	wt. %	Precision
Cl	0.34	0.02
Fe	17.38	0.08
F	1.24	0.59
Na	1.40	0.04
K	0.85	0.02
Mn	0.84	0.06
Si	20.96	0.02
Al	3.01	0.02
Mg	4.94	0.02
Ca	7.50	0.02
Ti	0.69	0.08

X-Ray Diffraction

X-ray diffraction patterns were obtained using a Guinier-Hagg focusing camera (CuKα radiation). The data were transformed to $^{o}2\theta$ by referring to an internal spinel standard admixed with the sample. The data were then indexed and used as input to the cell-refinement program of Appleman & Evans (1973). The mole fraction of Or was calculated from the cell volume using the equation of Kroll & Ribbe (1983). The degree of order, expressed by t_1O, was calculated using the expressions of Blasi (1977). An content of albite or plagioclase was estimated using a β^*-γ^* plot (Smith 1974, Fig. 7-44). Error in N_{Or} and t_1O is estimated to be $\pm$0.015. The samples used were either mineral separates obtained by C. Gariepy or chip samples of K-feldspar from a hand specimen.

Mineral Separates

Whole-rock samples were crushed using a jaw crusher with porcelain plates and an agate cone grinder. The finest-grained fraction was then removed by repeatedly filling and emptying

water from a beaker containing the crushed rock. The coarser grains were cleaned with acetone and sieved through nylon screens in plastic containers to obtain a size fraction between 100 and 250 um. Magnetite was removed using a magnet, and mafic and felsic grains were separated using a Frantz magnetic separator. A plastic "Teflon" overlay stuck to a board was used to separate biotite from other mafic minerals, as biotite tended to "stick" to the board. Purification of the mineral separates was achieved using the heavy liquids bromoform (S.G. 2.8899) and methylene iodide (S.G. 3.325), which in some cases were diluted by acetone (S.G. 0.792). Finally, samples were hand-picked for further purity.

Fe^{3+} Determinations and Oxygen Isotopes

Fe^{3+} determinations by wet chemistry were carried out by J.-L. Bouvier of the Geological Survey of Canada using the modified Pratt method for FeO and total Fe_2O_3. Oxygen isotope analyses were carried out by Dr. K. Muehlenbachs of the University of Alberta. Oxygen was extracted from rock and mineral samples by the BrF_5 method (Clayton and Mayeda 1963), and analyzed as CO_2 using a dual-collector mass spectrometer. Analytical precision (1σ), as reported by Sturchio and Muehlenbachs (1985), is $0.14^{o}/oo$ (SMOW). Three of four replicate analyses of the McGerrigle rocks fall within this range (Table 6.1).

APPENDIX II. SAMPLE DESCRIPTIONS

Sample descriptions are given for all samples from which electron microprobe data were obtained. More detailed sample descriptions are available from the author. Chemical analyses are available for all samples with the prefix MG. In the following descriptions, * indicates that the mineral is secondary or has completely recrystallized, ** indicates that the mineral is at least in part secondary or has partly recrystallized, and *** indicates that the mineral is also present in the groundmass.

Mafic and Mesocratic Intermediate Rock types

MG6: Fine-grained mafic inclusion; porphyritic [plagioclase** (labradorite (An56-57) forms a compound grain with titansalite; calcic oligoclase to andesine (An23-45) for resorbed core surrounded by a rim of oligoclase (An20)), augite to titansalite**, pseudomorphs (after clinopyroxene?) with an amphibole core and biotite rim, and magnetite**,*** (resorbed?)], groundmass [calcic oligoclase* (An21), magnesio-hornblende*, titaniferous biotite*, ilmenite**, hematite*, pyrite, apatite, zircon, chlorite*, titanite*, and epidote*], abundant amygdules [amphibole (oscillatory zoned from actinolitic hornblende to magnesio-hornblende), titanite, calcite, chlorite, apatite, K-feldspar, allanite, and ilmenite].

MG9: Biotite-pyroxene diorite; fine- to medium-grained, from inclusion exhibiting a chilled margin with a syenite (MG8), plagioclase**, minor perthitic K-feldspar, rare interstitial nepheline, pale green sodian salite*, biotite*, minor green amphibole*, magnetite**, ilmenite**, pyrite, pyrrhotite, chalcopyrite, apatite, zircon, titanite*, chlorite*, epidote*.

MG23: Amphibole-dominant monzodiorite; medium- to coarse-grained, appears in the field to be gradational with gabbro (MG25), sodic oligoclase to sodic andesine**(An10-38), perthitic K-feldspar (Or98), quartz, subophitic titaniferous augite to titanaugite**, pale green clinopyroxene*, actinolitic hornblende*, titaniferous biotite*, magnetite**, ilmenite**, pyrite, pyrrhotite, chalcopyrite, apatite, zircon, titanite*, calcite*, chlorite*, epidote*, rare secondary bodies (of garnet?) may be present along biotite cleavages.

MG24: Fine-grained mafic inclusion; fine- to medium-grained,

from a chilled pillow in granite, plagioclase**, minor perthitic K-feldspar, pale green salite*, kaersutite**, green amphibole*, titanbiotite*, magnetite**, ilmenite**, pyrite, pyrrhotite, chalcopyrite, apatite** (may occur in linear trains or parallel sheaves of needles), zircon, allanite (secondary?),titanite*, chlorite*, epidote*, calcite*, elongate pods or lenses of garnet(?)* and pumpellyite(?)* are observed along biotite cleavages.

MG25: Gabbro; medium- to coarse-grained, plagioclase**, rare pink-brown pyroxene**, colorless or pale green (sodian) salite* (some grains exhibit intergrowths of clinopyroxenes of slightly different composition), red brown amphibole**, green amphibole*, biotite*, magnetite**, ilmenite**, pyrite, pyrrhotite, chalcopyrite, apatite, zircon, titanite*, chlorite*, epidote*, elongate bodies may be present along biotite cleavages (garnet?*).

MG26: Amphibole-dominant diorite or monzodiorite; fine- to medium-grained, part of an inclusion with a cuspate margin in K-feldspar-dominant granite, porphyritic [plagioclase (highly sericitized)], groundmass (plagioclase**, perthitic K-feldspar, minor pale green clinopyroxene*, magnesio-hornblende to actinolitic hornblende*, titaniferous biotite*, magnetite**, ilmenite**, pyrite, chalcopyrite, apatite, zircon, titanite*, epidote*, chlorite*), abundant amygdules [chlorite, K-feldspar, amphibole (some oscillatory zoning), sodic plagioclase, epidote, calcite, zircon, titanite, pyrite, Fe-Ti oxides].

MG29: Biotite-pyroxene monzodiorite; fine- to medium-grained, sample contains common fine-grained mafic inclusions and exhibits a heterogeneous color index, plagioclase**, perthitic K-feldspar (coarser-grained concentration of K-feldspar may represent an infilled miarolitic cavity), colorless to pale green sodian salite** (some grains exhibit sector or irregular zoning), titaniferous biotite, very minor green amphibole*, magnetite**, ilmenite**, pyrite, apatite, zircon, titanite*, calcite*, chlorite*.

MG53: Amphibole-dominant monzodiorite; fine- to medium-grained, sodic oligoclase to calcic andesine** (An15-41), perthitic K-feldspar (Or92), quartz, colorless to pale brown clinopyroxene**, pale green clinopyroxene*, magnesio-hornblende*, titaniferous biotite*, magnetite**, ilmenite**, pyrite, apatite, zircon, titanite*, allanite (secondary?), chlorite*.

MG61: Alkali basaltic dyke; porphyritic [plagioclase**,***, globular aggregates of secondary minerals (pseudomorphs after olivine or clinopyroxene?)], rare titansalite cores to kaersutite**, green amphibole*, biotite**, pyrite, chalcopyrite, apatite, titanite*, epidote*, chlorite*, calcite*.

MG64: Gabbro; medium-grained, labradorite (An62-67), andesine*

(An32-33), titansalite** (subophitic, hourglass zoning), colorless sodian salite*, kaersutite** (overgrowths on or replacing titansalite, interstitial), green amphibole*, titaniferous biotite** (may contain secondary ilmenite), magnetite**, ilmenite**, pyrite, chalcopyrite, pyrrhotite, apatite, chlorite* (including diabantite), elongate bodies (garnet?*) are observed along biotite cleavages.

MG68: Fine-grained mafic inclusion, porphyritic [plagioclase**,***, sodian salite to titaniferous diopside (augite)**, pseudomorphs (after clinopyroxene?) that have a core of amphibole, titanite and Fe-Ti oxides and a rim of biotite, magnetite**, ***], groundmass [magnesio-hornblende*, titaniferous biotite* (dominant mineral along contact with granodiorite), ilmenite**, hematite*, pyrite, apatite, zircon, calcite*, titanite*, chlorite*, epidote*], abundant amygdules [sodic plagioclase, K-feldspar, chlorite, allanite(?), biotite, zircon, titanite, Fe-Ti oxides, quartz, amphibole (oscillatory zoned from magnesio-hornblende to actinolitic hornblende), epidote, calcite, apatite], garnet(?) forming due to alteration of biotite.

83-77: Biotite-pyroxene monzodiorite; fine- to medium-grained, albite to sodic andesine (An5-30**), perthitic K-feldspar, pale green to bright green sodian ferroaugite** (some grains exhibit sector or irregular zoning), minor green amphibole*, titanbiotite, magnetite**, ilmenite**, pyrite, pyrrhotite, apatite, zircon, titanite*, allanite(?), hematite*.

MG87: Amphibole-dominant quartz monzodiorite; medium-grained; plagioclase** (rounded resorbed cores observed in some laths), perthitic K-feldspar (Or90), quartz, augite to titaniferous augite**, green amphibole*, very minor biotite*, magnetite**, ilmenite**, pyrite, chalcopyrite, apatite, zircon, titanite*, hematite*.

MG90: Biotite-pyroxene diorite; medium- to coarse-grained, sodic to calcic oligoclase** (An14-27), perthitic K-feldspar**, sodian salite* (irregular intergrowths of clinopyroxene of slightly different composition), minor green amphibole*, titaniferous biotite* (forms apparent pseudomorphs with salite and titanite), magnetite**, ilmenite**, pyrite, apatite, titanite*, chlorite*.

MG97: Fine-grained mafic inclusion; chilled margin with white granodiorite, porphyritic [plagioclase**,***, pseudomorphs after clinopyroxene? that are cored by amphibole, titanite and colorless clinopyroxene and rimmed by biotite (may form compound grains with plagioclase)], sodian salite* (concentrated along chilled margin), groundmass [actinolitic hornblende to magnesian hastingsite**, titaniferous biotite* (dominant mafic mineral at the chilled margin), magnetite**, ilmenite**, pyrite, apatite, chlorite*, titanite*], rare amygdules (titanite, ilmenite, apatite, amphibole, pyrite and plagioclase).

83-109: Endoskarn; medium- to coarse-grained, plagioclase**, colorless diopside* (fills microfractures or forms intergrowth with plagioclase), extremely rare oxide remnants (hematite?), apatite, titanite*, rutile*.

84-556: Amphibole-dominant monzodiorite; fine- to medium-grained, slightly porphyritic [sodic oligoclase to labradorite**,*** (An14-53)], perthitic K-feldspar, quartz, pale brown titaniferous augite**, pale green (sodian) salite* (may exhibit irregular zoning or intergrowths of clinopyroxene of slightly different composition), magnesio-hornblende*, titaniferous biotite*, magnetite**, ilmenite**, pyrite, zircon, apatite** (concentrated in secondary plagioclase and clinopyroxene), allanite(?), titanite*, chlorite*, possible infilled miarolitic cavity (K-feldspar, quartz and amphibole).

Quartz-Poor Felsic Rock Types

MG8: Syenite; fine- to medium-grained, slightly porphyritic [mantled albite to sodic oligoclase** (An3-18), medium-grained felsic clot (plagioclase, subhedral grain of sodian augite*)], perthitic K-feldspar (Or97-98), quartz, sodian ferroaugite, interstitial actinolitic hornblende to actinolite (rare patchy zoning), minor titaniferous biotite, magnetite**, ilmenite**, pyrite, pyrrhotite, apatite (including possible xenocrysts), zircon, allanite, titanite**.

MG10: Plagioclase-phyric syenite; fine- to medium-grained, porphyritic [partly mantled plagioclase**, medium-grained felsic clots (plagioclase**, clinopyroxene**, kaersutite**, magnetite**, apatite), mafic clots (clinopyroxene pseudomorphs?)], perthitic K-feldspar, unzoned plagioclase, quartz, sodian salite to augite** (rare oscillatory zoned grains), interstitial actinolitic or ferro-actinolitic hornblende, titanbiotite, magnetite**, ilmenite**, hematite*, apatite, zircon, allanite(?), titanite*, chlorite*.

83-16: Plagioclase-phyric quartz monzonite; fine- to coarse-grained, porphyritic [partly mantled plagioclase** that may form compound grains (plagioclase, augite**), rare perthitic K-feldspar***], mafic clots (pseudomorphs), unzoned plagioclase, quartz, magnesio-hornblende, titaniferous biotite, magnetite**, ilmenite**, hematite*, apatite, zircon, allanite, titanite*, chlorite*.

MG20: Syenite to monzonite; fine- to medium-grained, slightly porphyritic (mantled plagioclase**, perthitic K-feldspar***), unzoned plagioclase, quartz, minor salite, interstitial green amphibole, biotite, magnetite**, ilmenite**, pyrite, apatite, zircon, chevkinite(?), chlorite*.

84-23: Alkali syenite; fine- to medium-grained, fine-grained xenolith (plagioclase**, biotite*, apatite, opaque minerals), perthitic K-feldspar (Or93-94; may exhibit well-developed rim of secondary albite), mantled plagioclase**, quartz, aegirine-

augite commonly with (replacing along cleavages and fractures) a core of sodian augite (aegirine-augite rims are not visible on grains included in K-feldspar), winchite or actinolite (weak zoning may be present), minor titaniferous biotite, magnetite**, ilmenite**, pyrite, pyrrhotite(?), apatite, zircon, allanite(?), titanite**.

83-31: Alkali-feldspar syenite; medium-grained, perthitic K-feldspar, mantled plagioclase**, quartz, interstitial magnesio-hornblende (some grains exhibit patchy zoning), minor biotite, magnetite**, ilmenite**, hematite*, apatite, zircon.

MG40: Plagioclase-phyric syenite; fine- to medium-grained, porphyritic [mantled albite to calcic oligoclase** (An3-31) that may form compound grains (plagioclase, clinopyroxene), mafic clots (pseudomorphs of clinopyroxene?)], unzoned plagioclase, perthitic K-feldspar (Or94), quartz, sodian augite**, interstitial ferro-hornblende (some grains exhibit slight zonation), titaniferous biotite, magnetite**, ilmenite**, pyrite(?), pyrrhotite(?), apatite, zircon, chevkinite(?).

MG44: Quartz monzonite; medium- to coarse-grained, plagioclase** (may occur in a clot of highly recrystallized grains), perthitic K-feldspar (Or93; may contain an internal rim of plagioclase), quartz, rare remnants of clinopyroxene**, euhedral ferroedenite (some grains exhibit well-developed concentric zoning), titaniferous biotite**, magnetite**, ilmenite**, pyrite, apatite, zircon, allanite, titanite**, chlorite*.

MG52: Plagioclase-phyric quartz monzonite; medium- to coarse-grained, porphyritic [mantled plagioclase** that may form clots (plagioclase, clinopyroxene**, oxide minerals, apatite)] unzoned plagioclase, perthitic K-feldspar (Or94; may contain an internal rim of plagioclase), quartz, augite**, subhedral magnesio-hornblende, titaniferous biotite, magnetite**, ilmenite**, pyrite, chalcopyrite, apatite, zircon, allanite.

MG63: Quartz monzonite; medium-grained, sodic oligoclase to sodic andesine** (An10-34; some laths are highly recrystallized), perthitic K-feldspar (Or95, rare grains exhibit zoning), quartz, subhedral actinolitic hornblende, titaniferous biotite, magnetite**, ilmenite**, pyrite, apatite, zircon, allanite, titanite (secondary?), chlorite*.

MG66: Quartz monzonite; fine- to medium-grained, mafic minerals heterogeneously distributed forming slight banding, albite to calcic andesine** (An7-49; some grains mantled by K-feldspar, others highly recrystallized), perthitic K-feldspar (Or92), quartz, rare remnants of clinopyroxene**, subhedral magnesio-hornblende, titaniferous biotite, magnetite**, ilmenite**, pyrite, apatite, zircon, allanite, titanite*, hematite*, chlorite*.

Granites

MG3: White granodiorite; fine- to medium-grained, oriented inclusions of green and brown biotite plus apatite(?) in quartz and plagioclase** (sodic oligoclase to labradorite; An19-59), minor K-feldspar, titaniferous biotite, apatite, zircon, chlorite*, epidote*, garnet(?)* forms bodies along biotite cleavages.

MG42: Granite porphyry, fine- to medium-grained, porphyritic [sodic oligoclase to labradorite** (An14-50; some phenocrysts fractured or highly recrystallized), perthitic K-feldspar***, quartz*** (may exhibit a skeletal shape), magnesio-hornblende*** (may contain a core of edenitic hornblende or clinopyroxene** remnants), titaniferous biotite***, rare mafic clots], unzoned plagioclase, magnetite**, ilmenite**, hematite*, pyrite(?), apatite, zircon, allanite, titanite (secondary?), chlorite*, epidote*.

MG46: Plagioclase-dominant granite; medium- to coarse-grained, slightly porphyritic [sodic oligoclase to labradorite*** (An12-52; many laths are highly recrystallized)], perthitic K-feldspar (Or93), quartz (may exhibit a skeletal shape), magnesio-hornblende, titaniferous biotite, magnetite**, ilmenite**, hematite*, pyrite, apatite, zircon, allanite, titanite (secondary?), chlorite*.

MG51: Granite porphyry; fine- to coarse-grained, porphyritic [plagioclase** (some laths are highly recrystallized), perthitic K-feldspar (Or94***), quartz*** (apparently underwent polygonization), titaniferous biotite***, magnesio-hornblende***], unzoned plagioclase, magnetite**, ilmenite**, pyrite(?), apatite, zircon, allanite, titanite*, chlorite*.

83-55: K-feldspar-dominant granite; medium- to coarse-grained, perthitic K-feldspar, plagioclase** (some laths are highly recrystallized), quartz, titaniferous biotite, ferro-hornblende, magnetite**, ilmenite**, hematite*, zircon, apatite.

MG57: K-feldspar-dominant granite; medium- to coarse-grained; perthitic K-feldspar (Or93; may contain an internal rim of plagioclase), plagioclase** (some laths are highly recrystallized), quartz, ferro-hornblende to ferro-edenite, titaniferous biotite, magnetite**, ilmenite**, hematite*, apatite, zircon, titanite**.

MG68: White granodiorite coexists with a fine-grained mafic inclusion, fine- to medium-grained, plagioclase** (some laths are highly recrystallized), perthitic K-feldspar, quartz, titanbiotite, rare green amphibole (n.a.), magnetite**, ilmenite**, hematite*, apatite, zircon, titanite*, chlorite*, epidote*, calcite*, garnet(?)* forms bodies along biotite cleavages.

MG83: K-feldspar-porphyritic granite; medium- to coarse-grained, porphyritic [perthitic K-feldspar*** (Or94; may exhibit a rapakivi texture)], oligoclase** (An11-24; some laths are highly recrystallized), quartz, ferro-hornblende, titaniferous biotite, magnetite**, ilmenite**, pyrite, apatite, zircon, allanite, titanite (secondary?), chlorite*.

MG97: White granodiorite coexists with a chilled mafic inclusion, fine- to medium-grained, plagioclase**, perthitic K-feldspar, quartz, sodian salite, magnesio-hornblende to actinolite, rare biotite (n.a.), magnetite**, ilmenite**, pyrite, apatite, zircon, allanite, titanite*, epidote*.

Nepheline Syenites

MG16: Miaskitic nepheline syenite; fine- to coarse-grained, trachytic texture, porphyritic [perthitic K-feldspar*** (Or100), manganiferous titaniferous biotite***, aegirine-augite***], albite, nepheline (Ne73.7Ks20.8Qtz5.5), magnetite** (may have pyrophanite lamellae), titanite**, zircon, apatite.

MG37: Peralkaline tinguaite; fine- to medium-grained, subtrachytic texture, slightly porphyritic [perthitic K-feldspar (Or96)], minor albite, nepheline (Ne73.3Ks23.7Qtz3.0), zoned aegirine to titanian aegirine (rare glomeroporphyritic texture), manganoan potassium arfvedsonite [forms a fine-grained mafic clot as well as an amphibole pseudomorph (with pectolite, aegirine and fluorite)], manganiferous titaniferous lepidomelane, sodalite, aenigmatite, astrophyllite, pectolite**, eucolite-eudialyte(?), fluorite**.

MG39: Peralkaline tinguaite; fine- to medium-grained, trachytic texture, porphyritic [perthitic K-feldspar*** (glomeroporphyritic texture, recrystallized remnants of plagioclase), nepheline*** (Ne72.3Ks21.0Qtz6.7), aegirine*** (weak zoning, forms a mafic clot), sodalite***], manganiferous titaniferous Mg-rich biotite (also remnants in aegirine), minor albite, magnetite, hematite*, pyrophanite*, apatite, zircon, fluorite**, pectolite(?), titanite*.

MG94: Intermediate tinguaite; fine- to medium-grained, subtrachytic texture, porphyritic [perthitic K-feldspar (Or96; glomeroporphyritic texture), aegirine-augite***], perthitic K-feldspar (Or94), minor albite, nepheline (Ne74.0Ks21.7Qtz4.3), manganiferous titaniferous lepidomelane, magnetite**, ilmenite**, very minor sodalite(?), apatite, zircon, wohlerite, pyrochlore, rosenbushite-gotzenite(?), titanite*.

MG98: White cognate inclusion; medium-grained, perthitic K-feldspar (glomeroporphyritic texture), minor albite, nepheline is replaced by secondary cancrinite(?) and pectolite(?), aegirine (some patchy zoning), manganiferous titaniferous lepidomelane (may be rimmed by aegirine), sodic amphibole, magnetite**, hematite*, apatite, zircon, fluorite, sodalite, astrophyllite (inclusions in biotite), titanite**, calcite*.

APPENDIX III. MODAL COMPOSITION OF SELECTED SAMPLES

With the exception of MG40, the modes were determined by J. Whalen and are derived from 2000 point counts on a 16 by 10 cm stained slab and 1200 points on a thin section. The mode for MG40, determined by the author, is derived from 2246 point counts on a thin section. Results expressed as volume %. Abbreviations for rock types listed in the appendices are as follows. DIOR: diorite, MZDI: monzodiorite, GABB: gabbro, ENDO: endoskarn, QMDI: quartz monzodiorite, MAFI: fine-grained mafic inclusion, MDYK: alkali basaltic dyke, SYEN: syenite, PSYN: plagioclase-phyric syenite, AFSY: alkali-feldspar syenite, MONZ: monzonite, ALKS: alkali syenite, QTMZ: quartz monzonite, PQMZ: plagioclase-phyric quartz monzonite, PDGR: plagioclase-dominant granite, GP: granite porphyry, KFDG: K-feldspar-dominant granite, WTGD: white granodiorite, KFPG: K-feldspar porphyritic granite, MIAS: miaskitic nepheline syenite, ITIN: intermediate tinguaite, PTIN: peralkaline tinguaite, WINC: white cognate inclusion.

TABLE A3.1. MODAL COMPOSITION OF SELECTED MAFIC AND MESOCRATIC INTERMEDIATE SAMPLES

Number	1	2	3	4	5	6	7	8
Rock Type	DIOR	MZDI	GABB	MZDI	ENDO	GABB	QMDI	DIOR
Sample	MG9	MG23	MG25	MG29	MG55	MG64	MG87	MG90
Quartz	0.0	1.8	0.0	0.0	0.0	0.0	8.1	0.0
Nepheline	0.3	0.0	0.0	0.0	0.0	0.0	0.0	0.0
K-Feldspar	0.2	15.0	0.0	20.3	0.0	0.0	21.9	3.2
Plagioclase	63.7	54.1	61.1	42.7	64.9	52.1	49.2	38.3
Biotite	29.0	6.9	9.7	23.1	0.0	12.4	0.1	42.1
Amphibole	1.4	10.7	21.2	0.7	0.0	25.3	14.2	0.5
Clinopyroxene	1.6	3.4	3.2	0.4	25.1	6.1	2.2	0.4
Titanite	2.7	1.0	0.7	0.9	7.3	0.0	0.9	2.0
Zircon	0.1	tr	tr	0.1	0.1	0.0	0.1	0.0
Apatite	1.0	1.5	0.0	1.4	2.6	0.9	0.6	1.5
Allanite	0.0	0.0	0.0	0.0	0.0	0.0	0.0	0.0
Opaques	tr	5.6	3.4	2.4	0.0	3.2	2.0	3.2
Rutile	0.0	0.0	0.0	0.0	tr	0.0	0.0	0.0

TABLE A3.2. MODAL COMPOSITION OF SELECTED QUARTZ-POOR FELSIC SAMPLES

Number	1	2	3	4	5
Rock Type	PSYN	QTMZ	PQMZ	QTMZ	QTMZ
Sample	MG40	MG44	MG52	MG63	MG66
Quartz	3.0	8.8	11.0	14.6	13.5
K-Feldspar	57.7*	46.5	34.2	35.0	31.7
Plagioclase	27.8*	33.6	*41.1	45.4	43.2
Biotite	2.1	1.6	4.8	1.0	4.4
Amphibole	6.7	6.7	4.2	2.5	5.5
Clinopyroxene	tr	tr	0.9	0.0	tr
Titanite	0.0	0.1	0.0	0.1	tr
Zircon	0.1	0.1	tr	0.1	0.1
Apatite	1.1	tr	1.1	tr	0.2
Allanite	0.0	tr	tr	tr	0.1
Chevkinite(?)	tr	0.0	0.0	0.0	0.0
Opaques	1.4	2.7	2.8	1.3	1.4

*: 17.1 % of the plagioclase occurs as mantled, commonly partially recrystallized phenocrysts while 10.7 % occurs within the groundmass as unzoned, twinned grains.

TABLE A3.3. MODAL COMPOSITION OF SELECTED SAMPLES OF GRANITE

Number	1	2	3	4
Rock Type	PDGR	GP	KFDG	KFPG
Sample	MG46	MG51	MG57	MG83
Quartz	27.2	8.2	27.4	27.1
K-Feldspar	25.4	10.2	42.4	33.5
Plagioclase	40.3	27.7	25.7	35.3
Biotite	4.0	2.5	2.3	2.0
Amphibole	2.3	1.7	1.0	1.7
Matrix	0.0	48.5	0.0	0.0
Titanite	tr	0.1	tr	0.2
Zircon	tr	0.1	tr	tr
Apatite	tr	tr	0.1	tr
Allanite	tr	tr	0.0	tr
Opaques	0.9	1.0	1.2	0.2

TABLE A3.4. MODAL COMPOSITION OF TWO SAMPLES OF NEPHELINE SYENITE

Number	1	2
Rock Type	MIAS	PTIN
Sample	MG16	MG37
Nepheline	9.2	19.3
K-Feldspar	78.3	61.8
Sodalite	0.0	2.8
Biotite	4.6	0.2
Amphibole	0.0	3.5
Clinopyroxene	3.0	11.9
Astrophyllite	0.0	tr
Aenigmatite	0.0	0.6
Titanite	1.9	0.0
Zircon	2.2	0.0
Eucolite(?)	0.0	tr
Apatite	tr	tr
Opaques	0.8	0.0
Fluorite	0.0	tr
Pectolite	0.0	tr

APPENDIX IV. CHEMICAL COMPOSITION AND NORMATIVE MINERALOGY OF SELECTED SAMPLES

*: analysis supplied by Dr. C. Gariépy, **: analysis carried out at McGill University by XRF on a Philips PW1400 X-ray spectrometer unit using fused pellets by Mr. T. Ahmedali. Normative mineralogy calculated by Dr. C. Gariépy. Rock types defined in Appendix III. T: total iron, expressed as Fe or as FeO. D. I. (differentiation index) is equal to normative Q+Or+Ab+Ne+Ks+Lc.

TABLE A4.1. CHEMICAL COMPOSITION AND NORMATIVE MINERALOGY OF SELECTED MAFIC AND MESOCRATIC INTERMEDIATE SAMPLES

Number	1	2	3	4	5	6	7	8	9	10	11	12	13	14
Rock Type	MAFI	DIOR	MZDI	MAFI	GABB	MAFI	MZDI	MZDI	MDYK	GABB	MZDI	QMDI	ENDO	DIOR
Sample	MG6MM	MG9M	MG23MM	MG24M	MG25M	MG26M	MG29MM	MG53M	MG61MM	MG64MM	MG71M	MG87MM	MG86M	MG90MM
SiO2 wt. %	51.96	51.91	55.45	47.57	47.96	51.77	59.69	56.23	45.59	48.19	54.83	60.69	53.17	53.17
TiO2	1.84	1.98	2.09	2.74	2.25	2.36	0.93	2.00	2.23	1.88	1.88	1.14	1.66	2.04
Al2O3	16.82	17.68	16.14	16.84	17.43	16.46	18.14	16.82	17.81	17.40	17.52	16.39	19.10	17.71
Fe2O3	2.38	2.76	3.12	4.28	3.20	2.28	1.81	2.13	3.17	2.68	2.65	2.11	0.55	2.86
FeOMM	6.38	5.58	5.48	7.58	7.00	7.00	3.58	5.38	7.18	6.98	4.60	3.38	3.18	5.48
FeOT	8.37	7.98	8.21	11.35	9.95	8.98	5.13	7.22	9.95	9.24	6.98	5.28	3.59	7.97
MnO	0.17	0.18	0.17	0.18	0.17	0.17	0.16	0.17	0.19	0.17	0.12	0.18	0.05	0.16
MgO	5.56	3.39	2.71	5.15	5.29	4.12	1.33	2.69	6.42	6.85	2.84	2.37	4.29	2.65
CaO	7.43	5.11	5.29	6.96	8.71	5.85	2.57	5.84	11.12	8.41	4.58	5.97	14.18	5.52
Na2O	4.64	5.52	4.76	3.75	3.85	4.29	7.83	4.78	3.34	3.95	4.44	3.94	3.58	5.74
K2O	1.88	2.54	3.85	2.38	1.58	2.61	3.64	3.19	1.38	1.72	3.39	3.85	0.59	2.86
P2O5	0.77	0.98	0.68	0.57	0.44	0.78	0.45	0.67	0.68	0.69	0.68	0.27	0.29	0.89
Cr2O3	0.02	0.0	0.0	0.01	0.01	0.01	0.0	0.0	0.01	0.01	0.0	0.0	0.0	0.0
Total	98.81	97.39	99.06	97.85	97.91	97.54	99.25	98.94	98.24	98.77	97.37	99.33	99.56	99.82
H2Om	1.38	0.98	0.61	1.55	1.42	1.52	0.45	0.58	2.14	1.33	0.86	0.58	1.45	0.78
CO2m	0.17	0.14	0.12	0.16	0.15	0.28	0.14	0.58	0.28	0.15	0.85	0.04	0.15	0.19
Mg/(Mg+FeT)	0.54	0.43	0.37	0.45	0.49	0.45	0.32	0.48	0.53	0.57	0.42	0.45	0.75	0.37
(Na+K)/Al	0.68	0.67	0.69	0.61	0.46	0.60	0.85	0.67	0.41	0.48	0.63	0.68	0.34	0.71
Fe3+/FeT	0.25	0.31	0.34	0.34	0.38	0.22	0.32	0.27	0.29	0.25	0.25	0.36	0.19	0.32
CIPW wt. %														
Qtz	0.0	0.0	2.69	0.0	0.0	0.0	0.0	2.65	0.0	0.0	2.94	11.48	1.16	0.0
Cor	0.0	0.0	0.0	0.0	0.0	0.0	0.0	0.0	0.0	0.0	0.14	0.0	0.0	0.0
Or	10.74	15.11	18.16	13.88	9.85	15.00	21.63	19.04	8.29	10.27	20.34	10.13	3.50	17.03
Ab	39.66	45.62	40.58	30.95	29.86	37.18	57.53	40.16	17.58	26.97	37.75	33.53	30.41	42.66
An	17.75	17.15	13.77	22.80	26.44	18.39	7.23	15.53	27.79	24.93	10.67	10.13	34.44	14.22
Neph	0.0	0.74	0.0	0.79	1.83	0.0	1.24	0.0	6.83	3.69	0.0	0.0	0.0	3.40
Wo	0.0	0.0	0.0	0.0	0.0	0.0	0.0	0.0	0.0	0.0	0.0	0.0	1.22	0.0
HyDi	0.32	1.16	3.00	4.95	8.24	3.33	1.23	2.63	14.03	7.56	0.0	5.06	23.14	4.00
FsDi	3.63	0.59	2.06	2.85	3.70	2.12	1.19	1.71	5.42	2.99	0.0	2.27	1.46	2.44
Augt	11.95	1.74	5.06	7.00	11.94	5.45	2.42	4.34	19.45	10.55	0.0	0.13	24.59	6.52
Enst	0.07	0.0	5.04	0.0	0.0	4.04	0.0	5.55	0.0	0.0	7.46	3.22	0.0	0.0
Fsal	0.04	0.0	3.14	0.0	0.0	3.53	0.0	4.15	0.0	0.0	3.53	1.43	0.0	0.0
Hy	0.11	0.0	0.10	0.0	0.0	0.30	0.0	9.69	0.0	0.0	10.99	4.65	0.0	0.0
Fo	7.05	5.49	0.0	7.57	6.75	2.89	1.94	0.0	6.83	9.63	0.0	0.0	0.0	3.33
Fa	3.00	3.53	0.0	3.96	3.63	2.32	2.38	0.0	3.33	4.01	0.0	0.0	0.0	2.51
Ol	10.93	9.03	0.0	11.53	10.57	5.21	4.31	0.0	10.16	14.43	0.0	0.0	0.0	5.85
Mag	3.37	4.23	4.56	6.34	4.85	3.27	2.64	3.12	4.67	3.81	4.82	3.06	0.00	4.18
Ilm	3.53	3.87	4.0	5.31	4.36	4.59	1.78	3.84	4.38	3.61	3.48	2.18	3.17	3.90
Apat	1.87	2.38	2.13	1.48	1.00	1.73	1.09	1.63	1.66	1.68	1.67	0.65	0.78	2.16
Chrm	0.04	0.0	0.0	0.01	0.01	0.0	0.0	0.0	0.02	0.01	0.0	0.0	0.01	0.0
D.I.	58.4	61.47	61.43	45.62	40.74	52.98	80.4	61.85	31.9	48.93	61.83	63.14	35.67	63.09

TABLE A4.2. CHEMICAL COMPOSITION AND NORMATIVE MINERALOGY OF SELECTED QUARTZ-POOR FELSIC SAMPLES

Number	1	2	3	4	5	6	7	8
Rock Type	SYEN	PSYN	MONZ	PSYN	QTM2	PQM2	QTM2	QTM2
Sample	M88**	M810**	M820*	M840**	M844**	M852*	M863*	M866**
SiO2 wt. %	65.22	63.56	65.8	64.39	66.09	62.65	67.48	68.82
TiO2	0.53	0.61	0.4	0.69	0.52	1.04	0.38	0.42
Al2O3	17.41	17.32	17.75	17.28	16.54	16.66	16.97	16.12
Fe2O3	1.78	1.81	1.90	1.88	1.13	1.47	1.86	0.81
FeO***	1.58	2.18	1.68	2.68	2.88	3.28	1.28	1.78
FeOT	3.18	3.75	3.51	3.58	3.82	4.52	2.15	2.43
MnO	0.12	0.12	0.06	0.14	0.08	0.11	0.04	0.06
MgO	0.51	0.89	0.32	0.69	0.51	1.25	0.45	0.66
CaO	1.11	1.71	1.21	1.64	1.42	2.78	1.98	2.04
Na2O	6.71	6.28	5.51	6.28	5.58	4.58	5.29	5.28
K2O	5.14	4.91	5.51	4.84	5.35	4.72	4.18	3.92
P2O5	0.16	0.27	0.12	0.19	0.14	0.32	0.12	0.12
Total	100.19	99.5	99.38	99.74	99.36	98.62	99.07	99.87
H2O*	0.16	0.36	0.18	0.15	0.16	0.35	0.15	0.21
CO2*	0.11	0.16	0.11	0.06	0.07	0.18	0.08	0.08
Mg/(Mg+FeT)*	0.25	0.31	0.15	0.27	0.24	0.33	0.27	0.34
A/NCK	0.93	0.93	1.03	0.93	0.94	0.96	1.01	0.98
(Na+K)/Al	0.95	0.90	0.85	0.90	0.91	0.75	0.77	0.79
Fe3+/FeT	0.51	0.44	0.52	0.26	0.34	0.29	0.44	0.38
CIPW wt. %								
Qtz	4.85	4.08	0.81	4.33	9.21	10.37	16.24	17.71
Cor	0.0	0.0	0.81	0.0	0.0	0.01	0.52	0.0
Or	30.31	29.11	32.76	28.63	31.78	28.27	24.45	23.17
Ab	56.66	52.64	46.98	53.19	47.47	38.59	45.17	44.81
An	2.28	4.96	5.26	4.67	4.31	11.46	9.12	9.87
MgDi	1.27	1.82	0.8	0.83	0.71	0.0	0.0	0.2
FeDi	0.58	0.63	0.8	1.29	0.99	0.0	0.0	0.2
Augt	1.82	1.65	0.8	2.12	1.78	0.8	0.8	0.4
Enst	0.68	1.75	0.8	1.34	0.96	3.16	1.13	1.55
Fesl	0.34	1.25	0.83	2.39	1.51	3.21	0.79	1.77
Hy	1.82	3.88	1.63	3.72	2.46	6.36	1.92	3.32
Mag	2.58	2.63	2.77	1.45	1.65	2.16	1.55	1.17
Ilm	1.88	1.16	0.76	1.31	0.99	2.88	0.73	0.88
Apat	0.38	0.65	0.29	0.46	0.34	0.78	0.29	0.29
D.I.	91.8	85.83	88.47	86.15	88.46	77.23	85.86	84.89

TABLE A4.3. CHEMICAL COMPOSITION AND NORMATIVE MINERALOGY OF SELECTED SAMPLES OF GRANITE

Number	1	2	3	4	5	6
Rock Type	WTGD	GP	PDGR	GP	KFDG	KFPG
Sample	MG3*	MG42*	MG46**	MG51*	MG57*	MG83**
SiO2 wt. %	70.05	72.05	72.02	72.70	72.40	73.02
TiO2	0.20	0.34	0.36	0.35	0.29	0.25
Al2O3	16.28	14.89	14.49	14.33	13.66	14.03
Fe2O3	0.35	1.12	0.97	0.70	0.82	0.83
FeO***	1.40	1.30	1.50	1.50	1.00	1.00
FeOT	1.71	2.31	2.37	2.13	1.74	1.75
MnO	0.04	0.05	0.05	0.05	0.05	0.05
MgO	0.96	0.61	0.50	0.48	0.32	0.29
CaO	3.43	2.11	1.94	1.51	1.01	1.28
Na2O	4.54	4.13	4.06	3.77	3.88	4.24
K2O	1.61	3.37	3.97	4.53	4.78	4.33
P2O5	0.10	0.13	0.10	0.14	0.11	0.06
Total	98.96	100.10	99.96	100.06	98.32	99.38
H2O*	0.41	0.22	0.21	0.20	0.20	0.22
CO2*	0.25	0.09	0.07	0.10	0.16	0.16
FeT/(FeT+Mg)*	0.50	0.68	0.71	0.71	0.75	0.75
A/CNK	1.05	1.04	1.00	1.03	1.02	1.00
(Na+K)/Al	0.57	0.70	0.76	0.77	0.85	0.83
Fe3+/FeT	0.19	0.44	0.37	0.30	0.43	0.43
CIPW wt. %						
Qtz	28.35	29.58	27.84	29.08	29.34	28.49
Cor	1.08	0.92	0.16	0.81	0.54	0.13
Or	9.61	19.89	23.45	26.75	28.72	25.73
Ab	38.81	34.90	34.34	31.87	33.38	36.08
An	16.53	9.61	9.14	6.57	4.36	6.14
Enst	2.42	1.52	1.25	1.19	0.81	0.73
Fesl	2.05	1.00	1.45	1.70	0.79	0.83
Hy	4.47	2.52	2.70	2.89	1.61	1.56
Mag	0.51	1.62	1.41	1.01	1.21	1.21
Ilm	0.38	0.64	0.68	0.66	0.56	0.48
Apat	0.24	0.31	0.24	0.34	0.27	0.15
D.I.	76.77	84.37	85.63	87.70	91.44	90.30

TABLE A4.4. CHEMICAL COMPOSITION AND NORMATIVE MINERALOGY OF SELECTED SAMPLES OF NEPHELINE SYENITE

Number	1	2	3	4
Rock Type	MIAS	PTIN	PTIN	ITIN
Sample	MG16**	MG3[illegible]**	MG39**	MG94**
SiO2 wt. %	61.24	59.56	59.97	60.77
TiO2	0.67	0.29	0.30	0.30
Al2O3	19.04	19.30	19.69	20.06
Fe2O3	1.87	3.05	3.64	2.51
FeO	1.40	0.90	0.40	1.40
FeOT	3.08	3.64	3.68	3.66
MnO	0.16	0.27	0.27	0.24
MgO	0.44	0.0	0.04	0.03
CaO	1.28	0.86	0.78	0.77
Na2O	7.09	9.35	9.28	8.78
K2O	5.58	5.05	5.13	5.05
P2O5	0.14	0.04	0.04	0.03
ZrO2	0.10	0.24	0.24	0.18
Total	99.01	99.31	99.78	100.12
H2O	0.60	0.75	0.50	0.29
CO2	0.13	0.08	0.09	0.03
FeT/(FeT+Mg)	0.80	1.00	0.98	0.99
(Na+K)/Al	0.93	1.06	1.06	0.99
Fe3+/FeT	0.54	0.75	0.89	0.62
CIPW wt. %				
Or	33.28	30.04	30.45	29.80
Ab	51.77	42.78	44.23	50.58
An	3.68	0.0	0.0	0.41
Neph	4.76	16.75	15.61	12.79
Acm	0.0	5.23	5.14	0.0
Wo	0.0	1.13	1.40	0.87
MgDi	1.34	0.0	0.22	0.16
FeDi	0.23	1.21	0.0	0.84
Augt	1.57	1.21	0.22	1.00
Fo	0.34	0.0	0.0	0.0
Fa	0.07	0.0	0.0	0.0
Ol	0.42	0.0	0.0	0.0
Mag	2.74	1.83	1.31	3.63
Hm	0.0	0.0	0.98	0.0
Ilm	1.28	0.55	0.57	0.57
Zir	0.16	0.37	0.37	0.27
Ap	0.34	0.10	0.10	0.07
D.I.	89.81	89.57	90.29	93.17

APPENDIX V. SELECTED COMPOSITIONS OF PLAGIOCLASE AND NEPHELINE

Both minerals are recalculated on the basis of 32 oxygen atoms. Endmembers for plagioclase (in mole %) are Ab: albite, An: anorthite, Or: orthoclase. Endmembers for nepheline (in wt. %) are Ne: nepheline, Ks: kalsilite, FeNe: ferri-nepheline, An: anorthite, Qtz: quartz. Rock types are defined in Appendix III. See Appendix I for analytical conditions.

TABLE A5.1. SELECTED COMPOSITIONS OF PLAGIOCLASE FROM MAFIC AND MESOCRATIC INTERMEDIATE SAMPLES

Number	1	2	3	4	5	6	7	8	9	10	11	12	13	14	15	16
Rock Type	MAFI	MAFI	MAFI	MAFI	MZDI	MZDI	MZDI	MZDI	GABB	GABB	MZDI	MZDI	DIOR	DIOR	MZDI	MZDI
Sample	MG6-1	MG6-3c	MG6-3r	MG6-2	MG23-1c	MG23-1r	MG53-3c	MG53-1r	MG64-1c	MG64-r	83-77c	83-77r	MG98-1c	MG98-1r	84-556c	84-556r
SiO2 wt. %	53.97	57.00	61.44	62.97	58.05	66.18	56.87	65.13	52.20	60.53	60.72	67.79	61.72	65.94	54.28	64.61
Al2O3	28.89	27.15	24.19	23.16	26.90	21.29	26.70	21.86	30.51	25.00	24.70	20.62	24.15	22.13	28.44	22.33
TiO2	0.05	0.07	0.0	0.0	0.0	0.02	0.0	0.0	0.09	0.0	0.0	0.0	0.0	0.04	0.08	0.17
FeO	0.23	0.05	0.09	0.27	0.17	0.23	0.15	0.20	0.13	0.17	0.18	0.06	0.12	0.19	0.17	0.19
MgO	0.0	0.0	0.0	0.0	0.0	0.0	0.25	0.0	0.0	0.0	0.0	0.0	0.0	0.0	0.0	0.0
CaO	11.56	9.19	5.67	4.16	7.62	2.21	8.84	2.91	13.34	6.46	5.94	0.96	5.58	2.72	10.99	3.17
Na2O	4.61	5.94	7.60	8.48	6.83	9.38	5.61	9.10	3.71	7.38	7.67	9.43	7.99	8.67	5.18	8.32
K2O	0.24	0.25	0.31	0.27	0.23	0.39	1.28	0.21	0.0	0.05	0.21	0.91	0.50	0.56	0.19	0.22
Total	99.55	99.65	99.30	99.31	98.80	99.62	98.90	99.49	99.90	99.57	99.42	99.77	100.06	100.25	99.33	99.01
Si	9.823	10.291	11.047	11.271	10.515	11.778	10.344	11.614	9.586	10.867	10.893	12.039	10.983	11.787	9.863	11.639
Al	6.198	5.777	5.126	4.886	5.529	4.466	5.724	4.594	6.549	5.290	5.223	4.316	5.065	4.631	6.091	4.741
Fe3+	0.0	0.0	0.0	0.0	0.0	0.0	0.0	0.0	0.0	0.0	0.0	0.0	0.0	0.0	0.0	0.0
Ti	0.007	0.010	0.0	0.0	0.0	0.003	0.0	0.0	0.012	0.0	0.0	0.0	0.0	0.005	0.011	0.023
Fe2+	0.035	0.008	0.014	0.040	0.026	0.034	0.023	0.042	0.020	0.026	0.027	0.009	0.018	0.028	0.026	0.029
Mg	0.0	0.0	0.0	0.0	0.0	0.0	0.068	0.0	0.0	0.0	0.0	0.0	0.0	0.0	0.0	0.0
Ca	2.264	1.778	1.092	0.798	1.479	0.421	1.567	0.556	2.683	1.243	1.142	0.183	1.064	0.517	2.140	0.612
Na	1.627	2.079	2.649	2.943	2.399	3.209	1.970	3.146	1.310	2.569	2.668	3.247	2.757	2.984	1.825	2.906
K	0.056	0.058	0.071	0.062	0.053	0.089	0.297	0.048	0.0	0.007	0.048	0.206	0.114	0.127	0.044	0.051
Ab mol. %	41.32	53.12	69.49	77.48	61.02	86.29	51.49	83.90	33.48	67.28	69.16	89.31	78.07	82.25	45.53	81.44
An	57.26	45.41	28.65	20.98	37.62	11.33	40.78	14.83	66.52	32.54	29.68	5.02	27.04	14.26	53.38	17.15
Or	1.42	1.47	1.86	1.62	1.35	2.38	7.73	1.27	0.0	0.18	1.25	5.67	2.89	3.58	1.10	1.42

1: labradorite (forms a compound xenocryst? with titansalite), 2: calcic andesine (core of oscillatory zoned, resorbed grain), 3: calcic oligoclase (rim of the same resorbed grain as 2), 4: calcic oligoclase (groundmass), 5: sodic andesine (partially recrystallized core), 6: sodic oligoclase (recrystallized rim), 7: calcic andesine (partially recrystallized core), 8: sodic oligoclase (recrystallized rim), 9: labradorite (core), 10: sodic andesine (recrystallized rim), 11: calcic oligoclase (partially recrystallized core), 12: albite (recrystallized rim), 13: calcic oligoclase (partially recrystallized core), 14: sodic oligoclase (recrystallized rim), 15: labradorite (partially recrystallized core), 16: sodic oligoclase (recrystallized rim).

TABLE A5.2. SELECTED COMPOSITIONS OF PLAGIOCLASE FROM QUARTZ-POOR FELSIC SAMPLES

Number	1	2	3	4	5	6	7	8	9
Rock Type	SYEN	SYEN	SYEN	PSYN	PSYN	QTZM	QTZM	QTZM	QTZM
Sample	MG8-2c	MG8-2r	MG8-3	MG48-2c	MG48-3r	MG63-4c	MG63-4r	MG66-3c	MG66-3r
SiO2 wt. %	64.86	69.85	70.16	61.48	66.78	59.72	65.48	56.12	66.52
Al2O3	22.66	20.83	20.18	24.86	21.75	25.85	22.38	27.68	20.58
TiO2	0.0	0.05	0.02	0.0	0.05	0.03	0.09	0.07	0.04
FeO	0.05	0.11	0.0	0.04	0.05	0.14	0.19	0.0	0.14
MgO	0.01	0.0	0.0	0.0	0.0	0.01	0.0	0.19	0.0
CaO	3.42	0.58	0.0	6.27	1.43	6.42	2.76	9.88	1.62
Na2O	9.87	10.65	10.85	7.59	9.38	7.37	8.74	5.52	10.23
K2O	0.39	0.17	0.07	0.27	0.38	0.38	0.36	0.10	0.24
Total	100.46	100.62	100.48	100.51	99.66	99.84	99.82	99.64	99.37
Si	11.442	12.087	12.378	10.921	11.856	10.765	11.669	10.148	11.794
Al	4.712	4.132	4.177	5.205	4.557	5.322	4.663	5.900	4.301
Fe3+	0.0	0.0	0.0	0.0	0.0	0.0	0.0	0.0	0.0
Ti	0.0	0.004	0.003	0.0	0.007	0.004	0.012	0.010	0.005
Fe2+	0.007	0.016	0.0	0.006	0.007	0.021	0.020	0.0	0.021
Mg	0.003	0.0	0.0	0.0	0.0	0.003	0.0	0.051	0.0
Ca	0.646	0.109	0.0	1.193	0.272	1.240	0.527	1.914	0.308
Na	3.182	3.614	3.435	2.614	3.233	2.576	3.020	1.935	3.517
K	0.088	0.038	0.016	0.061	0.068	0.069	0.002	0.042	0.054
Ab mol. %	80.86	96.18	99.54	67.57	90.47	66.31	83.22	49.74	90.67
An	16.85	2.89	0.0	30.85	7.62	31.92	14.52	49.20	7.93
Or	2.29	1.01	0.46	1.58	1.90	1.78	2.26	1.07	1.40

1:sodic oligoclase (partially recrystallized core of a partly mantled grain), 2: albite (rim of the same grain as 1), 3: albite (exsolved from K-feldspar), 4: sodic andesine (partially recrystallized core of a mantled phenocryst), 5: albite (recrystallized rim of a mantled phenocryst), 6: sodic andesine (partially recrystallized core), 7: sodic oligoclase (recrystallized rim), 8: calcic andesine (partially recrystallized core), 9: albite (recrystallized rim).

TABLE A5.3. SELECTED COMPOSITIONS OF PLAGIOCLASE FROM SAMPLES OF GRANITE

Number	1	2	3	4	5	6	7	8
Rock Type	WTGD	WTGD	GP	GP	TFGR	TFGR	KFPG	KFPG
Sample	MG3-1c	MG3-1r	MG42-4c	MG42-4r	MG46-4c	MG46-4r	MG83-2c	MG83-3r
SiO2 wt. %	53.68	63.10	55.67	65.15	55.45	65.41	63.01	65.71
Al2O3	29.26	23.36	27.91	21.55	28.33	21.97	23.33	21.21
TiO2	0.09	0.17	0.0	0.0	0.12	0.05	0.09	0.0
FeO	0.06	0.15	0.15	0.28	0.23	0.07	0.13	0.12
MgO	0.0	0.0	0.0	0.0	0.0	0.0	0.0	0.0
CaO	11.72	4.48	10.15	2.02	10.47	2.60	4.70	2.36
Na2O	4.48	7.99	5.53	9.76	5.31	8.90	8.54	9.52
K2O	0.16	0.20	0.14	0.26	0.10	0.29	0.35	0.51
Total	99.45	99.37	99.55	99.74	100.09	99.37	100.23	99.43
Si	9.704	11.334	10.079	11.532	10.003	11.691	11.171	11.607
Al	6.206	4.945	5.956	4.496	6.024	4.620	4.875	4.446
Fe3+	0.0	0.0	0.0	0.0	0.0	0.0	0.0	0.0
Ti	0.012	0.023	0.0	0.0	0.016	0.007	0.012	0.0
Fe2+	0.009	0.023	0.023	0.030	0.035	0.010	0.019	0.010
Mg	0.0	0.0	0.0	0.0	0.0	0.0	0.0	0.0
Ca	2.209	0.047	1.969	0.535	2.024	0.513	0.900	0.450
Na	1.503	2.703	1.941	3.349	1.057	3.004	2.935	3.203
K	0.037	0.046	0.032	0.059	0.041	0.066	0.079	0.116
Ab mol. %	40.50	75.71	49.24	84.95	47.35	84.19	74.03	85.31
An	58.55	23.04	49.94	13.56	51.59	14.01	23.15	11.69
Or	0.95	1.25	0.82	1.49	1.06	1.00	2.02	3.01

1:labradorite (partially recrystallized core), 2: calcic oligoclase (recrystallized rim), 3: calcic andesine (partially recrystallized core), 4: sodic oligoclase (rim), 5: labradorite (partially recrystallized core), 6: sodic oligoclase (recrystallized rim), 7: calcic oligoclase (partially recrystallized core), 8: sodic oligoclase (rim).

TABLE A5.4. SELECTED COMPOSITIONS OF NEPHELINE FROM SAMPLES OF NEPHELINE SYENITE

Number	1	2	3	4
Rock Type	MIAS	PTIN	PTIN	ITIN
Analysis	MG16 Av(4)	MG37 Av(4)	MG39 Av(2)	MG94-1 Av(3)
SiO2 wt. %	45.53	43.52	46.05	44.90
Al2O3	34.01	34.25	33.30	34.22
TiO2	0.04	0.01	0.02	0.0
Fe2O3	0.46	0.19	0.38	0.72
MgO	0.0	0.01	0.0	0.01
CaO	0.24	0.0	0.14	0.03
Na2O	14.96	15.80	15.45	15.21
K2O	5.70	6.93	6.06	5.97
Total	100.94	100.71	101.40	101.06
Si	8.562	8.311	8.647	8.466
Al	7.538	7.709	7.370	7.605
Ti	0.006	0.001	0.003	0.0
Fe3+	0.064	0.027	0.053	0.102
Mg	0.0	0.003	0.0	0.003
Ca	0.048	0.0	0.028	0.006
Na	5.455	5.850	5.625	5.560
K	1.367	1.688	1.452	1.436
Ne wt. %	67.76	72.09	70.15	68.43
Ks	19.14	23.27	20.35	20.05
FeNe	0.98	0.40	0.81	1.55
An	1.19	0.0	0.69	0.15
Qtz*	5.10	3.01	6.52	4.02

The amount of excess SiO_2 is calculated by subtracting the amount of Al plus Fe^{3+} from Si.

APPENDIX VI. X-RAY DIFFRACTION RESULTS FOR K-FELDSPAR AND PLAGIOCLASE

Analytical procedures and methods are described in Appendix I.

*: reciprocal cell, **: traces of microcline present. P: phenocryst, M: matrix, Pl: plagioclase, Or: orthoclase, Mi: microcline, Ab: albite lamellae in K-feldspar.

Units: a, b and c in angstrom units (Å), unit-cell volume V in $Å^3$, a^*, b^* and c^* in $Å^{-1}$, and interaxial angles in degrees.

Rock types are defined in Appendix III.

TABLE A6.1. APPROXIMATE COMPOSITION AND DEGREE OF Al-Si ORDER IN THE K-FELDSPAR

Sample	Rock Type	N_{Or}^{V}	t_1o+t_1m	t_1o-t_1m	t_1o
MG8Or	SYEN	0.979	0.912	0	0.46
MG8Mi	SYEN	0.971	1.014	0.720	0.87
MG16	MIAS	1.014	0.893	0	0.45
MG23	MZDI	0.979	0.818	0	0.41
84-23Or	ALKS	0.936	0.836	0	0.42
84-23Mi	ALKS	0.928	0.891	0.676	0.78
MG28	KFDG	0.951	0.884	0	0.44
MG36	QTMZ	0.918	0.842	0	0.42
MG37	PTIN	0.956	0.739	0	0.37
MG40	PSYN	0.936	0.805	0	0.40
MG44	QTMZ	0.933	0.899	0	0.45
MG46	PDGR	0.927	0.777	0	0.39
MG47	KFDG	0.911	0.848	0	0.42
MG51	GP	0.942	0.797	0	0.40
MG52	PQMZ	0.942	0.808	0	0.40
MG53	MZDI	0.918	0.788	0	0.39
MG57	KFDG	0.927	0.806	0	0.40
MG60	KFDG	0.927	0.855	0	0.43
MG62	QTMZ	0.937	0.866	0	0.43
MG63	QTMZ	0.946	0.863	0	0.43
MG66	QTMZ	0.917	0.838	0	0.42
MG71	MZDI	0.946	0.802	0	0.40
MG73	QTMZ	0.922	0.859	0	0.43
MG83	KFPG	0.935	0.866	0	0.43
MG87	QMDI	0.899	0.804	0	0.40
MG94P	ITIN	0.960	0.724	0	0.36
MG94M	ITIN	0.938	0.789	0	0.40

TABLE A6.2. APPROXIMATE COMPOSITION AND DEGREE OF Al-Si ORDER OF PLAGIOCLASE

Sample	Rock Type	An	Degree of order
MG8	SYEN	1	ordered
MG9Pl	DIOR	18	ordered
MG16	MIAS	0	slightly disordered
MG23	MZDI	5	slightly disordered
MG23Pl	MZDI	14	slightly disordered
84-23Or	ALKS	3	ordered
84-23Mi	ALKS	0	ordered
MG28	KFDG	0	ordered
MG36	QTMZ	4	slightly disordered
MG37	PTIN	0	ordered
MG40	PSYN	2	ordered
MG44	QTMZ	4	ordered
MG46	PDGR	2	slightly disordered
MG47	KFDG	2	ordered
MG51	GP	4	slightly disordered
MG52	PQMZ	4	ordered
MG53	MZDI	13	ordered
MG57	KFDG	3	ordered
MG60	KFDG	3	ordered
MG62	QTMZ	2	ordered
MG63	QTMZ	0	ordered
MG63Pl	QTMZ	15	ordered
MG64Pl	GABB	17	slightly disordered
MG66	QTMZ	2	ordered
MG71	MZDI	14	ordered
MG73	QTMZ	11	ordered
MG83	KFPG	0	ordered
MG83Pl	KFPG	14	slightly disordered
MG87	QMDI	3	ordered
MG94P	ITIN	0	ordered
MG94M	ITIN	0	ordered

TABLE A6:3. UNIT-CELL PARAMETERS OF K-FELDSPAR AND PLAGIOCLASE FROM SELECTED MAFIC AND MESOCRATIC INTERMEDIATE SAMPLES

Sample	Rock Type	a	b	c	α	β	γ	V	a*	b*	c*	α*	β*	γ*
M89P1	DIOR	8.1526	12.8228	7.1381	93.983	116.471	88.673	666.34	0.137832	0.078178	0.156843	86.211	63.555	89.588
		0.0012	0.0023	0.0012	0.019	0.011	0.017	0.14	0.000021	0.000015	0.000024	0.018	0.011	0.016
M823P1	MZDI	8.1412	12.8096	7.1582	94.113	116.589	88.526	664.24	0.137417	0.078336	0.156779	86.136	63.448	89.589
		0.0021	0.0000	0.0015	0.020	0.018	0.025	0.68	0.000035	0.000018	0.000033	0.025	0.018	0.022
M8230r	MZDI	8.5076	12.9885	7.2061	90	115.929	90	722.16	0.129581	0.077856	0.154527	90	64.071	90
		0.0030	0.0114	0.0017		0.029		1.11	0.000036	0.000015	0.000045		0.029	
Ab		8.1411	12.8113	7.1501	94.109	116.599	88.518	664.32	0.13742	0.07852	0.15678	86.345	63.526	90.232
		0.0022	0.0000	0.0017	0.020	0.018	0.026	0.69						
M8630r	MZDI	8.5744	12.9818	7.1989	90	116.036	90	719.96	0.129799	0.077835	0.154599	90	63.964	90
		0.0012	0.0019	0.0011		0.012		0.14	0.000019	0.000011	0.000021		0.012	
Ab		8.1494	12.8043	7.1451	94.179	116.484	88.365	665.56	0.137097	0.078308	0.156719	86.145	63.561	89.745
		0.0007	0.0012	0.0006	0.010	0.010	0.012	0.09	0.000014	0.000008	0.000021	0.010	0.010	0.012
M864P1	GABB	8.1491	12.8998	7.1389	93.891	116.579	88.728	664.16	0.137371	0.078249	0.156961	86.285	63.444	89.476
		0.0017	0.0027	0.0013	0.019	0.017	0.019	0.17	0.000040	0.000016	0.000023	0.019	0.017	0.019
M8710r	MZDI	8.5863	12.9888	7.2006	90	116.048	90	720.99	0.129632	0.077842	0.154579	90	63.952	90
		0.0022	0.0033	0.0017		0.019		0.23	0.000039	0.000019	0.000034		0.019	
Ab		8.1498	12.7768	7.1491	94.249	116.545	88.377	663.17	0.137177	0.078489	0.156929	86.061	63.500	89.693
		0.0023	0.0033	0.0023	0.043	0.042	0.036	0.37	0.000065	0.000021	0.000076	0.051	0.042	0.045
M8870r**	QMDI	8.5644	12.9816	7.2014	90	116.062	90	719.24	0.129978	0.077832	0.154580	90	63.938	90
		0.0024	0.0028	0.0015		0.020		0.22	0.000041	0.000017	0.000032		0.020	
Ab		8.1306	12.7855	7.1528	94.213	116.488	87.918	663.62	0.137419	0.078426	0.156541	86.333	63.507	90.238
		0.0024	0.0031	0.0018	0.035	0.025	0.041	0.24	0.000036	0.000018	0.000031	0.028	0.024	0.035

TABLE A6.4. UNIT-CELL PARAMETERS OF K-FELDSPAR AND PLAGIOCLASE FROM SELECTED QUARTZ-POOR FELSIC SAMPLES

Sample	Rock Type	a	b	c	α	β	γ	V	a*	b*	c*	α*	β*	γ*
M880r	SYEN	8.5919	12.9650	7.2106	90	115.962	90	722.16	0.129453	0.077131	0.154250	90	64.038	90
		0.0029	0.0037	0.0020		0.034		0.36	0.000059	0.000022	0.000060		0.034	
Mi		8.5797	12.9609	7.2236	90.582	115.964	88.321	721.87	0.129691	0.077189	0.153978	90.259	64.039	91.622
		0.0026	0.0055	0.0027	0.035	0.026	0.026	0.45	0.000054	0.000033	0.000054	0.034	0.026	0.044
Ab		8.1389	12.7862	7.1691	94.274	116.592	87.755	664.34	0.137495	0.078429	0.156525	86.343	63.495	90.374
		0.0010	0.0015	0.0012	0.017	0.012	0.014	0.12	0.000021	0.000010	0.000026	0.017	0.011	0.014
84-230r	ALKS	8.5756	12.9811	7.2059	90	116.057	90	720.64	0.129883	0.077035	0.154476	90	63.943	90
		0.0016	0.0033	0.0012		0.015		0.20	0.000038	0.000019	0.000029		0.015	
Ab		8.1332	12.7984	7.1586	94.183	116.597	87.879	664.11	0.137505	0.078393	0.156535	86.382	63.400	90.288
		0.0011	0.0011	0.0007	0.010	0.009	0.010	0.09	0.000018	0.000007	0.000014	0.011	0.008	0.019
Mi		8.5745	12.9683	7.2106	90.474	115.931	88.378	720.33	0.129738	0.077191	0.154213	90.265	64.071	91.582
		0.0019	0.0033	0.0013	0.021	0.024	0.030	0.23	0.000032	0.000020	0.000041	0.023	0.024	0.031
Ab		8.1376	12.7869	7.1581	94.187	116.621	87.738	664.08	0.137463	0.078416	0.156567	86.453	63.465	90.443
		0.0010	0.0012	0.0010	0.015	0.014	0.009	0.12	0.000024	0.000008	0.000029	0.016	0.015	0.010
M6360r	QTHZ	8.5717	12.9769	7.2051	90	116.059	90	719.97	0.129865	0.077060	0.154497	90	63.941	90
		0.0017	0.0021	0.0011		0.015		0.18	0.000031	0.000012	0.000026		0.015	
Ab		8.1442	12.7896	7.1556	94.242	116.624	87.893	664.47	0.137352	0.078404	0.156651	86.318	63.452	90.233
		0.0006	0.0011	0.0007	0.011	0.007	0.010	0.08	0.000011	0.000007	0.000015	0.010	0.007	0.009
M6480r	PSYN	8.5779	12.9832	7.2022	90	116.049	90	720.62	0.129768	0.077023	0.154545	90	63.951	90
		0.0015	0.0016	0.0010		0.012		0.13	0.000024	0.000009	0.000018		0.012	
Ab		8.1431	12.7873	7.1574	94.206	116.590	87.884	664.65	0.137331	0.078415	0.156551	86.395	63.492	90.352
		0.0006	0.0011	0.0008	0.011	0.011	0.008	0.10	0.000016	0.000006	0.000025	0.012	0.011	0.008
M6440r	QTHZ	8.5778	12.9642	7.2005	90	115.993	90	720.53	0.129788	0.077135	0.154337	90	64.006	90
		0.0012	0.0019	0.0011		0.016		0.15	0.000028	0.000011	0.000029		0.016	
Ab		8.1435	12.7731	7.1539	94.215	116.587	87.904	663.64	0.137329	0.078503	0.156632	86.334	63.489	90.236
		0.0014	0.0031	0.0012	0.021	0.021	0.024	0.20	0.000031	0.000018	0.000037	0.021	0.021	0.025
M6520r	PQHZ	8.5841	12.9794	7.2011	90	116.040	90	720.84	0.129663	0.077045	0.154564	90	63.956	90
		0.0016	0.0025	0.0013		0.019		0.20	0.000026	0.000015	0.000033		0.019	
Ab		8.1456	13.0122	7.1433	93.643	116.548	88.193	675.81	0.137262	0.077007	0.156721	86.829	63.516	90.201
		0.0009	0.0025	0.0005	0.024	0.011	0.022	0.15	0.000020	0.000016	0.000018	0.019	0.011	0.018
M6620r	QTHZ	8.5787	12.9732	7.2071	90	116.042	90	720.66	0.129748	0.077082	0.154432	90	63.958	90
		0.0008	0.0010	0.0006		0.008		0.09	0.000015	0.000006	0.000015		0.008	
Ab		8.1444	12.7987	7.1549	94.213	116.607	87.844	664.60	0.137329	0.078396	0.156634	86.367	63.472	90.304
		0.0010	0.0027	0.0014	0.016	0.015	0.018	0.17	0.000036	0.000016	0.000033	0.017	0.015	0.019
M6630P1	QTHZ	8.1467	12.8219	7.1328	94.864	116.536	88.549	665.35	0.137286	0.078198	0.156944	86.181	63.498	89.593
		0.0020	0.0029	0.0017	0.025	0.019	0.026	0.20	0.000037	0.000018	0.000036	0.022	0.019	0.024
Or		8.5767	12.9784	7.2087	90	116.037	90	720.98	0.129764	0.077051	0.154391	90	63.963	90
		0.0010	0.0016	0.0008		0.010		0.11	0.000018	0.000010	0.000017		0.010	
Ab		8.1461	12.7849	7.1552	94.192	116.589	87.919	664.48	0.03727	0.07845	0.15660	86.329	63.526	90.463
		0.0029	0.0121	0.0023	0.036	0.026	0.027	1.03						
M6660r	QTHZ	8.5712	12.9761	7.2043	90	116.041	90	719.92	0.129853	0.077065	0.154490	90	63.959	90
		0.0016	0.0024	0.0012		0.014		0.17	0.000029	0.000014	0.000024		0.014	
Ab		8.1265	12.7963	7.1506	94.092	116.598	87.906	663.13	0.137628	0.078355	0.156697	86.472	63.477	90.295
		0.0030	0.0024	0.0016	0.031	0.024	0.024	0.22	0.000036	0.000015	0.000031	0.028	0.024	0.021

TABLE A6.5. UNIT-CELL PARAMETERS OF K-FELDSPAR AND PLAGIOCLASE FROM SELECTED SAMPLES OF GRANITE

Sample	Rock Type	a	b	c	α	β	γ	V	a*	b*	c*	α*	β*	γ*
H6280r**	KFDG	8.5901	12.9645	7.2064	90	116.025	90	721.17	0.129549	0.077134	0.154424	90	63.975	90
		0.0033	0.0042	0.0020		0.034		0.37	0.000066	0.000025	0.000059		0.034	
	Ab	8.1440	12.7850	7.1529	94.108	116.520	87.763	662.99	0.137243	0.078613	0.156588	86.434	63.556	90.412
		0.0013	0.0050	0.0012	0.021	0.020	0.020	0.23	0.000030	0.000030	0.000025	0.023	0.020	0.021
H6460r	PDGR	8.5700	12.9018	7.1976	90	116.018	90	720.28	0.129723	0.077831	0.154603	90	63.982	90
		0.0015	0.0020	0.0012		0.013		0.16	0.000024	0.000012	0.000027		0.013	
	Ab	8.1367	12.7861	7.1631	94.169	116.656	87.782	664.18	0.137536	0.078426	0.156589	86.447	63.427	90.391
		0.0030	0.0043	0.0030	0.050	0.040	0.041	0.35	0.000052	0.000028	0.000060	0.050	0.040	0.042
H6470r	KFDG	8.5725	12.9706	7.2036	90	116.029	90	719.72	0.129823	0.077897	0.154489	90	63.971	90
		0.0026	0.0033	0.0016		0.020		0.25	0.000048	0.000019	0.000033		0.020	
	Ab	8.1368	12.7868	7.1536	94.247	116.596	87.799	663.63	0.137458	0.078427	0.156649	86.352	63.406	90.337
		0.0013	0.0022	0.0013	0.019	0.015	0.017	0.15	0.000026	0.000014	0.000032	0.018	0.015	0.016
H6510r	GP	8.5826	12.9821	7.2006	90	116.048	90	720.84	0.129680	0.077829	0.154568	90	63.960	90
		0.0017	0.0017	0.0011		0.013		0.16	0.000027	0.000018	0.000024		0.013	
	Ab	8.1408	12.7900	7.1552	94.209	116.613	87.938	664.28	0.137395	0.078398	0.156641	86.325	63.460	90.200
		0.0022	0.0040	0.0014	0.022	0.030	0.021	0.24	0.000061	0.000024	0.000053	0.022	0.030	0.021
H6570r**	KFDG	8.5806	12.9743	7.1989	90	116.002	90	720.31	0.129667	0.077875	0.154555	90	63.998	90
		0.0014	0.0019	0.0013		0.013		0.16	0.000028	0.000011	0.000030		0.013	
	Ab	8.1398	12.7878	7.1515	94.182	116.526	87.804	664.21	0.137386	0.078414	0.156597	86.381	63.552	90.208
		0.0022	0.0029	0.0019	0.035	0.022	0.027	0.22	0.000047	0.000017	0.000042	0.032	0.022	0.026
H6690r	PDGR	8.5752	12.9739	7.2059	90	116.041	90	720.29	0.129792	0.077878	0.154486	90	63.959	90
		0.0007	0.0014	0.0008		0.008		0.10	0.000012	0.000008	0.000015		0.008	
	Ab	8.1391	12.7906	7.1563	94.205	116.598	87.873	664.34	0.137396	0.078483	0.156595	86.272	63.408	90.236
		0.0017	0.0039	0.0022	0.054	0.028	0.029	0.34	0.000038	0.000026	0.000066	0.055	0.028	0.032
H6835P1	KFPG	8.1520	12.8197	7.1422	94.039	116.546	88.531	666.84	0.137129	0.078281	0.156855	86.218	63.489	89.626
		0.0016	0.0018	0.0013	0.021	0.014	0.019	0.15	0.000027	0.000012	0.000027	0.018	0.014	0.016
	Or	8.5779	12.9710	7.2063	90	116.011	90	720.59	0.129717	0.077896	0.154488	90	63.989	90
		0.0019	0.0021	0.0012		0.017		0.19	0.000031	0.000013	0.000030		0.019	
	Ab	8.1394	12.8010	7.1529	94.229	116.631	87.857	663.97	0.13744	0.07839	0.15671	86.329	63.526	90.463
		0.0016	0.0061	0.0012	0.019	0.014	0.018	~0.54						

TABLE A6.6. UNIT-CELL PARAMETERS OF K-FELDSPAR AND PLAGIOCLASE FROM SELECTED SAMPLES OF NEPHELINE SYENITE

Sample	Rock Type	a	b	c	α	β	γ	V	a*	b*	c*	α*	β*	γ*
MB160	Orthoclase MIAS	8.6830	12.9867	7.2157	90	116.183	90	723.39	0.129530	0.077808	0.154433	90	63.817	90
		0.0051	0.0039	0.0025		0.031		0.36	0.000065	0.000023	0.000052		0.031	
	Ab	8.1306	12.7967	7.1601	94.326	116.679	87.756	664.48	0.137513	0.078378	0.156633	86.286	63.407	90.341
		0.0010	0.0016	0.0012	0.017	0.014	0.012	0.15	0.000023	0.000018	0.000034	0.019	0.014	0.015
MB370	Orthoclase PTIN	8.6809	13.0049	7.2012	90	116.260	90	721.34	0.129020	0.076894	0.154948	90	63.740	90
		0.0052	0.0073	0.0042		0.048		0.44	0.000068	0.000043	0.000094		0.048	
ϕ	Ab	8.1308	12.7933	7.1564	94.248	116.608	87.662	663.88	0.137418	0.078446	0.156683	86.428	63.491	90.494
		0.0012	0.0023	0.0014	0.018	0.019	0.013	0.19	0.000032	0.000014	0.000041	0.024	0.019	0.017
MB940	Orthoclase PTIN	8.6905	12.9983	7.1964	90	116.122	90	721.48	0.129651	0.076933	0.154767	90	63.878	90
		0.0040	0.0068	0.0030		0.040		0.37	0.000064	0.000048	0.000062		0.040	
	Ab/P	8.1406	12.7894	7.1608	94.307	116.621	87.682	664.60	0.137411	0.078413	0.156628	86.343	63.469	90.437
		0.0009	0.0017	0.0012	0.019	0.012	0.014	0.13	0.000018	0.000017	0.000026	0.018	0.012	0.014
	Orthoclase	8.6881	12.9792	7.1984	90	116.077	90	720.78	0.129637	0.077047	0.154664	90	63.923	90
		0.0025	0.0033	0.0026		0.022		0.26	0.000041	0.000028	0.000059		0.022	
«	Ab/M	8.1346	12.7868	7.1586	94.257	116.615	87.686	663.88	0.137505	0.078431	0.156567	86.397	63.467	90.458
		0.0009	0.0011	0.0007	0.011	0.010	0.009	0.09	0.000010	0.000007	0.000016	0.010	0.010	0.009

APPENDIX VII. SELECTED COMPOSITIONS OF CLINOPYROXENE

Fe_2O_3 and formula calculated by normalizing to 4 cations and then adjusting the Fe^{3+} content so that the total number of oxygen atoms is equal to six, following the recommendations of Robinson (1980).

Nomenclature after Poldervaart and Hess (1951), Deer et al. (1978), Rock (1982) and Curtis and Currie (1981). Titanian aegirines are defined as aegirines containing more than 0.1 atoms of Ti per formula unit (Rønsbo et al. 1977).

Rock types defined in Appendix III. Av(n): average of n analyses. T: total iron, expressed as Fe or as FeO. % others is equal to the largest of three parameters: 1) (Na per six oxygen atoms) x 100, 2) (^{iv}Al per 6 oxygen atoms) x 100, and 3) (^{vi}Al + $^{vi}Fe^{3+}$ + ^{vi}Cr + ^{vi}Ti per 6 oxygen atoms) x 100 (Cameron and Papike 1981). See Appendix I for analytical conditions.

1:titansalite (forms a compound xenocryst(?) with labradorite; Fig. 2.4.4), 2: titaniferous salite (partially recrystallized xenocryst?), 3: augite (partially recrystallized xenocryst?), 4: titaniferous augite (partially recrystallized grain), 5: titaniferous augite (partially recrystallized grain), 6: titanaugite (partially recrystallized grain), 5: titaniferous augite (partially recrystallized grain), 6: titanaugite (partially recrystallized grain), 7: titansalite (groundmass of dyke), 8: Low-Ti sector of zoned titansalite (Fig. 2.9.1), 9: high-Ti sector of zoned titansalite (same grain as 8), 10: titaniferous augite (partially recrystallized xenocryst?), 11: titaniferous diopside (partially recrystallized xenocryst?), 12: sodian salite (partially recrystallized xenocryst?), 13: augite (partially recrystallized grain), 14: augite (partially recrystallized grain), 15: titaniferous augite (partially recrystallized grain), 16: titaniferous augite (partially recrystallized grain).

TABLE A7.1. SELECTED COMPOSITIONS OF "PRIMARY" CLINOPYROXENE FROM MAFIC AND MESOCRATIC INTERMEDIATE SAMPLES

Number	1	2	3	4	5	6	7	8	9	10	11	12	13	14	15	16
Rock Type	MAFI	MAFI	MAFI	M2DI	M2DI	M2DI	MDYK	GABB	GABB	MAFI	MAFI	MAFI	QMDI	QMDI	QMDI	M2DI
Sample	MG6-1	MG6-2	MG6-3	MG23-1	MG23-3	MG23-5	MG61	MG64-3a	MG64-3b	MG68-2	MG68-3	MG68-1	MG87-1	MG87-2	MG87-3	84-556
	Av(7)	Av(2)	Av(2)	Av(2)	Av(2)	Av(2)	Av(2)	Av(3)	Av(5)	Av(3)	Av(4)	Av(2)	Av(2)	Av(2)	Av(4)	Av(3)
SiO2 wt. %	47.82	47.26	49.30	50.63	51.02	48.94	43.82	49.58	46.51	50.50	49.45	51.27	51.76	51.93	49.99	50.63
Al2O3	6.26	8.40	5.72	2.46	2.53	4.43	8.89	4.16	6.81	4.81	6.80	4.36	1.94	2.70	3.46	3.91
Fe2O3	3.68	3.20	3.05	4.26	2.77	3.82	2.95	3.20	4.27	2.19	2.33	4.29	1.54	1.51	3.63	1.86
TiO2	2.16	1.71	0.91	1.04	1.32	2.08	5.17	1.71	2.67	1.23	1.06	0.61	0.73	0.97	1.31	1.57
Cr2O3	0.01	0.20	0.0	0.03	0.0	0.03	n.d.	0.05	0.03	0.03	0.32	0.20	0.02	0.04	0.04	n.d.
MgO	13.48	12.03	15.16	15.94	15.22	13.56	10.97	14.62	12.87	13.91	14.06	13.44	15.89	16.44	15.40	14.31
FeO	4.20	3.71	4.00	4.01	5.90	5.92	6.88	4.30	4.01	6.47	3.20	2.56	7.70	6.00	5.46	5.81
FeOT	7.52	6.69	6.82	8.64	8.47	8.63	9.54	7.18	7.86	8.44	5.37	6.42	9.09	7.36	8.72	7.48
MnO	0.17	0.13	0.13	0.29	0.37	0.25	0.24	0.15	0.14	0.37	0.12	0.06	0.32	0.20	0.17	0.30
CaO	21.13	21.24	20.47	19.91	20.28	20.78	20.99	21.99	22.00	20.19	21.04	21.46	19.22	20.17	20.45	20.71
Na2O	0.77	0.69	0.52	0.53	0.59	0.74	0.75	0.58	0.59	0.86	0.78	1.68	0.34	0.35	0.36	0.82
Total	99.68	99.73	99.42	99.89	100.08	99.74	100.66	100.16	99.91	99.76	99.95	100.00	99.46	100.31	100.26	99.92
Si	1.780	1.751	1.826	1.877	1.891	1.828	1.644	1.834	1.736	1.878	1.812	1.885	1.927	1.906	1.858	1.875
AlTET	0.220	0.249	0.174	0.107	0.109	0.172	0.356	0.166	0.264	0.122	0.188	0.115	0.073	0.094	0.150	0.125
AlOCT	0.054	0.121	0.076	0.0	0.001	0.023	0.036	0.016	0.036	0.053	0.106	0.074	0.013	0.023	0.001	0.045
Fe3+	0.101	0.089	0.085	0.119	0.077	0.086	0.083	0.089	0.120	0.061	0.064	0.119	0.043	0.042	0.101	0.052
Ti	0.060	0.048	0.025	0.029	0.037	0.058	0.146	0.048	0.075	0.034	0.029	0.017	0.020	0.027	0.036	0.044
Cr	0.000	0.000	0.000	0.001	0.000	0.001	0.000	0.001	0.001	0.001	0.009	0.000	0.001	0.001	0.001	0.000
Mg	0.748	0.700	0.836	0.881	0.841	0.755	0.613	0.801	0.716	0.771	0.812	0.737	0.882	0.899	0.850	0.798
Fe2+	0.133	0.115	0.126	0.149	0.186	0.186	0.216	0.133	0.125	0.201	0.100	0.079	0.240	0.184	0.169	0.180
Mn	0.005	0.004	0.004	0.009	0.012	0.008	0.008	0.005	0.004	0.012	0.004	0.002	0.010	0.006	0.005	0.009
Ca	0.842	0.843	0.811	0.791	0.805	0.832	0.843	0.872	0.880	0.804	0.826	0.845	0.767	0.793	0.811	0.822
Na	0.056	0.064	0.037	0.038	0.042	0.054	0.055	0.036	0.043	0.062	0.058	0.120	0.025	0.025	0.026	0.059
Mg/(Mg+FeT)	0.762	0.776	0.798	0.767	0.762	0.737	0.672	0.783	0.745	0.746	0.831	0.789	0.757	0.799	0.758	0.773
% Others	22.8	26.6	18.6	14.9	11.5	17.2	35.6	16.6	26.4	14.9	20.8	21.8	7.7	9.4	15.8	14.1
Ti/ivAl	0.271	0.189	0.144	0.271	0.339	0.337	0.410	0.289	0.284	0.276	0.154	0.149	0.274	0.287	0.248	0.352
Fe3+/FeT	0.432	0.436	0.493	0.444	0.294	0.315	0.278	0.491	0.490	0.233	0.390	0.681	0.152	0.186	0.374	0.224

TABLE A7.2. SELECTED COMPOSITIONS OF SECONDARY CLINOPYROXENE FROM MAFIC AND MESOCRATIC INTERMEDIATE SAMPLES

Number	1	2	3	4	5	6	7	8	9	10	11	12	13	14
Rock Type	DIOR	MAFI	GABB	GABB	MZDI	GABB	MZDI	MZDI	DIOR	DIOR	MAFI	ENDO	MZDI	MZDI
Sample	M69	M824	M825-1a	M825-1b	M629	M664	83-77	83-77	M890-4a	M890-4b	M697	83-189	556-5a	556-5b
	Av(4)	Av(5)	Av(1)	Av(2)	Av(2)	Av(3)	Av(2)	Av(2)	Av(3)	Av(3)	Av(5)	Av(4)	Av(2)	Av(3)
SiO2 wt. %	52.32	53.17	51.81	53.27	50.77	52.91	51.76	52.82	50.61	51.97	52.20	53.67	53.23	51.70
Al2O3	0.96	0.42	1.01	0.37	0.81	1.34	0.45	0.64	1.95	0.91	0.44	0.34	0.55	1.40
Fe2O3	2.96	1.31	3.12	0.45	2.55	1.81	3.44	1.90	4.15	2.56	2.31	0.33	0.19	0.73
TiO2	0.15	0.08	0.38	0.04	0.54	0.53	0.22	0.26	0.36	0.15	0.17	0.03	0.09	0.36
Cr2O3	0.0	0.01	0.0	0.0	0.0	0.0	n.d.	n.d.	0.01	0.0	0.0	0.0	n.d.	n.d.
MgO	11.57	12.71	11.20	13.23	9.09	14.07	6.40	8.82	10.21	11.27	12.30	15.10	12.53	11.11
FeO'	8.54	8.86	8.55	7.55	12.00	5.94	16.63	14.00	8.34	8.78	9.13	4.20	9.43	11.00
FeOT	11.19	10.04	11.36	7.95	14.37	7.57	19.73	15.79	12.07	11.01	11.21	4.49	9.60	11.74
MnO	0.01	0.55	0.34	0.35	1.25	0.33	1.53	1.58	0.75	0.00	0.66	0.11	0.61	0.74
CaO	22.68	22.91	21.86	23.90	21.00	22.35	18.31	20.75	22.06	22.72	21.62	25.02	22.59	21.20
Na2O	0.79	0.40	1.14	0.33	0.70	0.81	1.95	0.96	1.14	0.77	0.60	0.20	0.52	0.70
Total	100.76	100.50	99.49	99.56	99.75	100.09	100.69	101.01	99.50	99.06	99.51	98.99	99.74	99.10
Si	1.962	1.987	1.964	1.996	1.950	1.960	2.006	1.986	1.920	1.967	1.977	1.994	2.002	1.974
AlTET	0.030	0.013	0.036	0.004	0.037	0.040	0.0	0.014	0.072	0.033	0.020	0.006	0.0	0.026
AlOCT	0.004	0.006	0.009	0.013	0.000	0.018	0.021	0.015	0.016	0.000	0.000	0.009	0.024	0.037
Fe3	0.083	0.037	0.089	0.013	0.074	0.050	0.100	0.065	0.119	0.073	0.066	0.009	0.006	0.021
Ti	0.004	0.002	0.011	0.001	0.016	0.015	0.006	0.007	0.010	0.004	0.005	0.001	0.003	0.010
Cr	0.000	0.000	0.000	0.000	0.000	0.000	0.000	0.000	0.000	0.000	0.000	0.000	0.000	0.000
Mg	0.647	0.708	0.637	0.739	0.523	0.777	0.378	0.502	0.500	0.636	0.694	0.836	0.702	0.632
Fe2	0.268	0.277	0.271	0.237	0.398	0.184	0.539	0.450	0.266	0.275	0.289	0.130	0.296	0.354
Mn	0.026	0.017	0.011	0.011	0.041	0.010	0.050	0.051	0.024	0.026	0.021	0.003	0.019	0.024
Ca	0.911	0.917	0.888	0.963	0.904	0.887	0.760	0.849	0.901	0.921	0.877	0.996	0.910	0.870
Na	0.057	0.035	0.004	0.024	0.050	0.058	0.147	0.071	0.004	0.057	0.050	0.014	0.038	0.052
Mg/(Mg+FeT)	0.648	0.693	0.639	0.749	0.538	0.769	0.367	0.499	0.601	0.646	0.662	0.857	0.700	0.628
% Others	9.1	4.5	10.9	2.7	8.5	8.3	14.7	7.7	14.5	8.5	6.8	1.9	3.8	6.8
Fe3+/FeT	0.236	0.118	0.247	0.052	0.159	0.214	0.156	0.109	0.309	0.218	0.186	0.65	0.017	0.056

1: sodian salite, 2: salite, 3: sodian salite (pale green zone), 4: salite (colorless zone of the same grain as 3), 5: sodian salite, 6: sodian salite (apparent inclusion in titansalite; Fig. 2.9.2), 7: sodian ferroaugite (bright green zone), 8: sodian ferroaugite (pale green zone) 9: sodian salite (pale green zone), 10: sodian salite (colorless zone of the same grain as 9), 11: sodian salite (at chilled margin with white granodiorite), 12: diopside , 13: salite (colorless zone), 14: sodian salite (green zone of the same grain as 13).

TABLE A7.3. SELECTED COMPOSITIONS OF CLINOPYROXENE FROM QUARTZ-POOR FELSIC SAMPLES

Number	1	2	3	4	5	6	7	8	9	10	11	12	13	14
Rock Type	SYEN	SYEN	PSYN	PSYN	PSYN	PSYN	PSYN	PSYN	MONZ	ALKS	ALKS	PSYN	PSYN	PQMZ
Sample	MB8-4	MB8-1	MG10-2a	MG10-2b	MG10-2c	MG10-2b	MG10-2a	83-16	MG20	84-23	84-23	MG48-3	MG48-2	MG52-1
	Av(3)	Av(2)	Av(1)	Av(1)	Av(1)	Av(1)	Av(1)	Av(4)	Av(4)	Av(2)	Av(2)	Av(3)	Av(1)	Av(2)
SiO2 wt. %	51.22	52.05	51.27	50.58	50.68	51.06	50.82	52.17	52.36	53.41	52.84	51.67	50.46	52.62
Al2O3	0.38	1.24	1.47	2.36	2.52	2.33	1.81	0.85	0.43	0.29	0.29	1.16	1.09	0.49
Fe2O3	4.17	0.8	3.13	3.81	2.61	3.21	4.13	0.77	1.00	0.48	7.06	2.17	2.62	0.8
TiO2	0.20	0.58	0.37	0.67	0.68	0.62	0.49	0.32	0.18	0.05	0.12	0.51	0.33	0.24
Cr2O3	0.0	0.0	0.0	0.01	0.03	0.00	0.00	0.0	0.03	n.d.	n.d.	0.0	0.01	n.d.
MgO	0.18	12.18	11.95	14.73	13.76	14.83	14.87	12.90	11.48	11.75	7.62	12.58	9.83	10.11
FeO,	13.42	10.91	8.49	5.24	7.09	5.81	5.92	9.44	10.77	12.33	11.65	9.36	12.59	14.47
FeOT	17.17	10.91	11.31	8.67	9.44	8.78	9.63	10.13	11.75	12.69	18.00	11.32	14.95	14.47
MnO	1.39	0.88	0.78	0.54	0.61	0.44	0.71	0.95	1.32	0.78	1.19	0.95	1.48	1.18
CaO	19.28	20.74	21.41	20.35	20.12	20.19	20.38	20.79	21.60	20.61	16.79	20.60	19.93	21.87
Na2O	1.60	0.72	0.88	0.62	0.67	0.66	0.73	0.57	0.56	0.76	3.31	0.78	0.77	0.52
Total	99.60	100.82	99.59	98.83	98.69	99.15	99.85	98.76	99.66	100.38	100.87	99.63	99.83	100.78
Si	1.987	1.988	1.941	1.897	1.912	1.918	1.914	1.982	1.992	2.014	2.011	1.954	1.956	2.002
AlTET	0.013	0.012	0.059	0.103	0.088	0.090	0.088	0.018	0.008	0.000	0.000	0.046	0.044	0.000
AlOCT	0.000	0.043	0.007	0.002	0.024	0.013	0.000	0.020	0.011	0.013	0.013	0.006	0.006	0.022
Fe3	0.122	0.000	0.089	0.108	0.074	0.090	0.117	0.022	0.031	0.011	0.202	0.062	0.076	0.000
Ti	0.006	0.016	0.011	0.019	0.019	0.017	0.014	0.009	0.003	0.001	0.003	0.015	0.010	0.007
Cr	0.000	0.000	0.000	0.000	0.001	0.000	0.000	0.0	0.001	0.000	0.000	0.000	0.000	0.000
Mg	0.473	0.683	0.674	0.825	0.775	0.827	0.798	0.730	0.647	0.660	0.432	0.705	0.568	0.573
Fe2	0.436	0.343	0.269	0.165	0.224	0.182	0.186	0.308	0.343	0.389	0.371	0.296	0.408	0.460
Mn	0.046	0.025	0.022	0.017	0.020	0.014	0.023	0.031	0.043	0.022	0.038	0.030	0.046	0.038
Ca	0.798	0.836	0.869	0.819	0.814	0.809	0.822	0.846	0.881	0.833	0.685	0.835	0.828	0.859
Na	0.120	0.053	0.059	0.045	0.049	0.048	0.053	0.042	0.041	0.056	0.244	0.051	0.058	0.038
Mg/(Mg+FeT)	0.489	0.666	0.653	0.752	0.722	0.753	0.723	0.694	0.633	0.623	0.438	0.663	0.548	0.555
% Others	12.0	5.9	10.8	12.9	11.8	12.0	13.1	5.1	4.6	5.6	24.4	8.3	9.2	3.8
Fe3+/FeT	0.219	0.000	0.261	0.396	0.248	0.331	0.386	0.068	0.083	0.028	0.353	0.173	0.157	0.000

1: sodian ferroaugite, 2: sodian augite (recrystallized xenocryst at the core of a compound xenocryst dominated by plagioclase) 3: sodian salite (core of oscillatory zoned grain; Fig. 3.1.3), 4-7: augite (sucessive zones from core to rim of the same grain as 3), 8: augite (partially recrystallized xenocryst?), 9: salite, 10: sodian augite (colorless core), 11: aegirine-augite (green rim of the same grain as 10) 12: sodian augite (attached to a mantled plagioclase xenocryst), 13: sodian augite (partially recrystallized), 14: augite (recrystallized grain)

TABLE A7.4. SELECTED COMPOSITIONS OF CLINOPYROXENE FROM SAMPLES OF NEPHELINE SYENITE

Number	1	2	3	4	5	6	7	8	9	10	11	12	13	14
Rock Type	MIRS	PTIN	PTIN	PTIN	PTIN	PTIN	PTIN	PTIN	PTIN	PTIN	ITIN	ITIN	ITIN	MINC
Sample	MG16	MG37-1a	MG37-1b	MG37	MG39	MG39-3a	MG39-3b	MG39-1a	MG39-1b	MG39	MG94-2a	MG94-2b	MG94-1	MG98
	Av(10)	Av(4)	Av(1)	Av(1)	Av(1)	Av(1)	Av(1)	Av(1)	Av(1)	Av(1)	Av(2)	Av(1)	Av(1)	Av(1)
SiO2 wt. %	51.00	52.72	52.39	53.31	52.17	52.41	52.88	52.34	52.80	52.69	50.31	50.98	50.96	53.41
Al2O3	1.54	1.36	1.12	2.28	1.22	1.32	1.02	1.14	1.04	1.49	1.29	1.18	1.18	0.89
Fe2O3	11.54	26.47	21.25	21.00	22.34	25.59	23.87	28.72	25.83	25.00	14.42	17.21	18.75	25.70
TiO2	0.40	1.70	3.54	1.07	3.44	0.64	1.54	0.63	1.49	0.16	0.42	0.43	0.50	1.16
MgO	6.60	0.27	0.37	2.33	0.29	0.41	0.44	0.51	0.38	1.58	2.43	1.61	1.33	0.51
FeO	6.39	2.75	5.52	2.96	4.06	4.43	4.95	1.21	3.57	1.97	9.18	7.29	7.12	3.62
FeOT	16.77	26.57	24.64	21.86	24.16	27.46	26.71	27.85	26.82	24.47	22.16	22.78	23.99	26.75
MnO	1.60	0.39	0.57	1.74	0.65	0.55	0.80	0.53	0.61	2.64	2.34	2.02	2.06	0.58
ZrO2	0.29	0.02	1.03	0.12	n.d.	0.14	n.d.	0.20	0.00	0.16	0.70	n.d.	n.d.	n.d.
CaO	16.64	1.58	0.98	4.00	2.54	2.77	3.13	2.58	2.77	5.21	12.19	10.92	9.78	3.31
Na2O	4.44	12.71	12.70	10.73	12.29	11.66	11.66	12.36	12.10	10.59	6.36	7.58	8.04	11.90
Total	100.60	99.97	100.27	100.34	99.00	99.91	99.49	100.22	100.60	101.49	99.63	99.22	99.72	101.16
Si	1.945	2.010	2.004	2.011	2.000	2.013	2.033	1.997	2.009	1.992	1.973	1.994	1.987	2.021
AlTET	0.055	0.000	0.000	0.000	0.000	0.000	0.000	0.003	0.000	0.008	0.027	0.006	0.013	0.000
AlOCT	0.014	0.061	0.050	0.101	0.055	0.060	0.046	0.049	0.047	0.058	0.033	0.049	0.041	0.040
Fe3	0.331	0.760	0.612	0.596	0.647	0.740	0.668	0.825	0.740	0.711	0.426	0.507	0.550	0.732
Ti	0.014	0.049	0.102	0.030	0.100	0.018	0.045	0.018	0.043	0.005	0.012	0.013	0.015	0.033
Mg	0.375	0.015	0.021	0.131	0.017	0.023	0.025	0.029	0.022	0.089	0.142	0.094	0.077	0.029
Fe2	0.203	0.000	0.176	0.093	0.131	0.142	0.169	0.039	0.114	0.062	0.301	0.239	0.232	0.115
Mn	0.052	0.013	0.018	0.056	0.021	0.018	0.026	0.017	0.020	0.085	0.078	0.067	0.068	0.019
Zr	0.005	0.000	0.034	0.002	0.000	0.003	0.000	0.004	0.001	0.003	0.013	0.000	0.000	0.000
Ca	0.679	0.065	0.040	0.194	0.105	0.114	0.129	0.105	0.113	0.211	0.512	0.458	0.409	0.134
Na	0.328	0.940	0.942	0.785	0.917	0.860	0.869	0.915	0.893	0.776	0.485	0.575	0.608	0.879
Mg/(Mg+FeT)	0.413	0.017	0.026	0.160	0.021	0.025	0.029	0.032	0.025	0.103	0.163	0.112	0.090	0.033
Mg/(Mg+Fe2+)	0.648	0.149	0.107	0.584	0.113	0.142	0.137	0.429	0.159	0.588	0.320	0.282	0.250	0.201
Fe3+/FeT	0.628	0.896	0.777	0.865	0.832	0.839	0.888	0.955	0.867	0.920	0.586	0.688	0.703	0.864

*: average of 4 analyses.
1: aegirine-augite, 2: aegirine (core), 3: titanian aegirine (rim of the same grain as 2), 4: aegirine (late-stage pale brown rim), 5: Ti-rich aegirine, 6: aegirine (core of phenocryst), 7: aegirine (rim of the same phenocryst as 6), 8: aegirine (core of groundmass grain), 9: aegirine (rim of the same grain as 8), 10: aegirine-augite (recrystallized grain), 11: aegirine-augite (lighter zone), 12: aegirine-augite (darker zone of the same grain as 11), 13: aegirine-augite, 14: aegirine.

APPENDIX VIII. SELECTED COMPOSITIONS OF AMPHIBOLE

*: Fe_2O_3 calculated by the method of Laird and Albee (1981) using a computer program written by Dr. A. Hynes. For other compositions Fe_2O_3 was obtained or estimated from wet chemical data (Table 2.1). Formula in each case is based on 23 oxygen atoms.

Nomenclature after Leake (1978).

Rock types defined in Appendix III. Av(n): average of n analyses. T: total iron, expressed as Fe or as FeO. Ch. Excess: $2Ti + {}^{vi}Al + {}^{vi}Fe^{3+}$ (from wet chemistry) + NaA + K - ${}^{iv}(Al + Fe^{3+})$. See Appendix I for analytical methods and conditions.

TABLE A8.1. SELECTED COMPOSITIONS OF KAERSUTITE

Number	1	2	3	4
Rock Type	PSYN	MAFI	MDYK	GABB
Sample	MG10-5 Av(2)	MG24 Av(2)	MG61 Av(4)	MG64 Av(6)
SiO2 wt. %	41.74	41.98	39.91	41.59
Al2O3	10.90	10.02	12.66	11.99
TiO2	5.70	4.41	6.83	5.04
FeOT	15.19	17.47	12.53	11.58
FeO	14.16*	15.21*	11.89*	10.06*
Fe2O3	1.14	2.52	0.71	1.69
MnO	0.50	0.49	0.25	0.22
MgO	10.23	9.73	11.58	13.21
CaO	10.26	10.90	10.79	11.24
Na2O	2.68	2.22	2.84	2.82
K2O	1.01	1.04	0.85	1.03
F	0.33	0.06	0.10	0.16
Cl	0.07	0.07	0.01	0.04
Total	98.46	98.35	98.31	98.84
O=F,Cl	0.15	0.04	0.04	0.08
Si	6.219	6.299	5.901	6.070
AlZ	1.781	1.701	2.099	1.930
Fe3Z	0.0	0.0	0.0	0.0
AlY	0.133	0.071	0.108	0.133
Ti	0.639	0.498	0.759	0.553
Fe2	1.765	1.908	1.471	1.227
Fe3Y	0.128	0.284	0.079	0.186
Mn	0.063	0.062	0.031	0.027
Mg	2.272	2.176	2.552	2.874
XOct	0.0	0.0	0.0	0.0
Ca	1.638	1.752	1.709	1.758
NaM4	0.362	0.248	0.291	0.242
NaA	0.412	0.398	0.524	0.556
K	0.192	0.199	0.160	0.192
F	0.156	0.028	0.047	0.074
Cl	0.018	0.018	0.003	0.010
NaA+K	0.604	0.597	0.684	0.747
Mg/(Mg+Fe2+)	0.563	0.533	0.634	0.701
FeT/(FeT+Mg)	0.454	0.502	0.378	0.330
Fe3+/FeT	0.068	0.130	0.051	0.132

1:part of a compound xenocryst dominated by plagioclase (Fig. 3.1.5), 3: present in the groundmass of an alkali basaltic dyke.

1:magnesio-hornblende (groundmass), 2: magnesio-hornblende (oscillatory-zoned grain inside an amygdule), 3: actinolitic hornblende (same grain as 2), 4: actinolitic hornblende, 5: magnesio-hornblende, 6: magnesio-hornblende, 7: actinolitic hornblende (groundmass), 8: magnesio-hornblende (oscillatory-zoned grain inside an amygdule), 9: magnesio-hornblende (same grain as 8), 10: magnesian hastingsite (groundmass), 11: edenitic hornblende (groundmass), 12: magnesio-hornblende (groundmass), 13: actinolitic hornblende (groundmass), 14: magnesio-hornblende.

TABLE A8.2. SELECTED COMPOSITIONS OF GREEN AMPHIBOLE FROM MAFIC AND MESOCRATIC INTERMEDIATE SAMPLES

Number	1	2	3	4	5	6	7	8	9	10	11	12	13	14
Rock Type	MAFI	MAFI	MAFI	MZDI	MAFI	MZDI	MAFI	MAFI	MAFI	MAFI	MAFI	MAFI	MAFI	MZDI
Sample	M86-3	M86-4	M86-4	M823	M826	M853	M868-3	M868-4a	M868-4b	M897	M897	M897	M897	84-856
	Av(4)	Av(1)	Av(1)	Av(7)	Av(9)	Av(8)	Av(3)	Av(1)	Av(1)	Av(1)	Av(1)	Av(1)	Av(1)	Av(6)
SiO2 wt. %	49.76	47.20	50.25	49.97	49.63	48.29	50.87	47.96	50.87	41.68	45.42	49.50	51.64	49.17
Al2O3	5.25	7.81	4.73	4.51	4.64	5.33	4.65	6.44	5.00	11.62	8.73	6.81	4.19	5.36
TiO2	1.00	1.00	0.95	1.04	1.16	1.22	1.12	1.01	0.97	2.10	1.61	0.37	0.36	1.06
FeOT	14.71	15.76	14.54	16.29	17.24	17.05	14.59	14.32	15.16	10.34	15.62	14.93	13.10	14.09
FeO	11.65	12.43	11.40	12.07	13.64	14.07	11.63	11.35	12.01	14.47	12.30	11.70	10.39	11.74
Fe2O3	3.4	3.7	3.4	3.8	4.0	4.2	3.4	3.3	3.5	4.3	3.6	3.5	3.1	3.5
MnO	0.36	0.37	0.29	0.34	0.50	0.53	0.45	0.23	0.44	0.32	0.31	0.37	0.37	0.40
MgO	13.66	12.70	14.09	12.91	12.52	11.70	13.90	14.42	13.92	9.90	11.66	13.26	14.72	13.35
CaO	11.47	11.03	11.40	10.02	11.04	11.06	11.25	10.70	11.20	11.33	11.01	11.96	12.20	11.39
Na2O	0.00	1.69	1.01	1.32	1.16	1.30	0.92	1.73	1.16	2.20	1.07	1.4	0.06	1.26
K2O	0.50	0.71	0.49	0.47	0.47	0.50	0.44	0.66	0.54	1.01	0.00	0.44	0.20	0.56
F	0.11	0.05	0.05	0.21	0.16	0.45	0.12	0.05	0.0	0.35	0.40	0.0	0.0	0.29
Cl	0.15	0.22	0.10	0.17	0.15	0.24	0.13	0.20	0.21	0.00	0.13	0.09	0.03	0.11
Total	98.19	98.92	98.26	98.50	98.97	98.73	97.90	98.76	98.97	99.44	98.52	99.46	98.05	98.00
O=F,Cl	0.00	0.07	0.06	0.13	0.10	0.24	0.00	0.07	0.05	0.17	0.20	0.02	0.01	0.15
Si	7.237	6.909	7.293	7.302	7.249	7.133	7.290	6.959	7.242	6.214	6.700	7.119	7.457	7.193
Al2	0.763	1.091	0.707	0.698	0.751	0.867	0.710	1.041	0.758	1.786	1.292	0.881	0.543	0.807
Fe32	0.0	0.0	0.0	0.0	0.0	0.0	0.0	0.0	0.0	0.0	0.0	0.0	0.0	0.0
Al1	0.137	0.117	0.102	0.070	0.048	0.061	0.000	0.000	0.094	0.256	0.220	0.273	0.140	0.115
Ti	0.110	0.100	0.104	0.114	0.127	0.136	0.123	0.107	0.106	0.244	0.179	0.040	0.039	0.117
Fe2	1.417	1.519	1.393	1.573	1.666	1.730	1.404	1.377	1.403	1.004	1.529	1.417	1.201	1.436
Fe3+	0.372	0.407	0.371	0.410	0.440	0.467	0.373	0.360	0.301	0.402	0.400	0.379	0.336	0.305
Mn	0.044	0.046	0.036	0.047	0.062	0.066	0.055	0.020	0.054	0.040	0.039	0.045	0.045	0.050
Mg	2.961	2.766	3.040	2.012	2.726	2.576	3.054	3.119	3.001	2.210	2.567	2.042	3.160	2.911
Mgct	0.061	0.053	0.004	0.062	0.069	0.045	0.076	0.142	0.000	0.045	-0.069	-0.004	-0.020	0.020
Ca	1.707	1.727	1.773	1.694	1.720	1.750	1.755	1.676	1.736	1.010	1.069	1.043	1.003	1.705
Na(A)	0.162	0.220	0.174	0.244	0.204	0.206	0.169	0.102	0.176	0.146	0.131	0.157	0.117	0.194
Na(M	0.006	0.269	0.110	0.130	0.125	0.166	0.091	0.304	0.149	0.513	0.404	0.253	0.123	0.163
K	0.093	0.132	0.091	0.000	0.000	0.109	0.002	0.104	0.100	0.192	0.151	0.001	0.057	0.105
F	0.051	0.023	0.023	0.097	0.074	0.210	0.055	0.023	0.0	0.165	0.107	0.0	0.0	0.134
Cl	0.037	0.054	0.044	0.042	0.037	0.060	0.032	0.049	0.051	0.020	0.033	0.022	0.007	0.027
Na+K	0.179	0.391	0.281	0.218	0.212	0.275	0.173	0.400	0.249	0.705	0.555	0.314	0.159	0.267
Mg/(Fe2+Mg)	0.676	0.646	0.686	0.641	0.621	0.597	0.684	0.694	0.674	0.551	0.627	0.667	0.716	0.670
FeT/(FeT+Mg)	0.327	0.410	0.367	0.415	0.436	0.461	0.369	0.350	0.379	0.500	0.429	0.387	0.334	0.385
Fe3+/FeT	0.208	0.211	0.210	0.210	0.209	0.212	0.210	0.207	0.208	0.211	0.207	0.211	0.212	0.212
Ch. Excess	-	-	-	-	-	0.200	-	-	-	-	-	-	-	-

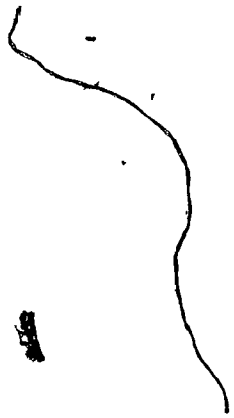

1: actinolite, 2: ferro-actinolitic hornblende, 3: winchite, 4: actinolite, 5: magnesio-hornblende, 6: ferro-hornblende, 7: ferro-edenite (core of zoned grains), 8: ferroedenite (rim of the same grains as 7), 9: magnesio-hornblende, 10: actinolitic hornblende, 11: magnesio-hornblende (core of weakly zoned grain), 12: magnesio-hornblende (rim of same grain as 11).

TABLE A8.3. SELECTED COMPOSITIONS OF AMPHIBOLE FROM QUARTZ-POOR FELSIC SAMPLES

Number	1	2	3	4	5	6	7	8	9	10	11	12
Rock Type	SYEN	PSYN	ALKS	ALKS	AFSY	PSYN	QTM2	QTM2	PQM2	QTM2	QTM2	QTM2
Sample	M88	M818	84-23	84-23	83-31	M640	M644-1c	M644-1r	M652	M665	M666-1c	M666-1r
	Av(5)	Av(7)	Av(3)	Av(2)	Av(11)	Av(6)	Av(3)	Av(4)	Av(7)	Av(7)	Av(3)	Av(2)
SiO2 wt. %	50.00	49.55	52.45	52.49	47.86	46.78	46.27	44.77	48.00	50.14	48.47	48.12
Al2O3	2.85	3.46	1.65	2.55	4.66	5.15	6.28	6.95	5.10	4.69	5.20	5.22
TiO2	1.14	1.35	1.19	0.86	0.99	1.40	1.58	1.91	1.21	0.91	1.13	0.99
FeOT	18.42	22.34	18.75	15.80	20.92	24.15	20.42	23.82	19.93	15.21	18.39	18.93
FeO	14.82	18.29	11.13*	11.66*	17.14	20.19	18.71	21.15	15.70	11.00	14.45	14.80
Fe2O3	4.0	4.5	8.47	4.61	4.2	4.4	1.9	2.1	4.7	3.7	4.4	4.5
MnO	1.00	1.41	0.90	0.61	1.21	1.21	0.60	0.60	0.90	0.63	0.59	0.59
MgO	11.06	9.04	11.00	13.50	9.91	7.69	9.35	7.79	10.50	13.05	11.06	10.37
CaO	0.69	0.76	7.02	9.49	9.81	9.45	9.96	10.07	10.50	10.99	10.39	10.42
Na2O	2.21	1.55	3.31	2.55	1.99	2.16	2.42	2.59	1.67	1.60	1.84	1.80
K2O	0.70	0.54	0.85	0.47	0.69	0.71	0.76	0.90	0.64	0.54	0.54	0.62
F	1.25	0.57	0.94	0.77	0.99	0.83	1.11	1.10	0.70	0.82	1.05	0.77
Cl	0.06	0.10	0.05	0.06	0.17	0.19	0.20	0.31	0.21	0.09	0.16	0.10
Total	90.90	99.32	90.55	90.87	90.37	99.75	90.69	99.75	99.75	90.60	90.77	90.11
O=F,Cl	0.54	0.10	0.40	0.34	0.46	0.39	0.55	0.55	0.34	0.37	0.47	0.35
Si	7.507	7.575	7.627	7.574	7.140	7.091	7.015	6.850	7.119	7.312	7.107	7.195
AlZ	0.492	0.607	0.205	0.426	0.855	0.909	0.907	1.170	0.001	0.600	0.015	0.005
Fe3+	0.001	0.020	0.090	0.0	0.027	0.0	0.0	0.0	0.0	0.0	0.0	0.0
AlY	0.0	0.0	0.0	0.005	0.0	0.000	0.154	0.076	0.009	0.119	0.096	0.110
Ti	0.126	0.151	0.130	0.095	0.115	0.160	0.100	0.219	0.135	0.100	0.126	0.111
Fe2+	1.029	2.276	1.305	1.407	2.175	2.560	2.571	2.696	1.944	1.449	1.790	1.061
FeSY	0.444	0.404	0.057	0.500	0.455	0.502	0.217	0.241	0.524	0.406	0.491	0.506
Mn	0.135	0.170	0.121	0.075	0.155	0.155	0.077	0.000	0.115	0.070	0.074	0.075
Mg	2.600	2.102	2.550	2.921	2.241	1.730	2.112	1.771	2.535	2.057	2.444	2.311
NOct	0.142	0.271	0.0	0.0	0.157	0.122	0.092	0.091	0.060	-0.012	0.021	-0.021
Ca	1.574	1.597	1.094	1.467	1.595	1.552	1.617	1.646	1.679	1.717	1.651	1.669
NaM4	0.404	0.552	0.905	0.555	0.269	0.546	0.291	0.265	0.261	0.205	0.529	0.551
NaA	0.140	0.109	0.020	0.101	0.517	0.209	0.420	0.505	0.210	0.170	0.200	0.214
K	0.152	0.065	0.154	0.007	0.154	0.157	0.147	0.175	0.121	0.100	0.102	0.110
F	0.505	0.174	0.432	0.351	0.475	0.390	0.532	0.531	0.320	0.570	0.405	0.364
Cl	0.015	0.025	0.007	0.015	0.044	0.049	0.072	0.000	0.055	0.022	0.040	0.025
NaA+K	0.200	0.174	0.102	0.267	0.450	0.426	0.567	0.670	0.339	0.270	0.305	0.333
Mg/(Mg+Fe2+)	0.500	0.409	0.654	0.675	0.507	0.404	0.471	0.397	0.546	0.662	0.577	0.554
FeT/(FeT+Mg)	0.466	0.560	0.471	0.395	0.542	0.630	0.551	0.624	0.514	0.395	0.405	0.506
Fe3+/FeT	0.196	0.194	0.467	0.262	0.197	0.164	0.004	0.002	0.212	0.219	0.215	0.214
Ch. Excess	0.405	-	-	-	-	0.347	0.291	0.265	-	0.307	0.320	0.370

1: magnesio-hornblende (interstitial grain), 2: edenitic hornblende (brown core of a zoned phenocryst), 3: magnesio-hornblende (intermediate zone of same grain as 2), 4: magnesio-hornblende (rim of same grain as 2), 5: magnesio-hornblende, 6: magnesio-hornblende, 7: ferro-hornblende, 8: ferro-hornblende, 9: ferro-edenite, 10: ferro-hornblende, 11: magnesio-hornblende (core of compositionally zoned grain), 12: actinolite (rim of the same grain as 11).

TABLE A7.4. SELECTED COMPOSITIONS OF AMPHIBOLE FROM SAMPLES OF GRANITE

Number	1	2	3	4	5	6	7	8	9	10	11	12
Rock Type	GP	GP	GP	GP	PDGR	GP	KFDG	KFDG	KFDG	KFPG	WTGD	WTGD
Sample	MG42-1 Av(5)	MG42-3c Av(3)	MG42-3i Av(3)	MG42-3r Av(2)	MG46 Av(9)	MG51 Av(7)	83-55 Av(8)	MG57 Av(7)	MG57-2 Av(2)	MG83 Av(6)	MG97-4c Av(1)	MG97-4r Av(2)
SiO2 wt. %	47.74	46.29	48.38	47.25	47.11	46.69	46.42	46.48	45.68	46.68	48.94	52.88
Al2O3	5.85	9.29	6.29	6.19	6.28	6.41	5.74	5.98	6.24	6.19	4.86	3.28
TiO2	1.08	1.72	1.19	1.41	1.33	1.43	1.15	1.09	1.32	1.08	0.91	0.69
FeOT	19.58	11.98	16.21	18.48	17.93	19.84	21.78	22.88	23.14	21.81	15.61	14.61
FeO	15.36	9.46	12.79	14.53	14.06	15.78	17.81	17.22	18.81	17.84	12.19	11.37
Fe2O3	4.6	2.8	3.8	4.3	4.3	4.6	5.3	5.4	5.7	5.3	3.8	3.6
MnO	0.78	0.26	0.69	0.75	0.63	0.87	0.98	1.19	0.94	1.04	0.64	0.62
MgO	10.38	14.35	12.86	10.85	11.52	10.14	8.95	8.37	7.95	8.51	13.39	14.55
CaO	10.86	11.52	10.83	11.81	10.59	10.89	10.25	10.68	10.94	10.52	10.73	10.87
Na2O	1.52	2.64	2.08	1.64	1.83	1.86	1.93	2.10	1.89	2.05	1.54	1.06
K2O	0.67	0.34	0.54	0.72	0.65	0.77	0.76	0.91	1.09	0.88	0.57	0.33
F	0.75	0.94	0.72	0.93	0.67	0.79	0.79	1.63	1.92	1.13	0.48	0.13
Cl	0.19	0.09	0.15	0.22	0.20	0.23	0.21	0.26	0.32	0.18	0.09	0.08
Total	98.96	99.08	99.68	99.04	98.76	100.08	99.11	100.33	101.12	100.08	97.87	98.51
O=F,Cl	0.36	0.42	0.34	0.44	0.33	0.38	0.38	0.75	0.88	0.52	0.19	0.07
Si	7.118	6.689	7.049	7.028	6.989	6.928	7.004	6.983	6.877	6.995	7.287	7.589
AlZ	0.898	1.311	0.951	0.988	1.011	1.072	0.996	1.017	1.107	1.005	0.793	0.491
FeSZ	0.0	0.0	0.0	0.0	0.0	0.0	0.0	0.0	0.015	0.0	0.0	0.0
AlY	0.004	0.271	0.138	0.105	0.073	0.049	0.025	0.038	0.0	0.000	0.051	0.053
Ti	0.112	0.187	0.138	0.108	0.148	0.168	0.138	0.123	0.149	0.122	0.101	0.075
Fe2	1.913	1.143	1.559	1.886	1.745	1.948	2.147	2.167	2.268	2.135	1.581	1.371
FeSY	0.516	0.384	0.417	0.481	0.488	0.514	0.682	0.612	0.638	0.598	0.421	0.391
Mn	0.088	0.032	0.085	0.094	0.079	0.109	0.125	0.152	0.128	0.132	0.088	0.076
Mg	2.384	3.091	2.728	2.357	2.547	2.245	2.013	1.878	1.784	1.901	2.939	3.127
XOct	0.817	0.828	0.848	0.819	0.875	0.825	0.842	0.839	0.849	0.825	0.893	0.892
Ca	1.735	1.782	1.691	1.765	1.685	1.731	1.657	1.709	1.765	1.689	1.695	1.679
NaM4	0.288	0.228	0.261	0.247	0.244	0.246	0.301	0.291	0.235	0.311	0.214	0.229
NaA	0.189	0.528	0.384	0.226	0.282	0.298	0.265	0.322	0.316	0.284	0.226	0.067
K	0.127	0.065	0.188	0.137	0.123	0.146	0.146	0.175	0.209	0.153	0.187	0.061
F	0.383	0.438	0.332	0.437	0.314	0.371	0.377	0.776	0.914	0.536	0.186	0.059
Cl	0.048	0.022	0.037	0.055	0.050	0.050	0.054	0.066	0.082	0.046	0.022	0.020
NaM4+K	0.316	0.582	0.484	0.363	0.485	0.435	0.410	0.497	0.526	0.437	0.333	0.128
Mg/(Mg+Fe2+)	0.546	0.730	0.636	0.564	0.594	0.535	0.484	0.464	0.440	0.471	0.662	0.695
FeT/(FeT+Mg)	0.513	0.319	0.428	0.496	0.466	0.523	0.577	0.597	0.628	0.598	0.395	0.368
Fe3+/FeT	0.212	0.218	0.211	0.218	0.216	0.209	0.219	0.228	0.252	0.219	0.219	0.222
Ch. Excess	-	-	-	-	0.245	0.247	-	-	-	0.362	-	-

TABLE A8.5. SELECTED COMPOSITION OF AMPHIBOLE FROM A PERALKALINE TINGUAITE

Number	1	2
Rock Type	PTIN	PTIN
Sample	MG37-I Av(6)	MG37-P Av(5)
SiO2	50.57	50.96
Al2O3	1.29	0.96
TiO2	0.98	0.91
FeOT	29.57	27.97
FeO	28.7*	25.8*
Fe2O3	1.0	2.4
MnO	3.14	2.66
MgO	1.24	2.12
CaO	1.48	0.82
Na2O	7.84	7.71
K2O	2.48	3.20
F	0.89	1.06
Cl	0.02	0.01
Total	99.15	97.92
O=F,Cl	0.38	0.45
Si	8.011	8.121
AlZ	0.0	0.0
Fe3Z	0.0	0.0
AlY	0.241	0.180
Ti	0.117	0.109
Fe2	3.803	3.438
Fe3Y	0.114	0.289
Mn	0.421	0.359
Mg	0.293	0.504
XOct	0.0	0.0
Ca	0.251	0.140
NaM4	1.749	1.860
NaA	0.659	0.522
K	0.501	0.650
F	0.446	0.534
Cl	0.005	0.003
NaA+K	1.160	1.173
Mg/(Mg+Fe2+)	0.071	0.128
Fe/(Fe+Mg)	0.930	0.881
Fe3+/FeT	0.029	0.076

1: manganoan potassium arfvedsonite (interstitial grains), 2) manganoan potassium arfvedsonite (phenocrysts).

APPENDIX IX. SELECTED COMPOSITIONS OF BIOTITE

*: all Fe treated as FeO. For other compositions Fe_2O_3 was obtained or estimated from wet chemical data (Table 2.1). In both cases the formula is based on 11 oxygen atoms.

Nomenclature after Deer et al. (1975) and Rock (1982).

Rock types defined in Appendix III. Av(n): average of n analyses. T: total iron, expressed as Fe or as FeO. See Appendix I for analytical methods and conditions.

TABLE A9.1. SELECTED COMPOSITIONS OF BIOTITE FROM MAFIC AND MESOCRATIC INTERMEDIATE SAMPLES

Number	1	2	3	4	5	6	7	8	9	10	11	12
Rock Type	MAFI	MZDI	MAFI	MAFI	MZDI	MZDI	GABB	MAFI	MZDI	DIOR	MAFI	MZDI
Sample	M66	M823	M624	M626	M629	M663	M664	M668	83-77	M698	M697	84-556
	Av(6)	Av(8)	Av(1)	Av(4)	Av(5)	Av(6)	Av(6)	Av(2)	Av(3)	Av(6)	Av(4)	Av(5)
SiO2 wt. %	37.49	37.81	37.82	37.24	36.28	37.11	37.98	37.34	37.06	35.94	37.66	37.25
Al2O3	13.90	13.89	12.98	13.44	12.52	12.90	14.65	14.29	12.29	13.73	14.06	13.57
TiO2	4.26	4.18	5.27	3.45	4.27	4.07	3.85	3.63	4.38	4.25	3.15	4.10
FeOT	19.44	20.46	18.98	21.24	24.25	21.05	16.82	19.37	23.91	22.35	17.42	19.84
FeO	16.92	17.84	16.46	18.46	20.74	18.17	13.86	16.85	20.40	19.11	15.08	16.52
Fe2O3	2.8	2.9	2.8	3.1	3.9	3.2	2.4	2.8	3.9	3.6	2.6	2.8
MnO	0.16	0.25	0.18	0.14	0.49	0.22	0.14	0.15	0.52	0.49	0.16	0.25
MgO	11.75	11.19	12.33	10.92	8.36	10.40	14.81	11.81	8.72	9.58	13.15	11.67
CaO	0.02	0.01	0.03	0.01	0.02	0.01	0.01	0.02	0.01	0.01	0.04	0.01
Na2O	0.13	0.12	0.10	0.11	0.07	0.07	0.79	0.10	0.09	0.06	0.13	0.10
K2O	9.75	9.66	9.36	9.72	10.26	9.77	8.41	9.22	9.60	10.02	9.52	9.43
F	0.12	0.43	0.22	0.41	0.34	0.79	0.05	0.07	0.03	0.17	0.16	0.41
Cl	0.42	0.35	0.22	0.32	0.27	0.48	0.17	0.48	0.31	0.34	0.17	0.28
Total	97.58	96.77	97.63	97.05	97.23	96.75	97.96	96.56	97.69	97.15	95.77	96.15
O=F,Cl	0.15	0.26	0.14	0.24	0.20	0.44	0.06	0.12	0.42	0.15	0.11	0.24
Si	2.800	2.811	2.810	2.824	2.800	2.836	2.780	2.806	2.840	2.758	2.829	2.819
Al2	1.200	1.172	1.137	1.176	1.141	1.162	1.220	1.194	1.110	1.238	1.171	1.181
Fe3Z	0.0	0.017	0.054	0.0	0.058	0.002	0.0	0.0	0.050	0.011	0.0	0.0
AlY	0.023	0.0	0.0	0.026	0.0	0.0	0.044	0.071	0.0	0.0	0.074	0.029
TiY	0.239	0.239	0.294	0.196	0.248	0.234	0.212	0.205	0.252	0.246	0.178	0.233
Fe3Y	0.157	0.149	0.103	0.177	0.169	0.182	0.132	0.158	0.174	0.196	0.147	0.159
Y1	0.420	0.387	0.397	0.398	0.417	0.416	0.388	0.435	0.427	0.448	0.399	0.422
MgY	1.308	1.267	1.365	1.234	0.963	1.185	1.616	1.323	0.996	1.093	1.472	1.316
FeY	1.057	1.133	1.023	1.170	1.342	1.161	0.848	1.059	1.307	1.223	0.947	1.046
MnY	0.010	0.016	0.011	0.009	0.032	0.014	0.009	0.010	0.034	0.032	0.010	0.016
NaY	0.0	0.0	0.0	0.0	0.010	0.0	0.0	0.0	0.0	0.0	0.0	0.0
Y2	2.375	2.416	2.399	2.414	2.347	2.368	2.473	2.391	2.337	2.347	2.438	2.378
K	0.929	0.936	0.887	0.940	1.012	0.952	0.785	0.884	0.938	0.978	0.912	0.910
NaX	0.019	0.010	0.014	0.016	0.0	0.010	0.112	0.015	0.013	0.009	0.019	0.015
CaX	0.002	0.001	0.002	0.001	0.002	0.001	0.001	0.002	0.001	0.001	0.003	0.001
A	0.949	0.964	0.904	0.957	1.014	0.964	0.898	0.900	0.953	0.988	0.934	0.926
F	0.028	0.103	0.052	0.098	0.083	0.191	0.012	0.017	0.201	0.041	0.038	0.098
Cl	0.053	0.045	0.028	0.041	0.035	0.062	0.021	0.051	0.040	0.044	0.022	0.036
FeT/(FeT+Mg)	0.481	0.506	0.463	0.522	0.620	0.532	0.378	0.479	0.606	0.567	0.426	0.478
Fe3+/FeT	0.138	0.128	0.133	0.131	0.145	0.137	0.135	0.139	0.147	0.145	0.134	0.132
Mg/(Mg+Fe2+)	0.553	0.528	0.572	0.513	0.418	0.505	0.656	0.555	0.432	0.472	0.608	0.557

1-2: titaniferous biotite; 3: titanbiotite, 4-8: titaniferous biotite, 9: titanbiotite, 10-12: titaniferous biotite

TABLE A9.2. SELECTED COMPOSITIONS OF BIOTITE FROM QUARTZ-POOR FELSIC SAMPLES

Number	1	2	3	4	5	6	7	8
Rock Type	SYEN	PSYN	ALKS	PSYN	QTZM	PQM2	QTZM	QTZM
Sample	MG8 Av(7)	MG10 Av(4)	WX25* Av(4)	MG48 Av(8)	MG44 Av(7)	MG52 Av(6)	MG63 Av(7)	MG66 Av(6)
SiO2 wt. %	36.45	36.25	38.83	36.92	37.38	36.68	37.80	36.69
Al2O3	13.17	12.26	11.08	11.85	11.93	12.54	13.08	12.67
TiO2	4.15	5.11	4.06	3.64	3.39	4.09	4.02	3.79
FeOT	22.75	25.29	20.10	27.02	24.52	25.26	19.13	23.06
FeO	19.31	21.51	20.10	23.96	20.85	19.21	16.62	18.82
Fe2O3	3.9	4.2	0.0	3.4	4.1	4.5	3.9	4.7
MnO	0.39	0.40	0.39	0.47	0.25	0.34	0.24	0.27
MgO	9.69	7.98	11.87	7.19	8.74	9.62	11.62	9.54
CaO	0.0	0.04	0.0	0.01	0.01	0.02	0.01	0.0
Na2O	0.10	0.04	0.12	0.09	0.07	0.12	0.06	0.10
K2O	10.06	9.42	9.87	9.72	9.79	9.68	10.04	9.75
F	1.04	0.67	1.12	1.64	1.76	1.20	1.20	1.41
Cl	0.21	0.38	0.07	0.33	0.42	0.46	0.33	0.29
Total	97.87	97.87	97.82	98.44	97.85	97.86	97.31	97.37
O=F,Cl	0.49	0.37	0.49	0.77	0.83	0.61	0.61	0.66
Si	2.788	2.789	2.954	2.878	2.884	2.887	2.846	2.817
Al2	1.186	1.113	0.995	1.084	1.086	1.131	1.154	1.146
Fe32	0.855	0.898	0.855	0.846	0.831	0.865	0.0	0.857
AlY	0.0	0.0	0.0	0.0	0.0	0.0	0.0	0.0
TiY	0.257	0.296	0.232	0.213	0.197	0.235	0.228	0.219
Fe3Y	0.186	0.145	0.0	0.152	0.207	0.196	0.221	0.235
YI	0.422	0.441	0.232	0.365	0.404	0.432	0.448	0.455
MgY	1.182	0.916	1.346	0.833	1.086	1.097	1.304	1.092
FeY	1.255	1.386	1.226	1.558	1.344	1.229	0.984	1.208
MnY	0.025	0.026	0.025	0.031	0.016	0.022	0.015	0.018
NaY	0.0	0.0	0.0	0.0	0.0	0.0	0.0	0.0
Y2	2.368	2.327	2.697	2.422	2.366	2.348	2.385	2.317
K	0.979	0.926	0.958	0.964	0.964	0.945	0.964	0.956
NaX	0.015	0.006	0.018	0.014	0.018	0.018	0.009	0.015
CaX	0.0	0.005	0.0	0.001	0.001	0.002	0.001	0.0
X	0.994	0.934	0.976	0.978	0.975	0.964	0.974	0.970
F	0.251	0.165	0.269	0.403	0.427	0.290	0.305	0.342
Cl	0.027	0.050	0.009	0.043	0.055	0.060	0.042	0.038
FeT/(FeT+Mg)	0.568	0.640	0.487	0.678	0.612	0.576	0.488	0.575
Fe3+/FeT	0.158	0.149	0.041	0.115	0.158	0.174	0.183	0.183
Mg/(Mg+Fe2+)	0.472	0.398	0.525	0.348	0.428	0.472	0.578	0.475

1: titaniferous biotite, 2: titanbiotite, 3-8: titaniferous biotite

TABLE A9.3. SELECTED COMPOSITIONS OF BIOTITE FROM SAMPLES OF GRANITE

Number	1	2	3	4	5	6	7	8	9
Rock Type	WTGD	WTGD	GP	PDGR	GP	KFDG	KFDG	WTGD	KFPG
Sample	M63a	M63b	M642	M646	M651	85-88	M667	M668	M683
	Av(8)	Av(3)	Av(6)	Av(5)	Av(7)	Av(7)	Av(5)	Av(6)	Av(8)
SiO2 wt. %	37.56	38.89	37.48	36.46	37.74	37.19	38.67	37.45	37.44
Al2O3	14.57	15.66	12.99	12.87	12.38	11.82	11.71	13.62	12.48
TiO2	2.72	0.96	4.16	4.81	3.66	3.62	3.52	4.58	3.64
FeOT	19.12	17.43	20.38	22.38	22.73	24.14	22.38	19.41	24.28
FeO	16.61	14.28	16.87	18.43	18.86	19.37	17.89	15.98	19.51
Fe2O3	3.9	3.6	3.9	4.3	4.3	5.3	4.9	3.9	5.3
MnO	0.33	0.28	0.37	0.28	0.39	0.38	0.45	0.19	0.48
MgO	12.68	13.77	11.15	10.35	10.58	8.96	10.33	11.64	9.85
CaO	0.07	0.0	0.01	0.02	0.02	0.01	0.01	0.0	0.02
Na2O	0.12	0.07	0.09	0.15	0.09	0.11	0.09	0.12	0.08
K2O	8.98	8.81	9.57	9.84	9.78	9.64	9.84	9.87	9.68
F	0.11	0.21	1.39	1.36	1.52	1.51	3.11	0.24	1.45
Cl	0.41	0.39	0.39	0.39	0.42	0.38	0.44	0.36	0.34
Total	96.09	96.31	97.78	97.72	98.93	97.69	99.55	97.69	98.69
O=F,Cl	0.14	0.18	0.67	0.66	0.75	0.72	1.41	0.18	0.68
Si	2.801	2.886	2.827	2.786	2.847	2.862	2.914	2.795	2.845
Al2	1.199	1.144	1.155	1.159	1.101	1.072	1.048	1.197	1.117
FeSZ	0.0	0.0	0.018	0.056	0.053	0.066	0.046	0.018	0.039
AlY	0.082	0.222	0.0	0.0	0.0	0.0	0.0	0.0	0.0
TiY	0.153	0.065	0.236	0.238	0.208	0.209	0.199	0.257	0.208
FeSY	0.219	0.195	0.283	0.191	0.192	0.241	0.252	0.209	0.264
Y1	0.454	0.478	0.459	0.421	0.399	0.458	0.431	0.466	0.471
MgY	1.486	1.519	1.264	1.178	1.181	1.028	1.168	1.294	1.024
FeY	0.974	0.884	1.064	1.177	1.198	1.247	1.127	0.992	1.259
MnY	0.021	0.016	0.024	0.013	0.025	0.033	0.029	0.012	0.031
NaY	0.0	0.0	0.0	0.0	0.0	0.0	0.0	0.0	0.0
Y2	2.481	2.419	2.342	2.369	2.395	2.387	2.316	2.298	2.295
K	0.864	0.852	0.921	0.969	0.941	0.946	0.946	0.939	0.938
NaX	0.017	0.010	0.013	0.022	0.013	0.016	0.013	0.017	0.012
CaX	0.006	0.0	0.001	0.002	0.002	0.001	0.001	0.0	0.002
X	0.877	0.862	0.936	0.993	0.956	0.964	0.960	0.956	0.943
F	0.026	0.049	0.332	0.329	0.363	0.367	0.741	0.057	0.343
Cl	0.052	0.049	0.050	0.050	0.054	0.050	0.056	0.046	0.044
FeT/(FeT+Mg)	0.489	0.415	0.586	0.547	0.548	0.602	0.548	0.485	0.601
Fe3+/FeT	0.184	0.181	0.172	0.174	0.178	0.198	0.198	0.181	0.196
Mg/(Mg+Fe2+)	0.691	0.632	0.541	0.500	0.498	0.452	0.507	0.566	0.453

1-7: titaniferous biotite, 8: titanbiotite, 9: titaniferous biotite

1: manganiferous titaniferous biotite, 2: manganiferous titaniferous lepidomelane (interstitial grain), 3: manganiferous titaniferous lepidomelane (interstitial grain), 4: manganiferous titaniferous Mg-biotite (inclusion in aegirine phenocryst; Fig. 5.3.2), 5-6: manganiferous titaniferous Mg-biotite (groundmass), 7: manganiferous titaniferous lepidomelane, 8: manganiferous titaniferous lepidomelane (inclusion in aegirine phenocryst), 9: manganiferous titaniferous lepidomelane (interstitial grain).

TABLE A9.4. SELECTED COMPOSITIONS OF BIOTITE FROM SAMPLES OF NEPHELINE SYENITE

Number	1	2	3	4	5	6	7	8	9
Rock Type	MIAS	PTIN	PTIN	PTIN	PTIN	PTIN	ITIN	WINC	WINC
Sample	M816 Av(6)	M637-2 Av(2)	M637-4 Av(4)	M639-8* Av(4)	M639-9a* Av(1)	M639-9b* Av(1)	M694 Av(4)	M690-1 Av(3)	M690-2 Av(3)
SiO2 wt. %	37.39	38.88	37.35	41.88	40.47	40.78	35.67	37.77	36.86
Al2O3	12.82	10.78	10.61	12.58	13.84	14.01	11.58	10.35	9.38
TiO2	2.71	1.77	2.86	2.56	3.25	1.56	3.74	3.42	3.74
FeOT	22.28	27.57	30.18	9.18	9.33	9.28	30.57	26.79	29.15
FeO	16.34	21.99	23.98	9.18	9.33	9.28	24.16	21.38	23.21
Fe2O3	6.6	6.2	6.8	0.0	0.0	0.0	6.9	6.1	6.6
MnO	1.77	4.21	3.17	4.28	4.69	4.85	3.87	4.45	4.8
MgO	9.46	5.88	2.58	14.98	12.51	14.74	2.58	5.38	2.68
CaO	0.01	0.0	0.0	0.01	0.01	0.0	0.0	0.01	0.0
Na2O	0.15	0.06	0.06	0.16	0.17	0.08	0,18	0.08	0.06
K2O	9.18	9.88	9.62	9.34	8.98	9.18	9.75	10.17	10.05
F	1.28	0.15	0.16	3.17	2.12	2.88	0.13	0.23	0.16
Cl	0.02	0.02	0.02	0.01	0.04	0.0	0.02	0.0	0.01
Total	97.15	96.79	96.26	96.57	95.71	94.66	97.48	97.08	96.68
O=F,Cl	0.53	0.07	0.07	1.34	0.90	0.04	0.06	0.10	0.07
Si	2.952	3.014	3.001	3.005	3.066	3.034	2.945	2.990	2.967
Al2	1.148	0.986	0.999	0.915	0.934	0.966	1.001	0.966	0.890
Fe3Z	0.0	0.0	0.0	0.0	0.0	0.0	0.074	0.044	0.143
AlY	0.004	0.021	0.006	0.177	0.238	0.265	0.0	0.0	0.0
TiY	0.155	0.106	0.124	0.142	0.185	0.087	0.224	0.204	0.226
Fe3Y	0.579	0.378	0.411	0.0	0.0	0.0	0.348	0.319	0.267
Y1	0.838	0.497	0.542	0.318	0.415	0.363	0.564	0.523	0.484
MgY	1.875	0.449	0.299	1.636	1.413	1.638	0.297	0.389	0.322
FeY	1.042	1.489	1.612	0.561	0.591	0.579	1.611	1.418	1.563
MnY	0.114	0.285	0.216	0.262	0.301	0.264	0.287	0.298	0.275
NaY	0.0	0.009	0.0	0.0	0.0	0.0	0.007	0.012	0.009
Y2	2.252	2.199	2.127	2.458	2.386	2.471	2.125	2.118	2.166
K	0.893	1.008	0.986	0.878	0.868	0.865	0.992	1.027	1.032
NaX	0.019	0.0	0.009	0.025	0.025	0.012	0.008	0.0	0.0
CaX	0.001	0.0	0.0	0.001	0.001	0.0	0.0	0.001	0.0
X	0.913	1.0	0.996	0.901	0.894	0.877	1.0	1.028	1.032
F	0.382	0.038	0.041	0.738	0.508	0.672	0.033	0.058	0.041
Cl	0.005	0.005	0.005	0.001	0.005	0.0	0.005	0.0	0.001
FeT/(FeT+Mg)	0.569	0.805	0.871	0.255	0.295	0.261	0.872	0.828	0.859
Fe3+/FeT	0.267	0.202	0.203	–	–	–	0.204	0.205	0.204
Mg/(Mg+Fe2+)	0.588	0.255	0.157	0.745	0.705	0.739	0.156	0.216	0.171

APPENDIX X. SELECTED COMPOSITIONS OF OXIDE MINERALS

Fe_2O_3 was calculated for both ilmenite and magnetite following the procedure of Carmichael (1967). Formula based on 4 oxygen for magnetite and 3 oxygen for ilmenite.

Rock types defined in Appendix III. Av(n): average of n analyses. Endmembers are given in weight per cent. See Appendix I for analytical conditions.

TABLE A10.1. SELECTED COMPOSITIONS OF OXIDE MINERALS FROM MAFIC AND MESOCRATIC INTERMEDIATE SAMPLES

Number	1	2	3	4	5	6	7	8
Rock Type	MAFI	MAFI	MZDI	MZDI	MZDI	GABB	GABB	GABB
Sample	M86-4	M86-2	M823-4a	M823-4b	M823-1	M864-1a	M864-1b	M864-2
	Av(2)	Av(2)	Av(1)	Av(1)	Av(3)	Av(1)	Av(3)	Av(3)
Al2O3 wt. %	0.03	0.02	0.00	0.01	0.0	0.25	0.02	0.01
TiO2	0.02	48.38	0.76	49.15	49.85	0.25	50.00	50.61
FeO	90.04	47.33	91.75	45.61	46.06	92.04	46.00	46.00
MnO	0.04	2.65	0.06	2.06	2.04	0.0	2.11	2.00
MgO	0.0	0.05	0.05	0.07	0.07	0.05	0.20	0.36
NiO	0.05	0.03	0.02	0.0	0.06	0.0	0.06	0.02
V2O3	0.0	0.61	0.47	0.0	0.33	0.57	0.25	0.22
Cr2O3	0.02	0.01	0.0	0.0	0.05	0.02	0.06	0.0
Fe2O3	67.32	7.33	66.91	4.95	5.67	68.21	5.04	4.51
FeO	30.27	40.74	31.54	41.17	41.76	31.46	42.27	42.02
Total	97.74	99.79	99.09	98.19	100.58	100.81	100.00	100.55
Al	0.001	0.001	0.004	0.0	0.0	0.011	0.001	0.0
Ti	0.001	0.924	0.022	0.952	0.943	0.007	0.949	0.955
Fe3+	1.997	0.140	1.948	0.096	0.107	1.959	0.096	0.085
Fe2+	0.998	0.866	1.017	0.887	0.879	1.004	0.892	0.899
Mn	0.001	0.057	0.002	0.062	0.061	0.0	0.045	0.043
Mg	0.0	0.001	0.003	0.003	0.003	0.003	0.011	0.013
Ni	0.002	0.001	0.001	0.0	0.001	0.0	0.001	0.0
V	0.0	0.010	0.012	0.0	0.005	0.014	0.004	0.004
Cr	0.001	0.0	0.0	0.0	0.001	0.001	0.001	0.0
Fe2TiO4	0.0	-	1.06	-	-	0.56	-	-
Fe3O4	97.48	-	97.01	-	-	98.90	-	-
Mn2TiO4	0.0	-	0.09	-	-	0.0	-	-
MnFe2O4	0.13	-	0.0	-	-	0.0	-	-
FeTiO3	-	86.04	-	86.96	88.20	-	89.27	90.44
MnTiO3	-	5.63	-	6.08	6.04	-	4.49	4.25
MgTiO3	-	0.09	-	0.21	0.21	-	0.04	1.07

1,3,6: magnetite; 2,5,8: discrete grains of ilmenite; 4,7: ilmenite granules associated with magnetite

TABLE A10.2. SELECTED COMPOSITIONS OF OXIDE MINERALS FROM QUARTZ-POOR FELSIC SAMPLES

	1	2	3	4	5	6	7	8	9	10	11	12	13	14
Rock Type	PSYN	PSYN	PSYN	ALKS	ALKS	ALKS	PSYN	PSYN	PSYN	PQZM	PQZM	PQZM	QTZM	QTZM
Sample	MG10-1a	MG10-1b	MG10-2	WX23-2	WX23-1a	WX23-1b	MG40-4a	MG40-4b	MG40-3	MG52-4a	MG52-4b	MG52-3	MG66-2a	MG66-2b
	Av(1)	Av(1)	Av(1)	Av(1)	Av(1)	Av(3)	Av(2)	Av(2)	Av(1)	Av(1)	Av(2)	Av(2)	Av(1)	Av(1)
Al2O3 wt. %	0.16	0.01	0.0	0.05	0.02	0.0	0.13	0.03	0.0	0.20	0.02	0.01	0.12	0.0
TiO2	0.73	52.69	48.45	0.11	53.90	48.97	0.69	51.54	52.41	0.60	51.81	50.98	0.75	50.19
FeO	90.79	45.79	44.76	89.93	40.70	45.63	91.54	41.53	44.59	90.74	43.15	46.19	90.67	44.36
MnO	0.07	1.63	2.97	0.02	5.96	5.82	0.09	5.07	2.58	0.06	3.04	2.35	0.12	3.70
MgO	0.01	0.03	0.00	0.0	0.05	0.02	0.01	0.12	0.07	0.02	0.03	0.13	0.02	0.05
NiO	0.10	0.0	0.04	0.02	0.01	0.0	0.0	0.0	0.0	0.03	0.03	0.06	0.07	0.0
V2O3	0.21	0.13	0.0	0.42	0.0	0.13	0.23	0.33	0.0	0.28	0.21	0.23	0.0	0.40
Cr2O3	0.01	0.03	0.01	0.0	0.03	0.01	0.0	0.01	0.02	0.04	0.01	0.0	0.04	0.02
Fe2O3	66.20	1.28	4.07	66.36	0.0	6.14	66.85	8.59	8.22	66.32	8.59	3.36	66.27	3.41
FeO	31.15	42.64	40.38	30.22	40.70	38.18	31.39	41.00	44.39	31.06	42.62	43.17	31.04	41.29
Total	98.72	101.44	96.80	97.20	100.67	99.20	99.39	98.69	99.69	98.61	99.16	100.29	98.43	99.14
Al	0.007	0.0	0.0	0.002	0.001	0.0	0.006	0.001	0.0	0.009	0.001	0.0	0.006	0.0
Ti	0.021	0.986	0.962	0.003	1.011	0.949	0.020	0.991	0.998	0.018	0.992	0.966	0.022	0.963
Fe3+	1.944	0.024	0.096	1.980	0.0	0.118	1.948	0.011	0.004	1.947	0.011	0.064	1.949	0.065
Fe2+	1.015	0.888	0.882	1.002	0.849	0.813	1.017	0.877	0.940	1.014	0.900	0.910	1.015	0.881
Mn	0.002	0.098	0.066	0.001	0.126	0.126	0.003	0.110	0.055	0.002	0.003	0.050	0.004	0.080
Mg	0.001	0.001	0.003	0.0	0.002	0.001	0.001	0.005	0.003	0.001	0.001	0.005	0.001	0.002
Ni	0.003	0.0	0.001	0.001	0.0	0.0	0.0	0.0	0.0	0.001	0.001	0.001	0.002	0.0
V	0.006	0.002	0.0	0.011	0.0	0.002	0.006	0.006	0.0	0.007	0.003	0.004	0.0	0.008
Cr	0.0	0.001	0.0	0.0	0.001	0.0	0.0	0.0	0.0	0.001	0.0	0.0	0.001	0.0
Fe2TiO4	1.76	-	-	0.25	-	-	1.76	-	-	1.48	-	-	1.75	-
Fe3O4	96.10	-	-	96.22	-	-	96.92	-	-	96.16	-	-	96.00	-
MnTiO4	0.11	-	-	0.03	-	-	0.14	-	-	0.09	-	-	0.19	-
FeTiO3	-	90.05	85.28	-	89.41	88.48	-	86.59	93.75	-	90.01	91.18	-	87.22
MnTiO3	-	9.84	6.32	-	12.67	12.38	-	10.78	5.49	-	8.17	5.00	-	7.87
MgTiO3	-	0.09	0.24	-	0.15	0.06	-	0.36	0.21	-	0.09	0.39	-	0.15

1,4,7,10,13: magnetite; 2,5,8,11,14: ilmenite granules associated with magnetite; 3,6,9,12: discrete grains of ilmenite

TABLE A10.3. SELECTED COMPOSITIONS OF OXIDE MINERALS FROM SAMPLES OF GRANITE

Number	1	2	3	4	5	6	7	8	9
Rock Type	PDGR	PDGR	PDGR	KFDG	KFDG	KFDG	KFPG	KFPG	KFPG
Sample	M646-2a Av(2)	M646-2b Av(1)	M646-1 Av(5)	M657-2a Av(1)	M657-2b Av(1)	M657-3 Av(3)	M683-1a Av(1)	M683-1b Av(1)	M683-2 Av(1)
Al2O3 wt. %	0.09	0.0	0.01	0.12	0.0	0.01	0.15	0.02	0.03
TiO2	1.01	51.06	51.30	0.31	50.35	50.71	0.29	50.47	50.91
FeO	91.17	43.72	43.51	89.77	41.76	43.23	90.00	41.87	43.76
MnO	0.06	4.85	4.22	0.09	6.14	4.73	0.10	6.13	4.47
MgO	0.0	0.04	0.05	0.01	0.02	0.05	0.0	0.04	0.02
NiO	0.01	0.00	0.01	0.0	0.0	0.01	0.0	0.01	0.04
V2O3	0.34	0.0	0.26	0.0	0.0	0.06	0.0	0.56	0.05
Cr2O3	0.03	0.14	0.0	0.01	0.05	0.02	0.0	0.0	0.0
Fe2O3	66.10	3.16	1.95	66.11	3.04	2.00	66.35	3.09	2.07
FeO	31.69	40.87	41.76	30.28	39.02	40.71	30.30	39.09	41.18
Total	99.33	100.19	99.55	96.93	90.63	99.10	97.27	99.41	99.57
Al	0.004	0.0	0.0	0.000	0.0	0.0	0.007	0.001	0.001
Ti	0.029	0.969	0.979	0.009	0.970	0.972	0.009	0.965	0.972
Fe3+	1.927	0.060	0.037	1.976	0.059	0.054	1.976	0.059	0.055
Fe2+	1.027	0.862	0.896	1.006	0.836	0.868	1.005	0.832	0.874
Mn	0.002	0.103	0.091	0.003	0.133	0.102	0.003	0.132	0.096
Mg	0.0	0.002	0.002	0.001	0.001	0.002	0.0	0.002	0.001
Ni	0.0	0.002	0.0	0.0	0.0	0.0	0.0	0.0	0.001
V	0.009	0.0	0.004	0.0	0.0	0.001	0.0	0.009	0.001
Cr	0.001	0.003	0.0	0.0	0.001	0.0	0.0	0.0	0.0
Fe2TiO4	2.72	-	-	0.70	-	-	0.65	-	-
Fe3O4	95.84	-	-	95.86	-	-	96.20	-	-
Mn2TiO4	0.09	-	-	0.14	-	-	0.16	-	-
MnFe2O4	0.0	-	-	0.0	-	-	0.0	-	-
FeTiO3	-	86.33	88.19	-	82.41	85.90	-	82.57	86.97
MnTiO3	-	10.27	8.97	-	13.06	10.06	-	13.03	9.50
MgTiO3	-	0.12	0.15	-	0.06	0.15	-	0.12	0.06

1,4,7: magnetite; 2,5,8: ilmenite granules associated with magnetite; 3,6,9: discrete grains of ilmenite

TABLE A10.4. SELECTED COMPOSITIONS OF OXIDE MINERALS FROM SAMPLES OF NEPHELINE SYENITE

Number	1	2	3	4	5	6
Rock Type	MIAS	MIAS	PTIN	PTIN	PTIN	PTIN
Sample	MG16 Av(8)	MG16-2 Av(3)	MG39 Av(6)	MG39 Av(1)	MG94 Av(3)	MG94-4 Av(3)
Al2O3 wt. %	0.11	0.50	0.05	0.0	0.06	0.0
TiO2	0.29	49.86	0.11	52.65	0.74	50.78
FeO	91.36	5.23	83.38	3.40	90.94	32.28
MnO	1.23	41.48	8.71	41.53	0.72	14.45
MgO	0.01	0.01	0.05	0.10	0.01	0.03
NiO	0.05	0.02	0.0	0.0	0.03	0.02
V2O3	0.20	0.34	0.08	0.0	0.02	0.34
Cr2O3	0.02	0.0	0.0	0.0	0.0	0.0
Fe2O3	68.15	2.72	68.18	0.0	66.93	1.47
FeO	30.04	2.79	22.03	3.40	30.72	30.95
Total	100.10	97.71	99.21	97.68	99.22	98.05
Al	0.005	0.015	0.002	0.0	0.003	0.0
Ti	0.008	0.963	0.003	1.012	0.022	0.983
Fe3+	1.973	0.053	1.989	0.0	1.954	0.029
Fe2+	0.966	0.060	0.714	0.073	0.996	0.666
Mn	0.040	0.903	0.286	0.899	0.024	0.315
Mg	0.001	0.0	0.003	0.004	0.001	0.001
Ni	0.002	0.0	0.0	0.0	0.001	0.0
V	0.005	0.006	0.002	0.0	0.0	0.006
Cr	0.001	0.0	0.0	0.0	0.0	0.0
Fe2TiO4	0.0	-	0.0	-	0.86	-
Fe3O4	96.27	-	70.78	-	97.04	-
Mn2TiO4	0.70	-	0.17	-	1.13	-
MnFe2O4	2.54	-	27.97	-	0.0	-
FeTiO3	-	5.88	-	10.78	-	65.38
MnTiO3	-	88.20	-	88.31	-	30.73
MgTiO3	-	0.03	-	0.30	-	0.09

1: magnetite, 2: pyrophanite lamellae in magnetite, 3: Mn-rich magnetite, 4: secondary pyrophanite, 5: magnetite, 6: Mn-rich ilmenite.

APPENDIX XI. SELECTED COMPOSITIONS OF ACCESSORY MINERALS

Recalculation method indicated in brackets with the mineral description below the table.

Rock types defined in Appendix III. Av(n): average of n analyses. See Appendix I for analytical conditions.

TABLE A11.1. SELECTED COMPOSITIONS OF ACCESSORY MINERALS FROM MAFIC AND MESOCRATIC INTERMEDIATE SAMPLES

Number	1	2	3
Rock Type	MAFI	GABB	GABB
Sample	MG24	MG25	MG64
	Av(3)	Av(1)	Av(1)
SiO2 wt. %	33.85	33.17	34.07
Al2O3	8.23	0.01	13.55
TiO2	3.89	0.05	0.0
ZrO2	0.0	64.62	0.0
Nb2O3	0.0	0.0	1.61
MgO	0.12	0.02	14.58
FeO	15.35	0.03	23.90
MnO	0.13	0.0	0.0
CaO	34.73	0.0	1.02
Na2O	0.02	0.0	0.04
K2O	0.02	0.0	0.09
La2O3	n.d.	0.02	0.0
Ce2O3	n.d.	0.08	0.0
P2O5	n.d.	0.35	0.0
Cl	0.03	n.d.	n.d.
F	1.09	n.d.	n.d.
Total	97.00	98.35	88.86
O=F,Cl	0.47	0.0	0.0
Si	2.795	4.073	7.009
Al	0.801	0.001	3.286
Ti	0.242	0.005	0.0
Zr	0.0	3.869	0.0
Nb	0.0	0.0	0.150
Mg	0.015	0.004	4.471
Fe	1.060	0.003	4.112
Mn	0.009	0.0	0.0
Ca	3.073	0.0	0.225
Na	0.003	0.0	0.016
K	0.002	0.0	0.024
La	-	0.001	0.0
Ce	-	0.004	0.0
P	-	0.036	0.0
Cl	0.004	-	-
F	0.285	-	-

1: secondary garnet(?) located along biotite cleavages (8 cations), 2: zircon (16 oxygen atoms), 3: diabantite (28 oxygen atoms).

TABLE A11.2. SELECTED COMPOSITIONS OF ACCESSORY MINERALS FROM QUARTZ-POOR FELSIC SAMPLES

Number	1	2	3	4	5	6
Rock Type	SYEN	SYEN	SYEN	PSYN	PSYN	QTMZ
Sample	MG8-1c Av(1)	MG8-1r Av(1)	MG8-2 Av(2)	MG40-1 Av(2)	MG40-2 Av(2)	MG63 Av(2)
SiO2 wt. %	0.16	0.78	30.73	33.17	20.26	31.55
Al2O3	0.06	0.01	9.25	0.0	0.52	11.95
TiO2	0.0	0.0	3.09	0.0	16.40	2.27
ZrO2	0.0	0.0	n.d.	62.29	n.d.	n.d.
Nb2O3	0.17	0.13	n.d.	1.64	n.d.	n.d.
MgO	0.0	0.0	0.52	0.01	0.29	1.50
FeO	0.02	0.0	16.30	0.10	10.14	15.84
MnO	0.09	0.09	0.97	0.0	0.30	0.45
CaO	54.93	53.93	9.25	0.01	3.92	9.26
Na2O	0.22	0.26	0.16	0.0	0.01	0.05
K2O	0.04	0.02	0.20	0.09	0.0	0.0
La2O3	0.19	0.60	8.88	0.03	13.39	9.26
Ce2O3	0.48	1.15	11.26	0.04	20.74	12.68
Y2O3	n.d.	n.d.	0.02	n.d.	0.48	0.01
ThO2	n.d.	n.d.	0.66	n.d.	0.98	0.64
P2O5	42.63	41.77	0.01	0.39	0.08	0.03
Total	98.99	98.74	91.26	97.74	87.49	95.47
Si	0.013	0.066	3.184	4.108	4.414	3.099
Al	0.006	0.001	1.130	0.0	0.134	1.383
Ti	0.0	0.0	0.241	0.0	2.689	0.168
Zr	0.0	0.0	-	3.761	-	-
Nb	0.006	0.005	-	0.091	-	-
Mg	0.0	0.0	0.080	0.002	0.093	0.220
Fe	0.001	0.0	1.412	0.010	1.849	1.302
Mn	0.006	0.006	0.085	0.0	0.055	0.037
Ca	4.901	4.853	1.027	0.001	0.913	0.974
Na	0.036	0.042	0.031	0.0	0.004	0.010
K	0.004	0.002	0.026	0.014	0.0	0.0
La	0.006	0.019	0.339	0.001	1.076	0.336
Ce	0.015	0.035	0.427	0.002	1.656	0.456
Y	-	-	0.001	-	0.055	0.0
Th	-	-	0.016	-	0.048	0.014
P	3.005	2.970	0.001	0.041	0.014	0.003

1: brown core of apatite xenocryst(?) (8 cations), 2: clear rim of apatite xenocryst(?) (8 cations), 3, 6: allanite (8 cations), 4: zircon (16 oxygen atoms), 5: chevkinite(?) (13 cations)

1: titanite (12 cations), 2: aenigmatite (14 cations and 20 oxygen atoms), 3: astrophyllite (28 oxygen atoms), 4: sodalite (12 cations in Si-Al framework), 5: eucolite-eudialyte(?) (18.5 oxygen atoms), 6: pectolite (6 cations), 7: sodalite (12 cations in Si-Al framework), 8: zircon (16 oxygen atoms), 9: pyrochlore (4 cations), 10: wohlerite (6 cations), 11: Rosenbuschite-Gotzenite(?) (6 cations).

TABLE A11.3. SELECTED COMPOSITIONS OF ACCESSORY MINERALS FROM SAMPLES OF NEPHELINE SYENITE

Number	1	2	3	4	5	6	7	8	9	10	11
Rock-Type	MIAS	PTIN	PTIN	PTIN	PTIN	PTIN	PTIN	PTIN	ITIN	ITIN	ITIN
Sample	M816 Av(1)	M637a Av(4)	M637b Av(5)	M637c Av(4)	M637d Av(2)	M637e Av(3)	M639a Av(2)	M639b Av(1)	M694a Av(2)	M694b Av(2)	M694c Av(2)
SiO2 wt. %	30.83	42.49	35.87	40.19	56.75	52.91	30.41	34.82	0.0	30.41	31.21
Al2O3	0.72	0.34	1.19	34.24	0.88	0.01	31.17	0.82	0.0	0.01	0.0
TiO2	35.40	9.17	11.85	0.01	0.51	0.01	0.04	0.0	0.22	1.12	7.19
ZrO2	0.69	0.0	0.34	n.d.	12.69	0.0	n.d.	62.23	0.34	13.96	7.89
Nb2O5	1.58	0.23	1.23	n.d.	1.83	0.0	n.d.	0.0	43.54	11.19	1.36
MgO	0.0	0.29	0.60	0.0	0.01	0.01	0.0	0.0	0.01	0.07	0.0
FeO	1.56	34.34	26.42	0.18	5.57	1.14	0.21	0.14	0.19	0.39	0.14
MnO	0.11	5.25	7.97	0.02	2.58	4.29	0.02	0.02	0.09	1.24	0.76
CaO	28.78	0.05	1.89	0.0	12.28	26.19	0.07	0.0	16.94	26.12	28.92
Na2O	0.41	7.63	2.04	17.44	2.94	0.71	20.39	0.01	4.98	7.94	0.35
K2O	0.01	0.0	6.64	0.04	0.31	0.04	0.02	0.06	0.04	0.04	0.03
La2O3	0.38	n.d.	n.d.	n.d.	n.d.	0.02	n.d.	n.d.	0.66	0.06	0.36
Ce2O3	0.82	n.d	n.d.	n.d.	n.d.	0.06	n.d.	n.d.	1.55	0.22	0.87
P2O5	0.06	n.d.	n.d.	n.d.	n.d.	0.01	n.d.	n.d.	0.09	0.12	0.15
Cl	n.d.	0.10	0.02	0.24	0.76	n.d.	0.44	0.16	n.d.	n.d.	n.d.
F	n.d.	0.01	1.43	0.14	0.22	n.d.	0.16	0.0	n.d.	n.d.	n.d.
Total	97.45	99.85	96.11	98.58	95.27	93.48	96.96	97.42	76.63	92.86	87.21
O=F,Cl	-	0.05	0.62	1.92	0.26	-	1.97	0.04	-	-	-
Si	4.058	6.058	7.749	5.977	6.982	3.095	6.119	4.175	0.0	2.068	2.090
Al	0.115	0.057	0.383	6.001	0.012	0.001	5.853	0.119	0.0	0.0	0.0
Fe3	-	0.0	-	0.022	-	-	0.027	-	-	-	-
Ti	3.606	0.982	1.795	0.001	0.047	0.0	0.005	0.0	0.449	0.057	0.362
Zr	0.039	0.0	0.036	-	0.761	0.0	-	3.724	0.012	0.463	0.257
Nb	0.097	0.015	0.120	-	0.057	0.0	-	0.0	1.431	0.344	0.041
Mg	0.0	0.062	0.193	0.0	0.001	0.001	0.0	0.0	0.001	0.007	0.0
Fe+	0.176	-	4.773	-	0.575	0.056	-	0.014	0.011	0.022	0.008
Fe2	-	4.009	-	-	-	-	-	-	-	-	-
Mn	0.013	0.631	1.459	0.002	0.268	0.212	0.002	0.002	0.006	0.071	0.043
Ca	3.721	0.008	0.436	0.0	1.608	1.641	0.011	0.0	1.319	1.904	2.074
Na	0.107	2.106	0.856	5.029	0.708	0.908	6.298	0.002	0.702	1.047	1.004
K	0.002	0.0	1.858	0.007	0.049	0.003	0.004	0.009	0.004	0.003	0.003
La	0.019	-	-	-	-	0.001	-	-	0.018	0.002	0.009
Cr	0.041	-	-	-	-	0.001	-	-	0.041	0.005	0.021
P	0.007	-	-	-	-	0.0	-	-	0.006	0.007	0.008
Cl	-	0.024	0.008	2.076	0.158	-	2.279	0.033	-	-	-
F	-	0.005	1.002	0.067	0.006	-	0.008	0.0	-	-	-